INNOVATIVE APPLICATIONS OF TIRE DERIVED AGGREGATE (TDA) FOR BURIED PIPES AND CULVERTS

by

Ahmed Mahgoub

Submitted in partial fulfilment of the requirements
for the degree of Doctor of Philosophy

at

Dalhousie University
Halifax, Nova Scotia
September 2019

This thesis is dedicated to my beloved parents; Gamaleldin and Iman.

Rest in peace dad! See you soon.

TABLE OF CONTENTS

LIST OF TABLES

LIST OF FIGURES

ABSTRACT

Social well being and economic prosperity are tied together in a mutually supportive and interdependent scheme. Achieving prosperity is highly related to the socio-economic well being and cannot be achieved without strong and supportive civil infrastructures. Soil-metal structures including buried bridges, culverts, and pipelines are key supporting pillars for the economic prosperity of developed communities.

In densely populated and congested urban centers, the interaction between surface structures and buried utilities are unavoidable. For instance, placing the pipe at a shallow depth attracts substantial additional earth pressures and loads causing overstressing and/or unacceptable deformations of the buried pipe. There are several alternatives that may be used to mitigate this situation. These alternatives include using induced trench construction, using lightweight fill material to reduce the imposed loads, and finally relocation of utilities which is the most expensive and less desirable alternative. The characteristics of the used backfill material control the pipe-soil interaction mechanism and sequentially the amount of exerted pressures. Using lightweight compressible materials above buried structures has long been investigated to reduce the stresses above buried pipes.

In this thesis innovative applications for using tire derived aggregates (TDA) as a lightweight backfill material to protect and improve the performance of buried structures under static and seismic loading conditions were investigated experimentally and numerically. Exploring useful uses for TDA (produced from recycled scrap tires) in civil engineering applications helps to reduce the environmental impacts that could be caused by disposing the tires in landfills which is becoming a scares resource by time. Full-scale field tests were carried to examine the feasibility of protecting pre-existing pipes, located underneath shallow foundations, by using TDA as an engineered stress-reduction fill above the pipes and underneath a concrete footing. Additionally, the study was extended to investigate the behaviour of rigid footings resting on a surface of conventional backfill materials overlying a TDA layer with different thicknesses. Furthermore, a comprehensive three-dimensional modelling exercise using the finite element (FE) code PLAXIS 3D was conducted to study the effect of changing various key parameters, i.e., the thickness of the TDA layer, the shape and configuration of the TDA cross-section, etc., on the performance of the system.

Another four full-scale tests were executed in the lab to investigate the feasibility of using TDA around corrugated steel culverts to enhance their performance under service loading. Afterward, 3D finite element models were developed for the different tested configurations to investigate crucial parameters affecting the culvert performance and to optimize the design of the proposed TDA system. In addition, a coupled TDA Geocell stress bridging system was developed utilizing three additional full-scale tests and a comprehensive 3D modelling component. The developed system uses a geocell reinforced top granular backfill layer over the TDA layer to induce a stress arching mechanism capable of reducing the imposed stresses on the underneath pipe and control the surface settlement.

Finally, the last part of this research focuses on evaluating the seismic design of open bottom large span metal arch culverts in the Canadian Highway Bridge Design Code (CHBDC) and developing an innovative system using TDA to mitigate the seismic hazards in high seismicity regions. Based on the results of the conducted study, a set of recommendations for the analysis and design of buried structures are proposed.

LIST OF ABBREVIATIONS AND SYMBOLS USED

Abbreviations

AASHTO	*American Association of State Highway and Transportation Officials*
ASCE	*American Society of Civil Engineers*
ASTM	*American Society for Testing and Materials*
CHBDC	*Canadian Highway Bridge Design Code*
CSA	*Canadian Standards Association*
CSP	*Corrugated Steel Plate*
DIC	*Digital Image Correlation*
FE	*Finite Element*
HSM	*Hardening Soil Model*
HSM-Small	*Hardening Soil Model with Small Strain*
LVDT	*Linear Variable Differential Transformers*
LRFD	*Load and Resistance Factor Design*
MC	*Mohr Coulomb*
NF	*Flexibility Number*
NCHRP	*National Cooperative Highway Research Program*
NBCC	*National Building Code of Canada*
ONT	*Ontario*
PGA	*Peak Ground Acceleration*
PSA_{targ}	*Targeted Spectrum Acceleration*
SPT	*Standard Penetration Test*
SSI	*Soil Structure Interaction*
TDA	*Tire Derived Aggregate*
TDF	*Tire-Derived Fuel*
UHS	*Uniform Hazard Spectrum*

Symbols

A	*Area*
a_x	*Horizontal Acceleration*
B	*Footing width*

c'	*Effective cohesion*
C_u	*Undrained shear strength*
D	*Diameter*
d	*Depth*
D_F	*Foundation depth*
d_g	*Geocell embedment depth*
E	*Modulus of elasticity*
E_{50}	*Secant modulus*
E_{oed}	*Tangent stiffness from odometer test*
E_s	*Soil modulus of elasticity*
EI	*Bending stiffness*
EA	*Hoop stiffness*
F_{FD}	*Foundation depth factor*
F_{FW}	*Footing width factor*
F_s	*Footing shape factor*
F_φ	*Internal friction angle factor*
F_y	*Yield strength*
F_u	*Tensile strength*
F_1	*Fundamental frequency*
f_{max}	*Maximum frequency component of the inserted wave*
f_{cu}	*Ultimate compressive strength*
G	*Shear Modulus*
hc	*Backfill height above the culvert crown*
H	*Backfill height*
I	*Moment of inertia*
K	*Curvature*
K_o	*At-rest earth pressure coefficient*
L	*Length*
M	*Bending Moment*
N	*Thrust force*
P_{ref}	*Reference pressure*

P_a	*Atmospheric pressure*
R_{inter}	*Strength-reduction factor for the interface element*
R_f	*Reduction factor*
t_g	*Thickness of the top granular layer*
t	*TDA thickness*
W	*Width*
W_c	*Water content*
Vs	*Average soil shear velocity*
$V_{S\,min}$	*Lowest shear wave velocity*
XS	*Cross sectional area*
y	*Vertical distance from the neutral axis*
2D	*Two-Dimensional*
3D	*Three-Dimensional*
α	*First Rayleigh Damping scaler*
β	*Second Rayleigh Damping scaler*
γ	*Unit weight*
γ	*Shear strain*
Δh	*Settlement*
ε	*Strain*
ε_{ave}	*Average strain*
ε_1	*Strain at the inside corrugation valley*
ε_2	*Strain at the inside crest*
λ	*Wavelength*
°	*Degree*
σ_v	*Vertical stress*
σ_{eff}	*Vertical effective stress*
φ	*Angle of the internal friction*

ACKNOWLEDGEMENTS

My unreserved gratitude and praise are for Allah, the Most Compassionate and the Most Merciful. He has blessed me with his bounties, and he has given me the strength and courage to reach my goals during this journey.

Sincere thanks to my supervisor, Dr. Hany El Naggar who provided valuable and venerable guidance throughout this research. This thesis would not have been possible without his guidance and kind advice. I wish to extend my appreciation to my committee members, Dr. John Newhook and Dr. Farid Taheri for their helpful comments on my thesis and during my research. I also want to thank Dr. Nicholas Vlachopoulos for taking time to review this dissertation, attending my defense and providing a valuable feedback.

The financial support of the Natural Sciences and Engineering Council of Canada (NSERC) is gratefully acknowledged. In addition, I gratefully acknowledge the generosity of our research collaborator, Halifax C&D Recycling Limited for the donation of all TDA materials used in this project.

My deep appreciation and gratitude go out to my wife Samaa who is my partner in every step in my life and to my beloved daughters Roaa and Salma. Special thanks go to my immediate family Walaa, Ibrahim and Aya whom I have missed during the many years of being away from home. Thanks also go to my friends and colleagues, without whom I could not have succeeded in my endeavors.

CHAPTER 1 INTRODUCTION

1.1 STATEMENT OF THE PROBLEM

Routing utility conduits beneath buildings is sometimes unavoidable, especially in densely populated, congested urban centers. Placement of a pipe at a shallow depth can result in substantial additional earth pressure and loads, leading to overstressing and/or unacceptable deformation of the buried pipe. Various alternatives may be used to avoid this situation. These include induced trench construction, the use of lightweight fill material to reduce imposed embankment loads, utilization of a geogrid reinforced soil platform bridge, and the relocation of utilities (El Naggar et al. 2015).

The use of lightweight compressible materials such as geofoam, straw, compressible soil, leaves, and woodchips over buried structures to reduce the stress above buried pipelines and culverts has long been a focus of investigation (Sladen and Oswell 1988; Liedberg 1997; McAffee and Valsangkar 2005; Parker et al. 2008; Jiang 2008; Gu et al. 2009; Oshati et al. 2012; Turan et al. 2013; Ahmed et al. 2015; Al-Naddaf et al. 2019).

In order to meet environmental demands, rubber tires have been introduced as a lightweight backfill material for many civil engineering applications. Each year, large quantities of used tires are generated worldwide. Around one billion scrap tires have been discarded globally, over 250 million of them in the USA and 30 million in Canada (El Naggar et al. 2016). Promotion of the re-use and recycling of rubber tires has increased progressively since 1990, because of the environmental hazards associated with uncontrolled landfill disposal (Rubber Manufacturers Association 2017). As per the USA Scrap Tire Management Council, in 2000, 70% of scrap tires were recycled, as compared with only

6% in 1990. Scrap rubber tires can be recycled via tire-derived fuel (TDF), ground rubber applications, rubberized asphalt concrete mixtures, and tire-derived aggregate (TDA) in civil engineering applications (Rubber Manufacturers Association 2017). This trend aims to reduce the environmental hazards that can result from scrap tire stockpiles, which serve as an attractive habitat for insects and rodents. In addition, tire disposal has occupied large areas of land, which is now becoming scarcer (Rubber Manufacturers Association 2017). Fires at scrap tire landfill sites can also cause environmental and human disasters. For instance, in February 1990, at Hagersville, Ontario, Canada, 1700 people were evacuated from their homes because of a massive fire that took place at a landfill site with 12.6 million tires, resulting in severe contamination and toxic fumes (Pierre 2013). Thus, there is an urgent need to recycle waste tires, and civil engineering construction is one of the main markets in this regard (GC 2008). In addition, as discussed in the following section, shredded tire products have several desirable geotechnical properties that can enhance the overall performance of civil engineering infrastructure. In light of these considerations, the objective of this research project was to use lightweight TDA as a backfill material to improve the performance of buried pipes and culverts under static and seismic loading conditions.

1.2 BACKGROUND OVERVIEW

Tire-derived aggregate is generally used in civil engineering applications as a lightweight backfill material. It is commonly produced by cutting waste tires into relatively small pieces (12 to 300 mm). ASTM D6270 classifies TDA into two types: Type A has a smaller particle size and is usually used as an insulation material for road projects or a fill material behind retaining walls; whereas type B, which consists mainly of larger particles, is

primarily used as an embankment fill. Figure 1-1 shows examples of type A and type B TDA made from shredded tires. TDA has advantageous properties that enable it to be used in various civil engineering applications. It is lightweight, weighing only one-third to half as much as traditional granular backfill materials. The specific gravity of TDA ranges from 1.15 to 1.21, while the specific gravity of conventional backfill ranges from 2.55 to 2.75 (Edil 2005; Sparkes et al. 2019). In addition, Yoon et al. (2006) and GC (2008) reported that TDA has a higher compressibility and a lower cost than other lightweight backfill materials, such as geofoam or expanded polystyrene (EPS) blocks. Moreover, TDA is considered to be a durable material, which resists degradation in a severe working environment. TDA has been utilized as a drainage material under perforated leachate collection pipes (Rowe and McIsaac 2005). Shredded tire degradation resistance was tested by Chu (1998), who exposed shredded tires to varying climatic conditions for 18 months. The study showed that there was no particle degradation in the time frame and climatic conditions tested. Ab-Malek and Stevensson (1986) studied the effect of salt water on tire deterioration over a longer period. No serious deterioration was encountered in tires dumped in 24 m of salt water for 42 years; moreover, the pH value and amount of dissolved oxygen in the surrounding water were within acceptable ranges. Similar conclusions were drawn by Leclerq et al. (1990), who emphasized that buried civil engineering applications provide a safe environment for TDA in terms of degradation. Humphrey and Swett (2006) and Hennebert et al. (2014) also studied the effect of tire shreds on underground water and recommended some procedures to prevent harm to the water quality. In conclusion, except for corrosion that may affect the protruding steel, shredded tires have high durability, and

environmental concerns should no longer prevent TDA from being used in civil engineering applications.

On the other hand, Edil et al. (2005) showed that the permeability of TDA is ten times that of gravel when these materials are used in drainage applications. For instance, TDA has been used as a drainage layer for highways (Lawrence et al. 1999). Moreover, TDA is considered to be a good thermal insulator and is eight times more effective than regular soil in this regard (Eaton et al. 1994; Benson et al. 1996). Rashwan and Charette (2015) performed a full-scale study to investigate the feasibility of using TDA to replace natural materials for residential home basement slabs and walls, to enhance the heat insulation of the building and to decrease water retention around the walls. In addition, Rezaei et al. (2012) utilized TDA as an intermediate insulator layer beneath heat pump pipes.

Since the 1990s, the use of TDA as a light backfill material in embankment projects has been examined by many researchers (Bosscher et al. 1992; Hoppe 1998; Humphrey et al. 2000; Salgado et al. 2003; Yoon et al. 2006; Humphrey and Blumenthal 2010; Meles et al. 2014; Mills et al. 2015). Furthermore, the use of TDA as a backfill material for conventional retaining walls, mechanically stabilized earth (MSE) retaining walls and abutment projects has been investigated (Tweedie et al. 1998; Humphrey, 2008; Xiao et al. 2012). Moreover, TDA exhibits outstanding performance when used as a damping material for dynamic loads below rail lines and retaining walls subject to dynamic and/or earthquake loads (Wolfe et al. 2004; Xiao et al. 2012; Ahn and Cheng. 2014;).

TDA has been used in trench fill projects above buried pipes, culverts, and cut and cover tunnels to enhance the arching mechanism. Since TDA has high deformability, it can be advantageous for inducing a larger differential settlement between the soil prism above the

pipe and the adjacent soil. Consequently, a positive arching effect is achieved that reduces earth pressures. Meguid and Youssef (2018) performed an experiment to investigate the effectiveness of using a layer of TDA material above a 150-mm PVC pipe to decrease pipe stresses. The experimental program included small-scale laboratory tests (measuring 1.4 m × 1.0 m × 0.45 m) subjected to uniform upper stresses to simulate embankment loads. The study showed that using TDA above buried pipes under embankment loads decreased pipe crown stresses by 30%. Ni et al. (2018) developed finite element (FE) modelling to explore the usefulness a compressible layer above rigid buried pipes beneath high embankments. In addition, the study included a comparison between pipe behaviour with TDA and with expanded polystyrene (EPS) foam. The study concluded that TDA is as useful as any conventional compressible material and has the advantage of being inexpensive and abundantly available. Rodríguez et al. (2018) used a 2.0 m layer of TDA as a stress reduction layer above the crown of a 13 m diameter cut and cover concrete rail tunnel in northwestern Spain. A granular backfill layer 8 m thick was then placed above the TDA layer, up to the proposed level. During the tunnel construction, earth pressure cells above the tunnel lining were installed to measure the contact pressure. Settlement plates were installed above and below the TDA layer to monitor the TDA deformation during construction and the serviceability. In addition, thermistors were placed in the TDA layer to monitor the change in TDA temperature over time. Finally, five surveying targets were mounted on the inner surface of the tunnel, to measure tunnel deformation during the placement of backfill layers and the application of external loading. The research included a numerical study that used the commercial code FLAC3D to simulate the case study, to validate the results of the proposed numerical models. A parametric study was then

conducted to investigate changing TDA configurations above the tunnel. The study found that using TDA above a cut and cover tunnel significantly reduced the stress in the tunnel liners.

Researchers have conducted various laboratory experiments (for instance, using a direct shear box, triaxial testing, and odometers) to identify geotechnical properties (e.g., shear strength parameters, compressibility, etc.) of TDA and TDA mixtures with different soils. Many studies have been carried out to estimate the compressibility and modulus of elasticity of TDA by using odometer tests (e.g., Humphrey et al. 1992; Manion and Humphrey 1992; Edil and Bosscher 1992; Newcomb and Drescher 1994; Nickels and Humphrey 1997; Shalaby and Khan 2002; Moo-Young 2003; Meles et al. 2014; Mills et al. 2015). In these studies, the average compressibility ranged from 30% to 50%, depending upon the TDA particle size and the unit weight value achieved during the compaction. In addition, Wartman et al. (2007) carried out long-term, one-dimensional compression tests to measure the secondary compression index of TDA. The average secondary compression index was found to be 0.0065. Moreover, the study indicated that the secondary consolidation depends on the layer height, not on the applied loads or the particle size. Moreover, Ahn et al. (2014) reported field measurements of the TDA secondary compression index (i.e., creep), calculated from several embankment projects in the USA and Canada. They found that most of the settlement occurred during or shortly after construction, with a TDA secondary compression index ranging from 0.004 to 0.0047. These values are very comparable to those of stiff clay.

Many studies have been conducted by using large-scale direct shear tests and large triaxial tests to determine the shear strength parameters of TDA (Imtiaz Ahmed 1993; Cetin et al.

2006; Xiao et al. 2012; Reddy et al. 2015; El Naggar et al. 2016; Iranikhah 2018). As part of an ongoing research project at Dalhousie University to determine the mechanical properties of TDA materials and TDA mixtures, a comprehensive large-scale triaxial test (the triaxial cell has 6 inch diameter and 12 inch height) program was carried out by Ashari et al. (2017) and Ashari Ghomi (2018) to identify the failure envelope of the TDA material used in the study. The shear strength parameters obtained were the cohesion (c') and angle of internal friction (φ'). The results are confirmed by many reports in the literature. For example, Humphrey and Sandford (1993) used a large-scale direct shear box and found that type A TDA with particles measuring 13 to 76 mm had (φ') ranging from 19° to 25° and (c') ranging from 7.7 kPa to 11.5 kPa. Imtiaz Ahmed (1993) also used a large-scale triaxial test for TDA samples with a maximum size of 25.4 mm and found that the material had (φ') ranging from 27° to 34° and (c') ranging from 15.9 kPa to 20.3 kPa.

To study the dynamic performance of TDA as a backfill material for retaining walls, Ahn and Cheng (2014) performed a full-scale shake table test on a retaining wall with TDA backfill and compared the results with those of conventional backfill. They reported that TDA exerted less dynamic pressure on the wall in comparison to conventional soil, while resulting in greater displacement than was the case with conventional soil. In addition, Moussa and El Naggar (2019) conducted a series of large-scale cyclic triaxial tests to determine the dynamic properties of type A TDA (i.e., the damping ratio, and shear modulus reduction curves under different confining pressures). The TDA exhibited outstanding behaviour as a dampening material, with an approximately constant damping ratio ranging from 14% to 24%.

1.3 THESIS CONTRIBUTIONS AND OBJECTIVES

The primary objective of this research is to use lightweight tire-derived aggregate (TDA) backfill materials to improve the static and seismic performance of buried pipes and culverts. Previous studies (e.g., Ni et al. 2018; Meguid and Youssef 2018) used small-scale tests and numerical modelling to examine the use of TDA to create a positive arching mechanism over buried pipes under embankment loads (a technique referred to as induced trench installation). In the present research project, two full-scale tests were performed to investigate the feasibility of protecting pre-existing pipes located beneath shallow foundations by using TDA as an engineered stress reduction fill above the pipes and underneath a concrete footing. In addition, the study developed three-dimensional models of the tests by using the finite element (FE) code PLAXIS 3D to examine the effect of changing various key parameters (i.e., the thickness of the TDA layer, the shape and configuration of the TDA cross-section, and the pipe stiffness) on the system performance. Figure 1-2 presents a schematic drawing of the study conducted.

Three full-scale tests were then carried out to examine the behaviour of rigid footings resting on a surface of conventional backfill materials overlying a TDA layer with different thicknesses. The tests were followed by rigorous finite element analyses to examine the failure mechanism of shallow foundations over the TDA backfill material, and to study the effect of critical parameters on the footing performance. Subsequently, based on the calibrated finite element analysis, regression analyses were used to develop design equations to estimate the ultimate bearing capacity of shallow foundations built over a TDA layer, taking into account the granular layer thickness, TDA layer thickness, footing width, footing shape, footing depth, and allowable settlement.

Four full-scale tests were performed to investigate the use of a TDA backfill envelope around corrugated steel culverts (600 mm in diameter), to enhance the culvert performance under traffic loading. Figure 1-3 presents a schematic drawing of the configurations tested. Three-dimensional finite element modelling was then developed for the different configurations tested to investigate crucial parameters affecting the culvert performance.

Although TDA exhibits an outstanding performance in enhancing the arching mechanism over buried pipes, the corresponding settlement of the loaded surface increases significantly when the TDA is located at a shallow depth (located near to the surface). Therefore, this research project investigated the use of reinforced granular backfill over the TDA layer, by conducting three full-scale tests with a geocell layer in the upper part of the granular material above the TDA layer. Figure 1-4 presents a schematic drawing of the configurations tested. These tests utilized the same layout, loading conditions, and construction sequence as the previous set of tests (which used a TDA backfill envelope around a corrugated steel culvert), in order to illustrate the effectiveness of the geocell in reducing surface settlement and enhancing the arching mechanism.

The final part of this research focuses on evaluating the seismic design for open bottom large-span metal arch culverts in the Canadian Highway Bridge Design Code (CHBDC) and on developing an innovative system that uses TDA to mitigate seismic hazards in regions with high seismicity. First the static behaviour of a long-span metal culvert described in a well-documented field case study was verified. Full dynamic analyses were then performed with the aid of seismic records applicable to different cities across Canada, representing different levels of seismicity. The finite element analysis results were subsequently compared with the simplified seismic provisions of the CHBDC to evaluate

the seismic design of the code. The investigation was then extended by including a detailed parametric study to examine the effect of site subsurface conditions, foundation settings, culvert spans and cross-sections, and culvert configurations on metal culvert performance under earthquake loading conditions. Then an innovative solution which uses a TDA layer around a long-span metal arch culvert was developed to mitigate earthquake loads. Figure 1-5 presents a schematic drawing of the proposed solution.

1.4 THESIS OUTLINE

This thesis is presented in the "paper format" style. The chapters of the thesis present separate but related studies, each with its own introduction, methods, results, discussion, conclusions, and references. Tables and figures are provided at the end of each chapter. Chapters 2 and 7 have already been published, and Chapters 3, 4, 5 and 6 have been submitted to international peer-reviewed journals and are currently under review. Following a general introduction in Chapter 1, six original manuscripts are presented as Chapters 2 to 7. Finally, the overall findings of the research are summarized in Chapter 8.

The layout of the thesis chapters is as follows:

- Chapter 1 presents a general introduction and background overview.
- Chapter 2 discusses the merits of using TDA as an engineered stress reduction fill over pre-existing buried pipes. In Chapter 2, the results of two full-scale tests are presented and discussed, together with a comprehensive parametric study to investigate the feasibility of using TDA to protect pre-existing pipes. The work presented in this chapter is published as a journal paper entitled "Using TDA as an engineered stress

reduction fill over pre-existing buried pipes" in the ASCE Journal of Pipelines Systems Engineering and Practice.

- Chapter 3 presents the findings of three other full-scale field tests, conducted to explore the feasibility of using TDA beneath shallow foundations. In this chapter, the findings of a parametric study concerning the use of TDA beneath shallow foundations are also reported and discussed. The work presented in Chapter 3 is currently under the second round of revision and is expected to appear as a journal paper entitled "Using TDA underneath shallow foundations: Field tests and numerical modelling" in the ICE journal Géotechnique.
- Chapter 4 presents research aimed at developing design rules and procedures for shallow foundations built on TDA backfill. This paper is currently under review at the International Journal of Geotechnical Engineering.
- Chapter 5 presents the results of experimental work conducted to study an innovative application of TDA around corrugated steel pipe (CSP) culverts. The findings of a three-dimensional finite element model of the problem under consideration are also reported and discussed. The research presented in this chapter is currently under review at the ASCE Journal of Pipelines Systems Engineering and Practice.
- Chapter 6 presents a continuation of the work described in Chapter 5. In Chapter 6, a coupled TDA geocell stress bridging system for metal pipes is proposed to mitigate some of the serviceability issues discussed in the previous chapter. The research presented in Chapter 6 is currently under review at the ASCE Journal of Geotechnical and Geoenvironmental Engineering.

- Chapter 7 presents comprehensive research work conducted to evaluate the seismic provisions of the Canadian Highway Bridge Design Code (CHBDC). In this chapter, full dynamic analyses of arch culverts are provided, and the results obtained are compared with those from the seismic provisions of the CHBDC. Part of the work presented in this chapter is published as a journal paper entitled "Seismic design of metal arch culverts: Design codes vs. full dynamic analysis" in the Journal of Earthquake Engineering. In addition, a seismic mitigation scheme utilizing TDA around and/or under arch culverts is presented and discussed.
- Finally, Chapter 8 presents a general summary of the research described in this thesis, together with the conclusions drawn and recommendations for future work.

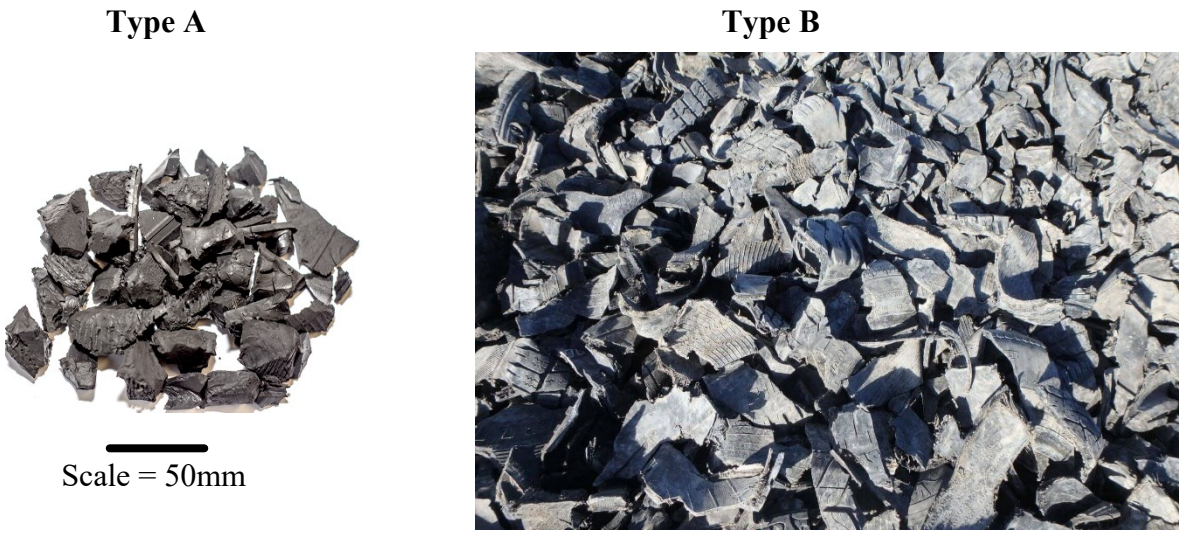

Figure 1-1 TDA types A and B

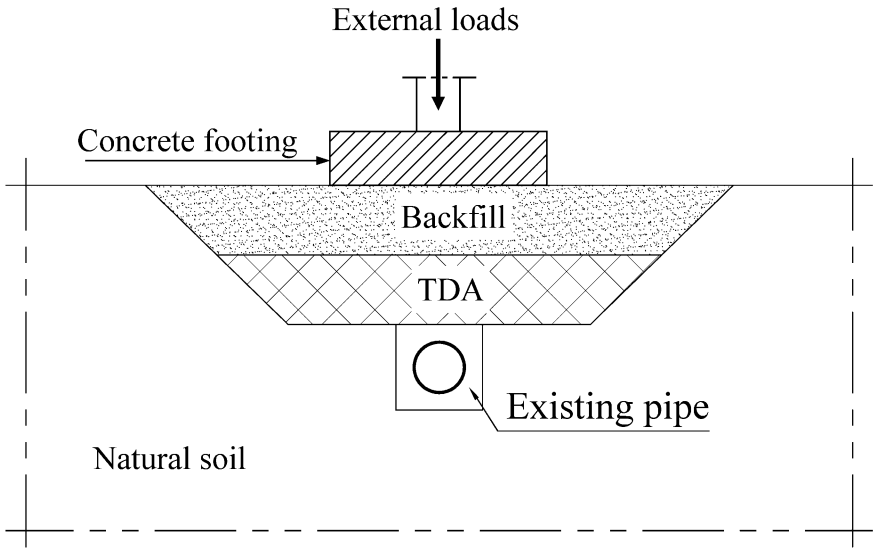

Figure 1-2 Schematic drawing of test setup that uses TDA above pre-existing pipes

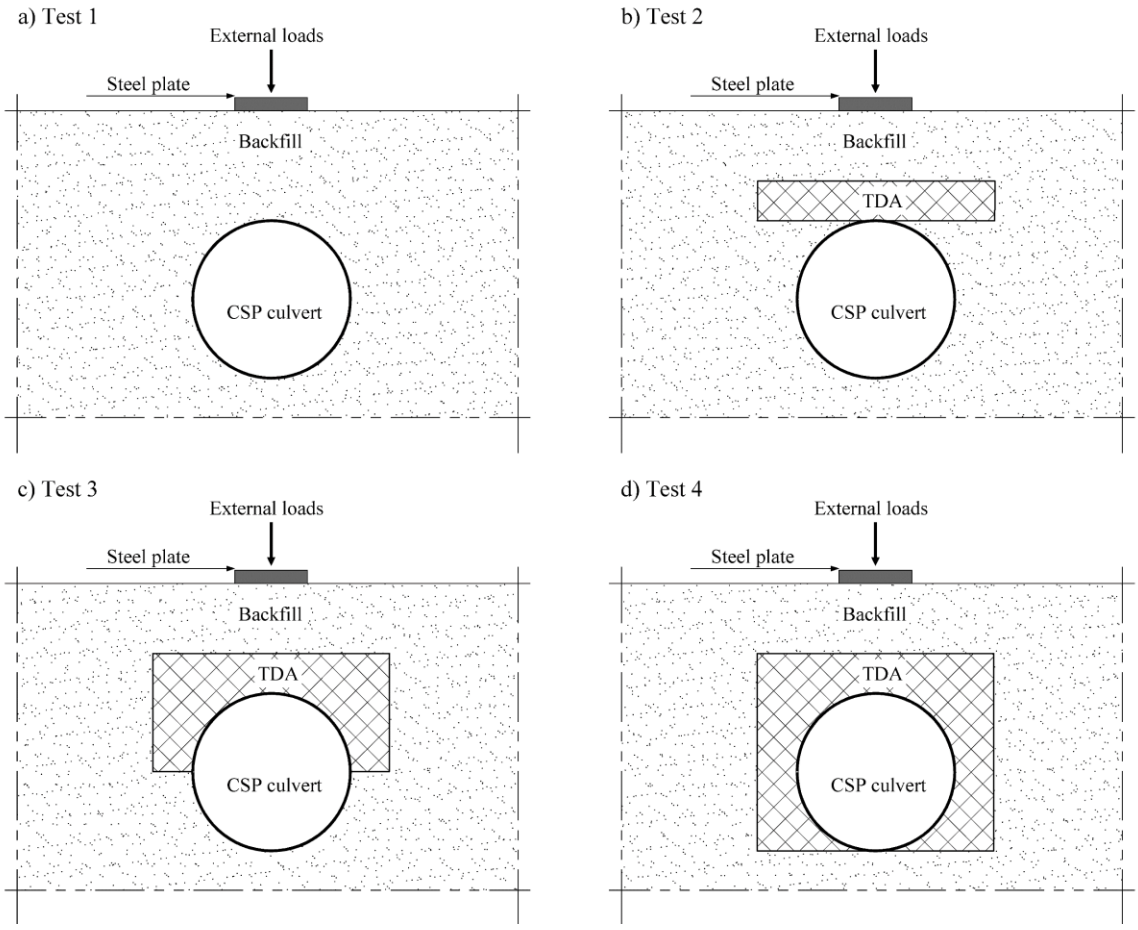

Figure 1-3 Schematic drawings of test setup that uses a TDA backfill envelope around CSP culverts

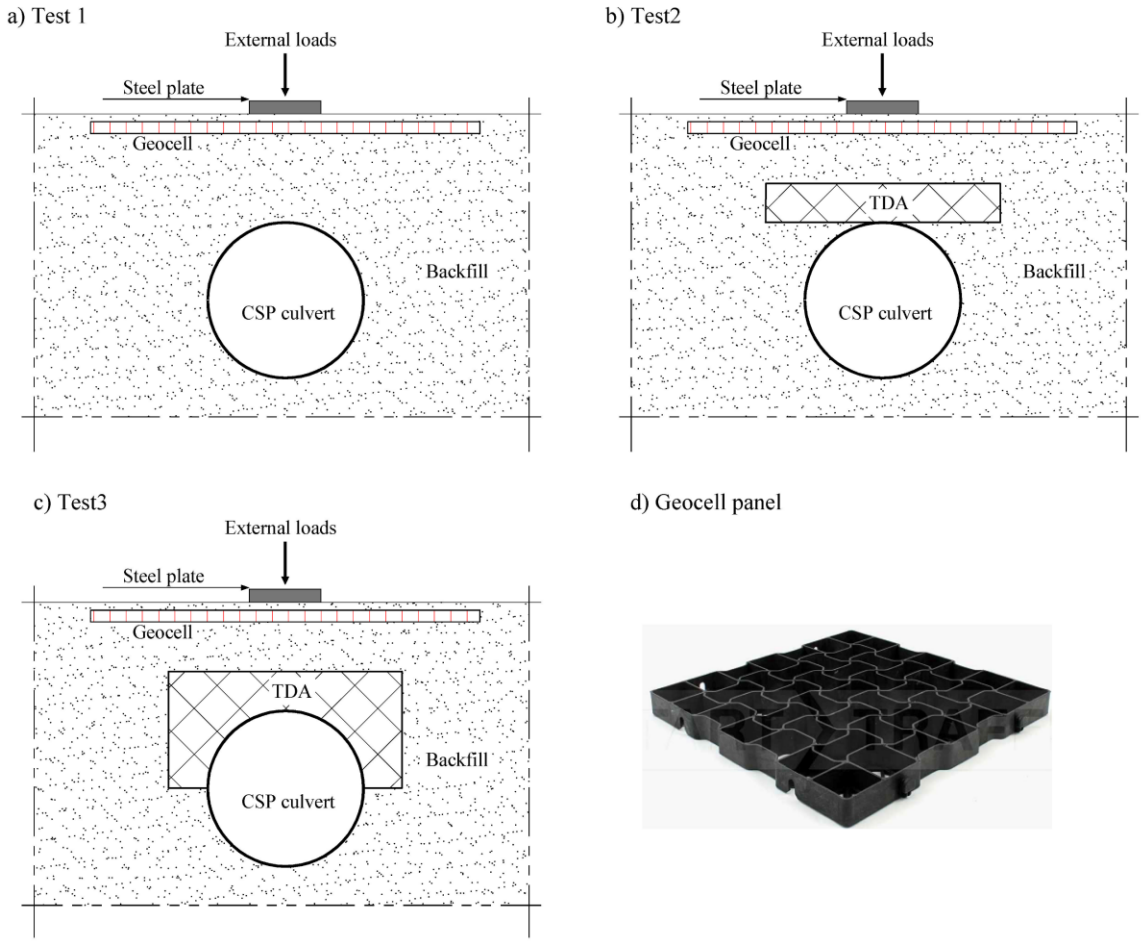

Figure 1-4 Schematic drawings of testing program that uses a coupled TDA geocell stress bridging system for metal pipes

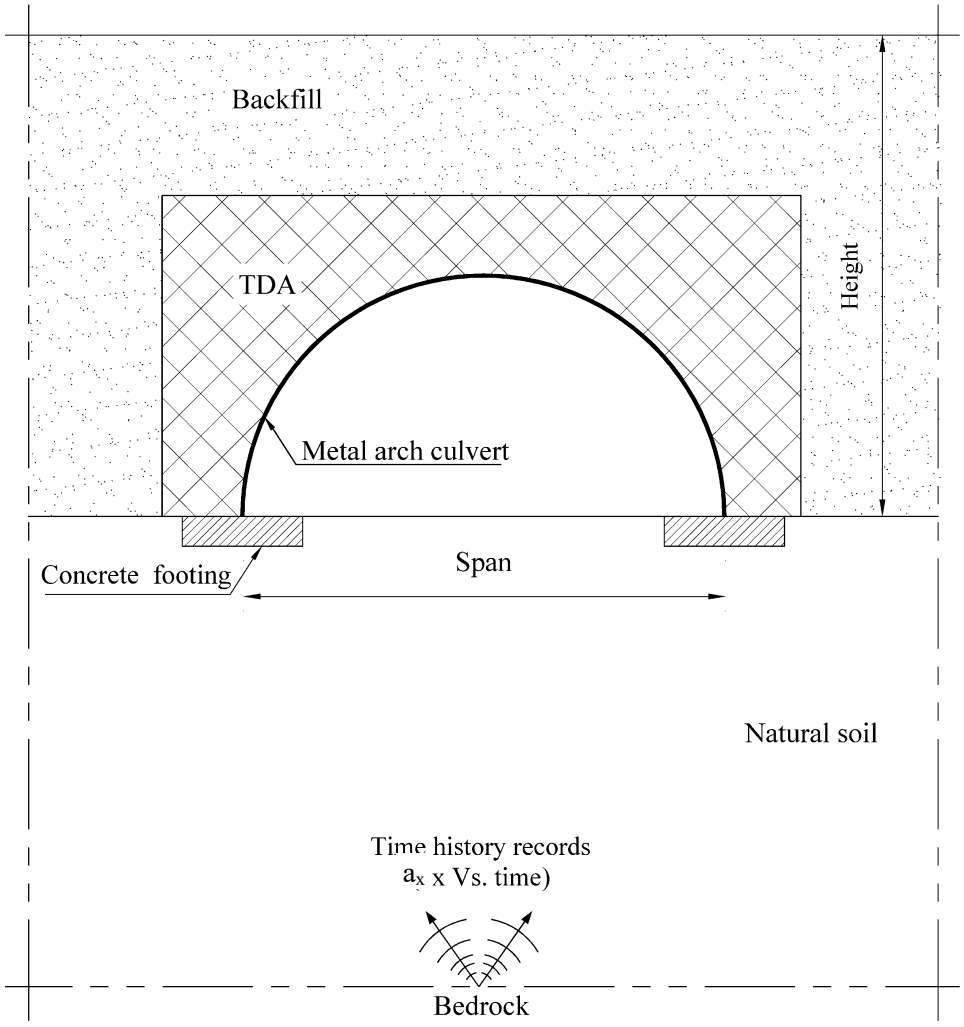

Figure 1-5 Schematic drawing of proposed solution which uses TDA as a damper material around arch culverts

1.5 REFERENCES

Ab-Malek K and Stevenson A (1986) The effect of 42-year immersion in seawater on natural rubber. Journal of materials science, 21(1):147-54.

Ahn I-S and Cheng L (2014) Tire derived aggregate for retaining wall backfill under earthquake loading. Construction and Building Materials **57**: 105–116, https://doi.org/10.1016/ j. conbuildmat.2014.01.091.

Ahmed Imtiaz (1993) Laboratory Study on Properties of Rubber-Soils.

Ahmed M, Tran V, Meguid MA (2015) On the role of geogrid reinforcement in reducing earth pressures on buried pipes. Soils Found, 55(3):588–99.

Ali Iranikhah (2018) Experimental Investigation on the Shear Strength Parameters and Deformability Behavior of Various Soil Types Mixed with Tire-Derived Aggregate. Master's thesis. Dalhousie University.

ASTM (2012) D 6270-12: Standard practice for use of scrap tires in civil engineering applications. ASTM International, West Conshohocken, PA, USA.

Ashari M and El Naggar H (2017) Evaluation of the physical properties of TDA-sand mixtures. In GeoOttawa, the 70th Canadian Geotechnical Conference Ottawa. Canadian Geotechnical Society.

Ashari Ghomi M (2018) Large-scale triaxial testing of sustainable TDA backfilling alternatives. Master's thesis. Dalhousie University.

Al-Naddaf M, Han J, Xu C, Rahmaninezhad SM (2019) Effect of geofoam on vertical stress distribution on buried structures subjected to static and cyclic footing loads. Journal of Pipeline Systems Engineering and Practice, 10(1):04018027.

Bali Reddy S, Pradeep Kumar D and Murali Krishna A (2015) Evaluation of the Optimum Mixing Ratio of a Sand-Tire Chips Mixture for Geoengineering Applications. Journal of Materials in Civil Engineering, 28(2), 6015007. https://doi.org/10.1061/(ASCE)MT.1943-5533.0001335

Benson CH, Olson MA and Bergstrom WR (1996) Temperatures of insulated landfill liner. Transportation Research Record **1534(1)**: 24–31, https://doi.org/10.3141/1534-05.

Bosscher PJ, Edil TB and Eldin NN (1992) Construction and performance of shredded waste-tire test embankment. Transportation Research Record **1345**: 44–52.

Cetin H, Fener M, and Gunaydin O (2006) Geotechnical properties of tire-cohesive clayey soil mixtures as a fill material. Engineering Geology, 88(1–2), 110–120. https://doi.org/10.1016/j.enggeo.2006.09.002

Chu, C-J (1998). A geotechnical investigation of the potential use of shredded scrap tires in soil stabilization. Ph.D. Dissertation, Kent State University, Kent, Ohio.

Eaton RA, Roberts RJ and Humphrey DN (1994) Gravel Road Test Sections Insulated with Scrap Tire Chips: Construction and First Year's Results. US Army Corps of Engineers, Cold Regions Research and Engineering Laboratory, Hanover, NH, USA. Special Report 94-21.

Edil TB, and Bosscher P J (1992) Development of engineering criteria for shredded or whole tires in highway applications. Report No. WI 14-92, Department of Civil and Environmental Engineering, University of Wisconsin, Madison, Wisconsin.

Edil TB (2005) A review of mechanical and chemical properties of shredded tires and soil mixtures. InRecycled Materials in Geotechnics (pp. 1-21).

El Naggar H, Turan A. and Valsangkar A. (2015) Earth pressure reduction system using geogrid-reinforced platform bridging for buried utilities. Journal of Geotechnical and Geoenvironmental Engineering, 141, No. 6, 04015024.

El Naggar H, Soleimani P, and Fakhroo A (2016) Strength and stiffness properties of green lightweight fill mixtures. Geotech. Geol. Eng. 34 (3): 867–876. https://doi.org/10.1007/s10706-016-0010-1.

GC (Geosyntec Consultants) (2008). Guidance Manual for Engineering Uses of Scrap Tires, Geosyntec Project No.: ME0012-11. Maryland Department of the Environmental Scrap Tire Programme, Columbia, MD, USA.

Gu Z, Song G, Liu W, Li P, Gao L, Li H, Hu X (2009) Preparation and properties of styrene butadiene rubber/natural rubber/organo-bentonite nanocomposites prepared from latex dispersions. Applied Clay Science, 46(3):241-4.

Hennebert P, Lambert S, Fouillen F and Charrasse B (2014) Assessing the environmental impact of shredded tires as embankment fill material. Canadian Geotechnical Journal, 51(5):469-78.

Hoppe EJ (1998) Field study of shredded-tire embankment. Transportation Research Record **1619(1)**: 47–54, https://doi.org/10.3141/1619-06.

Humphrey DN and Manion WP (1992) Properties of tire chips for lightweight fill. Proceeding: Grouting, Soil Improvement, and Geosynthetics, ASCE, New York, 1344–1355.

Humphrey DN, and Thomas Sandford (1993) Tire Chips as Lightweight Subgrade Fill and Retaining Wall Backfill, Symposium on Recovery and Effective Reuse of Discarded Materials and By- Products for Construction of Highway Facilities, no. 207: 20.

Humphrey DN, Whetten N, Weaver J, and Recker K (2000) Tire shreds as lightweight fill for construction on weak marine clay. Proceeding International Symposium on Coastal Geotechnical Engineering in Practice, Balkema, Rotterdam, The Netherlands, 611–616.

Humphrey DN, and Swett M (2006) Literature review of the water quality effects of tire derived aggregate and rubber modified asphalt pavement. Department of Civil and Environmental Engineering, University of Maine, Orono, ME, for U.S. Environmental Protection Agency Resource Conservation Challenge, November 29, 2006.

Humphrey DN (2008) Tire derived aggregate as lightweight fill for embankments and retaining walls. In Scrap Tire Derived Geomaterials — Opportunities and Challenges (Hazarika H and Yasuhara K (eds)). Taylor & Francis Group, London, UK, pp. 59–81.

Humphrey D and Blumenthal M (2010) The use of tire-derived aggregate in road construction applications. In Green Streets and Highways 2010: An Interactive Conference on the State of the Art and How to Achieve Sustainable Outcomes. ASCE, Reston, VA, USA, pp. 299–313.

Lawrence B, Humphrey D and Chen L-H (1999) Field trial of tire shreds as insulation for paved roads. In Tenth International Conference on Cold Regions Engineering: Putting Research into Practice. ASCE, Reston, VA, USA, pp. 428–439.

Leclerq B, Schaeffner M, Delmas P, Blivet JC and Matichard Y (1990) Durability of geotextiles: Pragmatic approach used in France. Geotextiles, Geomembranes and Related Products, Ed. Hoedt, D., Balkema, Rotterdam, 679-684.

Liedberg NSD (1997) Load reduction on a rigid pipe: pilot study of a soft cushion installation. Transp. Res. Rec. 1594, 217e223.

Jiang F, Gu A (2008) Breakage mitigation method for culverts under high embankments using Eps geofoam. In: Liu, H., Deng, A., Chu, J. (Eds.), Geotechnical Engineering for Disaster Mitigation and Rehabilitation. Springer, Berlin, Heidelberg.

Manion WP and Humphrey DN (1992) Use of tire chips as light weight and conventional embankment fill, Phase I-laboratory. Technical paper 91-1, Technical Services Division, Maine department of transportation, Maine.

Meguid MA, Youssef TA (2018) Experimental investigation of the earth pressure distribution on buried pipes backfilled with tire-derived aggregate. Transportation Geotechnics, 14:117-25.

Mills, B., H. El Naggar, and A. J. Valsangkar. 2015. “North American overview and Canadian perspective on the use of tire derived aggregate in highway embankment construction.” Chap. 22 in Vol. 2 of Ground improvement case histories, edited by Indraratna and Chu. New York: Elsevier.

Meles D, Bayat A, Hussien Shafiee M, Nassiri S, Gul M (2014) Investigation of tire derived aggregate as a fill material for highway embankment. International Journal of Geotechnical Engineering, 8(2):182-90.

McAffee RP, Valsangkar AJ, (2008) Field performance, centrifuge testing, and numerical modelling of an induced trench installation. Can. Geotechnical J. 45 (1), 85e101.

Moo-Young, Sellasie K, Zeroka D, and Sabnis G (2003) Physical and chemical properties of recycled tire shreds for use in construction, Journal of Environmental Engineering, 129(10), 921-929.

Moussa A and El Naggar H (2019) Dynamic properties of tire derived aggregates. In GeoSt.John's, the 72th Canadian Geotechnical Conference St John’s, Canada. Canadian Geotechnical Society.

Ni P, Qin X, Yi Y (2018) Numerical study of earth pressures on rigid pipes with tire-derived aggregate inclusions. Geosynthetics International, 25(5): 494-506.

Nickels WL (1995) The effect of tire shreds as subgrade fill on paved roads. M.S. Thesis, Department of Civil Engineering, University of Maine, Orono, Maine, 215.

Newcomb DE and Drescher A (1994) Engineering properties of shredded tires in lightweight fill applications. Transportation Research Record 1437, National Research Council, Transportation Research Board, Washington, D.C., 1-7.

Oshati OS, Valsangkar AJ, Schriver AB (2012) Earth pressures exerted on an induced trench cast-in-place double-cell rectangular box culvert. Canadian Geotechnical Journal, 49(11):1267–84.

Parker BA, McAffee RP, Valsangkar AJ (2008) Field performance and analysis of 3-m-diameter induced trench culvert under a 19.4-m soil cover. Transp Res Rec 2045(08):68–76.

Pierre DKS (2013) Canadian waste tire practices and their potential in sustainable construction. Dalhousie Journal of Interdisciplinary Management **9(1)**.

Rashwan S and Charette P (2015) Demonstration of the Viability of Using Tire Derived Aggregate (TDA) to Replace Natural Material (NM) in Residential Home Basement Construction. Summary report of the demonstration project at 263 Waverly Street, Winnipeg, Manitoba, Canada.

Rezaei A, Kolahdouz EM, Dargush, GF and Weber AS (2012) Ground source heat pump pipe performance with tire derived aggregate. International Journal of Heat and Mass Transfer, 55, No. 11, 2844–2853.

Rowe RK and McIsaac R (2005) Clogging of tire shreds and gravel permeated with landfill leachate. Journal of Geotechnical and Geoenvironmental Engineering, 131(6):682-93.

Rodríguez LM, Arroyo M, Cano MM (2018) Use of tire-derived aggregate in tunnel cut-and-cover. Canadian Geotechnical Journal, 55(7):968-78.

Rubber Manufacturers Association (2017) US scrap tire management summary 2005–2009. Rubber Manufacturers Association, Washington, DC, USA.

Salgado R, Yoon S and Siddiki NZ (2003) Construction of Tire Shreds Test Embankment. FHWA/IN/JTRP-2002/35, Joint Transportation Research Program, Indiana Department of Transportation and Purdue University, West Lafayette, IN, USA https://doi.org/10.1520/JAI103711.

Shalaby A and Khan RA (2002) Temperature monitoring and compressibility measurement of a tire shred embankment: Winnipeg, Manitoba, Canada. Transportation Research Record 1808, National Research Council, Transportation Research Board, Washington, D.C., 67-75.

Sladen, J A. and Oswell, J M. (1988). The induced trench method - a critical review and case history. Canadian Geotechnical Journal, 25(3), pp.541-549.

Sparkes J, El Naggar H and Valsangkar A (2019) Compressibility and shear strength properties of tire-derived aggregate mixed with lightweight aggregate. Journal of Pipeline Systems Engineering and Practice **10(1)**, https://doi.org/10.1061/(ASCE)PS.1949-1204.0000354.

Tweedie JJ, Humphrey DN and Sandford TC (1998) Full-scale field trials of tire shreds as lightweight retaining wall backfill under at-rest conditions. Transportation Research Record **1619**: 64–71, https://doi.org/10.3141/1619-08.

Turan A, El Naggar MH, and Dundas D (2013) Investigation of induced trench method using a full-scale test embankment. Geotech. Geol. Eng. 31 (2): 557–568. https://doi.org/10.1007/s10706-012-9608-0.

Wartman J, Natale M and Strenk P (2007) Immediate and time-dependent compression of tire derived aggregate. Journal of geotechnical and geoenvironmental engineering, 133(3), pp.245-256.

Wolfe SL, Humphrey DN and Wetzel EA (2004) Development of tire shred underlayment to reduce groundborne vibration from LRT track. In GeoTrans 2004, Los Angeles, CA. ASCE, Reston, VA, USA, pp. 750–759.

Xiao M, Bowen J, Graham M and Larralde J (2012) Comparison of seismic responses of geosynthetically reinforced walls with tire-derived aggregates and granular backfills. Journal of Materials in Civil Engineering **24(11)**: 1368–1377, https://doi.org/10.1061/(ASCE)MT.1943- 5533.0000514.

Yoon S, Prezzi M, Siddiki NZ and Kim B (2006) Construction of a test embankment using a sand-tire shred mixture as fill material. Waste Management **26(9)**: 1033–1044, https://doi.org/10.1016/j.wasman.2005.10.009.

CHAPTER 2 USING TDA AS AN ENGINEERED STRESS REDUCTION FILL OVER PRE-EXISTING BURIED PIPES

Ahmed Mahgoub and Hany El Naggar

Published in Journal of Pipeline Systems Engineering and Practice, Volume 10, 1

https://doi.org/10.1061/(ASCE)PS.1949-1204.0000362

2.1 INTRODUCTION

Buried utilities and pipelines, commonly known as lifelines, are usually exposed to large external stresses which may be unavoidable in certain circumstances. For example, foundations of new structures, particularly in urban and congested centres, often interfere with pre-existing lifelines imposing significant additional loads on them. In many instances, these loads would be unacceptably high causing overstressing and/or excessive deformations resulting in consequent damage and interruption of services. This may lead to a catastrophic social and economic impacts on the affected areas. Hence, dealing with this challenge is one of the main concerns that need to be addressed early in the design.

There are several available alternatives that can be used to mitigate this problem. These alternatives include: a) relocation of utilities, which is the most expensive option, b) using induced trench construction (this option will be discussed in detail later), and finally c) using lightweight fill material to reduce the external load.

Tire-derived aggregate (TDA) is an engineered sustainable fill material produced by shredding scrap tires into sizes ranging from 12 mm to 305 mm. In the literature, TDA is regularly referred to as tire chips or tire shreds according to the size. ASTM (2012) specifies two size ranges and gradations of TDA. Type A; with particle size ranging from

12 mm to 70 mm; which is suitable for backfilling around buried utilities, drainage, vibration damping, and insulation applications. Type B; with particle size ranging from 70 mm to 305 mm. Type B is suitable for use as backfilling material behind retaining walls and in highway embankments among several other useful civil engineering applications (Bosscher et al., 1992; Upton and Machau, 1993; Engstrom and Lamb, 1994; Dickson et al., 2000; and Mills and McGinn 2010).

Azevedo et al. (2012) estimated that each seven people alive produces one scrap tire per year on average. This average is not evenly scattered; advanced countries have a higher rate of scrap tires per capita compared to developing countries. In North America, approximately 250 million tires are discarded each year in the United States and 30 million in Canada (El Naggar et al. 2016). Disposal issues along with a continuing increase in tire production have increased tire stockpiles. Finding sustainable ways to dispose of these tires continues to be a severe problem throughout the world not only in North America. Consequently, shredding tires to TDA and using it in civil engineering applications provides a sustainable solution for these environmental problems. The economic and ecological benefits of using TDA as an engineered fill material are evident as large volumes of scrap tires are diverted from landfills and stockpiles and, at the same time, equal volumes of non-renewable aggregates are saved.

TDA has outstanding geotechnical properties, preserves its structural integrity, and weighs approximately 60% less than conventional geomaterials. TDA has been successfully used in several jurisdictions in North America and around the world since the early 1990s (Humphrey and Eaton, 1995; Dickson et al., 2001; Shalaby and Ahmed-Khan, 2002; Humphrey and Blumenthal, 2010; and Meles et al., 2013).

The lightweight characteristic of TDA coupled with its structural integrity makes it a suitable material to be used as an engineered backfill over existing pipes and underneath shallow foundations. In this paper, an innovative solution is introduced in which a layer of TDA is placed over a pre-existing pipe in a trench with a specific configuration to induce a special stress arching mechanism (i.e., stress bridging) that results in reduced, transferred pressures to the pipe.

Installation configuration and construction sequence have a critical effect on the soil arching and consequently the pipes' behaviour. Soil arching involves the transmission of the shear stress between the deforming soil mass and the adjoining buried pipe. Many researchers explained the soil arching phenomenon and the accompanying stress distribution mechanisms in different geotechnical engineering applications (e.g., Terzaghi, 1936 and 1943; Schlick, 1932; Wang and Yen, 1974; Luscher and Hoeg, 1964; Costa et al., 2009; and Rui et al., 2016). If a pipe is installed in a trench (ditch) configuration that is excavated from the original ground surface and then backfilled with a compressible material (e.g. TDA), positive soil arching tends to develop in the backfill surrounding the pipe. Consequently, the average vertical stress acting over the pipe due to the backfill will be less than the overburden stress caused by the own weight of the backfill ($\gamma_{fill} \times h_{fill}$). This technique is known as the induced trench method. On the other hand, when a rigid pipe is installed on the ground surface, and a wide backfilling layer is built around and above it, the pipe tends to act as a stiffer zone within the fill. Consequently, the average vertical stress acting on it tends to be greater than the overburden stress caused by the own weight of the backfill (i.e., negative soil arching occurs). These two conditions are illustrated schematically in Figure 2-1. Over the last century, many studies have been conducted to

clarify and investigate the effectiveness of the induced trench installation technique. The focus of these studies was set mainly on understanding the involved soil-structure interaction (e.g. Anderson, 1913; Marston, 1930; Spangler, 1950 a&b; Spangler and Handy,1973; McAffee and Valsangkar, 2008; McGuigan and Valsangkar, 2010 & 2011; and Turan et al., 2013).

This paper presents the results of two full-scale field tests which were conducted to evaluate the effectiveness of using a layer of TDA above existing metal pipes to enhance the stress arching mechanism. Furthermore, 3D Finite Element models (FEM) of the tests were developed to study the interaction mechanism of the considered problem, where the developed models were validated against the field tests results. Also, an extensive parametric study was carried out to examine the effect of several parameters on the performance of the investigated system.

2.2 METHODOLOGY

The following steps summarize the procedure that was followed in this study to investigate the benefits of using TDA as an engineered stress reduction fill over pre-existing buried pipes:

- Specifics of the conducted field tests were described including their layout, instrumentation details and construction procedures along with the collected measurements.
- Two 3D finite element models of the two testing setups were developed and calibrated against the results of the field tests.
- Then, a parametric study was conducted to examine the effect of the thickness of the

TDA layer, shape and configuration of the TDA cross-section and the pipe's stiffness (i.e., the pipe's flexibility) on the performance of the investigated system.

2.3 FIELD TEST OVERVIEW

Two full-scale field tests (Setup 1 and Setup 2) were conducted by the authors at a site in Antrim, NS, 65 km northeast of Halifax (44.92211 Longitude and -63.37710 Latitude). The purpose of these experiments was to evaluate the effectiveness of using a layer of TDA as a light backfilling material above metal pipes to enhance the stress arching mechanism (i.e., reducing the stresses over the buried pipes). The authors performed all the construction activities, the instrumentation installation and monitoring, and data collection. The first setup (Setup 1) involved a 1.0 m conventional compacted granular backfill (as a replacement soil) below a concrete footing and above a metal buried pipe; 200 mm in diameter and 6.3 mm thickness (see Figure 2-2a) which was used as the reference case. The second setup (Setup 2) was similar to the first one in geometry, layout and the construction procedures; the only difference was that the conventional backfill materials were replaced with a 0.5 m layer of granular fill overtop of a 0.5 m of TDA as shown in Figure 2-2b. The TDA used in this research was manufactured and shredded from passenger scrap tires and was classified as Type A per ASTM D6270-08. The field tests were constructed to measure the footing's settlement, the stresses above the buried pipe, and the changes in the pipe's internal stresses to assess the efficiency of each system.

2.3.1 Site Preparation and Characterizations

Prior to the construction of the two field tests, the site was levelled, and the topsoil was removed. Also, extensive site investigations were carried out to identify the soil properties of the site by drilling boreholes, performing standard penetration test (SPT) and extracting

samples by Shelby tubes for the lab tests (i.e. Atterberg limits, sieve analyses, shear box and triaxial tests). The in-situ soil was found to be 0.5 m of organic soil followed by a glacial till with sand and gravel. According to ASTM D2487, the till layer was classified as sandy lean clay with gravel. Additionally, shear box tests were conducted to deduct the drained shear strength parameters which resulted in a cohesion of 22 kPa and an angle of internal fiction of 20° for the till layer at the proposed foundation level. Moreover, the unconsolidated undrained triaxial tests showed that the C_u (undrained cohesion) for the till layer ranged from 100 to 140 kPa.

2.3.2 Backfill Materials Characterizations and the Concrete Footings

The TDA particles used in the tests was in the range of 13 mm to 63 mm with a unit weight of 7 kN/m^3. Intensive lab tests (i.e., sieve analysis, triaxial tests) were performed on the used TDA as a part of this project. Figure 2-3 shows the particle size distribution of the used TDA materials and Figure 2-4 shows the results of the triaxial testing (stress-strain curves) as described in Ashari and El Naggar (2017) and Ashari (2018). From the triaxial test results, the angle of internal friction was determined to be φ = 26.5° and the cohesion c' = 24 kPa.

Gravel backfill material was used for the full excavated depth in Setup 1 and the topping layer in Setup 2. Sieve analysis, Proctor test and triaxial tests were carried out to determine the soil classification, maximum dry density and the shear strength parameters. The gravel backfill material was classified as an A1 granular material with a maximum dry unit weight of 22.50 kN/m^3, the optimum water content was W_c= 7.5%, and the angle of internal friction

was $\varphi' = 44°$. Furthermore, clean fine sand was used to backfill the buried pipes as shown in Figure 2-2.

The square concrete footings had a width of 0.8 m and a thickness of 0.3 m with ultimate compressive strength (f_{cu}) of 60 MPa. The footings were cured after casting for 28 days before testing.

2.3.3 Instrumentation

Extensive instrumentation was used in each test to monitor the behaviour of the pipe, the transferred stresses throughout the backfill, and the footing's settlement during the test.

The strain gauges were mounted at the crown, springline and invert locations on the outer surface of the metal pipe of each setup in both circumferential and longitudinal directions (see Figure 2-2). These strain gauges were F series Foil strain gauges manufactured by Tokyo Sokki Kenkyujo company with operational temperature between $-196° \; to \; 150° \; C$ and grid resistance of 350 Ohms. The transferred pressure throughout the backfill was measured by pressure cells installed under the backfill and above the pipe at each test. The pressure cells used were 240-mm (9.5-in.) in diameter pressure transducers (LPTC09-S) manufactured by RST Instruments. Furthermore, four linear variable differential transformers (LVDT) manufactured by TE Connectivity were mounted on the top surface of the footing to measure the footing's settlement. These compact string pot LVDTs with voltage driver outputs provide a measurement with an accuracy of 0.25%. In addition, the loading on the footing was measured using a load cell as illustrated in Figure 2-2, while a hydraulic jack was used against a Komatsu dump truck, HM400, with a bucket filled with concrete blocks with a total weight exceeding 50 metric tons to apply a downward

concentrated load on the footing. Accordingly, the side concrete blocks in Figure 2-2 were placed to avoid any effect of the truck on the foundations during the loading (i.e., to transfer the load from the truck away from the testing trenches). All the data was acquired using a computerized data acquisition system. The in-situ density and moisture of the backfill materials were determined with a nuclear densitometer. Standard survey equipment was used to reach the proposed ground levels.

2.3.4 Test Procedure

As shown in Figure 2-2, two test pits were excavated to a depth of 1.0 m, then the pipes' trenches were dug with 0.3 m width and 0.3 m depth at the centre of each pit. Subsequently, a small layer of a clean sand bedding was placed before laying the pipes in the trenches and covering them with the same sand to eliminate any possible damages to the strain gauges. Two parallel piles of concrete blocks placed on top of each other on the opposite sides of the pits for the entire depth of the test pits. The concrete blocks were placed to support the weight of the truck's tires in a way that this load is transferred to the subsurface underneath and not to affect the layers immediately below the footings. Additionally, for each setup, a pressure cell was placed at the centre of the test pit overtop the pipe's trench to measure the stresses transferring to the pipe. After that, the pits were filled with the desired backfill materials in different layers, and each layer of the granular materials was compacted and tested to make sure it reached the desired compaction level (95% of the standard Proctor dry density). Even though in Setup 2, the proposed thickness of TDA was 500mm, an overbuild layer of 100 mm (20% of the total thickness) of TDA materials was added to compensate the settlement occurred after the placement of the cover of 500 mm of gravel-A1 materials. Thin polymeric membrane was used on top of the TDA layer to

segregate it from the gravel layer on top. The top surface of the test area was levelled, and the footing was placed on a predefined alignment such that the centre of the footing was directly positioned above the pressure transducer. After the footings were cured, the framework for the fixed beam as shown in Figure 2-2 was installed on top of them in a way such that if the footing was loaded and settled, the position of the framework remains stationary. Then from the framework, four LVDTs were attached to the four corners of the footings. In the centre of the footing, a metal plate was placed, and on top of that, a hydraulic jack was positioned. The Truck was positioned above the hydraulic jack in a way that the centre of the truck bucket (second axle of the truck) was aligned with the centre of the hydraulic jack as shown in Figure 2-5. A load cell was placed between the hydraulic jack and the truck. The load was applied incrementally every 20 kN with a hydraulic jack and maintained manually with a hand pump. The testing procedure was performed according to ASTM D 1196- 93 (ASTM, 1997), where the load increments were applied and maintained until the rate of the settlement was less than 0.03 mm/min over three consecutive minutes. The maximum load applied from the truck was 320 kN in Setup1 and 200 kN in Setup2. Where, Setup 1 was stopped once the truck was lifted due to the applied force by the hydraulic jack, and Setup 2 stopped when, an excessive settlement occurred, and strain gauges' readings were interrupted. The results of the field tests (i.e. pipe's strains, load cell readings, pressure transducers records and the footings' settlements) were then used to investigate the soil structure interaction (SSI) of the investigated systems and their effectiveness on the reduction of stresses received by the buried pipes. Unfortunately, during the construction and compaction, the two strain gauges in the pipe's invert in Setup 1 and the longitudinal strain gauge in the pipe's crown in Setup 2 were damaged. For each

setup, a 3D finite element model was prepared and verified against the collected tests' results. Figure 2-6 shows the punching shear failure that occurred in Setup 2. It can seen from the figure that the punching shear occurred along a semicircular perimeter approximately 150 mm away from the footing.

2.4 DEVELOPMENT OF THE FINITE ELEMENT MODELS

In order to investigate the stress reduction mechanism and the effectiveness of using the TDA materials as a platform bridging, finite-element analyses (FEAs) were carried out using the software package PLAXIS 3D-2017. The numerical analyses were conducted in two sets: The first set consisted of two finite element models which were used to verify the field tests results of Setup 1 and Setup 2 as the models were created to have the same geometry, layout, and construction procedures of the full-scale field tests. The 2nd set was developed to perform a parametric study to investigate the effect of changing several key parameters including the thickness of the TDA layer; shape and configuration of the TDA cross-section, and the pipe's flexibility on the performance of the proposed system. Figure 2-7 shows one of the developed numerical models used in the verification. The natural ground and the backfilling envelope were modelled using higher order 10-node triangular elements. The verification models comprised around 150,000 elements with an average element size of approximately 100 mm in the zone between the pipe and the concrete footing. The large number of small-sized elements assured high accuracy, especially at locations where nonlinear behaviour was anticipated.

2.4.1 Foundation Soil Layers and the Granular Backfill

An elastic-perfectly plastic soil constitutive model with Mohr-Coulomb failure criterion was used during the simulation for the native foundation soil, the granular Gravel-A1 layer, and the clean fine sand around the pipes due to the simplicity of the model and its suitability in such application. The strength parameters of the foundation soil were estimated from the site investigation conducted prior to the construction. Table 2.1 provides a summary of the soil parameters used in the numerical analysis.

2.4.2 TDA Material

TDA materials are lightweight nonlinear materials that are significantly affected by the level of applied confining stresses and strains. Consequently, the hyperbolic hardening soil model (Schanz et al. 1999) from the PLAXIS 3D library was used to model the stress-dependent variation of the stiffness of the TDA materials. The adopted hyperbolic hardening soil model is from the double-stiffness model's family, which is a refinement of the Duncan and Chang (1970) hyperbolic model. The hyperbolic hardening soil model used in this study supersedes the Duncan and Chang model because it uses the theory of plasticity rather than the theory of elasticity, accounts for the soils' dilatancy, and utilizes a yield cap. FE (finite element) TDA triaxial properties were modelled and calibrated to the TDA laboratory triaxial test results as per Ashari and El Naggar (2017) and Ashari (2018) in different confinement stresses to ensure that the hardening soil model exhibits the same stress-strain relationship as shown in Figure 2-4. The FE model verification used the laboratory triaxial sample's height and diameter (Figure 2-8). Figure 2-9 shows the comparison between the FE model and laboratory triaxial results. The figure showed that

good match was achieved using the hardening soil model and displayed its capability in simulating the TDA behaviour under different confining pressures.

2.4.3 Buried Pipes, Concrete Footings and Concrete Blocks

The metal pipes in the first stage of the FE analysis (the verification of the field tests) were modelled as volume elements using an elastic material model to measure the strain on the top surface of the pipes to be compared with the field test results. However, in the parametric study, the pipes were simulated using plate elements from the PLAXIS's library to help in estimating the pipes' straining actions directly from the analysis. In particular, the plate element of PLAXIS 3D allows for orthotropic elastic material behaviour and uses the axial and flexural rigidities. PLAXIS 3D treats the plate elements in the same manner as the conventional beam elements where the shear, bending and normal forces are considered in the element's formulation. Similarly, the concrete blocks were simulated using the elastic material model in drained conditions, while the concrete footings were modelled utilizing plate elements with the isotropic elastic material. Table 2.2 shows the used parameters for the steel and the concrete materials in the FE analysis. Furthermore, the friction behaviour at the pipes-soil interface and the concrete blocks-soil interface were modelled using the five-nodded interface elements from the PLAXIS's library, and the roughness of the interaction was modelled by utilizing a strength-reduction factor at the interface, $R_{inter} = 0.67$. As well as, horizontal interface elements were assigned between the TDA materials and the topsoil layer of Gravel-A1 materials with $R_{inter} = 0.30$ to simulate the placed smooth thin membrane as explained in the testing procedure above.

2.4.4 Boundary Conditions

A fully fixed boundary condition was assumed at the base of the models at a predefined depth below the pipe. In addition, as shown in Figure 2-7, one-quarter of the problem was modelled to benefit from the test setup's symmetry in the two horizontal directions, and therefore, the computational extent and number of elements were reduced. On the other hand, while, the lateral boundary conditions were assigned to be free in the vertical direction and fixed in the horizontal direction, only perpendicular lateral boundary conditions along the models' axes of symmetry were restrained. In addition, a sensitivity analysis was performed to check the effect of the model size, the lateral boundaries, and the mesh quality (the number of elements). Consequently, the model lateral boundaries were extended 5 times of the footing's width from each side and the FE model had 150, 000 elements.

2.4.5 Simulation of the Construction Process

The same staged construction sequence followed in the full-scale tests was simulated in the conducted 3D modelling as follows:

1. The initial in-situ stress state was installed using the K_o procedure in which the initial geostatic stresses were established assuming increasing vertical stress with depth ($\sigma_v = \gamma\, z$) and horizontal stresses based on $\sigma_h = K_o\, \sigma_v$. The groundwater table was assumed to be 0.5 m below the ground surface.
2. The excavation for the test pits and the pipes trenches to their specific depths were simulated by deactivating the soil elements inside the pits and the trenches.
3. The pipes were then placed in its locations and were covered by the clean sand in the trenches.

4. The backfill materials were placed, and the interface elements were activated between the concrete blocks and the backfill, and between the TDA material and the topsoil gravel.
5. The concrete footing was poured and constructed by activating the concrete plate.
6. External vertical loads on the footing were applied to represent the hydraulic jack loads.

Due to the large settlement and soil deformations in the verified model of Setup 2, the updating mesh option in PLAXIS was used to avoid any errors caused by the elements distortions.

2.4.6 Description of the Conducted Parametric Study

Figure 2-10 shows a brief description of the parametric study conducted to examine the behaviour of the pre-existing pipes which were overtopped by TDA materials utilized as a stress reduction media. An external load of 120 kPa was considered as a service load on the footing in all the models. This load represents 80% of the load that caused punching failure (see Figure 2-12) as will be discussed later. Four different configuration sets were used in the parametric study. Set 1 examines the effect of changing the TDA layer's thickness on the pipe's and footing's behaviour (Figure 2-10a). Set 2 studies the effects of the changes in the geometry of the TDA layer above the pipe by forming an induced trench in the TDA part with a lower trench side slope of 1H: 3V while the side slope of the upper part remained as 1H:1V. The variable (X) in this set represents the trench's lower width which was set to 0.5B, 1B, 1.5B and 2.5B, where B is the footing width (Figure 2-10b). Similarly, Set 3 studies the effect of the changes in the geometry of the TDA layer by changing the side slope of the induced trench (i.e., the lower TDA part) to 1H:1V, 1H:2V, 1H:3V, 1H:4V and 1H:5V. Also, two widths of 1B and 0.5B were used for the induced

trench to investigate its effect on the developed stress arching mechanism (Figure 2-10c). Finally, Set 4 investigates the effect of the pipe's flexibility on the performance. The flexibility was presented in terms of the flexibility number (*NF*) as expressed below:

$$NF = \frac{E_s \ D^3}{E \ I} \qquad (1)$$

where, E_s is the soil's modulus of elasticity (MPa), *D* is the pipe's diameter (mm), *E* is the modulus of elasticity of the pipe's material and *I* is the moment of inertia (mm^4/mm).

To represent different combinations of pipe materials and moments of inertia, different *NF* values of 25, 50, 100, 250, 500 and 1000 were considered. These different *NF* values were applied to two different geometries as can be seen in Figure 2-10d (Configuration 1 and Configuration 2).

For each set, the results (i.e. footing's settlement, maximum pipe's stresses and deformation) were normalized and compared with the results of the reference (control) case. As indicated in Figure 2-10, the field test in Setup 1 was the control case for Sets 1, 2 and 3. However, because of the geometrical differences, Setup 2 was used to normalize the results of Set 4.

2.5 RESULTS AND DISCUSSION

This section presents the results of the two full-scale tests (i.e. footing's settlement, pressure cell readings, and the measured strains on the pipe) in addition to the results of the developed numerical models. Then, the results of the parametric study were discussed to investigate the soil structure interaction (SSI) of the proposed configurations and their effects on the stress reduction and deformation of the pre-existing buried pipes.

2.5.1 Results of the Full-Scale Tests

Measurements taken during the field tests covered a wide range of behaviour. The results of the field tests (Setups 1 and 2) are presented here along with the results of the developed FE models to investigate the TDA behaviour as a backfilling material and to verify the developed models.

2.5.1.1 Transferred Pressure and Footing's Settlement

Figures 2-11 and 2-12 show the variation of the stresses measured at the bottom of the backfill (above the pipe's crown) and the corresponding footing's settlement during the gradual loading on the footings for Setup1 and 2, respectively. The figures show an excellent match between the results of the FE analyses and the measurements in the field. It can be seen from Figure 2-11 that the responses of the transferred pressure and the footing's settlement (of Setup 1) were almost linear with a slight nonlinearity at the onset. A change in the slope of the loading curve near the applied load of 95 kN (around 150 kPa) can be seen in Figure 2-12 for Setup 2. In which the nonlinear curve starts behaving linearly for loads over 95 kN. This can be related to the punching shear failure that occurred at this stress level. As the strong, rigid layer (granular material), located on the top of the elastic weak TDA layer failed, the response started a linear trend as being governed by the elasticity of the TDA layer. Moreover, it can be seen that the corresponding settlement at the punching load in Setup 2 was around 40 mm, while the settlement at the same applied load in Setup 1 was about 4 mm.

As a result of the existence of the TDA layer, in Figure 2-12 the pressure cell measurements varied from around 12 kPa to 52 kPa at applied loads ranging from 0 to 95 kN. However, in Set up 1 (Figure 2-11), the readings ranged between 22 to 110 kPa for the same applied

loads' range. Therefore, TDA exhibited an excellent behaviour in reducing the applied load to the pre-existing pipes, particularly before the punching failure happening.

Furthermore, Figure 2-13 confirmed the enhancement of the stress transferring mechanism of TDA by showing the transferring pressure as a percentage of the applied pressure for Setups 1 and 2. The figure indicates that in Setup 2, the TDA transferred up to 28% of the applied stresses until the punching shear happened in the granular cover, and then the percentage increased gradually due to the elastic behaviour of the TDA. On the other hand, in Setup 1, the percentage decreased gradually after reaching the optimum value (64%) at around 65 kPa due to the soil hardening in the granular backfilling material. Moreover, it can be seen from the same figure that the percentage of the transferred stress at 150 kPa in Setup 1 (55%) is about two times the percentage in Setup 2 (28%). This proves the excellent ability of TDA to act as an engineered stress reduction backfilling material.

2.5.1.2 Pipe's Strains

The strains of the outer surface of the pipe in Setups 1 and 2 were measured parallelly to the footing settlement and the transferring stresses. Figures 2-14 and 2-15 show the change of the pipes' strains induced by the external loading. Also, it can be seen that there is good compatibility between the FE results and the tests measurements. As mentioned in the test procedure, some strain gauges were damaged during the field tests, wherein Setup 1 only the radial and longitudinal strains at the crown and the radial strain at the springline were working. However, in Setup 2 only the circumferential strain gauge at the crown was damaged. By comparing the measured strains of the pipes in Setups 1 and 2, there is a notable increase of the circumferential strains at the springlines in Setup 1 compared to that of Setup 2. For example, at load increments of 50, 95, 150 and 200 kN, the strain is about

25, 55, 100 and 123 μm/m respectively for Setup 1, while they were only15, 30, 60 and 100 μm/m for Setup 2. Even though the transferred pressure to the pipe's crown in Setup 2 is less than Setup 1, the longitudinal strain in the pipe's crown in Setup 2 is more than that in Setup 1. Figure 2-16 shows the load transfer mechanism throughout the granular backfill and the TDA using FEA to explain why there are higher amounts of longitudinal strain in Setup 2. The figure shows the effective stress distribution induced by the footing loaded up to 77kN (120kPa) with the values of effective normal stresses developed on the interface between the pipe and the backfill along the length of the pipe. As shown in Figure 2-16a, in Setup 1, the compacted Gravel-A1 hardened during the loading and distributed the stress widely along the pipe in the longitudinal direction (about 2m along the pipe). While in Setup 2, Figure 2-16b, the TDA acted as a stress cushion that absorbed the imposed stresses and minimized (shortened) the exposed area of the pipe to the normal stresses (0.9 m along the pipe's longitudinal direction). In addition, it can be seen that the maximum stresses at the pipe's interface are 80 kPa and 52 kPa for Setups 1 and 2 respectively. Therefore, it can be understood that the pipe in Setup 2 will be free to bend more along the pipe's longitudinal axis due to the lesser area exposed to the high stresses coupled with the low stiffness of the TDA above the pipe. While the other pipe that is buried in the stiffer granular backfill in Setup 1, its ends uplift is resisted by higher normal stresses acting over a larger length. This trend will be explicitly shown hereafter in the results of the parametric study; particularly in the distinct effect of the pipe's stiffness (i.e. *NF*) on the pipe's longitudinal stresses.

2.5.2 Results of the Parametric Study

This section presents the results of the parametric study conducted to understand the effect of TDA in different configurations. As described in the parametric study, the pipes were simulated using plate elements instead of volume elements in the parametric study. Consequently, Figure 2-17 shows a comparison between the results of the developed FE model using plate elements versus the results of the model that simulated the pipe utilizing volume elements for Setup 2 testing configuration. It can be seen from Figure 2-17 that excellent matches were found in the pipe's deformation and the footing's settlement between the two models. Hence, it can be concluded that using the plate elements in this exercise will not affect the soil-structure interaction while saving computational time and facilitating the ease of calculations of the stresses.

2.5.2.1 The Effect of TDA Layer Thickness (Set 1)

Figure 2-18 shows the effect of using different TDA layer thicknesses on the response of the buried pipes and footings. The figure displays the corresponding normalized maximum radial and longitudinal stresses of the pipe accompanied by the footing's settlement.

It can be seen that, as the thickness of the TDA layer increases, the amount of stresses in pipes' walls decreases almost linearly. Even though the presence of TDA does not bring any significant change in the pipes longitudinal stresses compared to the control case (the percentage varies from 109% to 90%), a notable reduction of the radial stresses is found when using TDA. This reduction is in the range of 20% to 40% for TDA thicknesses ranging from 0.25B to 1B, respectively. On the other hand, the footing's settlement increased progressively with increasing the TDA thickness. However, this increase can be controlled by creating an optimum design for the super-structure and using the proper

allowable bearing capacity. In addition, other configurations of the cross-section of the TDA layer underneath the foundations may decrease the footing's settlement as discussed in the sections hereafter.

2.5.2.2 The Effect of Forming an Induced Trench Above the Pipe (Set 2)

To enhance the serviceability of the TDA underneath the foundation and decrease the settlement, the TDA backfilling area's configuration was changed as discussed previously and displayed in Figure 2-10b. Figure 2-19 shows the effects of changing the trench's base width versus the footing's settlement and the normalized pipe's maximum stresses. It can be seen from the figure that the normalized longitudinal and radial stresses decreased from 105% to 69% and from 73% to 49%, respectively with decreasing the trench base width. Moreover, the rate of the reduction in stresses increased as the base width decreases to less than 1B. This is because the upper soil layer (A1-Gravel) became so stiff that the stresses were transferred to the surrounding natural soils (stress bridging). It is worth to note that the trench with 0.5B base width has an upper width of 0.91B which is narrower than the punching shear zone. This can interrupt the punching shear failure and affect the stress path. Additionally, the reduction of the stresses comes with a significant decrease of the settlement. Therefore, it is evident that this change in the configuration of the TDA cross-section decreased the settlement. For this reason, the effect of changing the trench's slopes was also investigated in this research as shown below.

2.5.2.3 The Effect of Changing the Trench's Side Slopes (Set 3)

Figure 2-20 confirms the previously mentioned conclusion in the previous section. As the top width of the induced trench got narrower, the footing's settlement and the pipe's stresses decreased. The figure shows the normalized maximum stresses of the pipe in the

longitudinal and radial directions versus the utilized trench's side slopes. The behaviour was examined using two different base widths: 0.5B and 1B. With each base width, five different side slopes: 1H:1V, 1H:2V, 1H:3V, 1H:4V, 1H:5V were paired. It can be seen from Figure 2-20 that as the side slopes got steeper, the stresses and settlements decreased. For example, in the configuration with 0.5B base width, the normalized longitudinal and radial stresses decreased from 70% to 34% and 95% to 48%, respectively, as the slopes changed from 1H:1V to 1H:5V. Meanwhile, the footing's settlement reduced from 25mm to 16mm. The same trend was found to hold for the configuration with a base width of 1B.

2.5.2.4 The Effect of Pipe's Flexibility (Set 4)

In this section, the influence of the pipe's stiffness on the pipe's crown deformation and the developed maximum stresses are studied. It was observed that the stresses in the pipe's walls were reduced as the pipe's stiffness decreases due to the positive arching effect in the trench backfill. Figures 2-21 and 2-22 show the normalized maximum pipe stresses (in two directions) and the crown deflection versus the flexibility number (*NF*) in logarithmic scale for configurations 1 and 2 (as indicated in Figure 2-10d). The higher the *NF* number, the more flexible the pipe is. Figure 2-21 indicates that there is a correlation between the pipe's flexibility and it's longitudinal and radial stresses. As the *NF* increased from 25 to 1000, the longitudinal stresses decreased from 133% to 29%. Additionally, the radial stresses decreased from 110% to 55% with an increase in *NF* from 25 to 1000. In contrast, the accompanying normalized crown deflection increased from 80% to 265% when the pipe became less stiff (higher *NF* values). The same trend was observed in Figure 2-22 for the 2nd configuration. This figure shows that the longitudinal stresses dropped from 88% to 20%, and the radial stresses dropped from 75% to 36% for *NF* values from 25 to 1000.

Meanwhile, the pipe's crown deflection increased from 58% to 195%, when *NF* increased from 25 to 1000. Additionally, it can be seen from Figures 2-21 and 2-22 that the reduction rate in the longitudinal stresses is more than that of the radial stresses. This means that the pipe's flexibility has a more prominent effect on its longitudinal behaviour.

2.6 SUMMARY AND CONCLUSION

Two full-scale field tests were conducted to evaluate the benefits of using a layer of TDA above existing metal pipes to enhance the stress arching mechanism (i.e., stress bridging). In addition, the complicated pipe-soil interaction was investigated by monitoring the surface settlement, change of the pipe's wall strains and the pressure distribution over the pipe. Furthermore, 3D Finite Element models (FEM) of the tests were developed to study the interaction mechanism of the considered problem, where the developed models were validated against the field tests results. Finally, an extensive parametric study was conducted to examine the effect of some important parameters on the performance of the investigated system. The following conclusions can be drawn based on the results of the study:

- The field results showed that using a layer of TDA over the pipe is significantly effective in reducing the pipe's stresses and magnitude of transferred pressures compared to using conventional backfill.
- The employed hardening soil model showed its capability in simulating the TDA behaviour under different confining pressures.
- TDA acted as a stress cushion that absorbed the imposed stresses and minimized the exposed area of the pipe to the stresses.

- TDA reduced the pipe’s stresses in the range of 20% to 50% for TDA thicknesses of 0.25B to 1B, respectively (where B is the footing’s width). However, the footing’s settlement increased progressively with increasing the TDA thickness.
- Changing the configuration of the cross-section of the TDA layer underneath the foundations decreased the footing’s settlement and improved the serviceability substantially.
- It was observed that the stresses in the pipe’s wall were reduced as the pipe's stiffness decreases due to the positive arching effect in the trench backfill. Moreover, the reduction rate in the longitudinal stresses is more than that of the radial stresses. This means that the pipe’s flexibility has a more prominent effect on its longitudinal behaviour.

Table 2.1: Parameters used in the FEA

Layers	**Constitutive model**	**Unit weight (kN/m3)**	**E (MPa)**	**E_{50} (MPa)**	**E_{oed} (MPa)**	**Cohesion (kPa)**	**Angle of internal friction (°)**
Natural ground	MC	18	30	-	-	22	20
A1-Gravel	MC	22.5	40	-	-	-	44
Clean sand	MC	16	15	-	-	-	31
TDA	*HSM	7	-	2.75	2.2	24	26.5

Note: E = modulus of elasticity; E_{oed} = tangent stiffness from odometer test; E_{50} = secant modulus; HSM= hardening soil model; MC = Mohr Coulomb.
*The properties at P_{ref} = 25 kPa and R_f=0.95.

Table 2.2: Steel and concrete parameters

Layers	Constitutive model	Unit weight (kN/m^3)	E (GPa)
Steel	Elastic	78	180
Concrete	Elastic	24	39

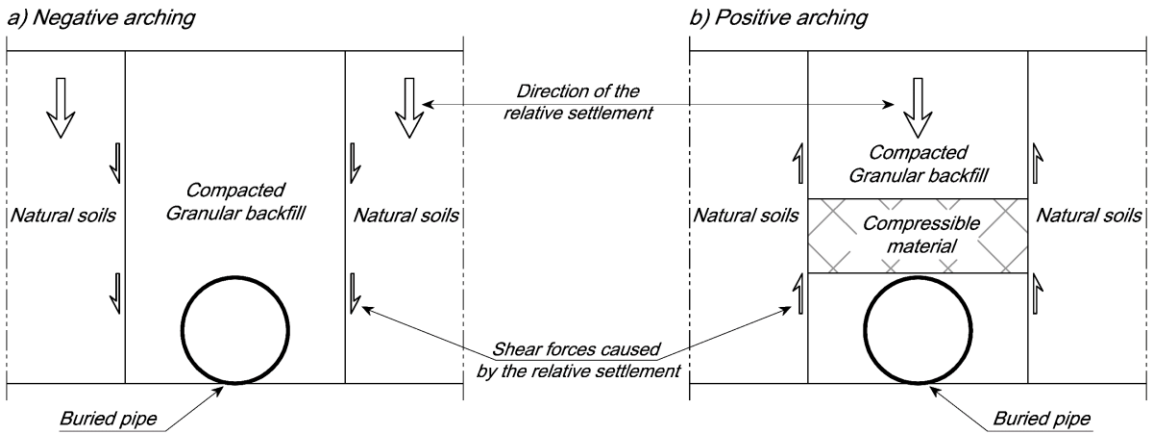

Figure 2-1 Schematic illustrations of the positive and negative arching mechanisms in pipe installations

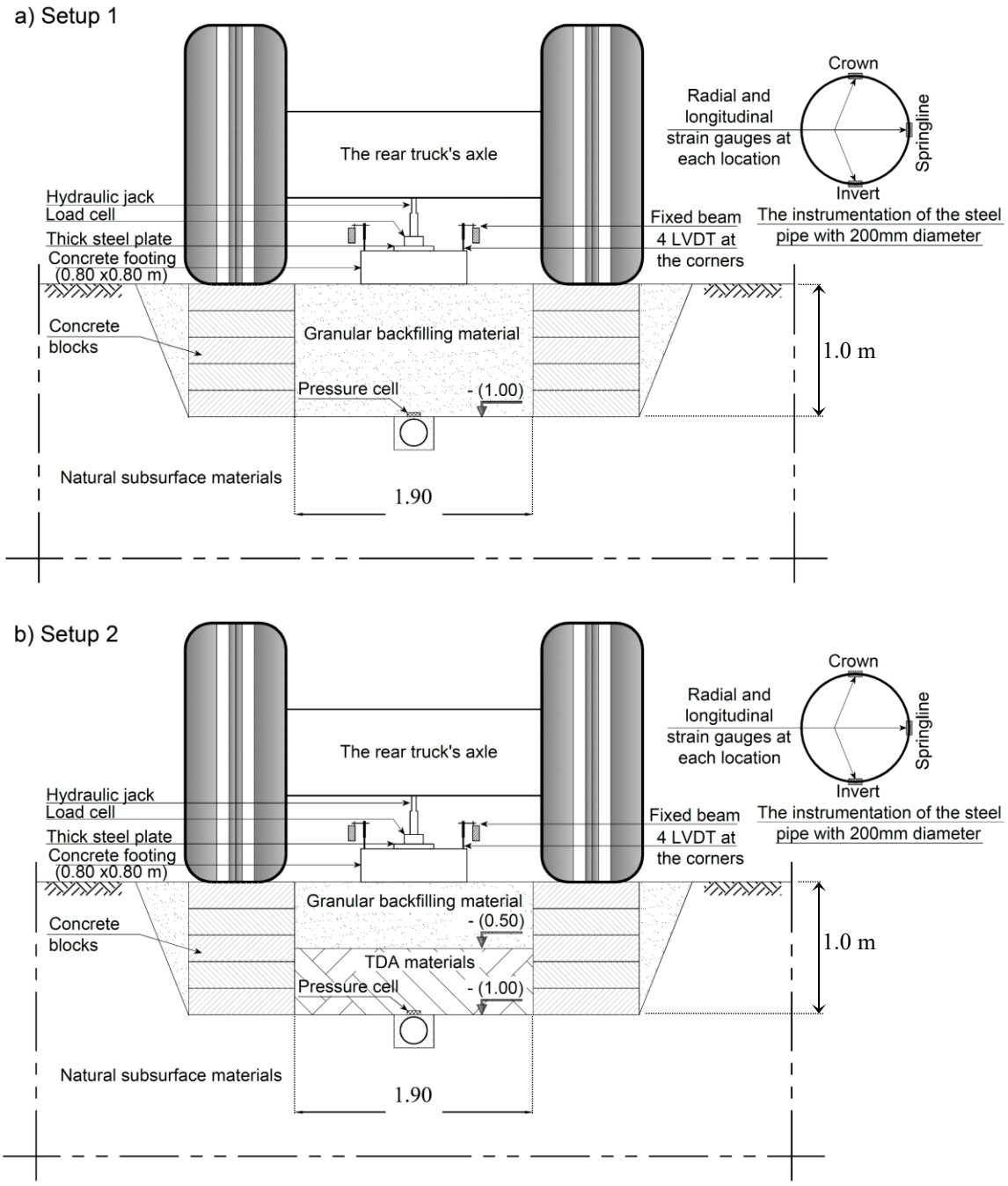

Figure 2-2 Layout of the field tests a) Setup 1, and b) Setup 2

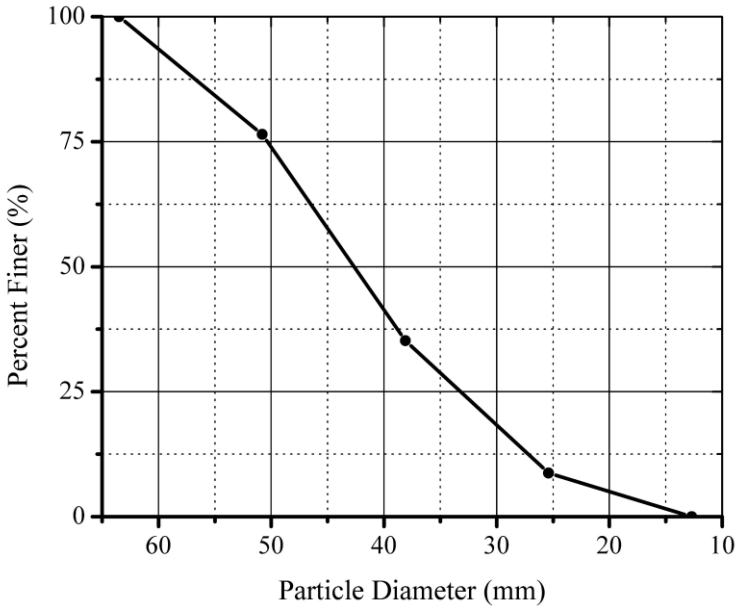

Figure 2-3 TDA Gradation (Ashari and El Naggar 2017)

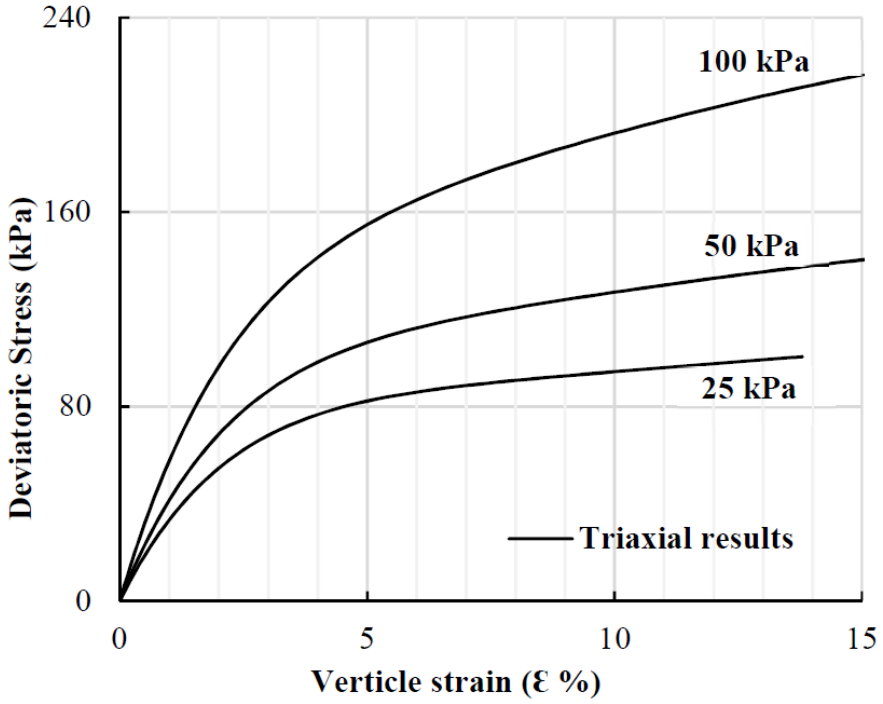

Figure 2-4 Deviatoric Stress vs. Axial Strain for TDA materials (Ashari 2018)

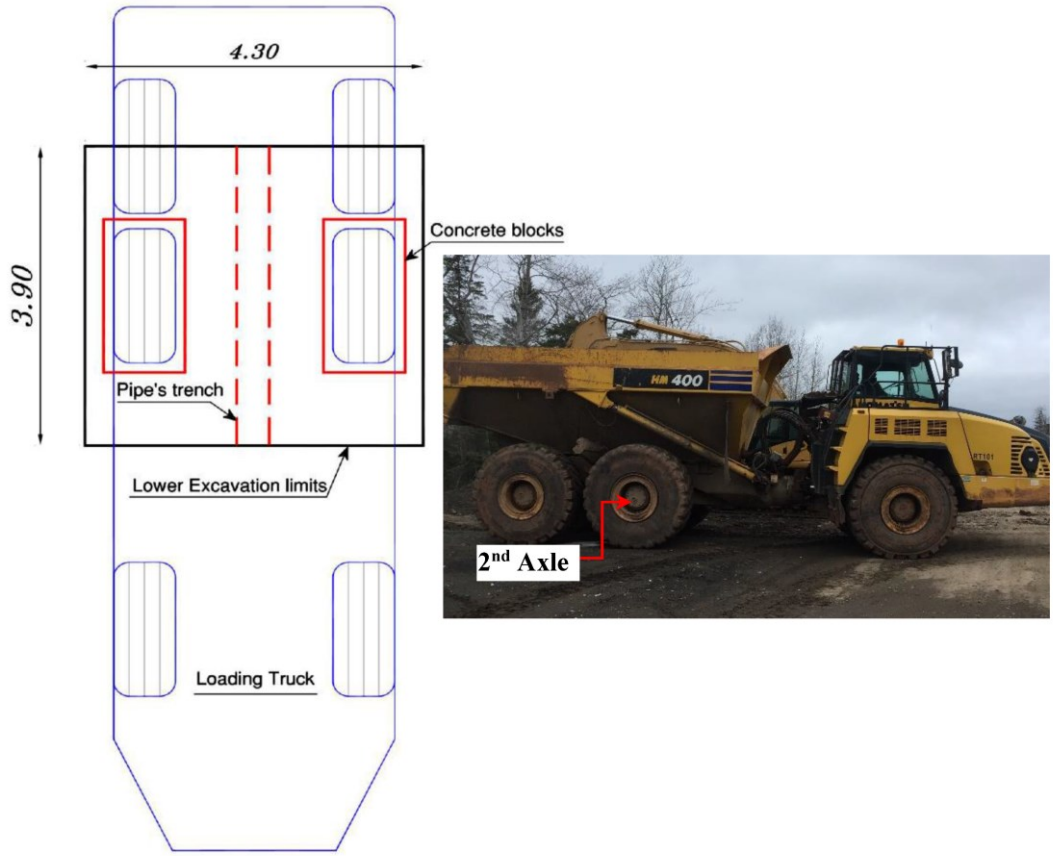

Figure 2-5 The loading truck's layout above the concrete blocks

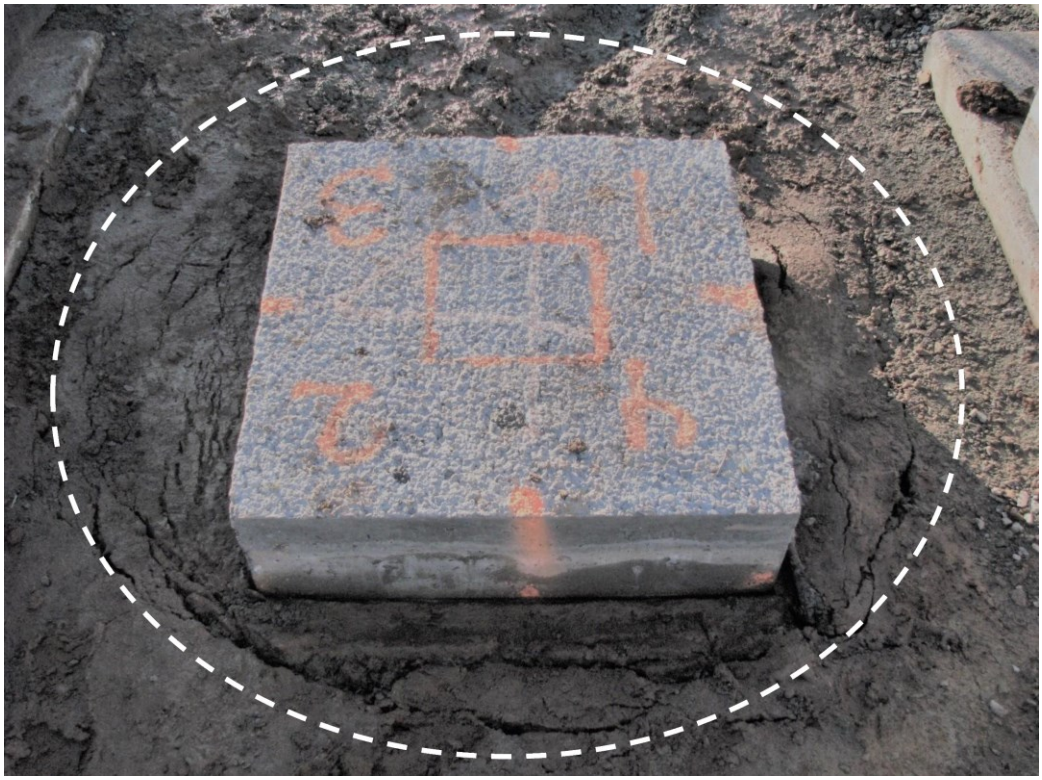

Figure 2-6 Punching failure of Setup 2

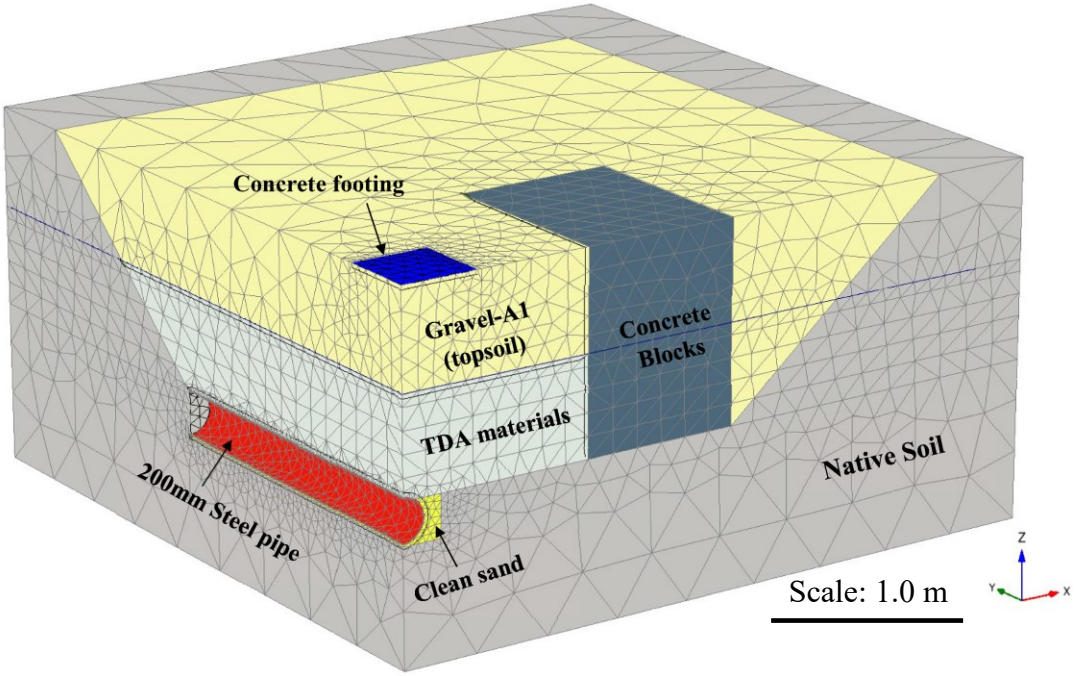

Figure 2-7 FE model of the Setup 2

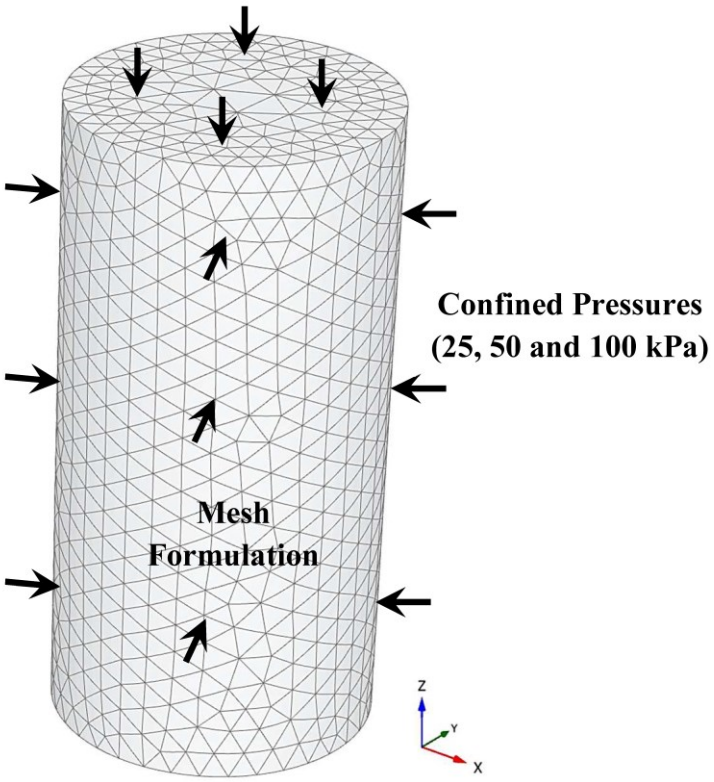

Figure 2-8 FE simulation of the triaxial test for the TDA using the Hardening soil model

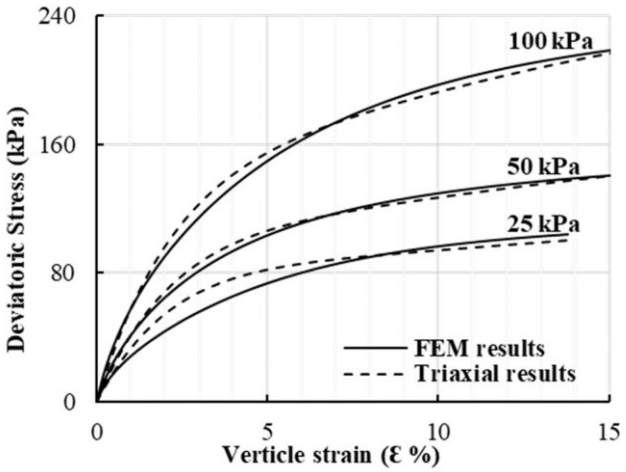

Figure 2-9 Verification of the TDA's behaviour in the FE simulations

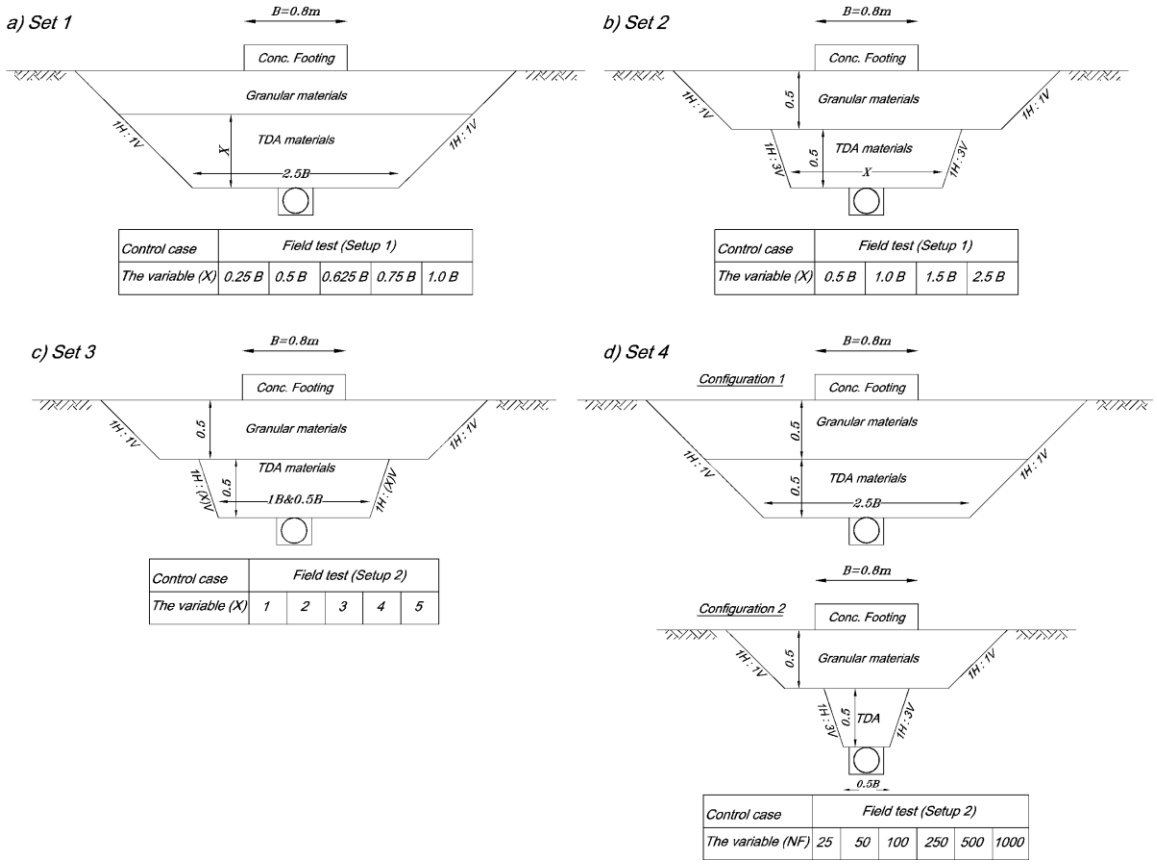

Figure 2-10 Illustrations of the different configuration sets considered in the parametric study

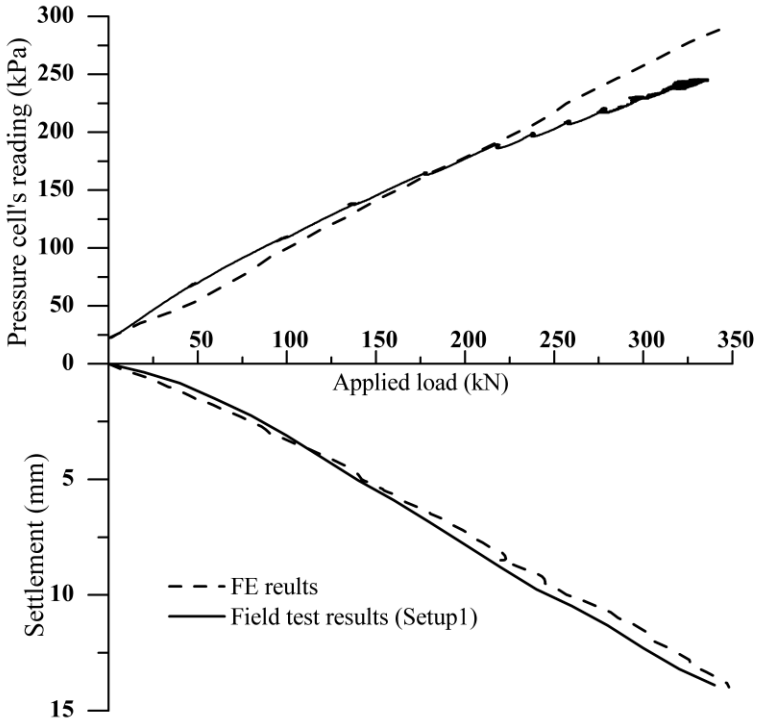

Figure 2-11 Comparison between the measured field test and the FE model results (Setup 1)

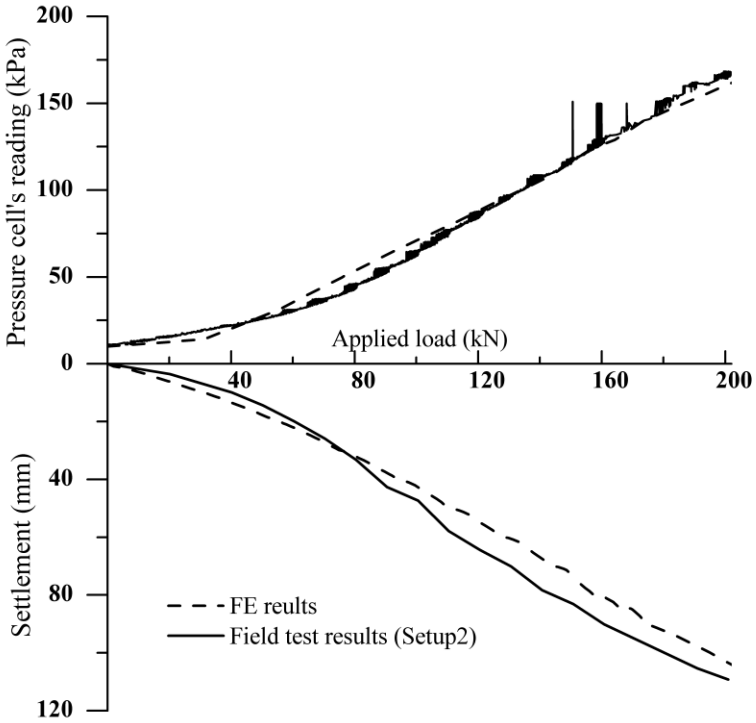

Figure 2-12 Comparison between the measured field test and the FE model results (Setup 2)

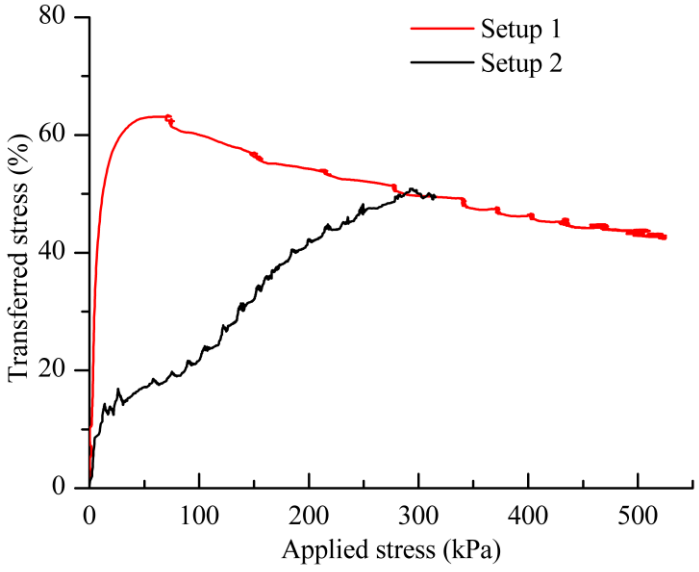

Figure 2-13 The percentage of the pressure transferred throughout the backfill layers of the two testing setups

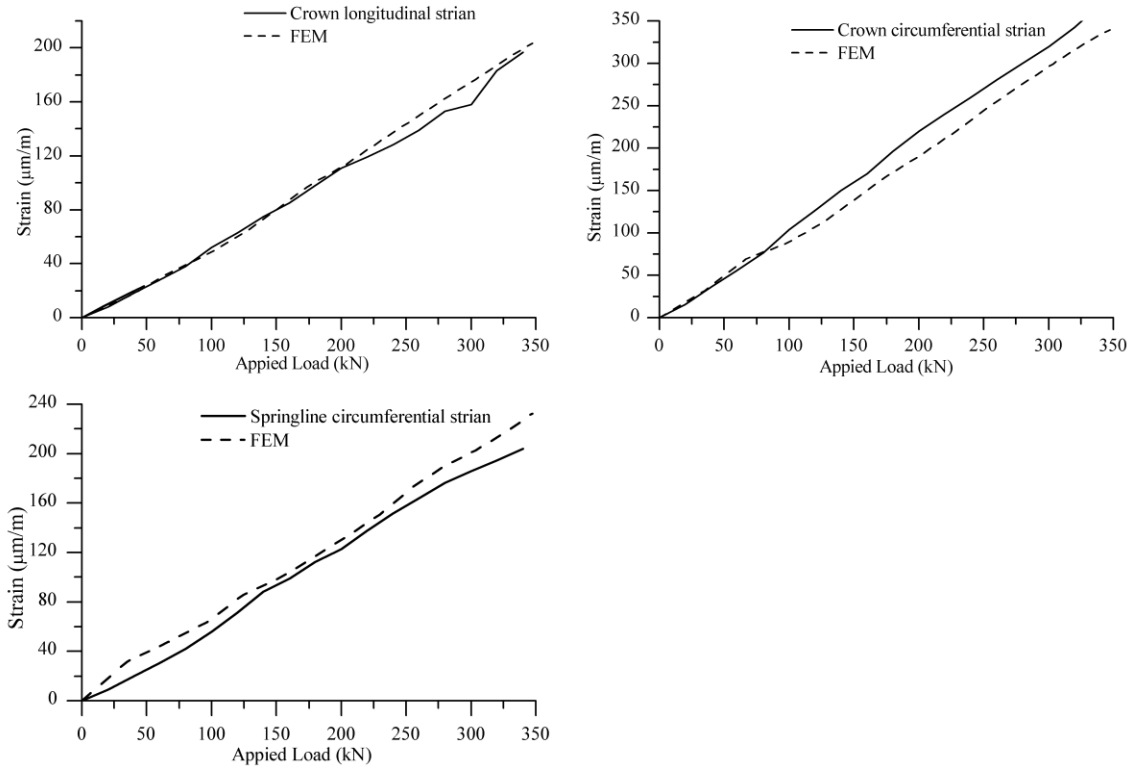

Figure 2-14 Pipe's surface strains in Setup 1

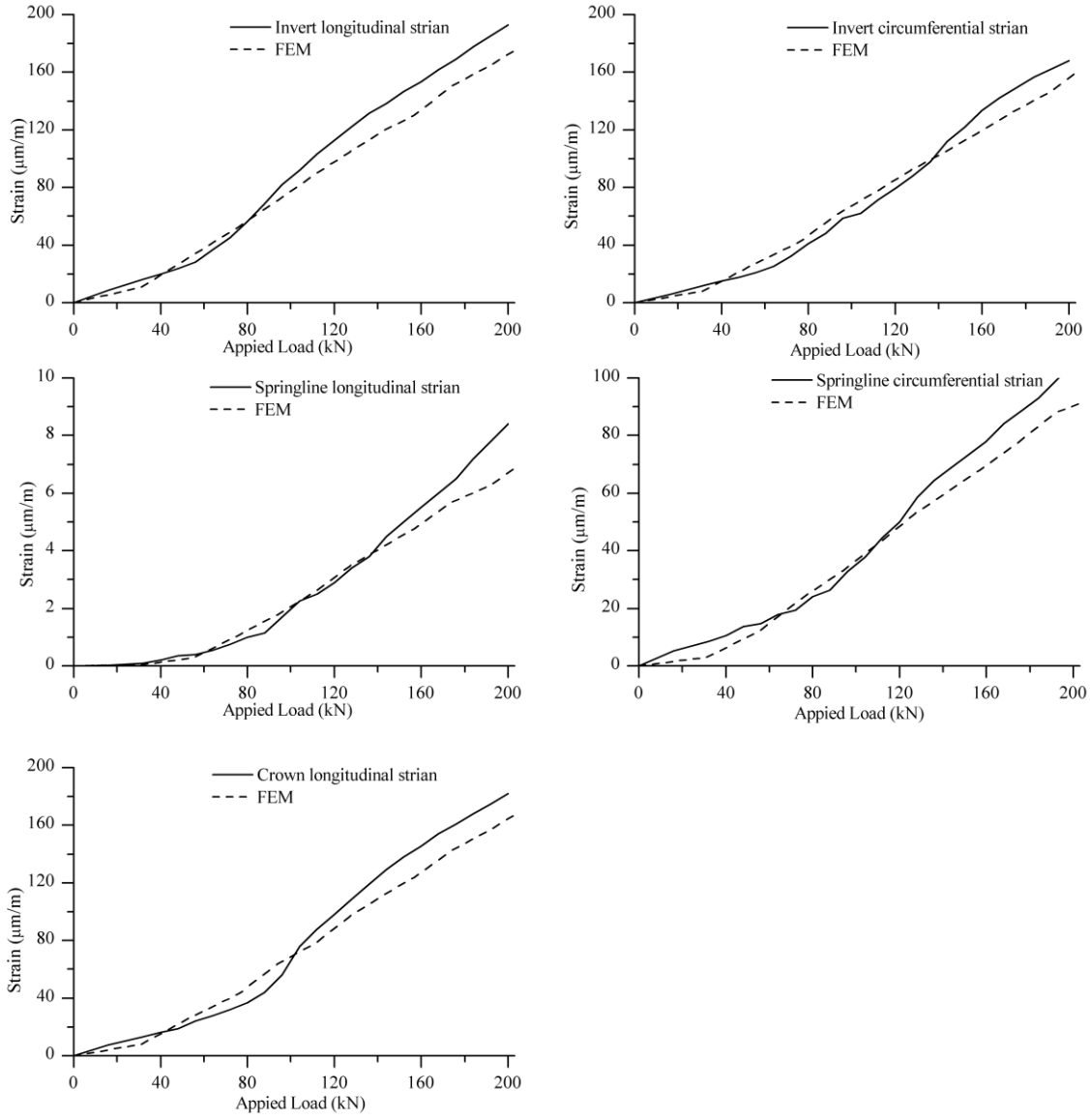

Figure 2-15 Pipe's surface strains in Setup 2

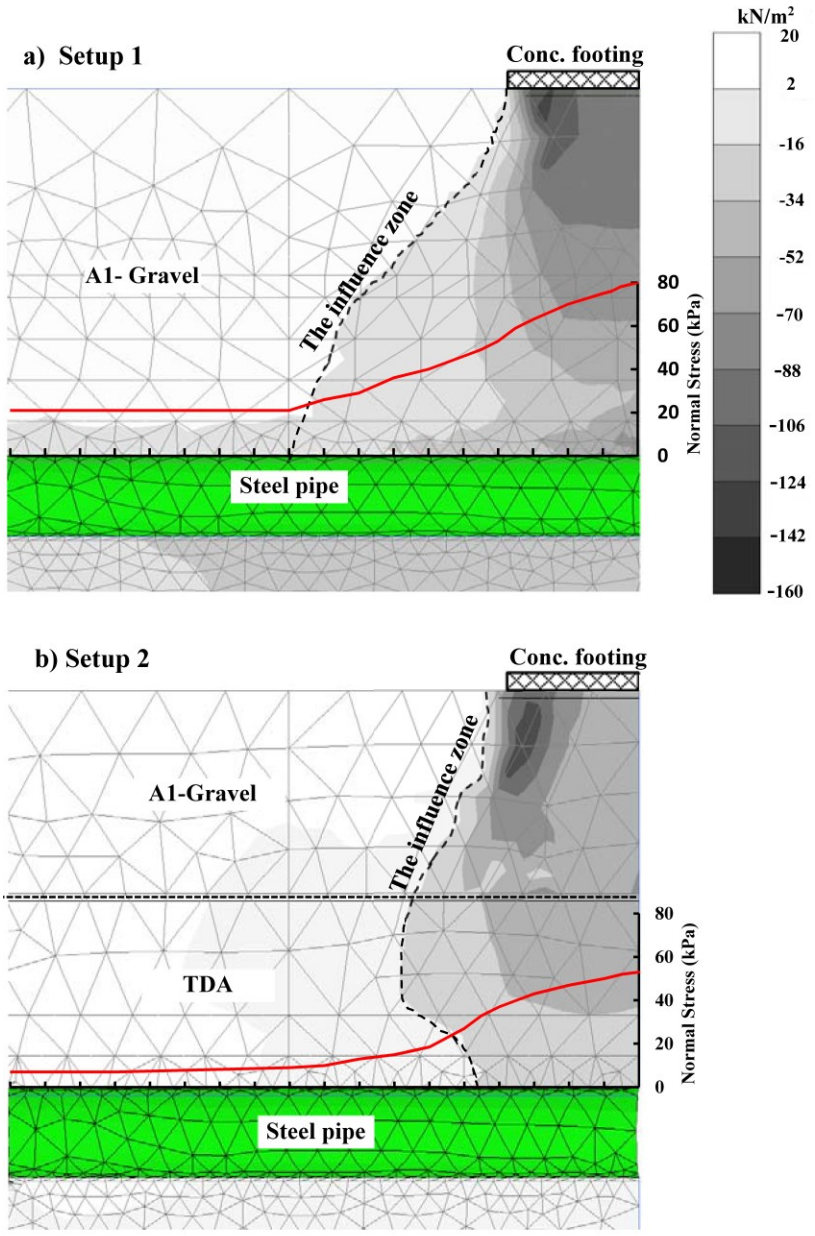

Figure 2-16 Illustration of the effective stress distribution throughout different backfill materials (developed arching mechanisms)

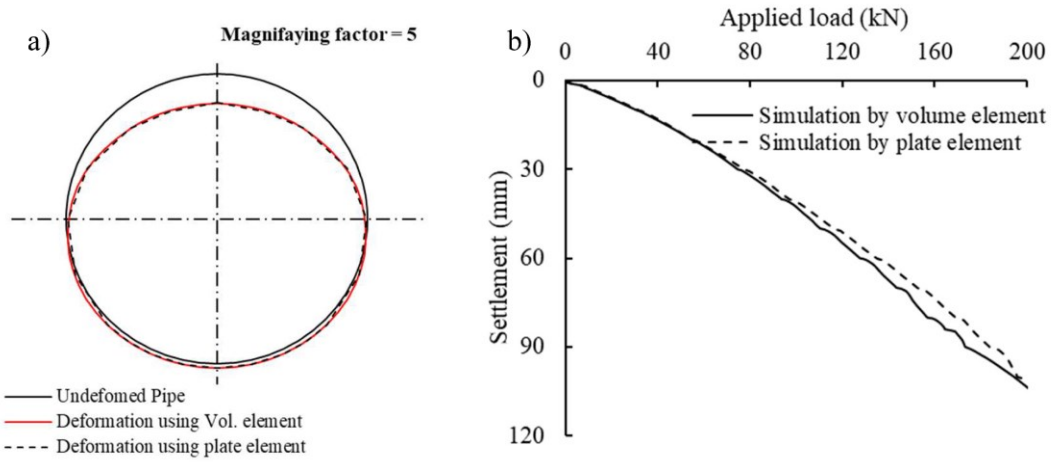

Figure 2-17 Effect of using different element types on the FE results; a) pipe deformation b) footing settlement

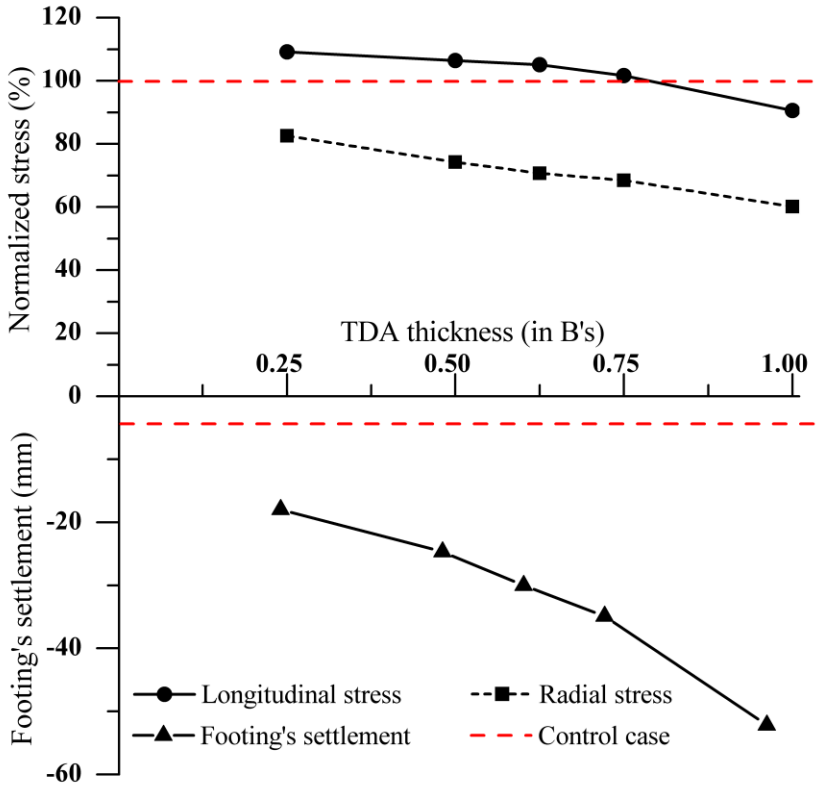

Figure 2-18 Effect of changing the TDA thickness on the pipe and footing's behaviour (Set 1 results)

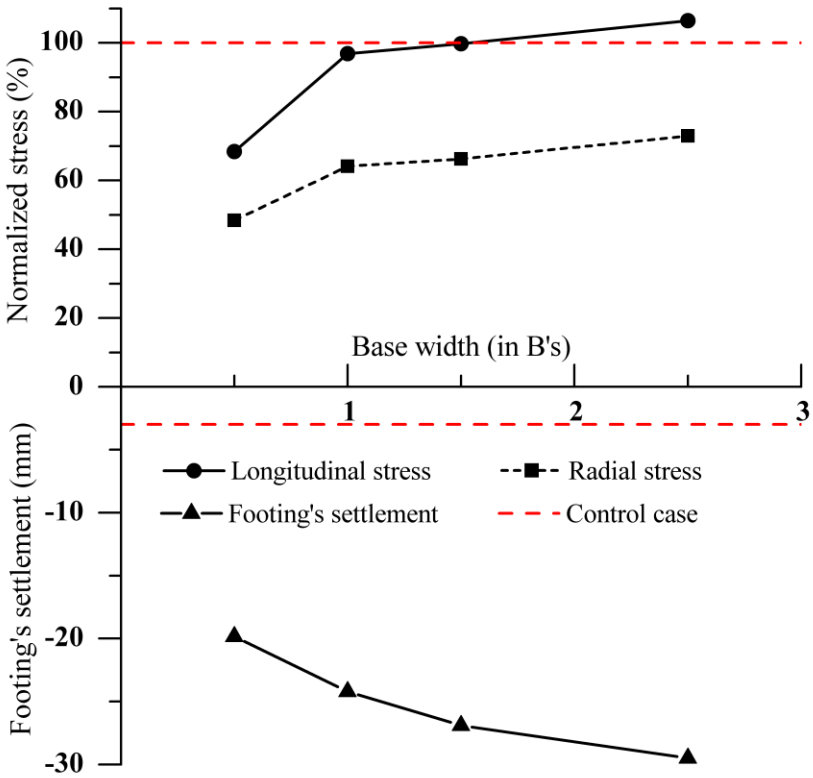

Figure 2-19 Effect of forming an induced trench above the pipe (Set 2 results)

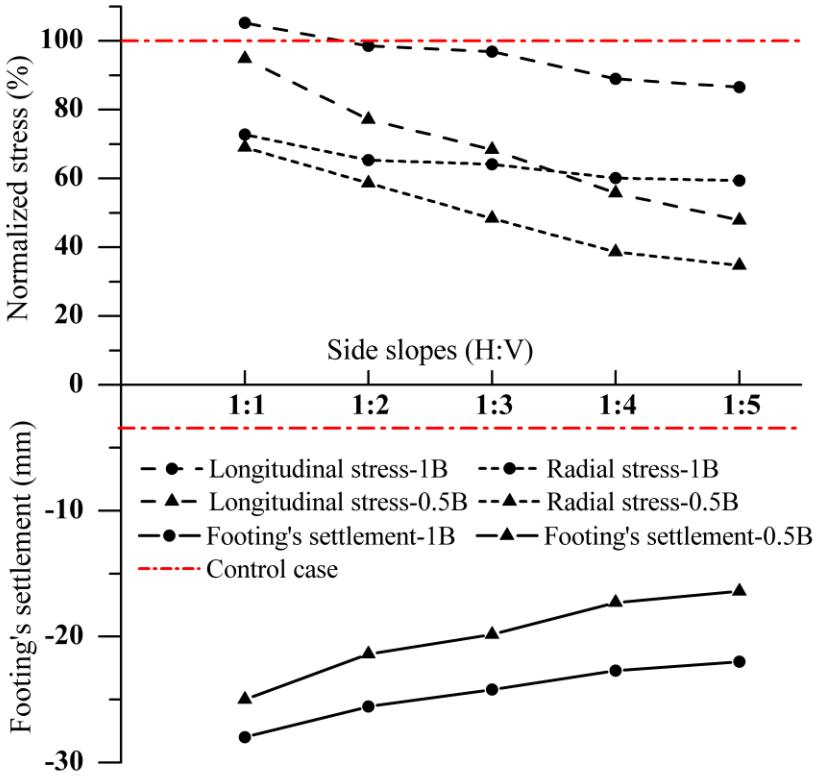

Figure 2-20 Effect of changing the trench's side slopes on the pipe and footing's behaviour (Set 3 results)

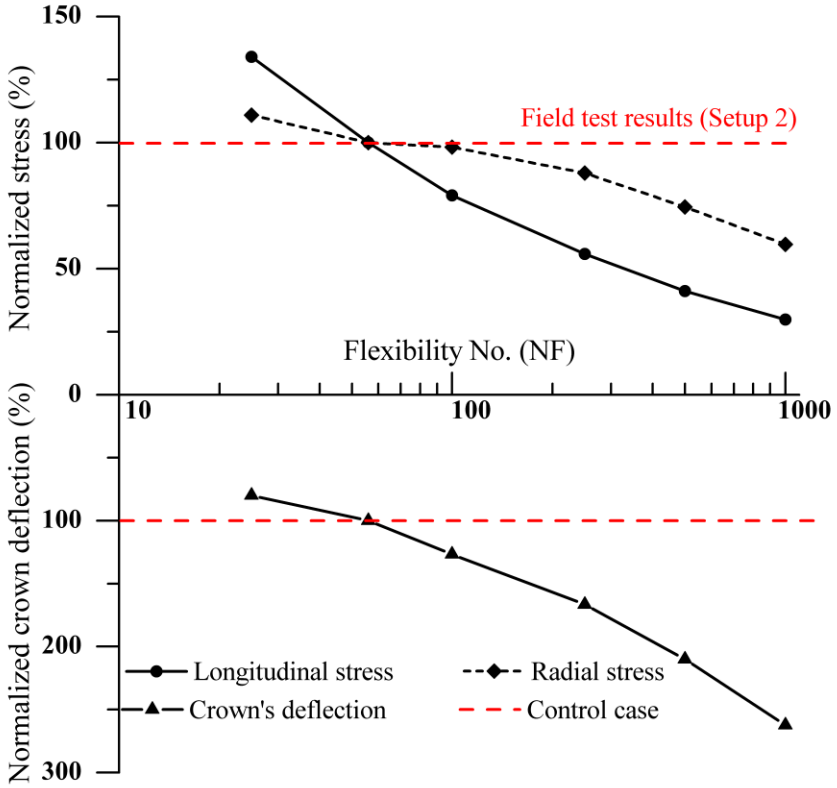

Figure 2-21 Effect of changing the pipe's flexibility number (NF) on the pipe's behaviour- 1st configuration (Set 4 results)

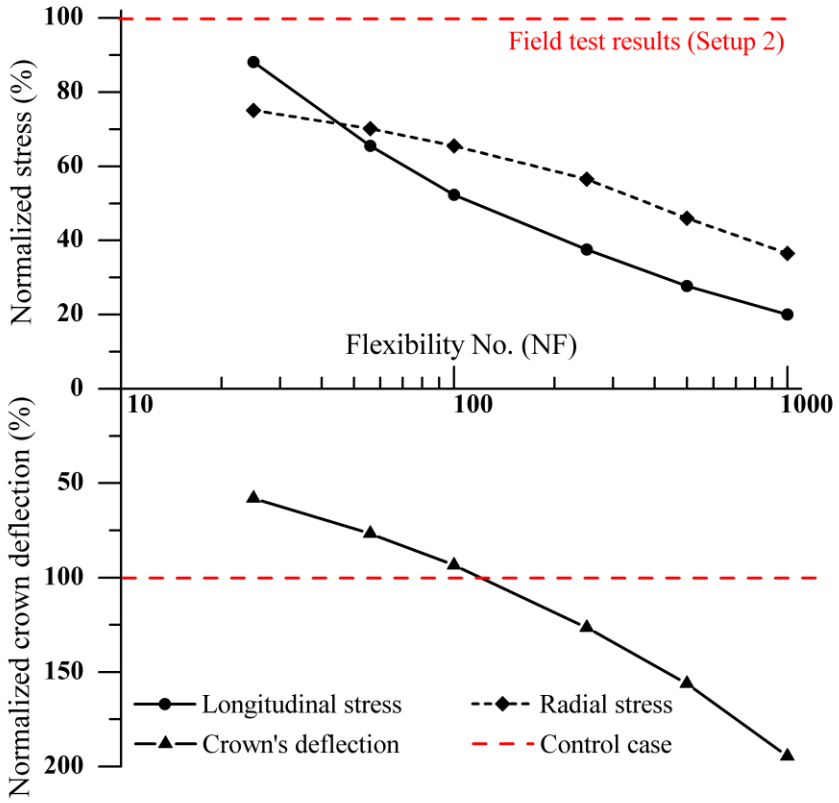

Figure 2-22 Effect of changing the pipe's flexibility number (NF) on the pipe's behaviour- 2nd configuration (Set 4 results)

2.7 REFERENCES

Anderson AO (1913) Vol. 31 of the theory of loads on pipes in ditches: And tests of cement and clay drain tile and sewer pipe. Ames, IA: Iowa State College of Agriculture and Mechanic Arts.

Ashari Ghomi M (2018) Large-scale triaxial testing of sustainable TDA backfilling alternatives. Master's thesis, Dalhousie Univ.

Ashari M and El Naggar H (2017) Evaluation of the physical properties of TDA-Sand mixtures. In GeoOttawa, the 70th Canadian Geotechnical Conf. Ottawa: Canadian Geotechnical Society.

ASTM (1997) Nonrepetitive static plate load tests of soils and flexible pavement components, for use in evaluation and design of airport and highway pavements. D 1196-93. West Conshohocken, PA: ASTM International.

ASTM (2012) Standard practice for use of scrap tires in civil engineering applications. D6270-12. West Conshohocken, PA: ASTM International.

ASTM (2017) Classification of soils for engineering purposes (Unified Soil Classification System). D2487-17. West Conshohocken, PA: ASTM International.

Azevedo F, Pacheco-Torgal F, Jesus C, De Aguiar JB, and Camões AF (2012) Properties and durability of HPC with tyre rubber wastes. Constr. Build. Mater. 34: 186–191. https://doi.org/10.1016/j .conbuildmat.2012.02.062.

Bosscher PJ, Edil TB and Eldin NN (1992) Construction and performance of a shredded waste tire test embankment. Transp. Res. Rec. 1345: 44–52.

Costa YD, Zornberg JG, Bueno BS, and Costa CL (2009) Failure mechanisms in sand over a deep active trapdoor. J. Geotech. Geoenviron. Eng. 135 (11): 1741–1753. https://doi.org/10.1061/(ASCE)GT.1943-5606.0000134.

Dickson, T, Dwyer D, and Humphrey D (2001) Prototype tire-shred embankment construction. Transp. Res. Rec. 1755: 160–167. https://doi.org/10.3141/1755-17.

Duncan JM, and Chang CY (1970) Nonlinear analysis of stress and strain in soils. J. Soil Mech. Found. Div. 96 (5): 1629–1653.

El Naggar H, Soleimani P, and Fakhroo A (2016) Strength and stiffness properties of green lightweight fill mixtures. Geotech. Geol. Eng. 34 (3): 867–876. https://doi.org/10.1007/s10706-016-0010-1.

Engstrom G, and Lamb R (1994) Using shredded waste tires as a lightweight fill material for road surfaces. Rep. No. MN-RD- 94-10. Minnesota, US: Dept. of Transportation.

Humphrey D, and Blumenthal M (2010) The use of tire-derived aggregate in road construction applications. In Green Streets and Highways 2010: An Interactive Conf. on the State of the Art and How to Achieve Sustainable Outcomes, 299–313. Reston, VA: ASCE.

Humphrey DN, and Eaton RA (1995) Field performance of tire chips as subgrade insulation for rural roads. In Proc., Transportation Research Board Conf. Washington, DC: Transportation Research Board.

Luscher U and Hoeg K (1964) The beneficial action of the surrounding soil on the load-carrying capacity of buried tubes. In Proc., Symp. On Soil-Structure Interaction. Tucson, AZ: University of Arizona.

McAffee RP and Valsangkar AJ (2008) Field performance, centrifuge testing, and numerical modelling of an induced trench installation. Can. Geotech. J. 45 (1): 85–101. https://doi.org/10.1139/T07-086.

McGuigan B L and Valsangkar AJ (2010) Centrifuge testing and numerical analysis of box culverts installed in induced trenches. Can. Geotech. J. 47 (2): 147–163. https://doi.org/10.1139/T09-085.

McGuigan BL and Valsangkar AJ (2011) Earth pressures on twin positive projecting and induced trench box culverts under high embankments. Can. Geotech. J. 48 (2): 173–185. https://doi.org/10.1139/T10-058.

Marston A (1930) The theory of external loads on closed conduits in the light of the latest experiments. In Vol. 9 of Proc., Highway research board. Washington, DC: Highway Research Board.

Meles D, Bayat A, Shafiee MH, Nassiri S and Gul M (2013) Field study on construction of highway embankment made from two tirederived aggregate types and tire-derived

aggregate mixed with soil as fill materials. In Transportation Research Board, 92 Annual meeting. Washington, DC. Washington, DC: Transportation Research Board.

Mills B and McGinn J (2010) Design, construction, and performance of a highway embankment failure repaired with tire-derived aggregate. Transp. Res. Rec. 2170: 90–99. https://doi.org/10.3141/2170-11.

Plaxis B (2017) Reference manual for PLAXIS 2D. Delft, Netherlands:Plaxis.

Rui R., Van Tol AA, Xia YY, Van Eekelen SJM, and Hu G (2016) Investigation of soil-arching development in dense sand by 2D model tests. Geotech. Test. J. 39 (3): 415–430. https://doi.org/10.1520/GTJ20150130.

Schanz T, Vermeer PA, and Bonnier PG (1999) The hardening soil model: Formulation and verification. In Beyond 2000 in computational geotechnics: 10 years of Plaxis, 281–296. Rotterdam, Netherlands: A.A. Balkema.

Schlick W J (1932) Loads on pipe in wide ditches, Bul. 108, Iowa Eng., Exp. Sta., 1–49. Ames, IA: Iowa State College.

Shalaby A and Khan RA (2002) Temperature monitoring and compressibility measurement of a tire shred embankment: Winnipeg, Manitoba, Canada. In Transportation research record 1808, 67–75. Washington, DC: National Research Council, Transportation Research Board.

Spangler MG (1950a) A theory of loads on negative projecting conduits. In Vol. 30 of Proc., Highway Research Board, 153–161. Washington, DC: Transportation Research Board.

Spangler MG (1950b) Field measurements of the settlement ratios of various highway culverts. Bulletin 171. Ames, IA: Iowa Engineering Experiment Station.

Spangler MG, and Handy RL (1973) Soil engineering. New York: Intext Educational.

Terzaghi, K (1936) A fundamental fallacy in earth pressure computations. J. Boston Soc. Civ. Eng. 23: 71–88.

Terzaghi K (1943) Theoretical soil mechanics. New York: Wiley.

Turan A, El Naggar MH, and Dundas D (2013) Investigation of induced trench method using a full-scale test embankment. Geotech. Geol. Eng. 31 (2): 557–568. https://doi.org/10.1007/s10706-012-9608-0.

Upton RJ, and Machan G (1993) Use of shredded tires for lightweight fill. Transp. Res. Rec. 1422: 36–45.

Wang WL and Yen BC (1974) Soil arching in slopes. J. Geotech. Eng. 100 (GT1): 61–78.

CHAPTER 3 USING TDA UNDERNEATH SHALLOW FOUNDATIONS: FIELD TESTS AND NUMERICAL MODELLING

Ahmed Mahgoub and Hany El Naggar

3.1 INTRODUCTION

Tire-derived aggregate (TDA), a recycled product made by shredding scrap tires into sizes ranging from 12 mm to 305 mm, can be used to replace natural aggregates in civil engineering applications. Each year, one billion scrap tires are discarded worldwide. Over 250 million of them are in the United States and 30 million in Canada (El Naggar et al. 2016). In the 1990s, tire recycling and reuse in North America and worldwide have increased considerably, with the aim of reducing the harmful effects of scrap tires on the environment. For instance, scrap tires in landfills provide an attractive habitat for mosquitoes and rodents (Rubber Manufacturers Association 2017). In addition, stockpiling scrape tires in tire landfills is hazardous and may cause uncontrolled fires such as the 1990 tire fire in Hagersville, Ontario, Canada (Pierre 2013).

The progressive development of tire recycling and reuse has resulted in a significant decrease in the disposal of scrap tire stockpiles in landfills. According to the Scrap Tire Management Council in the United States, in 2000, 70% of scrap tires were recycled as compared with only 6% in 1990. The 2017 Rubber Manufacturers Association report states that over 43% of scrap tires generated annually in the United States were recycled as tire-derived fuel (TDF). Although 25% of the tires were utilized in ground rubber applications, only 7.9% were recycled in civil engineering projects. Hence there is a current direction to

deviate a greater portion of the tires from being used as TDF to be used in civil applications to reduce the environmental concerns associated with burning tires.

TDA has outstanding properties making it suitable for use in a wide variety of civil applications, e.g., embankments, trench backfilling and road subgrades (Humphrey and Eaton 1995; Humphrey 2005; Humphrey 2008; Humphrey and Blumenthal 2010). In comparison to conventional backfill aggregates, TDA is an inexpensive, lightweight material. The specific gravity of TDA ranges from 1.15 to 1.21, whereas the specific gravity of natural backfills ranges from 2.55 to 2.75 (Edil 2005; Sparkes et al. 2019). In addition, the cost of scrap tires is about 25% of the cost of conventional backfill (Humphrey 2008). As reported in (Edil et al. 2004), the permeability of TDA is ten times that of gravel used in drainage applications. Moreover, TDA is considered to be a good thermal insulator, eight times more effective than natural soil (Eaton et al. 1994; Benson et al. 1996).

Many studies have been conducted to investigate the use of TDA in embankments, buried infrastructure and trench fill projects (Bosscher et al. 1992; Ahmed and Lovell 1993; Hoppe 1998; Salgado et al. 2003; Yoon et al. 2006; Humphrey and Blumenthal 2010; Mills et al. 2015; Mahgoub and El Naggar, 2019). Ahn et al. (2014) reported field measurements of the secondary compression index (i.e., creep) of TDA calculated from several embankment projects in the United States and Canada. They found that most of the occurred settlement happened during or shortly after the construction with TDA secondary compression index ranges from 0.004 to 0.0047; very comparable that of stiff clay. In addition, Wartman et al. (2007) carried out long-term, one-dimensional compression tests to measure the secondary compression index of TDA, the study found that the average

secondary compression index was 0.0065. Moreover, the study indicated that the secondary consolidation depends on the layer height, not the applied loads or the tires size.

In addition, the use of TDA as a backfill material for retaining walls and abutment projects has been investigated (Hoppe, 1998; Tweedie et al. 1998; Humphrey, 2008; Xiao et al. 2012). Studies have also examined the utilization of TDA as a subgrade thermal insulator and as a drainage layer for various civil applications (Eaton et al. 1994; Humphrey and Eaton 1995; Benson et al., 1996; Lawrence et al. 1999). Moreover, TDA exhibits an outstanding performance when used as a damping material for dynamic loads below rail lines and retaining walls subject to dynamic and/or earthquakes loads (Wolfe et al. 2004; Ahn and Cheng. 2014).

Even though there is a lack of studies investigating the use of TDA underneath shallow foundations. A study has been conducted by Mahgoub and El Naggar (2019) on the feasibility of protecting pre-existing pipes, located underneath shallow foundations, by using TDA as an engineered stress-reduction fill above the pipes and underneath a concrete footing. The study included two full-scale field tests to evaluate the usefulness of employing a TDA layer above existing metal pipes to enhance the stress arching mechanism. In addition, the study developed three-dimensional finite element models of the tests to study the effect of changing various key parameters (i.e., the thickness of the TDA layer, the shape and configuration of the TDA cross-section, and the pipe stiffness) on the performance of the system. However, the focus of the study was mainly on the behaviour of the buried pipes. In addition, Rashwan and Charette (2015) performed a full-scale study to investigate the feasibility of using TDA to replace natural materials in residential home basements, by using TDA around basement walls and underneath the

basement slabs (not the building footings). It was found that, in comparison to natural materials, TDA significantly reduced the lateral earth pressure on basement walls. In addition, the TDA noticeably enhanced the heat insulation of basement walls and slabs.

This paper examines rigid footings resting on a surface of conventional backfill materials overlying a TDA layer. The study includes three full-scale field tests with TDA layers of different thicknesses. Rigorous finite element analyses (FEA) are then developed to examine the failure mechanism of the shallow foundations over TDA as a backfill material, and to study the effect of critical parameters on the footing performance.

3.2 METHODOLOGY

The procedure used in this study can be summarized as follows:

- Three full-scale field tests were conducted. These are described in detail, including the layout, instrumentation, construction procedures, and measurements obtained.
- Three-dimensional finite element models of the three testing setups were developed and verified against the results of the field tests.

A parametric study was then conducted to examine the effects of the TDA layer thickness, footing geometry, foundation depth, and soil type on the performance of the system investigated.

3.3 FIELD TEST OVERVIEW AND SITE CHARACTERIZATION

Three rigid square concrete footings (for setups F1, F2 and F3) were constructed and tested at a site in Antrim, Nova Scotia, Canada, 65 km northeast of Halifax (see Figure A1 in Appendix A), to examine the behaviour of shallow foundations on a backfill of TDA materials. The square footings, 0.8 m wide and 0.3 m thick, were cast using high-strength

concrete and had an ultimate compressive strength, f_{cu}, of 60 MPa. For the first concrete footing (setup F1), which served as the control, 1.0 m of conventional compacted granular backfill was utilized as replacement soil beneath the footing. For the second footing (setup F2), a TDA layer 0.5 m thick beneath a 0.5 m layer of conventional granular materials was used underneath the footing; while for the third footing (setup F3), a TDA layer 0.7 m thick beneath a 0.3 m layer of conventional granular materials was used. Figure 3-1 illustrates the considered test configurations. To examine the performance of each configuration, field tests were designed to measure the loads applied to the concrete footing, the corresponding footing settlement, and the transferred stresses under the replacement layers.

Two boreholes were drilled to a depth of 10 m. A standard penetration test (SPT) was performed at different levels, and Shelby tubes were used to extract undisturbed soil samples for laboratory testing (i.e., Atterberg limits testing, sieve analyses, and triaxial tests).

The site investigation showed that the in-situ soil was primarily glacial till with sand and gravel (classified as sandy lean clay with gravel, according to ASTM D2487) underneath 0.5 m of organic soils. Atterberg limits and sieve analysis testing were performed for characterization purposes. In addition, triaxial tests were conducted to obtain the shear strength parameters for the till layer at the proposed foundation level. The undrained shear strength C_u ranged from 100 kPa to 140 kPa, and the drained shear strength parameter measurements yielded a cohesion of 22 kPa and an internal friction angle of 20°.

3.3.1 Backfill Materials

Gravel materials were used as a conventional backfill for the different setups. Sieve analyses and Proctor testing were carried out for soil classification purposes, and to determine the optimum water content and maximum dry density of the granular backfill used. The material was classified as A1 granular material with a maximum dry density of 22.5 kN/m^{3}and W_c= 7.5%. Triaxial tests were performed to obtain the shear strength parameters (φ' = 44°) and the modulus of elasticity E.

The TDA used in the field tests was TDA type A, in accordance with ASTM D6270-08, with sizes ranging from 13 mm to 63 mm, and a unit weight of 7 kN/m^3. The TDA was shredded and manufactured from passenger car scrap tires by the Halifax C&D Recycling company in Nova Scotia, Canada. The shear strength parameters of the TDA were determined by using large-scale triaxial tests. Proctor tests and sieve analyses were also performed to classify the material and to determine the maximum capacity. A more detailed description of the laboratory testing program is provided in (Ashari Ghomi 2018; Ashari et al. 2017). Ashari Ghomi (2018) performed large-scale triaxial tests to identify the failure envelope of the TDA material and used the tests results to develop a constitutive material model of the TDA; the triaxial test results for different confinement pressures are shown in Figure 3-2. For the used TDA, the drained internal friction angle *(φ')* was found to be 26.5° and the cohesion *(c')* was 24 kPa.

3.3.2 Instrumentation

To obtain the pressure distribution throughout the backfill, a 240 mm pressure cell (LPTC09-S) manufactured by RST Instruments was installed under the backfill, directly

below the centre of the concrete footing. Footing settlement was monitored by using four linear variable differential transformers (LVDT) manufactured by TE Connectivity. The transformers had a measuring capacity of 500 mm and were installed on the upper surface of the footing. A hydraulic jack was installed at the centre of the upper surface of each concrete footing to apply a concentrated downward load. Simultaneously, a loaded Komatsu HM400 dump truck weighing 50 metric tons, positioned on concrete slabs, was used to act as a reaction load above the hydraulic jack. The load on the footing was observed and controlled by using a load cell (see Figure 3-1). A computerized data acquisition system (Campbell 5000) was used to record the monitoring data every 0.1 second for the different setups.

3.3.3 Test Procedure

Prior to the field tests, the site was levelled, and the topsoil removed. The depth of each excavated pit was exactly one meter, as shown in Figure 3-1. The bottom of the pits was inspected to confirm the subsurface conditions indicated by the boreholes. Two parallel stacks of concrete slabs, each stack one meter high, were then placed in the pit, as illustrated in Figure A2 (a) in Appendix A. The concrete slabs were positioned so that the truck could drive onto them; in this way, the slabs could support the weight of the truck and could transfer this load to the subsurface below, without affecting the layers immediately underneath the footing. A pressure cell was then placed at the bottom of the test pit, aligned so as to be directly beneath the centre of the footing (see Figure A2 (b) in Appendix A).

Next, the excavated pits were filled with the desired layers of backfill materials for each test. Each layer of the gravel A1 was compacted and tested by using a nuclear densitometer, to ensure that the desired compaction level (95% of the standard Proctor dry density) was

achieved. For setups F2 and F3, an overbuild layer of the TDA was added to compensate for the settlement occurring after the addition of the gravel A1 materials (Figure A2 (c) in Appendix A). As shown in Figure A2 (d) in Appendix A, the TDA layer was covered with a thin polymeric membrane, to separate it from the top gravel layer. In addition, another sheet of the membrane was placed against the concrete slabs and the backfill to reduce any friction at the slabs boundary during the loading. The surface of the test area was then levelled, and the concrete for the three footings was poured. The footings were positioned so that they would be aligned with the buried pressure transducers (Figure A3 (a) in Appendix A). After casting, the footings were cured for 28 days before testing. Three-inch PVC pipe was installed near each footing to measure the groundwater level before the test. The groundwater level was encountered between 0.8 m to 0.9 m below the footings level.

Four LVDTs were placed on each footing, one at each corner of the footing. The hydraulic jack was then aligned with the centre of the footing and placed beneath the second-rear axle of the truck (Figueres. A3 (b) and A3 (c) in Appendix A). In addition, the load cell was mounted to measure the load applied to the footing.

The load was applied in 20 kN increments and was maintained until the rate of the settlement was less than 0.03 mm/min over three consecutive minutes, in accordance with ASTM D 1196-93 (ASTM, 1997). The maximum load applied by the truck was 340 kN for setup F1 and 260 kN for setups F2 and F3. Loading was stopped when the truck was lifted due to the force applied by the hydraulic jack (in F1), or when a clear punching shear failure could be seen in setups F2 and F3. Figure A4 in Appendix A shows the punching shear failure for the footings in setups F2 and F3. The failure appeared as a semi-circular cracked line located approximately 150 mm away from the edges of the footing.

Subsequently, 3D finite element models were developed for the field tests to investigate the failure mechanism of each configuration. The field test results, including the load-settlement curves and the stress transferred through the backfill, are presented in comparison with the finite element results in the following sections.

3.4 DESCRIPTION OF THE NUMERICAL MODELS

Finite element analyses (FEAs) were employed parametrically by using PLAXIS 3D-2017 to identify the failure mechanisms of the rigid footings above a TDA layer. Two sets of models were developed. The first set includes a simulation of the three conducted full-scale field tests to validate the models. The second set involves a detailed parametric study that was carried out to study the performance of the investigated system.

3.4.1 The First Set of Models – Simulation of the Field Tests

The geometry and construction sequence followed in the full-scale tests were simulated in the 3D modelling. Figure 3-3 shows the geometry of the FE model developed for the second setup (F2).

The natural soil and the backfill envelope were modelled by using higher order 10-node triangular elements. The verification models comprised approximately 40,000 elements. Due to the extensive settlement and soil deformation represented in the verified models for setups F2 and F3, the PLAXIS updating mesh option was used to account for large deformations and to avoid errors caused by element distortion. To avoid interference with the stress contours within the influence zone, a fully fixed boundary condition was assumed at the base of the model more than 4 times the footing width (B) below the foundation. One-quarter of the problem was modelled in order to benefit from the model symmetry in

the two horizontal directions and to reduce the computations and number of elements. For this reason, the perpendicular lateral boundary conditions along the model axes of symmetry were restrained. The outer lateral boundary conditions, which extended 3 times the width of the footing on each side, were assigned to be free in the vertical direction and fixed in the horizontal direction.

3.4.2 Material and Soil Properties

An elastic-perfectly plastic soil constitutive model with a Mohr-Coulomb failure criterion was used to simulate the natural soil and the granular (gravel A1) layer, due to the simplicity of the model and its suitability for this application.

An elastoplastic strain-hardening model (HSM) from the PLAXIS 3D library was used to represent the behaviour of the TDA materials. This double-stiffness model is used to model the stress-dependent variation of the soil stiffness due to different loading conditions (Schanz et al., 1999). Various studies have demonstrated the effectiveness of using the HSM model to simulate TDA behaviour (Bernal et al., 1996 and Ashari Ghomi, 2018). To investigate the ability of the HSM model to simulate TDA behaviour, Mahgoub and El Naggar (2019) developed FE models for the triaxial TDA tests that are presented in Ashari and El Naggar (2017) and Ashari Ghomi (2018). The study showed an excellent match between the stress-strain relationships resulting from the triaxial tests and the FE models.

Although the concrete slabs and concrete footings were simulated as volume elements by using the elastic material model, the concrete slabs were modelled in drained conditions, and the concrete footing was modelled as a non-porous material. Table 3.1 shows the

parameters used in the FE analyses of the natural soil, granular gravel A1 material, TDA and concrete.

Five-node interface elements were added between the TDA layer and the top granular layer, with a reduction factor (R_{inter}) of 0.30, to simulate the smooth thin polymeric membrane between them. The membrane between the concrete slabs and the surrounding soil was also simulated. In addition, an interface element with R_{inter} equal to 0.67 was added between the concrete footing and the soil to simulate the soil-structure interaction (SSI).

3.4.3 Construction Sequence

The construction sequence followed in the full-scale field tests was simulated in the 3D modelling. First, the initial in-situ stresses were established by using the K_0 procedure, in which the vertical stresses increase linearly with depth. The excavation was then simulated by deactivating the soil in the test pit. Subsequently, the proposed backfill material was placed, and the interface elements around the concrete slabs and above the TDA were activated. Finally, the concrete footing was cast, and progressive vertical loads were applied until failure.

3.4.4 The Second Set of Models – the Parametric Study

Table 3.2 and Figure 3-4 show the parameters used in the parametric study. The study investigated the behaviour of shallow foundations by changing the following key parameters: TDA layer thickness, internal friction angle (φ') of the top granular backfill, foundation depth, footing width, footing shape, and different subsurface conditions.

As shown in Table 3.2, the parametric study consisted of six groups of models. The first group (G1) examined the effect of changing the thickness of the TDA layer on the footing

performance. The footing width (B) used in G1 was 0.8 m, the backfill height (H) was 1.0 m (i.e., 1.25B), and the TDA thickness (t) ranged from 0.1 H to 0.7 H.

The second group (G2) investigated the effect of changing the internal friction angle (φ') of the top granular backfill on the footing behaviour. Angles of 28°, 32°, 36°, 40° and 44° were used to represent different granular backfill densities.

The third group (G3) examined the effect of the foundation depth (D_F) on the footing behaviour. The foundation depth (D_F) was varied from 0 B to 2.5 B.

The fourth group (G4) evaluated the effect of changing the footing width (B). The footing geometry used in G4 was square, as in the field tests. Footing widths from 0.5 H to 2.0 H were examined, with a TDA layer thickness of 0.5 H.

In the fifth group (G5), different footing geometries were considered in the FE analyses. The different geometries were represented by the ratio of the footing length (L) to the footing width (B). In the analyses, six (L/B) aspect ratios were used: 1, 2, 5, 10, 15, and 20. In addition, a circular footing with a diameter of B was also considered.

Finally, the sixth group (G6) investigated the effect of changing the subsurface conditions on the footing performance. The subsurface conditions considered were hard, stiff, medium, and soft clay. The soil properties for the stiff, medium and soft clay were selected from reasonable ranges from Look (2014), and Obrzud and Truty (2012) and presented in Table 3.3.

For all models in the G2, G3, G5 and G6 groups, a footing width (B) of 0.8 m, a backfill height (H) of 1.25 B, and a TDA layer thickness (t) of 0.5 H were used. It should be noted that the FE models in the parametric study were simulated without the presence of the concrete slabs existed in the field test. A comparison between the FE results in case of

using the concrete slabs and without them was presented and discussed in the results of the parametric study section.

3.5 RESULTS AND DISCUSSION

This section presents the results of the full-scale field tests along with the validation of the FE models. Also, the effect of the different parameters investigated in the parametric study on the performance of footings resting on backfill containing a TDA layer is presented and discussed.

3.5.1 Results of Full-Scale Field Tests and the First Set of Models

Figures 3-5, 3-6 and 3-7 show the results of the field tests of setups F1, F2, and F3, respectively, as compared with the results of the FE models. The figures plot the stresses measured at the bottom of the backfill and the corresponding footing settlement against the load applied to the footings.

In Figures 3-5 to 3-7, the solid lines represent the field test results. For setup F1 (Figure 3-5), a generally linear relationship between the applied load and the footing settlement was recorded. A direct relationship was also found between the applied load and the pressure measured at the bottom of the backfill. For setups F2 and F3 (Figures 3-6 and 3-7), it can be seen that for smaller applied loads, nonlinear footing settlement and transferred pressure responses were obtained, but above a certain load value, the responses increased linearly until the end of the test. For setup F2, the curve started being linear at a load value of 99 kN (corresponding to a pressure of 155 kPa in this case); while for setup F3, the curve started its linearity at a load value of 82 kN (128 kPa). This change in behaviour corresponds to the incidence of the punching shear failure of the strong layer overlying the

TDA layer. The FE results plotted as dashed lines in Figures 3-5, 3-6 and 3-7, demonstrate an excellent match with the field test measurements.

It can be seen from the results of F1 (Figure 3-5), that for applied loads of 99 kN and 82 kN (the values at which the punching shear failure occurred in setups F2 and F3), the readings of the pressure cell beneath the granular backfill of setup F1 were 103 kPa and 85 kPa, respectively. Figure 3-6 illustrates that in setup F2, where 50% of the granular backfill materials were replaced with a TDA layer, the pressure cell reading at an applied load of 99 kN (i.e., at the punching failure load of F2) was only 65 kPa. Likewise, in setup F3, where 70% of the granular backfill materials were replaced with a TDA layer, the pressure cell reading at the punching failure load of this case (i.e., 82 kN) was only 52 kPa. This demonstrates the effectiveness of the TDA layer in reducing the transferred pressure and enhancing the stress arching performance (an important feature when building on soft soils).

On the other hand, as a result of the presence of the TDA layer, the F2 and F3 footings settled by approximately 40 mm under the punching shear failure loads, in comparison the settlement values of footing F1 were 2.5 mm and 3.5 mm at applied loads of 82 kN and 99 kN, respectively. However, it should be noted that there are no limitations in the foundation design standards as to the total foundation settlement; the limits are set only for the differential settlement. The foundation total settlement is commonly governed by the building usage and the deflection tolerance of the utility connections. Though, for design purposes, it is possible to control the settlement values as described below in the discussion of the parametric study results.

In Figure 3-8, values obtained from the field tests are used to plot the stress transferred through the backfill (i.e., at the bottom of the backfill) as a percentage of the applied stress at the surface, for setups F1, F2 and F3. It can be seen that for setup F1, the percentage of the stress transferred through the granular backfill increased to 62.5% of the applied stress (near 60 kPa), and then gradually decreased with progressive loading, due to the soil hardening of the gravel material at high pressures. In contrast, in setups F2 and F3, the TDA layer transferred stresses reached up to 32% and 28%, respectively, until the punching shear failure of the top layer occurred. Above these values, with progressive loading, the percentages then increased gradually due to the elastic behaviour of the TDA. Figure 3-8 also indicates that following the punching shear failure, transferred stress percentages were greater in the F3 setup than in the F2 setup. This was because after the shear failure of the top layer occurred, the thicker TDA layer in the F3 setup accommodated more settlement. In the F1 setup, where only conventional backfill was used, the stresses transferred at applied stresses of 155 kPa and 128 kPa (the values at which the punching shear failure occurred in setups F2 and F3) were 55% and 58%, respectively, compared to 32% in F2 and 28% in F3. Hence, it can be clearly seen that the TDA is able to reduce the stress transfer rate by almost half of what the natural backfill is able to achieve, illustrating the TDA ability in enhancing the stress arching mechanism underneath shallow foundations.

Following validation against the field test results, the FE models were used to estimate the stress influence zones underneath the footings for setups F1, F2 and F3 (see Figure 3-9). For purposes of comparison, an applied external stress of 120 kPa on the footings was selected, which was less than the punching shear failure loads for setups F2 and F3. The stress bulbs shown in Figure 3-9 represent contour lines for transferred stress equal to 10%

of the applied stress. It can be seen that this stress extended to 2.45 B underneath the footing for setup F1, which was built on a conventional granular backfill. In contrast, due to the presence of the TDA layers, this stress contour extended only to 1.82 B and 1.68 B for setups F2 and F3, respectively. Thus, using a TDA layer underneath shallow foundations could be an inexpensive solution for many civil engineering and underground applications, such as building on soft or weak soils, or providing fill medium for pipelines and utilities near shallow foundations.

3.5.2 Results of the Parametric Study - the Second Set of Models

As explained earlier, one of the objectives of this study is to explore the influence of the investigated design parameters on the performance of shallow foundations built on a TDA backfill. Hence, a detailed interpretation of the conducted FE models for the parametric study was presented in this section. Additionally, as mentioned in the parametric study section above, the FE models in the parametric study were simulated without the concrete slabs. A comparison between the results (i.e., applied loads versus corresponding footing settlement) of the developed FE model using the concrete slabs and without them for the testing setup F2 is shown in Figure 3-10. The figure shows an excellent match between the results (i.e., with and without the side concrete slabs). Therefore, this comparison proves that the location of the concrete slabs (used as a platform for the loading truck) did not affect the behaviour.

3.5.2.1 Effect of TDA Layer Thickness (G1)

In Figure 3-11, for different TDA layer thicknesses, the footing settlement is plotted against the applied stress. It can be seen that decreasing the thickness of the TDA layer results in a notable increase in the sustained stresses at a given settlement value. For instance, for a

settlement value of 25 mm, the applied stresses on footings built on a backfill containing TDA layers with thicknesses of 0.1H, 0.2H, 0.3H, 0.4H, 0.5H, 0.6H and 0.7H reached 148 kPa, 128 kPa, 111kPa, 100 kPa, 77 kPa, 88 kPa and 66 kPa, respectively. Figure 3-12 shows that for settlement values of 25 mm, 40 mm, 60 mm and 100 mm, the applied stresses decrease linearly with increasing TDA layer thickness. In addition, Figure 3-12 indicates that for higher settlement values, the stresses decrease more sharply as the TDA layer thickness increases, which could be attributable to the hardening of TDA under large deformations. However, although increasing the TDA layer thickness is found to reduce the service pressure that can be used, it should be considered that the TDA layer offers significant benefits in decreasing the stress influence zone, as shown in Figure 3-9.

3.5.2.2 Effect of Internal Friction Angle of the Top Backfill Layer (G2)

Figure 3-13 shows the effect of the strength of the top granular layer on the footing performance. Figure 3-13 indicates that for cases where the top backfill layer has a relatively small angle of internal friction, φ', (i.e., loose material with shear strength parameters close to those of the TDA) an explicit nonlinear behaviour was encountered. In such cases, a combination of punching and bearing shear failure in the top granular layer occurs, causing most of the applied stress to be carried by the underlying TDA layer resulting in larger settlements. In contrast, punching shear failure was experienced when dense soils (i.e., having a high φ') with limited thickness, relative to the footing width, were utilized in the top backfill layer. The dense soils distributed the stresses over a larger area above the TDA layer, thus significantly reducing the settlement and enhancing the performance. Figure 3-14 uses soil deformation results from the FE models to compare the soil deformation underneath footings over very dense (φ'=44°) and loose (φ'=28°)

granular backfills. The stresses associated with a settlement value of 60 mm were found to be 191 kPa for the very dense and 106 kPa for the loose granular backfill. It can also be seen that the volume of soil with a settlement of 60 mm (indicated in black) and the extent of soil deformation are greater in the case of dense granular backfill (Figure 3-14a) than loose granular backfill (Figure 3-14b). This behaviour is reflected in the different values of applied stress associated with the same amount of settlement in the two cases. As illustrated in Figure 3-14a, a top backfill layer comprised of a material with a high density and shear strength forms a firm layer above the soft materials in the underlying TDA layer. In contrast, as shown in Figure 3-14b, loose materials in the top backfill layer result in a conical deformation over the TDA layer, thus causing the stresses to be transferred to a smaller volume of the underlying material.

3.5.2.3 Effect of Foundation Depth (G3)

Foundation depth is an important parameter which affects the bearing capacity of the soil. Figure 3-15 illustrates the effect of increasing the foundation depth on the footing behaviour. It can be seen that greater foundation depths result in a significant enhancement of the relationship between the stress applied to the footing and the corresponding settlement. For a settlement value of 25 mm, the applied stress was found to increase by 155% and 225%, as the foundation depth increased from 0 B to 1 B, and from 0 B to 2.5 B, respectively. Figure 3-15 was used to determine the values of the footing bearing capacity at specific settlement values that are plotted in Figure 3-16. In Figure 3-16, the applied stresses are plotted against the effective stress (γD_F) at the foundation level, where D_F represents the foundation depth, and γ represents the unit weight of the granular

material. From Figure 3-16 it can be seen that, for different settlement values, the applied stresses increase with an approximately constant slope.

3.5.2.4 Effect of Footing Width (G4)

In this section, the effect of changing the footing width on the footing performance was investigated for a constant backfill height, with 50% TDA and 50% overlying granular material. Stress-settlement relationships obtained from the models were plotted in Figure 3-17. It can be seen from this figure that as the width of the footing decreased with respect to the thickness of the top granular layer (t_g), the footing performance was governed by the top granular layer and the corresponding settlement decreased. While, the TDA layers controlled the behaviour if the footing width increased with respect to the top granular layer thickness; where most of the stresses were accommodated by the TDA. For this purpose, the applied stresses were plotted against the footing width, expressed as a function of the thickness of the top granular layer (t_g), in Figure 3-18 for settlement values of 25 mm, 40 mm, 60 mm and 100 mm. It can be seen that the sustained stresses decreased sharply when the footing width increased from $0.5t_g$ to $1t_g$; as with a footing width of $0.5t_g$, most of the stress influence zone was in the top granular layer. However, the stresses decreased slightly as the footing width increased from $1t_g$ to $4t_g$.

3.5.2.5 Effect of Footing Shape (G5)

Conventional bearing capacity theories for shallow foundations (e.g., Terzaghi, 1920) indicate that circular footings have the highest bearing capacity and strip footings have the lowest. As shown in Figure 3-19, the FE analyses in this study indicate that footings with square and circular shapes yield similar values with regard to the stress-settlement relationship and have a better performance than strip footings. It can also be seen from

Figure 3-19 that all of the footings with L/B aspect ratios equal to or greater than ten have very similar behaviour, i.e., L/B of 10 can be considered as the limiting border between the rectangular and strip footing behaviours in this case. For rectangular footings with aspect ratios ranging from 1 to 10, the stress capacity was found to decrease gradually as the aspect ratio increased.

3.5.2.6 Effect of the Condition of the Natural Soil (G6)

The effect of changing the condition of the natural in-situ soil located in the footing stress influence zone (below the TDA layer) was analysed while keeping the other parameters constant. Figure 3-20 plots stress-settlement relationships obtained from the models for different site conditions (i.e., hard clay, stiff clay, medium clay and soft clay). It can be seen that as the site conditions became weaker, the corresponding footing settlement in response to the applied stress increased. This can be attributed to the lower stiffness of the weak soils that receive part of the external stress. However, it should be noted that if a weak natural soil is located beyond the stress influence zone of the proposed footing, this effect is eliminated. Thus, a TDA layer can play a valuable role by helping to reduce the extent of the stress influence zone underneath the footing (Figure 3-9). For instance, as it can be seen in Figure 3-9, in the case of using a layer of TDA to replace 50% of the conventional granular backfill material (the total backfill height underneath the footing equals 1.25 B), the influence zone underneath the footing extended to 1.82 B (i.e., approximately 0.57B in the natural soil); and subsequently part of the stresses transferred to the natural soil. Therefore, if the natural soil gets weaker, more footing settlement will be anticipated. However, if the backfill layer is thick enough, the influence zone extent will be contained within the backfill layer, and the effect of the natural soil will be eliminated.

3.6 SUMMARY AND CONCLUSIONS

Three full-scale field tests were conducted to investigate the advantages of using type A tire-derived aggregate (TDA) as a backfill material underneath footings, and to compare TDA performance with that of conventional backfill materials. In addition, 3D finite element analyses were used to identify the failure mechanisms of the rigid footings over a TDA layer, and the models developed were validated against the field test results. An extensive parametric study was then performed to examine the effect of key parameters on the footing performance. The conducted parametric study included varying the following parameters: i) TDA layer thickness ranging from 0.3H to 0.7H (total backfill height), ii) Internal friction angle of the top granular backfill ranging from 28° to 44°, iii) Footing width, B, ranging from 0.5H to 2H, iv) Foundation depth, D_F, ranging from 0B to 2.5 B, v) Footing shape (square, circular, rectangular and strip foundations), and vi) Different subsurface conditions (hard, stiff, medium, and soft clay). Based on this research, the following conclusions can be drawn:

- The field test results show that, in comparison to the use of conventional backfill, the use of a TDA layer underneath shallow foundations achieves a significant improvement in transferring the stresses and reducing the stress influence zone underneath the footing.
- In the case of setups with an underlying TDA layer (F2 and F3), punching shear failure of the top granular layer is encountered, and this controls the footing behaviour.
- For a given settlement value, the corresponding sustained stresses on the footing decrease linearly as the thickness of the TDA layer increases.

- The use of denser soils (with a high internal friction angle, φ') in the top backfill layer above the TDA significantly improves the performance, because such soils form a firm layer that distributes the stress over a wider area. In contrast, loose materials in the top backfill layer result in a conical deformation over the TDA layer, thus causing the stresses to be transferred to a smaller area.
- Foundation depth is an important parameter governing the footing performance. For example, where B is the footing width, for a settlement value of 25 mm, the applied stress increases by 155% and 225% as the foundation depth increases from 0 B to 1 B, and from 0 B to 2.5 B, respectively.
- It can be concluded that as the width of the footing decreased with respect to the thickness of the top granular layer (t_g), the footing performance was governed by the top granular layer and the corresponding settlement decreased. While, the TDA layers controlled the behaviour if the footing width increased with respect to the top granular layer thickness; where most of the stresses were accommodated by the TDA.
- Square and circular footings yield similar values for the stress-settlement relationship.
- For rectangular footings with (L/B) aspect ratios ranging from 1 and 10, the stress capacity decreases gradually as the aspect ratio increases. However, further increasing the aspect ratio above a value of 10 has little effect on the footing behaviour.
- As natural soil conditions become weaker, footing settlement in response to applied stresses increases. However, a TDA layer can help to eliminate this effect by ensuring that the natural soil is beyond the footing stress influence zone.

Table 3.1: Parameters used in the FEA

Layers	Constitutive model	Unit weight (kN/m^3)	E (MPa)	E_{50} (MPa)	E_{oed} (MPa)	Cohesion (kPa)	Angle of internal friction (°)
*Natural soil	MC	18	30	-	-	22	20
Gravel A1	MC	22.5	40^{+}	-	-	-	44
TDA	**HSM	7	-	2.75	2.2	24	26.5
Concrete	Elastic Model	24	39000	-	-	-	-

Note: E = modulus of elasticity; E_{oed} = tangent stiffness from odometer test; E_{50} = secant modulus; HSM= hardening soil model; MC = Mohr-Coulomb.

*Undrained condition.

**The properties at P_{ref} = 25 kPa and R_f=0.95.

+This value was used for the verification of setup F1. For the remaining models in the parametric study, E=10.6+34.84 Z was used; where Z is the depth (m).

Table 3.2: Parametric study

Model group	**Footing width (*B*)**	**Backfill height (*H*)**	**TDA thickness (*t*)**	**Foundation depth (D_F)**	**Aspect ratio (*L/B*)**	***(φ')* of the granular material**	**Natural soil**
G1	0.8 m	1.25 B	(0.1, 0.2, 0.3, 0.4, 0.5, 0.6, 0.7) H	0 B	1	44°	Till
G2	0.8 m	1.25 B	0.5 H	0 B	1	28°, 32°, 36°, 40°, and 44°	Till
G3	0.8 m	1.25 B	0.5 H	(0, 0.25, 0.5, 1.0, 1.25, 1.5, 2, and 2.5) B	1	44°	Till
G4	(0.25, 0.5, 0.8, 1, 1.25, 1.5 and 2) H	1.0 m	0.5 H	0 B	1	44°	Till
G5	0.8 m	1.25 B	0.5 H	0 B	1, 2, 5, 10, 15, and 20	44°	Till
G6	0.8 m	1.25 B	0.5 H	0 B	1	44°	Hard, stiff, medium, and soft clay

Table 3.3: Soil properties for the soils used in the parametric study

Layers	E (MPa)	Undrained shear strength (kPa)	Cohesion (kPa)	Angle of internal friction (°)
*Hard clay	30	120	22	20
Stiff clay	20	80	20	18
Medium clay	8	50	15	16
Soft clay	4	25	10	15

*The natural soil

** The values for the stiff, medium and soft clay was selected from reasonable ranges from Look (2014), and Obrzud and Truty (2012)

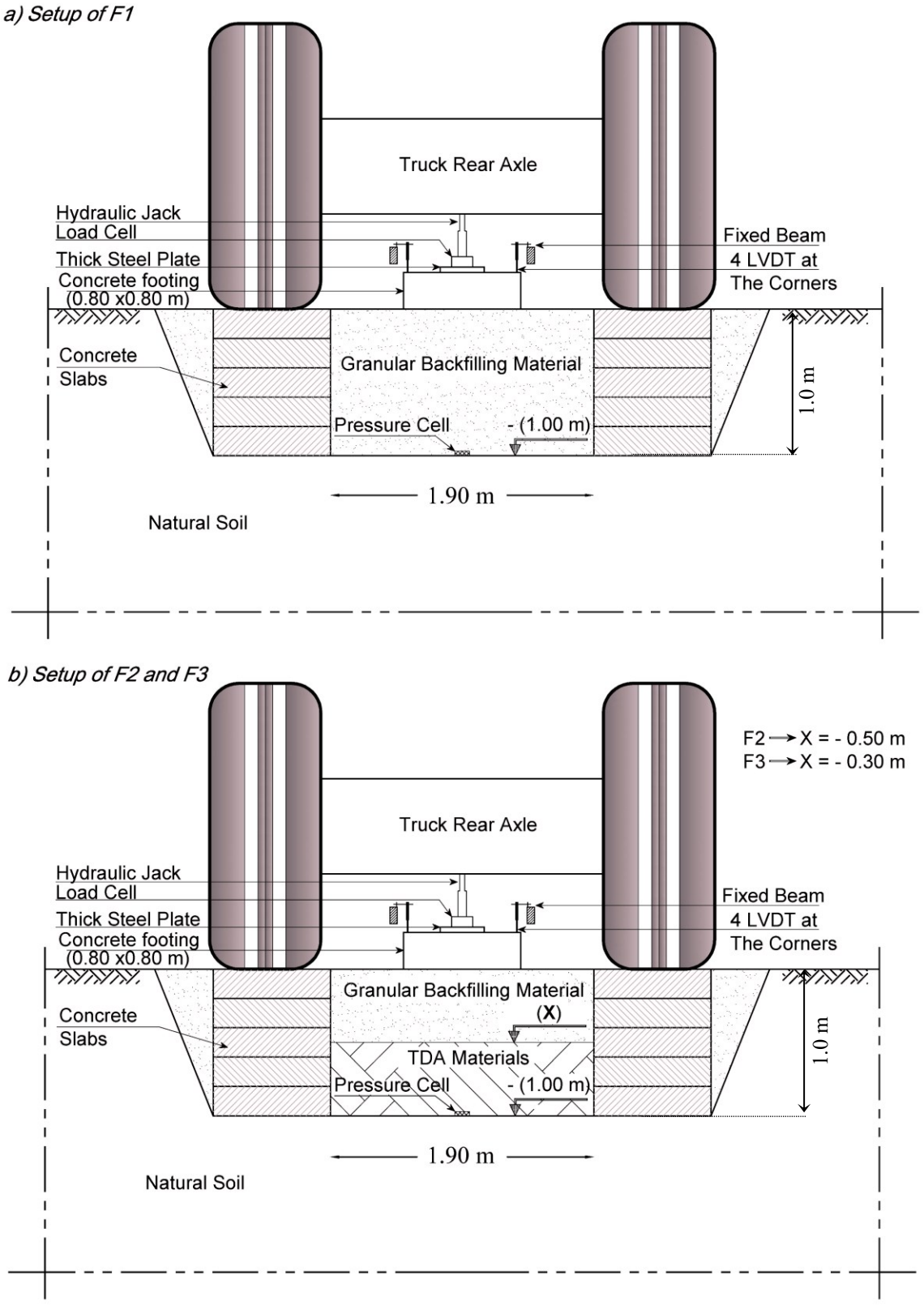

Figure 3-1 Layout of the field tests a) setup of F1, and b) setup of F2 and F3

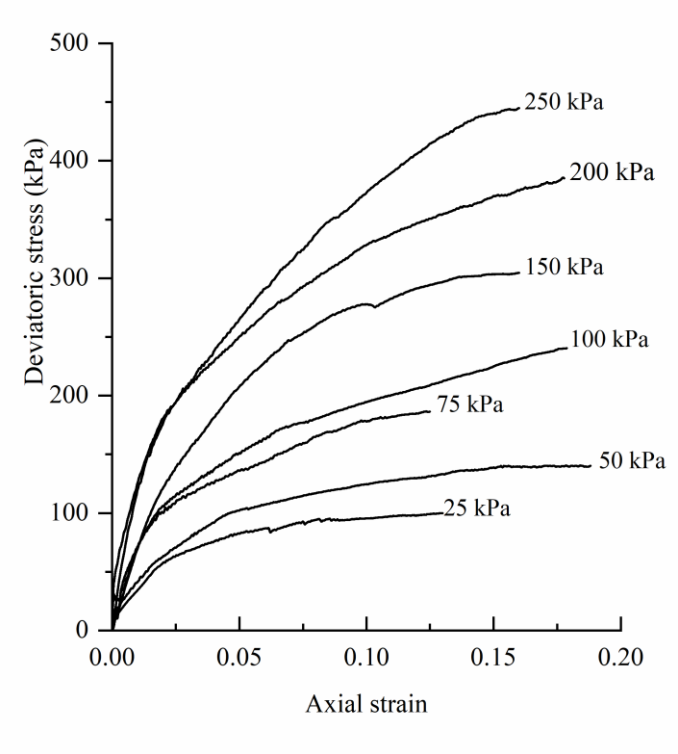

Figure 3-2 Deviatoric stress vs. axial strain for the TDA materials (Ashari Ghomi 2018)

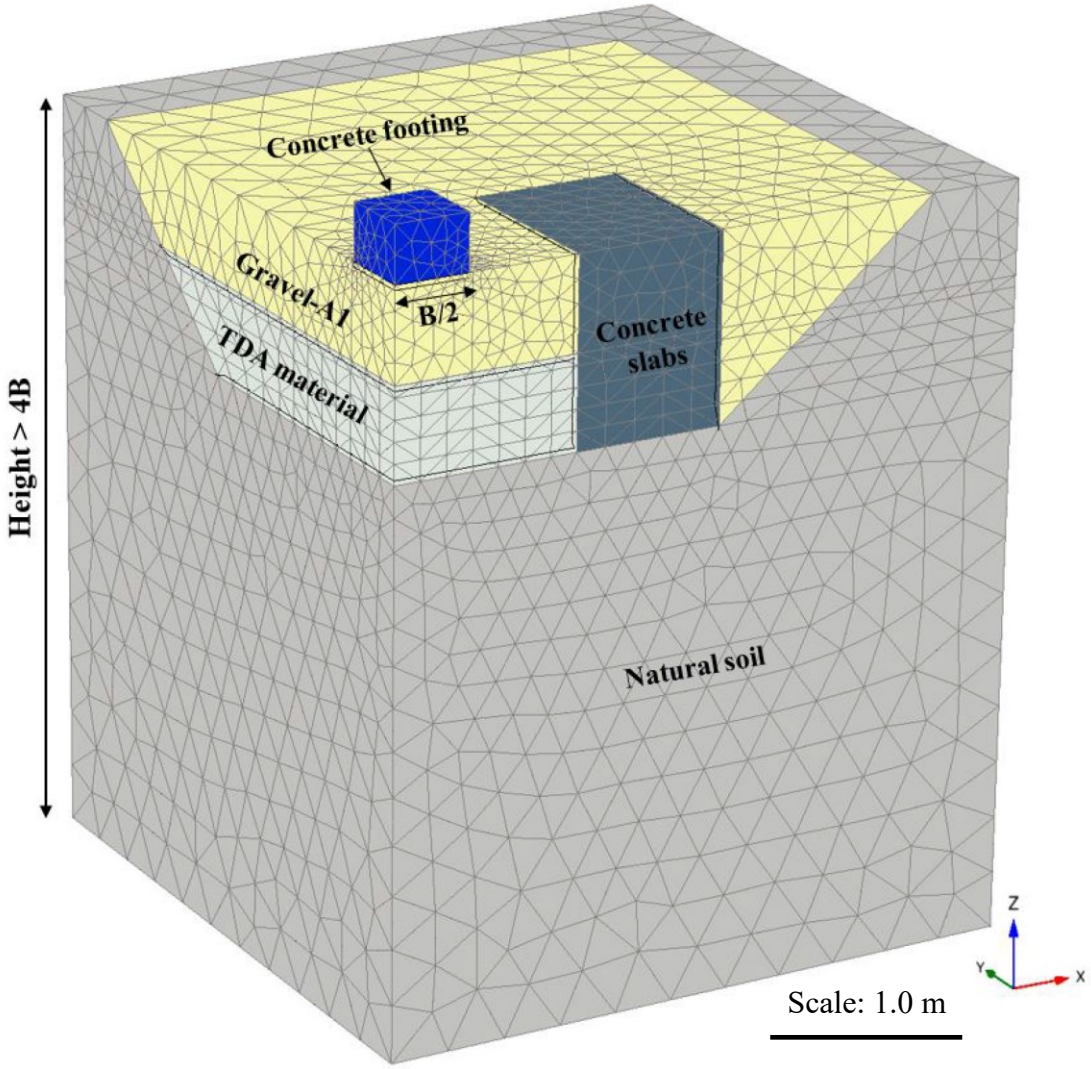

Figure 3-3 FE model of setup 2

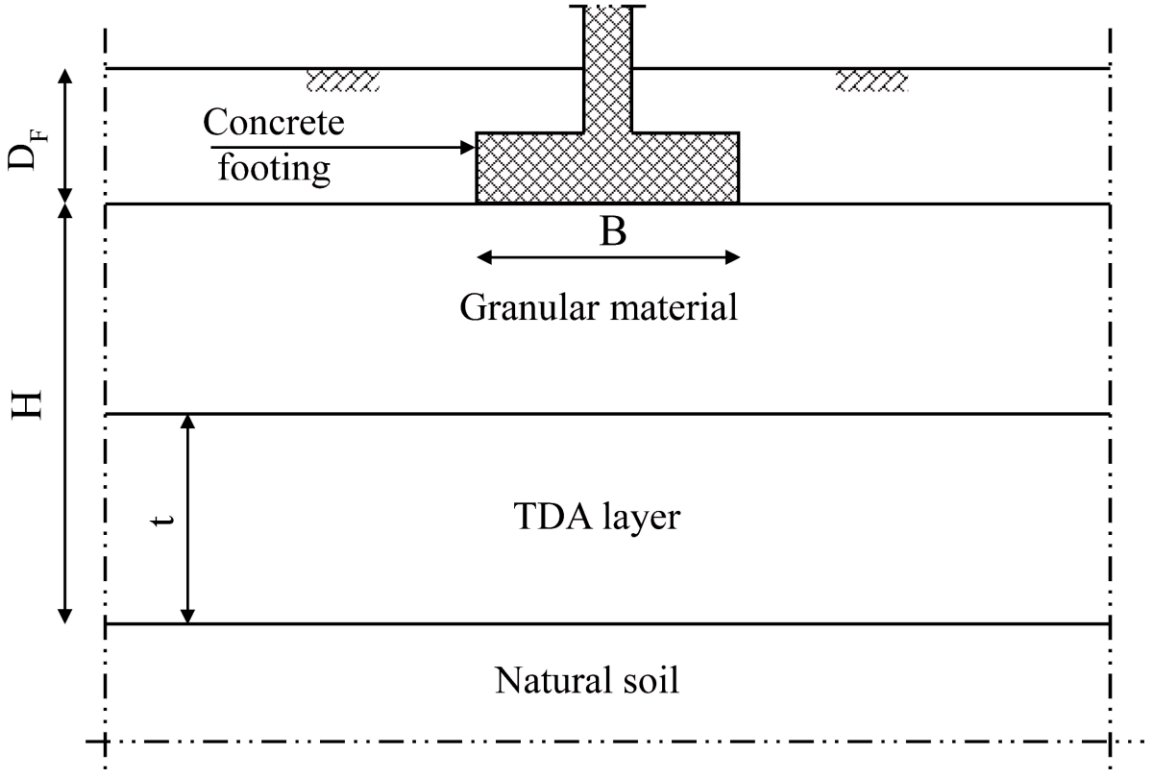

Figure 3-4 Key parameters of the parametric study

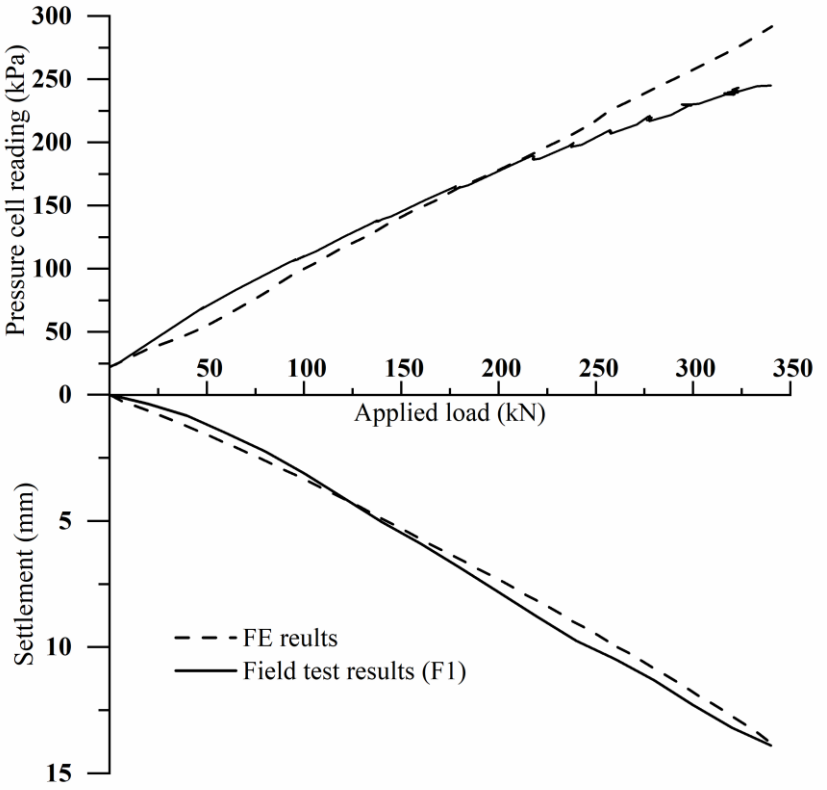

Figure 3-5 Comparison between field test measurements and FE model results for setup F1

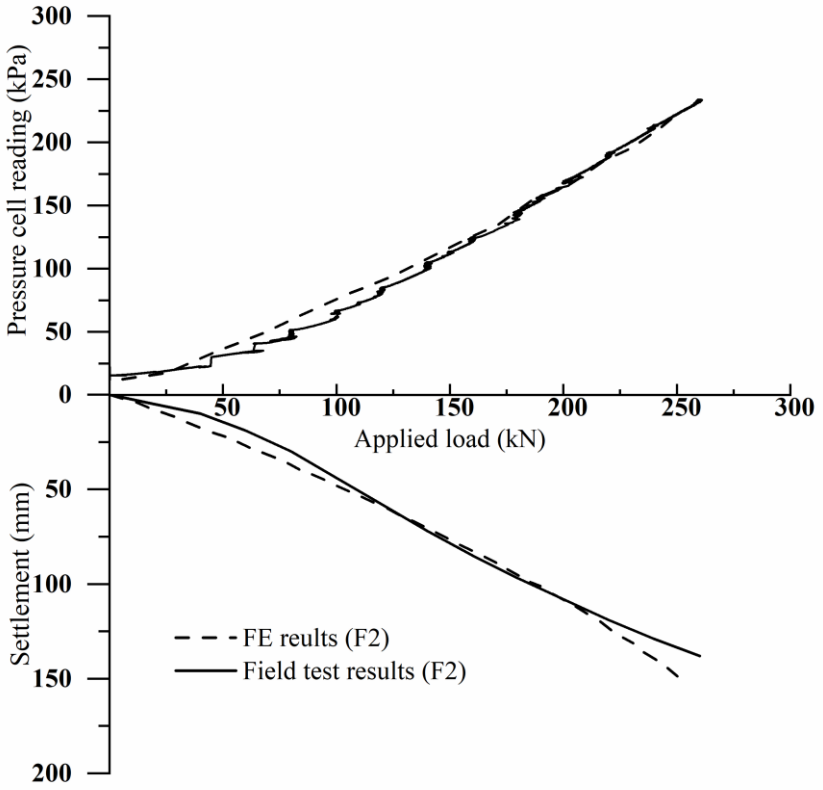

Figure 3-6 Comparison between field test measurements and FE model results for setup F2

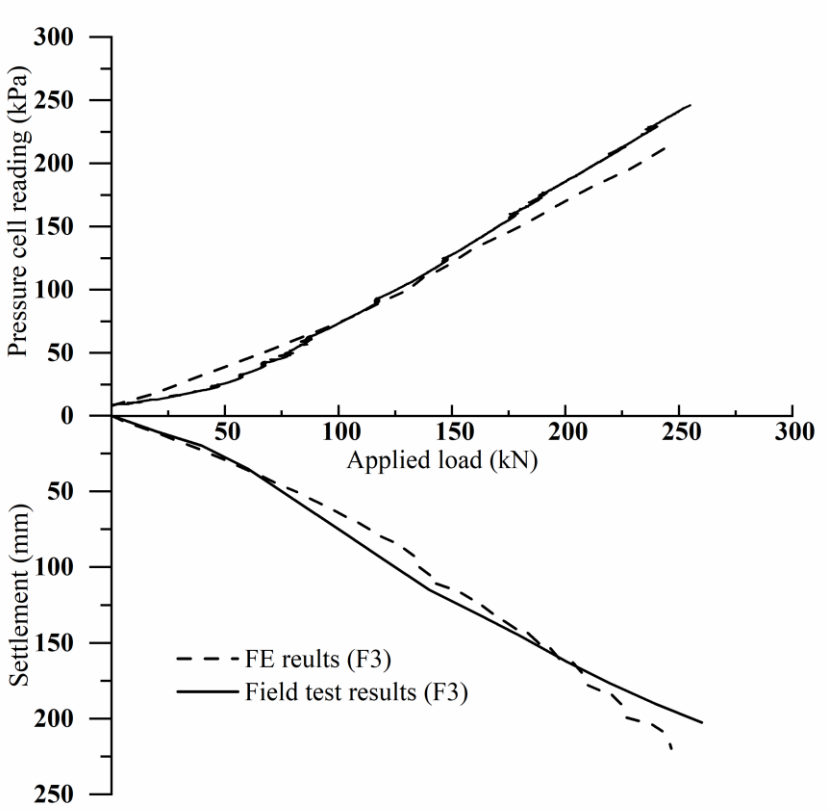

Figure 3-7 Comparison between field test measurements and FE model results for setup F3

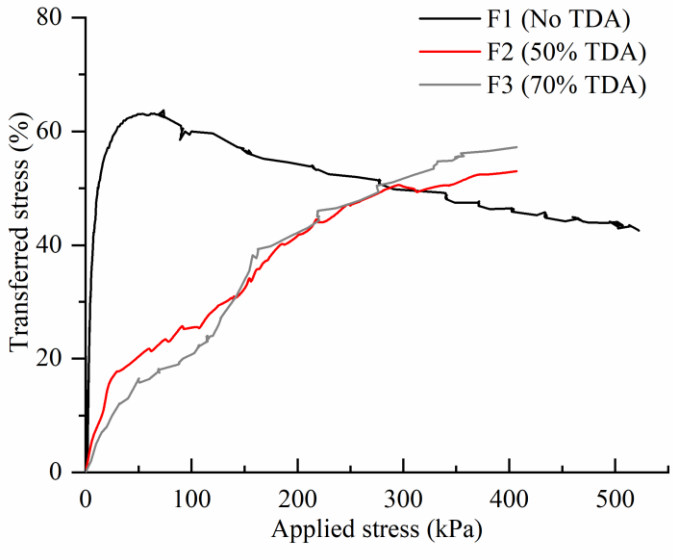

Figure 3-8 Percentage of stress transferred throughout the backfill layers of the three test setups

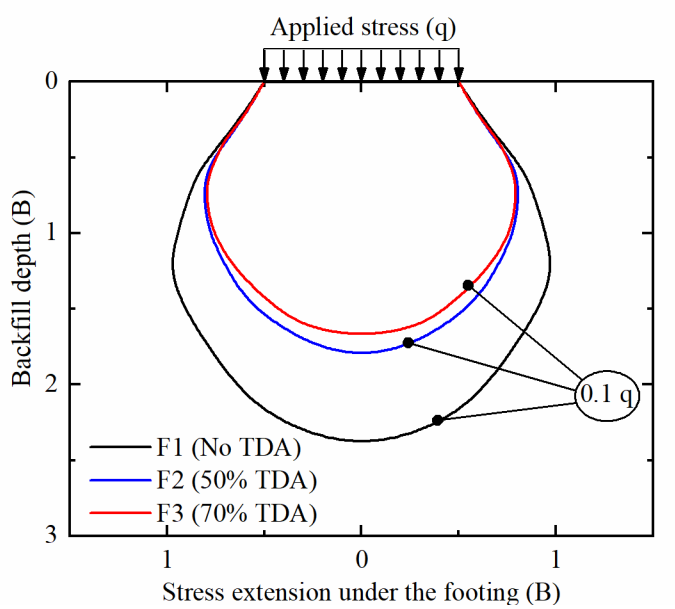

Figure 3-9 Stress influence zone underneath the test footings for setups F1, F2, and F3

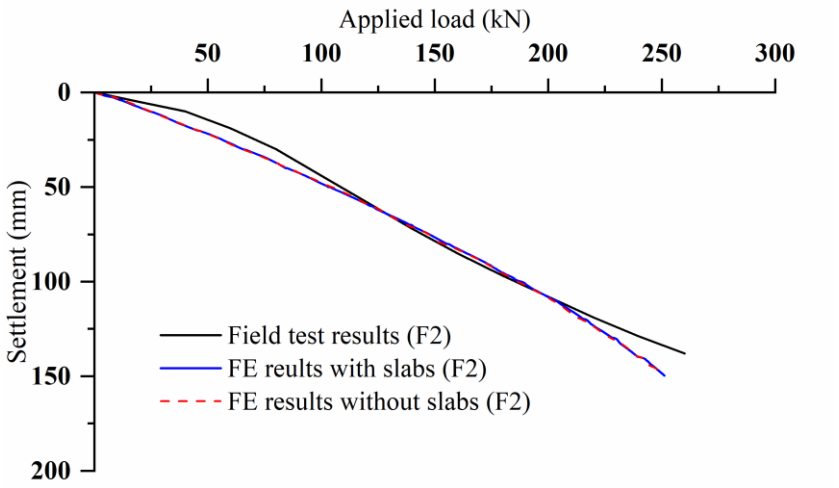

Figure 3-10 Effect of the concrete slabs on the footing behaviour in setup F2

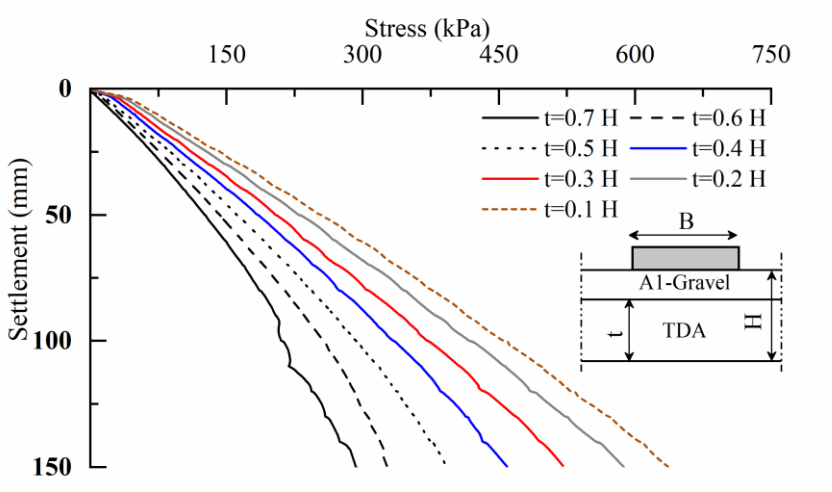

Figure 3-11 Footing stress-settlement relationships for different TDA layer thicknesses

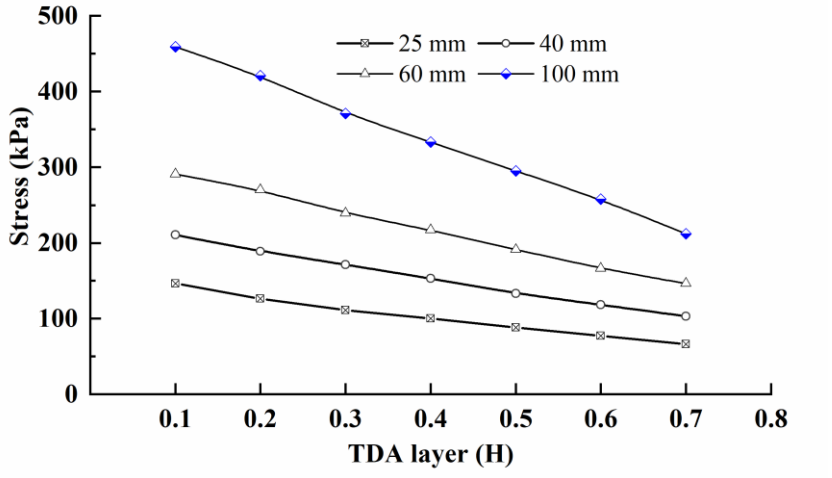

Figure 3-12 Effect of changing the TDA layer thickness for different settlement values

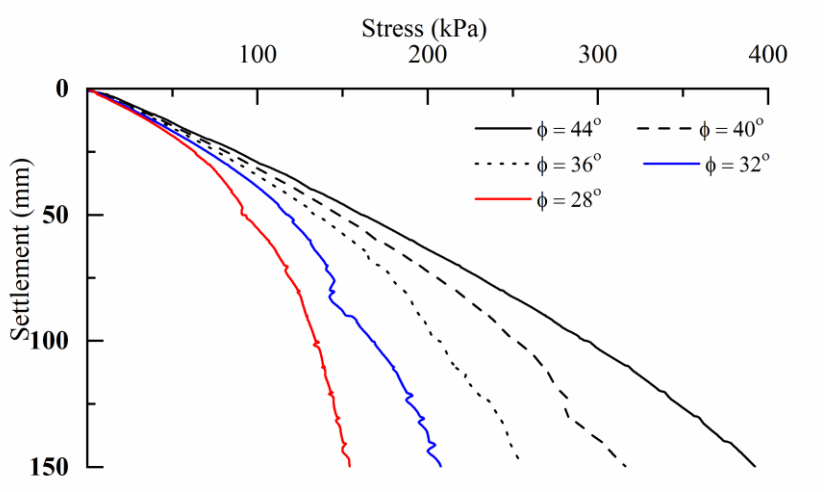

Figure 3-13 Effect of changing the internal friction angle of the granular material in the top backfill layer on the footing performance

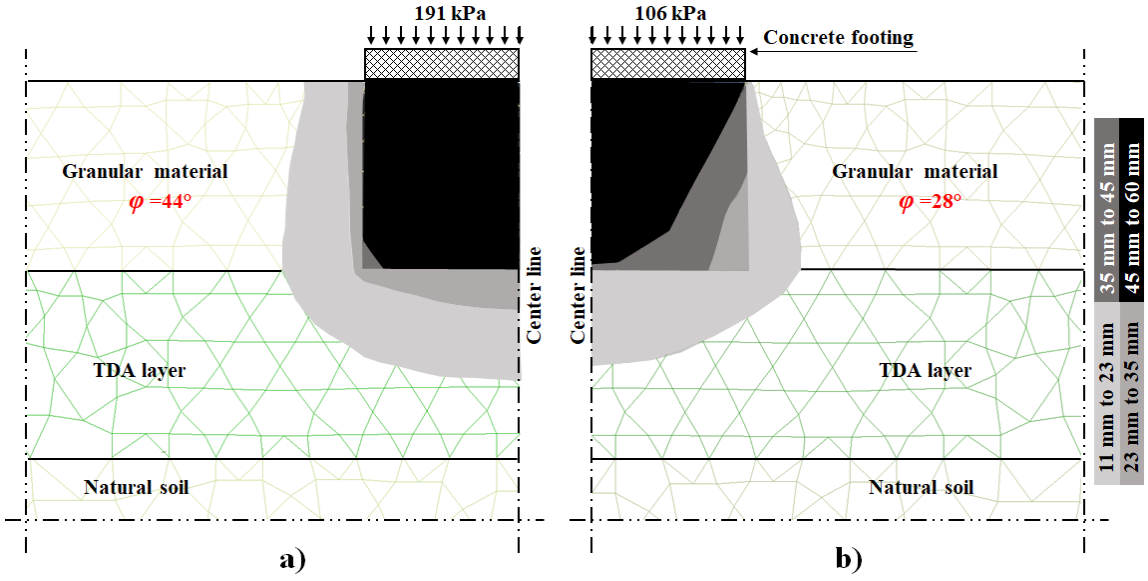

Figure 3-14 Soil deformation contours obtained by using a) very dense granular materials, and b) loose granular materials

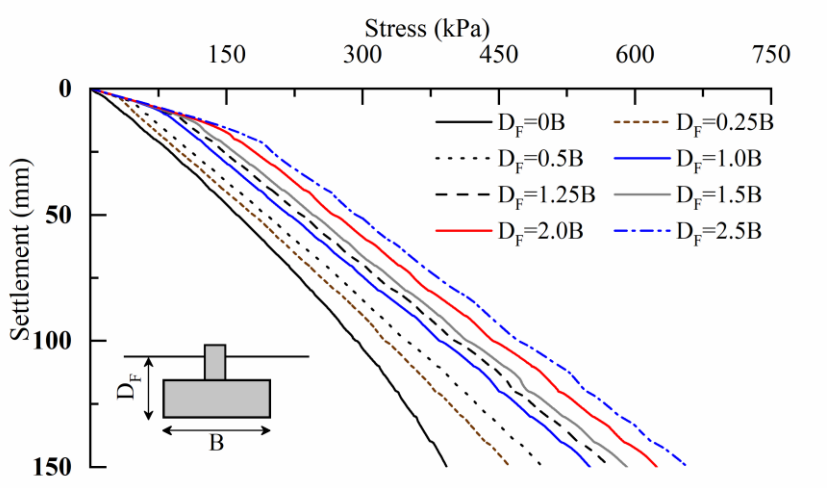

Figure 3-15 Effect of changing the foundation depth on the footing performance

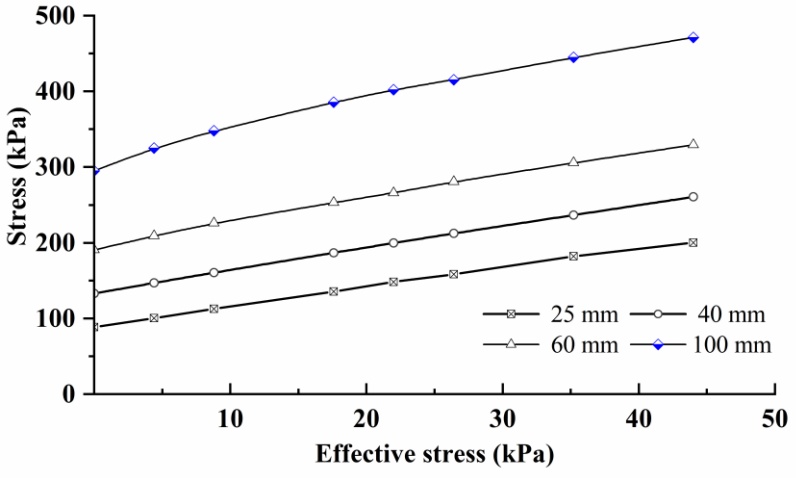

Figure 3-16 Effect of changing the effective stress at the foundation level on the footing bearing capacity

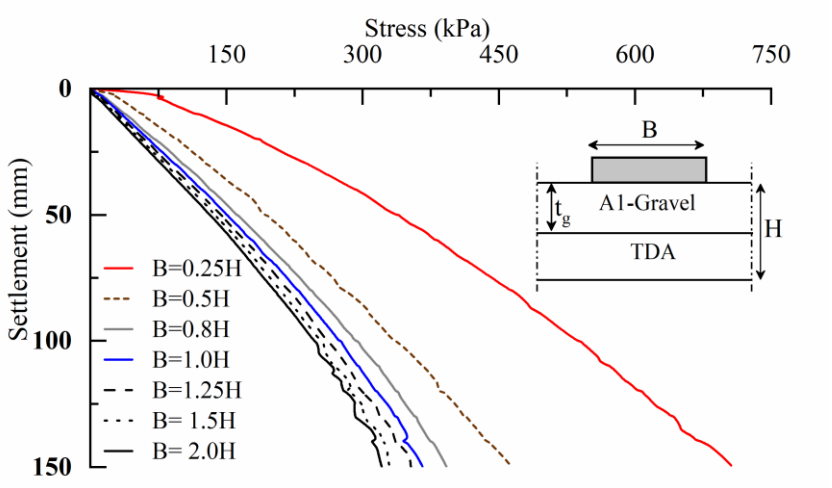

Figure 3-17 Effect of changing the footing width on the footing performance

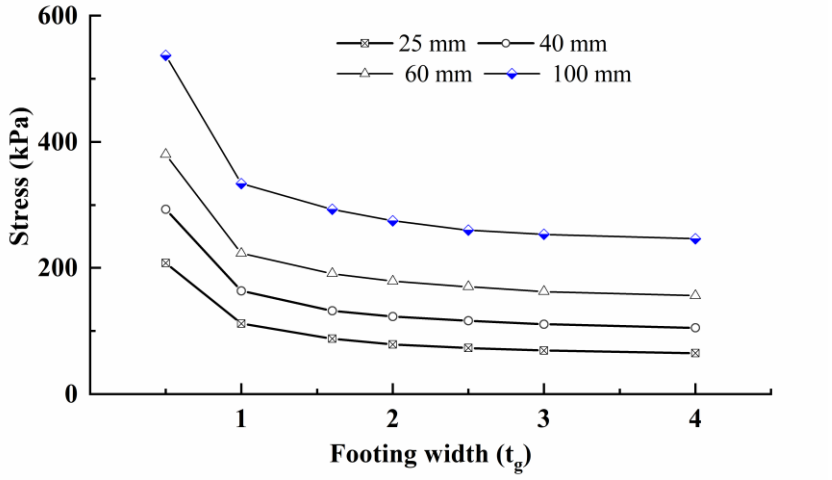

Figure 3-18 Effect of changing the footing width expressed as a function of the thickness of the top granular layer, for different settlement values

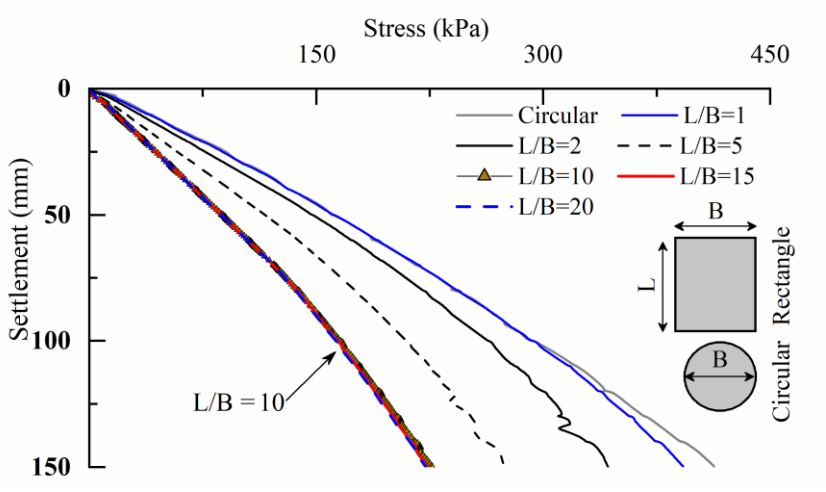

Figure 3-19 Effect of the footing geometry on the footing performance

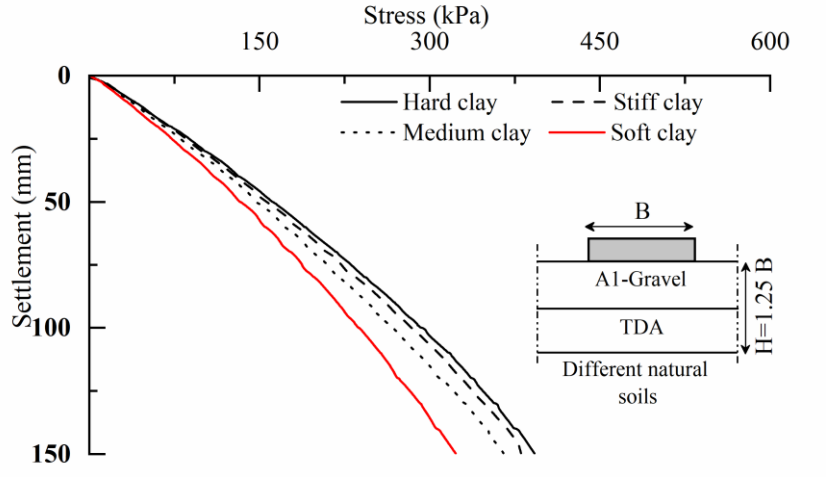

Figure 3-20 Effect of changing the natural soil conditions on the footing performance

3.7 REFERENCES

Ahmed I and Lovell CW (1993) Rubber soils as lightweight geomaterials. Transportation Research Record **1422**: 61–70.

Ahn I-S and Cheng L (2014) Tire derived aggregate for retaining wall backfill under earthquake loading. Construction and Building Materials **57**: 105–116, https://doi.org/10.1016/ j. conbuildmat.2014.01.091.

Ahn I-S, Cheng L, Fox PJ, Wright J, Patenaude S and Fujii B (2014) Material properties of large-size tire derived aggregate for civil engineering applications. Journal of Materials in Civil Engineering **27(9)**.

Ashari Ghomi M (2018) Large-scale triaxial testing of sustainable TDA backfilling alternatives. Master's thesis. Dalhousie University, https://dalspace.library.dal.ca/bitstream/handle/10222/73810/AshariGhomi-Mohammad-CIVL-March-2018.pdf?sequence=1.

Ashari M and El Naggar H (2017) Evaluation of the physical properties of TDA-sand mixtures. In GeoOttawa, the 70th Canadian Geotechnical Conference Ottawa. Canadian Geotechnical Society.

ASTM (1997) D 1196-93: Nonrepetitive static plate load tests of soils and flexible pavement components, for use in evaluation and design of airport and highway pavements. ASTM International, West Conshohocken, PA, USA.

ASTM (2012) D 6270-12: Standard practice for use of scrap tires in civil engineering applications. ASTM International, West Conshohocken, PA, USA.

ASTM (2017) D 2487-17: Classification of soils for engineering purposes (Unified Soil Classification System). ASTM International, West Conshohocken, PA, USA.

Benson CH, Olson MA and Bergstrom WR (1996) Temperatures of insulated landfill liner. Transportation Research Record **1534(1)**: 24–31, https://doi.org/10.3141/1534-05.

Bosscher PJ, Edil TB and Eldin NN (1992) Construction and performance of shredded waste-tire test embankment. Transportation Research Record **1345**: 44–52.

Eaton RA, Roberts RJ and Humphrey DN (1994) Gravel Road Test Sections Insulated with Scrap Tire Chips: Construction and First Year's Results. US Army Corps of Engineers, Cold Regions Research and Engineering Laboratory, Hanover, NH, USA. Special Report 94-21.

Edil TB, Fox PJ and Ahl SW (1992) Hydraulic conductivity and compressibility of waste tire chips. In 15th Madison Waste Conference, University of Wisconsin-Madison, Engineering Professional Development Department, Madison, WI, USA, pp. 49–61.

Edil TB and Bosscher PJ (1994) Engineering properties of tire chips and soil mixtures. Geotechnical Testing Journal **17(4)**: 453–464, https://doi.org/10.1520/GTJ10306J.

El Naggar H, Soleimani P and Fakhroo A (2016) Strength and stiffness properties of green lightweight fill mixtures. Geotechnical and Geological Engineering **34(3)**: 867–876, https://doi.org/10.1007/s10706-016-0010-1.

Hoppe EJ (1998) Field study of shredded-tire embankment. Transportation Research Record **1619(1)**: 47–54, https://doi.org/10.3141/1619-06.

Humphrey DN (2005) Tire Derived Aggregate – A New Road Building Material. In Seventh International Conference on the Bearing Capacity of Roads, Railways and Airfields, Trondheim, Norway, ARRB Group Limited, Vermont South, Australia.

Humphrey DN (2008) Tire derived aggregate as lightweight fill for embankments and retaining walls. In *Scrap Tire Derived Geomaterials — Opportunities and Challenges* (Hazarika H and Yasuhara K (eds)). Taylor & Francis Group, London, UK, pp. 59–81.

Humphrey DN and Eaton RA (1995) Field performance of tire chips as subgrade insulation for rural roads. In Sixth International Conference on Low-Volume Roads, Minneapolis, MN, Transportation Research Board, Washington, DC, USA, pp. 77–86.

Humphrey D and Blumenthal M (2010) The use of tire-derived aggregate in road construction applications. In *Green Streets and Highways 2010: An Interactive Conference on the State of the Art and How to Achieve Sustainable Outcomes*. ASCE, Reston, VA, USA, pp. 299–313.

Lawrence B, Humphrey D and Chen L-H (1999) Field trial of tire shreds as insulation for paved roads. In *Tenth International Conference on Cold Regions Engineering: Putting Research into Practice*. ASCE, Reston, VA, USA, pp. 428–439.

Look B (2014) Handbook of geotechnical investigation and design tables. CRC Press.

Mahgoub A and El Naggar H (2019) Using TDA as an engineered stress-reduction fill over preexisting buried pipes. Journal of Pipeline Systems Engineering and Practice **10(1)**, https://doi.org/10.1061/(ASCE)PS.1949-1204.0000362.

Mills, B., H. El Naggar, and A. J. Valsangkar. 2015. "North American overview and Canadian perspective on the use of tire derived aggregate in highway embankment construction." Chap. 22 in Vol. 2 of Ground improvement case histories, edited by Indraratna and Chu. New York: Elsevier.

Plaxis B (2016) Reference manual for PLAXIS 2D. Delft, Netherlands.

Pierre DKS (2013) Canadian waste tire practices and their potential in sustainable construction. Dalhousie Journal of Interdisciplinary Management **9(1)**.

Obrzud R and Truty A (2012) The hardening soil model-a practical guidebook z soil. PC100701 Report.

Rashwan S and Charette P (2015) Demonstration of the Viability of Using Tire Derived Aggregate (TDA) to Replace Natural Material (NM) in Residential Home Basement Construction. Summary report of the demonstration project at 263 Waverly Street, Winnipeg, Manitoba, Canada.

Rubber Manufacturers Association (2017) US scrap tire management summary 2005–2009. Rubber Manufacturers Association, Washington, DC, USA.

Salgado R, Yoon S and Siddiki NZ (2003) Construction of Tire Shreds Test Embankment. FHWA/IN/JTRP-2002/35, Joint Transportation Research Program, Indiana Department of Transportation and Purdue University, West Lafayette, IN, USA https://doi.org/10.1520/JAI103711.

Sparkes J, El Naggar H and Valsangkar A (2019) Compressibility and shear strength properties of tire-derived aggregate mixed with lightweight aggregate. Journal of Pipeline Systems Engineering and Practice **10(1)**, https://doi.org/10.1061/(ASCE)PS.1949-1204.0000354.

Tweedie JJ, Humphrey DN and Sandford TC (1998) Full-scale field trials of tire shreds as lightweight retaining wall backfill under at-rest conditions. Transportation Research Record **1619**: 64–71, https://doi.org/10.3141/1619-08.

Wartman J, Natale M and Strenk P (2007) Immediate and time-dependent compression of tire derived aggregate. Journal of geotechnical and geoenvironmental engineering, 133(3), pp.245-256.

Wolfe SL, Humphrey DN and Wetzel EA (2004) Development of tire shred underlayment to reduce groundborne vibration from LRT track. In GeoTrans 2004, Los Angeles, CA. ASCE, Reston, VA, USA, pp. 750–759.

Xiao M, Bowen J, Graham M and Larralde J (2012) Comparison of seismic responses of geosynthetically reinforced walls with tire-derived aggregates and granular backfills. Journal of Materials in Civil Engineering **24(11)**: 1368–1377, https://doi.org/10.1061/(ASCE)MT.1943- 5533.0000514.

Yoon S, Prezzi M, Siddiki NZ and Kim B (2006) Construction of a test embankment using a sand-tire shred mixture as fill material. Waste Management **26(9)**: 1033–1044, https://doi.org/10.1016/j.wasman.2005.10.009.

CHAPTER 4 USING TDA UNDERNEATH SHALLOW FOUNDATIONS: SIMPLIFIED DESIGN PROCEDURE

Ahmed Mahgoub and Hany El Naggar

4.1 INTRODUCTION

Shallow foundations are the simplest and most common type of foundation. In many instances, they are the most cost-effective choice to support superstructures, because they are relatively inexpensive to construct and do not require specialized construction equipment (Das 2016). Shallow foundations serve to distribute structural loads from the superstructure over larger areas of near-surface soil, so as to lower the magnitude of stresses induced by the applied loads to levels that can be tolerated by the foundation soils (Bowles 2001). When subsurface conditions are appropriate, shallow foundations can be used in various applications ranging from footings for signposts, to footings under buildings, to strip footings supporting retaining walls, to bridge piers and abutments. Isolated footings, which are the most common type of shallow foundation, are used to support single columns and their size is calculated based on the load acting on the supported columns and the allowable bearing capacity of the soil (Das 2016).

The distribution of soft soils in Canada and worldwide is very extensive (Quigley 1980, Lefebvre 1981 and Lefebvre et al. 1988). Buildings and other surface structures constructed on soft soils often face serious safety issues, where inadequate subsurface bearing capacity results in sliding failures and structural damage, leading to significant social and economic loss. Lightweight fills have been used in the foundation design of various projects on soft soils, to reduce the possibility of ultimate failure and serviceability failure (Stark et al.

2004, Zornberg, et al. 2005, and Elias et al. 2006). Ultimate failure is commonly described as the total collapse of the foundation. This failure mode is associated with the strength of the subsurface soil and is due to the bearing capacity failure of the soil beneath the foundation. The use of lightweight fills rather than conventional fill materials can reduce the load induced on underlying soils, thus providing a greater factor of safety to guard against ultimate failure. In contrast, serviceability failures can generally be described as settlement or movements of the foundation, i.e., excessive total settlements and/or differential settlements that would cause the foundation to be deemed unusable. Serviceability failures are generally associated with the compression of the subsurface soil underneath the foundation. Because lightweight fills reduce the load induced on underlying soils, they reduce the corresponding settlement.

Tire-derived aggregate (TDA) has been used for decades as a lightweight fill material for the construction on soft ground of roads, embankments, noise barriers, landslide stabilization measures, retaining wall backfill, building foundations, and bridge and road banks (Bosscher et al. 1992; Upton and Machau 1993; Engstrom and Lamb 1994; Humphrey and Eaton 1995; Dickson et al. 2001; Shalaby and Ahmed-Khan 2002; Humphrey 2008; Mills et al. 2015; El Naggar et al. 2016, Sparks et al. 2019; and Mahgoub and El Naggar 2019). TDA is an engineered fill material produced by shredding scrap tires into sizes ranging from 12 mm to 305 mm. In the literature, TDA is referred to as tire chips or tire shreds, depending on the particle size. ASTM (2012) specifies two TDA size ranges: Type A with a particle size ranging from 12 mm to 50 mm, and type B with a particle size ranging from 50 mm to 305 mm. TDA has excellent geotechnical properties, maintains its structural integrity, and weighs 60% less than coarse sand and as much as 70% less than

conventional gravel. This use of recycled tires has been growing exponentially over the past decade due to increasing environmental awareness, shrinking landfill resources, and advances achieved in the relevant processing technologies and equipment (Rashwan, 2015). The cost of TDA is only around 25% of the cost of conventional granular backfill (Humphrey 2008).

The light weight of TDA, combined with its structural integrity, thermal insulation capabilities and reasonable price, makes it suitable for use as an engineered backfill underneath shallow foundations. Rashwan (2015) used TDA as a backfill material around basement walls and beneath basement slabs (not the building footings). He reported that in comparison to conventional backfill materials, TDA resulted in a significant reduction of lateral earth pressures on the basement walls. Furthermore, there was a substantial improvement in heat insulation through the basement walls and slabs. The study also showed that the good drainage capability of TDA resulted in reduced moisture retention on the basement walls.

Mahgoub and El Naggar (2019a) used TDA as an engineered stress-reduction fill to protect pre-existing pipes located underneath shallow foundations. The study included two full-scale field tests to evaluate the merits and practicality of using a layer of TDA above existing metal pipes to enhance the stress arching mechanism. The paper also included extensive three-dimensional numerical modelling to investigate the effect of changing several key parameters (i.e., the thickness of the TDA layer, the shape and configuration of the TDA cross-section, and the pipe stiffness) on the performance of the system investigated.

In another study, Mahgoub and El Naggar (2019b) investigated the use TDA underneath shallow foundations, via three full-scale field tests and a comprehensive numerical modelling program. Rigorous 3D finite element models were developed to examine the failure mechanism of the proposed shallow foundation system and to study the effect on footing performance of key parameters including the TDA layer thickness, the internal friction angle (φ) of the upper granular backfill, the foundation depth, the footing width, the footing shape, and various subsurface conditions. It was shown that the use of a TDA layer as backfill underneath shallow foundations resulted in a significant improvement in transferring the stresses and reducing the stress influence zone underneath the footings in comparison to the use of conventional granular backfill. The results of the study combined with additional finite element (FE) analyses have been used to develop the desired simplified design equations presented in this paper, which permit calculation of the bearing capacity of backfill including TDA underneath a shallow foundation.

Limited information exists concerning design procedures and methodologies for using TDA underneath shallow foundations. The lack of comprehensive design methodology and guidelines is hindering the utilization of TDA in such applications. Hence, the main objective of this paper is to develop a design procedure for shallow foundations built over TDA layers.

Classical bearing capacity theories for shallow foundations were first developed for plane strain conditions, assuming that the supporting soil layer is relatively homogeneous and that the zone of shear deformation beneath the foundation is uniform. These approaches were eventually developed further to account for other factors that influence the bearing capacity, such as footing shape and depth, and soil anisotropy and nonuniformity. Shallow

foundations built over a TDA layer always include a layer of conventional granular backfill of limited thickness immediately below the foundation and above the TDA layer. If foundations rest on a relatively thin dense layer above the TDA layer, they may break through the dense layer into the TDA. In contrast, if the granular backfill layer above the TDA is weak and relatively thick, bearing capacity failure may be limited to the top stratum, unless both layers have relatively comparable individual bearing capacities. Since in this case the ultimate bearing capacity depends on the soil-structure interaction between the soil and the foundation, and the interaction between the conventional backfill layer and the underlying TDA layer, a semi-empirical design method utilizing regression analysis techniques is developed in this paper, based on the results of field tests and extensive numerical modelling presented in Mahgoub and El Naggar (2019b). The semi-empirical method developed is similar to the established design approach for shallow foundations, where a general bearing capacity formula is used together with specific bearing capacity factors that rely on effective strength parameters and various correction factors accounting for different aspects. The proposed design method estimates the ultimate bearing capacity of shallow foundations built over a TDA layer, taking into account the granular layer thickness, TDA layer thickness, footing width, footing shape, footing depth, and allowable settlement. The design equations developed are then validated by comparing their results to those obtained from finite element models for three different cases.

4.2 CASE STUDY USED TO DEVELOP THE DESIGN

In Mahgoub and El Naggar (2019b), three rigid square concrete footings (F1, F2 and F3) were constructed, instrumented and tested, as illustrated in Figure 4-1, to examine the behaviour of shallow foundations on a backfill of TDA materials. For the first footing (F1),

which served as the control case, 1.0 m of conventional compacted granular backfill was utilized to replace the soil beneath the concrete footing. The second footing (F2) was cast on a replacement layer comprised of 0.5 m of conventional granular materials overlying 0.5 m of TDA materials. For the third footing (F3), the replacement layer consisted of 0.3m of conventional granular materials overlying 0.7 of TDA materials. To investigate the performance of each configuration, field tests were designed to measure the loads applied to the concrete footings, the corresponding footing settlement, and the stresses beneath the replacement layer.

The TDA material used in this research was manufactured from shredded scrap tires of passenger cars and was classified as type A, in accordance with ASTM D6270-08. The TDA had a unit weight of 7 kN/m^3, with particle sizes ranging from 13 mm to 63 mm. Comprehensive material characterization tests (e.g., sieve analyses and triaxial tests) were performed to determine the geotechnical properties of the TDA used. Figure 4-2 shows the particle size distribution of the TDA material used, together with the results of triaxial testing as described in Ashari and El Naggar (2017). From the triaxial test results it was determined that the angle of internal friction $\varphi = 26.5°$ and the cohesion c' = 24 kPa. The TDA parameters obtained were used successfully to verify several finite element models against field studies, as described in Mahgoub and El Naggar (2019a) and Mahgoub and El Naggar (2019b).

Two sets of FE models were developed in this study, with the aid of PLAXIS 3D. A hardening soil model, used to simulate the TDA behaviour, was validated against the results of large triaxial tests on the TDA. The first set of FE models simulated the three full-scale tests to validate the models developed. The second set of FE models included an

intensive parametric study to examine the effect of key parameters on the behaviour of shallow foundations above a TDA layer. These parameters were the thickness of the TDA layer, different subsurface conditions, the foundation depth, various footing shapes, and the footing width.

Figure 4-3 compares the results of the field tests to the results of the FE analyses developed in the first set of models. The results show the relationship between the applied stresses and corresponding settlements, and the stresses transferred through the backfill of the different configurations tested. The FE models follow the dimensions, material properties and construction sequence of the field tests. The excellent match between the results of the FE models and those of the field tests demonstrates that the problem can be simulated by FE modelling. It can be seen from Figure 4-3 that in comparison to the use of conventional backfill, the use of a TDA layer underneath shallow foundations achieves a significant improvement in transferring the stresses and reducing the stress influence zone beneath the footing. It was found that in setups with an underlying TDA layer (setups F2 and F3), punching shear failure of the upper granular layer is encountered, which controls the footing behaviour.

The key parameters investigated in the parametric study were used as input parameters for the proposed design equations. Table 4.1 shows the approach used in the parametric study; more details are explained in Mahgoub and El Naggar (2019b). The following sections provide a comprehensive discussion of how each input parameter contributes to the equations.

4.3 DEVELOPMENT OF THE DESIGN EQUATIONS

The design equations rely on five main parameters that affect footing performance (i.e., the thickness of the TDA layer, the internal friction angle of the upper granular layer, the foundation depth, the footing width, and various footing shapes). The main purpose of the equations is to estimate the bearing capacity of a shallow foundation resting on TDA backfill, for a specific settlement value. Thus, the relationship between the footing sustained stresses and the corresponding settlement can be plotted. Figure 4-4 provides details of the parameters selected for the equations developed.

4.3.1 TDA Layer Thickness

As indicated in Table 4.1, the first group of models (G1) was used to deduce the effect of changing the thickness of the TDA layer on the footing sustained pressure. Figure 4-5 shows that for settlement values of 10 mm, 25 mm, 40 mm, 60 mm, 80 mm, and 100 mm, the footing sustained pressure decreased linearly with increasing TDA layer thickness (t). In Figure 4-5, the settlement values and the TDA layer thickness are normalized with respect to the backfill height (H). Figure 4-5 shows a direct relationship between the sustained pressure (q) and the TDA layer thickness, which can be described by Equation 1.

$$q = a\left(1 - \frac{t}{H}\right) + b \qquad (1)$$

where, a depends on the settlement value and TDA layer thickness utilized, and b is the bearing pressure of the footing when $t = H$, as illustrated in Figure 4-5.

The constants a and b can be calculated by using Equations 2 and 3.

$$a = 2570 \left(\frac{\Delta h}{H}\right)^{0.82} \quad (2)$$

where Δh is the proposed settlement.

$$\frac{b}{P_a} = 11.05 \frac{\Delta h}{H} \quad (3)$$

where P_a is the atmospheric pressure (100 kPa).

4.3.2 Foundation Depth

The foundation depth has a significant effect on footing bearing capacity values. In Figure 4-6, the effective stress at the foundation level, a function of the foundation depth (D_F) and the unit weight of the soil (γ), is plotted against the footing sustained pressure for different settlement values (i.e., 1%, 2.5%, 4%, 6%, 8%, and 10% of the backfill height *H*). It can be seen that, for different settlement values, the applied stresses increase with an approximately constant slope. A regression analysis was conducted by using the FE model results presented in Figure 4-6 to obtain the contributing factor, F_{FD}, for the proposed bearing capacity equation. The inclusion of F_{FD} in the equation yields

$$q = \left[a \left(1 - \frac{t}{H}\right) + b\right] F_{FD} \quad (4)$$

where F_{FD} is the foundation depth factor, which can be calculated by using Equation 5.

$$F_{FD} = c_1 \left(\frac{\gamma D_F}{P_a}\right) + 1 \quad (5)$$

where c_1 is a constant that can be calculated by using Equation 6 or Figure 4-7.

$$c_1 = -9127.8 \left(\frac{\Delta h}{H}\right)^3 + 2136.6 \left(\frac{\Delta h}{H}\right)^2 - 168.85 \frac{\Delta h}{H} + 6.1 \quad (6)$$

4.3.3 Footing Width

As indicated in Table 4.1, the fourth group of FE models (G4) was created to investigate the effect of different footing widths on the footing performance. As described in Mahgoub and El Naggar (2019b), when the footing width decreased with respect to the thickness of the top granular layer (t_g), the footing performance was governed by the upper granular layer, and the corresponding settlement decreased. Figure 4-8 shows the effect on footing performance of changing the footing width. It can be seen from the figure that there is a sharp decrease in the sustained pressure when the ratio of the footing width (B) to the thickness of the granular top layer (t_g) is less than 1.0. However, for values of B/t_g greater than 1.0, as the ratio increases, the sustained pressure decreases only slightly. Based on these results, a footing width factor (F_{FW}) was obtained for the general bearing capacity equation. F_{FW} can be calculated by using Equation 7.

$$F_{FW} = c_2 \left(\frac{B}{t_g}\right)^2 - c_3 \left(\frac{B}{t_g}\right) + c_4 \qquad (7)$$

If $\frac{B}{t_g} > 1$, Equations 8, 9 and 10 can be used to calculate c_2, c_3, and c_4; whereas if $\frac{B}{t_g} < 1.0$, Equations 11, 12 and 13 should be used to calculate c_2, c_3, and c_4, respectively:

$$c_2 = 0.0134 \left(\frac{\Delta h}{H}\right)^{-0.484} \qquad (8)$$

$$c_3 = 0.102 \left(\frac{\Delta h}{H}\right)^{-0.464} \qquad (9)$$

$$c_4 = 0.87 \left(\frac{\Delta h}{H}\right)^{-0.193} \qquad (10)$$

$$c_2 = 0 \qquad (11)$$

$$c_3 = 1.337\left(\frac{\Delta h}{H}\right)^{-0.27} \quad (12)$$

$$c_4 = 0.595\left(\frac{\Delta h}{H}\right)^{-0.365} \quad (13)$$

The footing width factor (F_{FW}) can thus be included in the general bearing capacity equation:

$$q = \left[a\left(1 - \frac{t}{H}\right) + b\right] F_{FD}\ F_{FW} \quad (14)$$

4.3.4 Footing Shape

As in conventional bearing capacity theories for shallow foundations, Mahgoub and El Naggar (2019b) found that circular or square footings (L/B = 1, where L is the footing length and B is the footing width) have the highest bearing capacity, whereas strip footings ($L/B > 10$) have the lowest bearing capacity. Figure 4-9 shows the relationship between the footing sustained pressure and the footing aspect ratio (L/B). It can be seen that the bearing capacity gradually decreases as the aspect ratio increases. The footing shape factor (F_s) was estimated from this figure. In Equation 15, a natural logarithmic relationship is used to calculate the footing shape factor (F_s).

$$F_s = c_5\ ln\left(\frac{L}{B}\right) + 1.05 \quad (15)$$

where c_5 can be calculated by using Equation 16:

$$c_5 = 0.021\ ln\left(\frac{\Delta h}{H}\right) - 0.14 \quad (16)$$

The equation for calculating the bearing capacity of a shallow foundation over backfill with a TDA layer can thus be written as:

$$q = \left[a\left(1 - \frac{t}{H}\right) + b\right] F_{DF}\ F_{FW}\ F_S \qquad (17)$$

4.3.5 Internal Friction Angle of the Top Layer

Based on numerical analyses by Mahgoub and El Naggar (2019b), Figure 4-10 shows the effect on footing performance of changing the internal friction angle (φ) of the upper granular layer. For these calculations a square footing is used, at a foundation level of 0 m, with different settlement values. It can be seen that with a low settlement value (10 mm), the footing sustained pressure increases only slightly as the internal friction angle increases. However, with a high settlement value (100 mm), there is a considerable increase in the footing sustained pressure as the internal friction angle increases. An internal friction angle factor (F_φ) is obtainable via the normalized sustained pressure by using different friction angles with the sustained pressure obtained for models with φ = 44. However, this factor was found to be significantly affected by the value of the effective pressure above the foundation level. Therefore, the FE models in the second group (G2) shown in Table 4.1 were reiterated with different foundation levels: 0 *B*, 0.5 *B*, 1.0 *B*, 2.0 *B*, and 2.5 *B*, representing effective pressures equivalent to 0 kPa, 8.8 kPa, 22 kPa, 35.2 kPa, and 44 kPa, respectively. In total, 25 FE models were developed to deduce the effect on footing performance of the internal friction angle of the upper granular layer. Regression analyses were then performed to obtain the (F_φ) factor, which was applied to the general equation (Equation 17) to include the effect of different materials in the upper granular layer. Figure 4-11 shows the effect on F_φ of different effective pressures, for a settlement value of 25 mm. The figure illustrates that F_φ, the internal friction angle of the upper granular layer, has different values for different effective pressures above the foundation level. Regression

analyses were carried out to obtain F_φ as a function of the internal friction angle of the upper granular layer, as it is affected by the effective pressure above the foundation level. The value of $F\varphi$ can be obtained by using Equations 18, 19 and 20, or by using Figure 4-12 directly.

$$F_\varphi = c_6 \, tan\varphi + c_7 \tag{18}$$

where c_6 and c_7 are coefficients which can be calculated by using Equations 19 and 20.

$$c_6 = c_{6a}\left(\frac{\Delta h}{H}\right)^3 + c_{6b}\left(\frac{\Delta h}{H}\right)^2 + \; c_{6c}\,\frac{\Delta h}{H} + c_{6d} \tag{19}$$

$$c_7 = c_{7a}\left(\frac{\Delta h}{H}\right)^3 + c_{7b}\left(\frac{\Delta h}{H}\right)^2 + \; c_{7c}\,\frac{\Delta h}{H} + c_{7d} \tag{20}$$

where $c_{6a}, c_{6b}, c_{6c}, c_{6d}, c_{7a}, c_{7b}, c_{7c}$ and c_{7d} are coefficients that can be calculated by using Equations 21 to 28.

$$c_{6a} = 816470\left(\frac{\gamma\, D_F}{P_a}\right)^4 - \; 904018\left(\frac{\gamma\, D_F}{P_a}\right)^3 + 326340\left(\frac{\gamma\, D_F}{P_a}\right)^2 - 34952\,\frac{\gamma\, D_F}{P_a} + 568.67 \tag{21}$$

$$c_{6b} = -179045\left(\frac{\gamma\, D_F}{P_a}\right)^4 + \; 904018\left(\frac{\gamma\, D_F}{P_a}\right)^3 - 72365\left(\frac{\gamma\, D_F}{P_a}\right)^2 + 8271.6\,\frac{\gamma\, D_F}{P_a} + 66.24 \tag{22}$$

$$c_{6c} = 11721\left(\frac{\gamma\, D_F}{P_a}\right)^4 - 13061\left(\frac{\gamma\, D_F}{P_a}\right)^3 + 4881.2\left(\frac{\gamma\, D_F}{P_a}\right)^2 - 629.16\,\frac{\gamma\, D_F}{P_a} + 7.14 \tag{23}$$

$$c_{6d} = -134.62\left(\frac{\gamma\, D_F}{P_a}\right)^4 + 150.78\left(\frac{\gamma\, D_F}{P_a}\right)^3 - 55.9\left(\frac{\gamma\, D_F}{P_a}\right)^2 + 7.25\,\frac{\gamma\, D_F}{P_a} + 0.45 \tag{24}$$

$$c_{7a} = -964472\left(\frac{\gamma\, D_F}{P_a}\right)^4 + 1030500\left(\frac{\gamma\, D_F}{P_a}\right)^3 - 354772\left(\frac{\gamma\, D_F}{P_a}\right)^2 + 36086\frac{\gamma\, D_F}{P_a} + 560.96$$

(25)

$$c_{7b} = 205975\left(\frac{\gamma\, D_F}{P_a}\right)^4 - 220015\left(\frac{\gamma\, D_F}{P_a}\right)^3 + 76503\left(\frac{\gamma\, D_F}{P_a}\right)^2 - 8264.7\frac{\gamma\, D_F}{P_a} - 75.054$$

(26)

$$c_{7c} = -13394\left(\frac{\gamma\, D_F}{P_a}\right)^4 + 14332\left(\frac{\gamma\, D_F}{P_a}\right)^3 - 5091.8\left(\frac{\gamma\, D_F}{P_a}\right)^2 + 619.66\frac{\gamma\, D_F}{P_a} - 5.79$$

(27)

$$c_{7d} = 173\left(\frac{\gamma\, D_F}{P_a}\right)^4 - 180.85\left(\frac{\gamma\, D_F}{P_a}\right)^3 + 61.98\left(\frac{\gamma\, D_F}{P_a}\right)^2 - 7.42\frac{\gamma\, D_F}{P_a} + 0.55$$

(28)

The effect of shearing parameters in the upper granular layer ($F\varphi$) can thus be included in the general bearing capacity equation:

$$q = \left[a\ \left(1 - \frac{t}{H}\right) + b\right]\ F_{DF}\ \ F_{FW}\ \ F_s\ \ F_\varphi \qquad (29)$$

4.4 SUMMARY OF THE PROPOSED DESIGN PROCEDURE

The design equations developed were then integrated into a design procedure to enable practitioners to calculate the bearing capacity of shallow foundations on backfill including a TDA layer, for a certain settlement value. For this purpose, Equations 1 to 29 should be used in sequence where applicable. Meanwhile, if the load settlement curve is required, the flowchart presented in Figure 4-13 summarizes the required steps to develop the full load settlement curve. The flowchart comprises seven steps. First, the parameters for the proposed system need to be specified. These include the backfill parameters (t, t_g, φ, and

H), footing geometry (B and L), effective pressure above the foundation level (γD_F), and target settlement value (Δh). These parameters are then used to calculate the bearing capacity of the footing for a specific settlement value. By repeating these steps with different settlement values, a full load-settlement curve can be obtained for any footing. A more detailed explanation is provided in the following section, where the design equations are used to plot load-settlement curves for three design examples (i.e., three footings with different shapes and different backfill dimensions). These results are then compared with the results of the FE analysis.

4.5 VALIDATION OF THE PROPOSED DESIGN EQUATIONS

In order to validate the proposed design equations, FE models were created for three design examples with hypothetical dimensions. To assess the suitability of the design equations, the results of the FE models for the design examples were then compared to the results of the developed design equations.

4.5.1 Development of the FE Models

The FE models developed were based on the assumptions described in Mahgoub and El Naggar (2019b). Figure 4-14 shows a schematic illustration of the three design examples considered. Table 4.2 shows the parameters selected for the design examples. It can be seen from Table 4.2 that the rectangular footing in Example 1 had a width of 1.0 m and a length of 2.0 m (i.e., $L/B = 2$). The total backfill height (H) underneath the footing was 1.0 m, with a TDA layer 0.5 m thick. The internal friction angle of the conventional backfill material was 40° and the foundation depth (D_F) was 0.5 m. Example 2 had a rectangular footing with an aspect ratio of $L/B = 4.67$, and a footing width of 0.75 m. Even though the same backfill height was used in this example (i.e., 1.0 m), the TDA layer was only 0.4 m thick.

In addition, the angle of internal friction of the top granular layer was 36° and the foundation depth was 1.0 m. Finally, for Example 3, strip footing was selected, with an aspect ratio of L/B = 10, a footing width of 1.0 m, and a foundation depth of 2.0 m. For this example, a layer of granular backfill material 1.0 m thick with an internal friction angle of 38° was placed over a TDA layer 0.5 m thick.

4.5.1.1 Finite Element Mesh

Ten-node tetrahedral finite elements from the element library of the FE package PLAXIS 3D v.2017 (PLAXIS bv. 2017) were used to model the soil continuum with the TDA layer. The lateral boundaries were placed at a distance of more than 4 times the width of the footing in each direction, to simulate an infinite medium in the horizontal dimension. The bottom boundary was placed at a depth of 4 times the footing width below the ground surface. Only one-quarter of the problem was modelled, so as to benefit from symmetry in the two horizontal directions. The size of the model was selected such that the artificial boundaries and boundary conditions would not affect the stress variation near the foundation, to ensure that the model could simulate the real in-situ state of stress. The model was constructed by using approximately 40,000 3D 10-node elements. The reason for using a large number of elements with a small size was to assure high accuracy of the results at locations where non-linear behaviour was anticipated, such as those in close proximity to the foundation. Interface elements were used to allow for slippage between the foundation and the surrounding soil, and between the TDA layer and the upper granular layer. Figure 4-15 illustrates a typical mesh used in this study.

4.5.1.2 Material Models

The stiffness of TDA, a nonlinear material, is significantly affected by confining stresses. The hyperbolic hardening soil model (Schanz et al., 1999) from the PLAXIS library was therefore used to model stress-dependent stiffness variations of the TDA layer. An elastic-perfectly plastic soil model with a Mohr-Coulomb failure criterion was used to simulate the behaviour of the upper granular layer and the native foundation soil due to the simplicity of the model and its suitability for such applications. The material properties adopted are summarized in Table 4.2.

The concrete footings were modelled by using volume tetrahedral elements with an isotropic elastic material, because it is not anticipated that the concrete will receive any appreciable stress relative to its material strength. Finally, the friction behaviour at the interfaces was modelled by using a strength-reduction factor at the interface, R_{inter} = 0.67. In addition, horizontal interface elements were assigned between the TDA layer and the top layer of gravel A1 materials, with a value of R_{inter} = 0.30. This simulated the smooth thin membrane that is used to separate the two layers.

4.5.2 Comparison Between Results of the FE Models and Those of the Design Equations

The equations were developed to calculate the rigid footing sustained pressure for different settlement values, so as to deduce the footing sustained pressure versus the corresponding settlement. Figures 4-16, 4-17, and 4-18 compare the results (i.e., the footing sustained pressure versus the corresponding settlement) of the FE models and the design equations, for the three examples. The very good agreement between the results of the FE models and

those of the design equations demonstrates the sound outcome of the design equations and their suitability for use in design.

4.6 SUMMARY AND CONCLUSIONS

In this study, design equations were integrated into a design procedure to calculate the sustained pressure for rigid footings over backfill with a TDA layer, for different settlement values. The equations were developed by using the field tests and intensive FE analyses described in Mahgoub and El Naggar (2019b). In addition, FE models of three design examples with hypothetical dimensions were created in order to compare their results with the results of the design equations. Very good agreement between the results demonstrates the sound outcome of the design equations. The following boundary conditions were utilized for the equations:

- The equations were developed for TDA type A materials.
- Due to the high permeability of TDA, the design equations were developed assuming drained conditions.
- A granular material layer with a minimum thickness of 0.3 H (where H is the total backfill height) should be placed underneath the footing, above the TDA layer.
- The equations were created by using various footing shapes (i.e., square, circular, rectangular and strip footings).
- The footing width, B, ranged from 0.5 H to 2 H.
- The equations did not include changes in subsurface conditions, where the TDA materials underneath the foundations helped to decrease the stress influence zone beneath the footings. However, the effect of changing the natural ground conditions is minimal as per Mahgoub and El Naggar (2019b).

Table 4.1: Parametric study

Model groups	Footing width (B)	Backfill height (H)	TDA thickness (t)	Foundation depth (D_F)	*Aspect ratio (L/B)	**(φ) of the granular material	Natural soil
G1	0.8 m	1.25 B	(0.1, 0.2, 0.3, 0.4, 0.5, 0.6, 0.7) H	0 B	1	44°	Till
G2	0.8 m	1.25 B	0.5 H	0 B	1	28°, 32°, 36°, 40°, and 44°	Till
G3	0.8 m	1.25 B	0.5 H	(0, 0.25, 0.5, 1.0, 1.25, 1.5, 2, and 2.5) B	1	44°	Till
G4	(0.125, 0.25, 0.5, 0.8, 1, 1.25, 1.5 and 2) H	1.0 m	0.5 H	0 B	1	44°	Till
G5	0.8 m	1.25 B	0.5 H	0 B	1, 2, 5, 10, 15, and 20	44°	Till
G6	0.8 m	1.25 B	0.5 H	0 B	1	44°	Hard, stiff, medium, and soft clay

*L is the footing length and B is the footing width.
**Internal friction angle of the upper granular layer

Table 4.2: Parameters selected for the validated examples

*Parameters	Example 1	Example 2	Example 3
B (m)	1.0	0.75	1.0
L (m)	2.0	3.5	10
t (m)	0.5	0.4	0.5
H (m)	1.0	1.0	1.5
**D_F (m)	0.5	1	2
φ (°)	40	36	38
Foundation soil	Assumed to be hard clay		

*All of the symbols are identified in Figure 4-4.
**Unit weight of the backfill above the foundation level = 22 kN/m^3

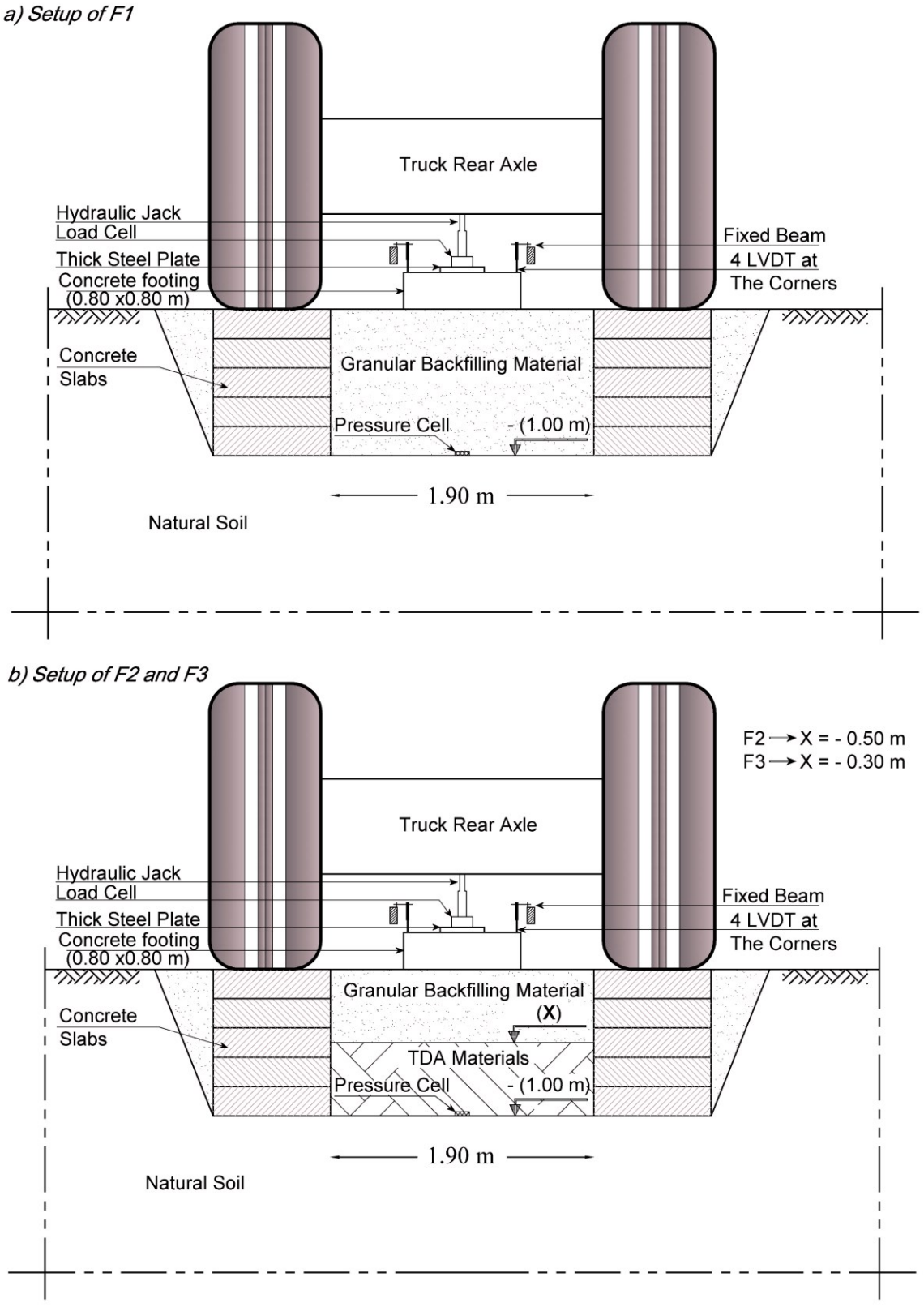

Figure 4-1 Layout of the field tests: a) setup of F1, and b) setup of F2 and F3

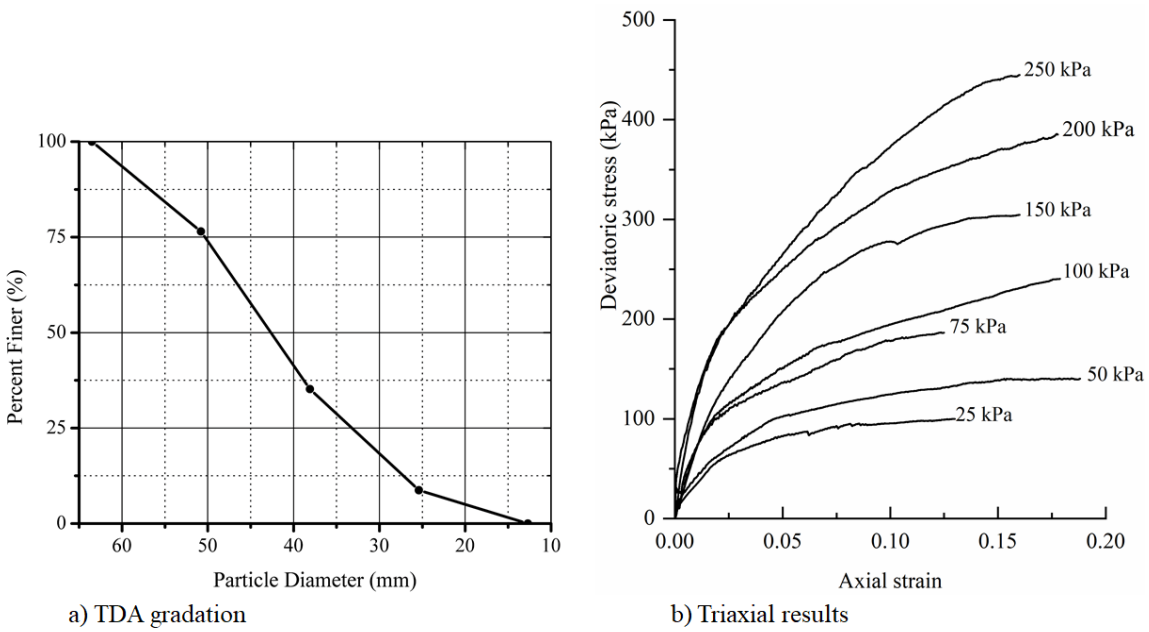

Figure 4-2 Characterization of TDA: a) TDA gradation, and b) deviatoric stress versus axial strain for TDA materials (Ashari Ghomi 2018).

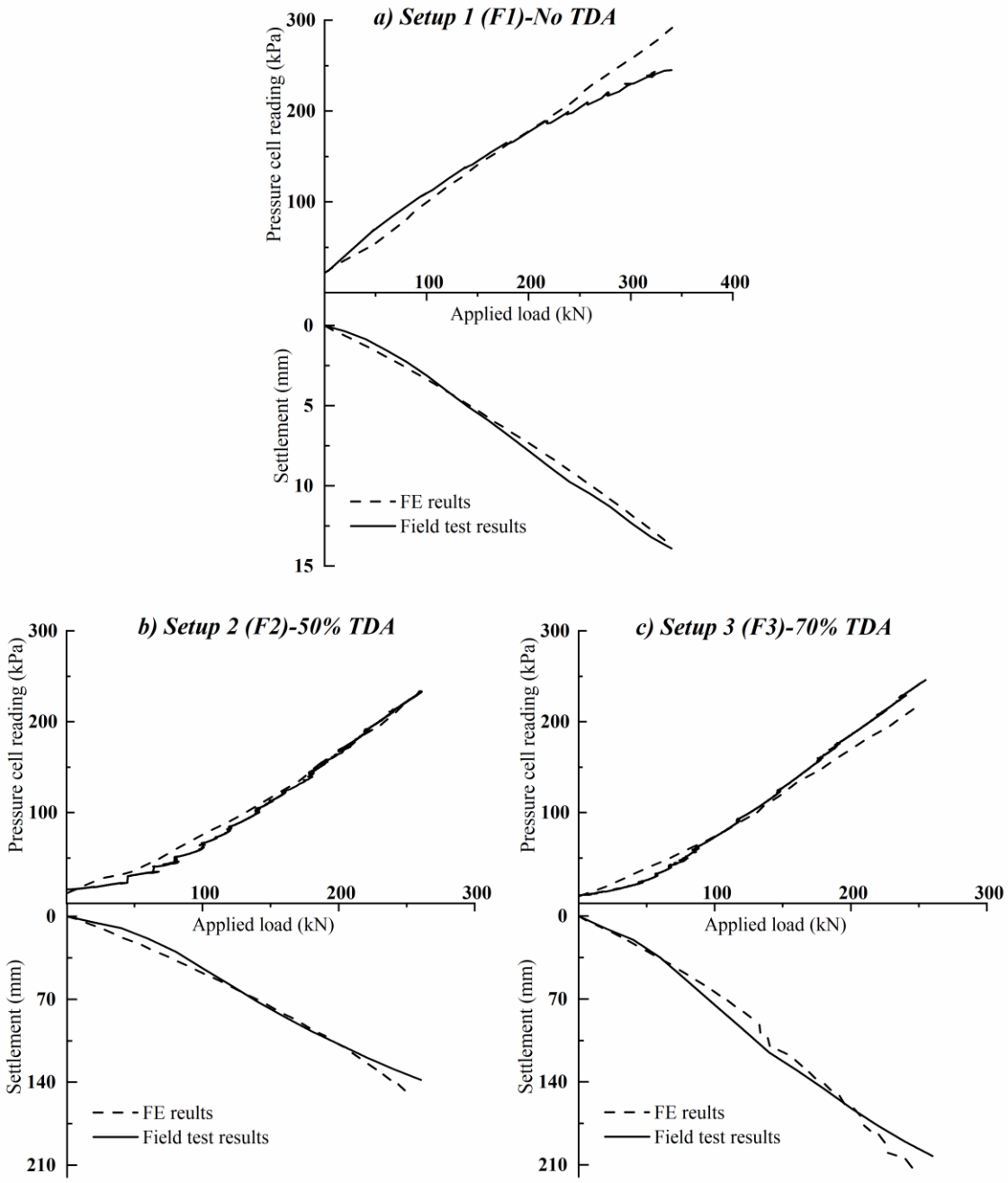

Figure 4-3 Comparison between field test measurements and FE model results.

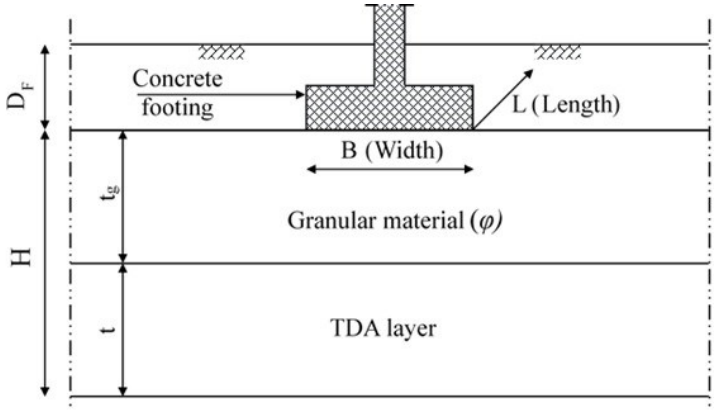

Figure 4-4 Parameters used in equation development.

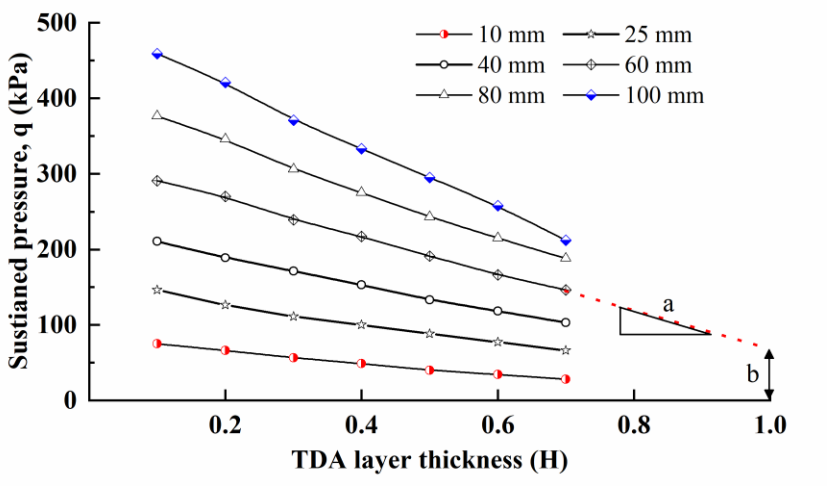

Figure 4-5 Effect of changing the TDA layer thickness on footing performance for specific settlement values.

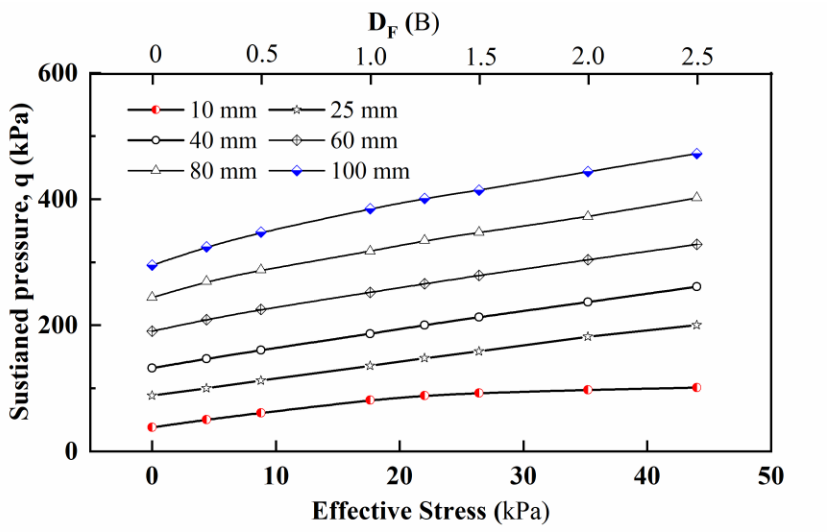

Figure 4-6 Effect on the footing bearing capacity of changing the effective stress at the foundation level.

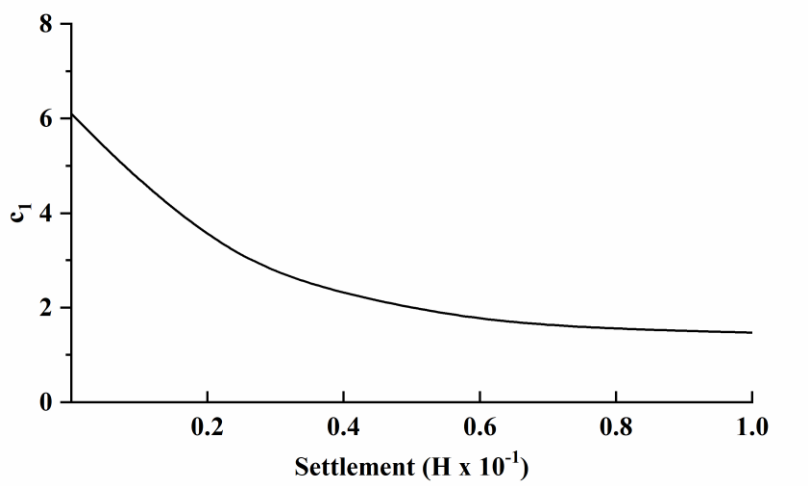

Figure 4-7 Constant (c1) for equation 5.

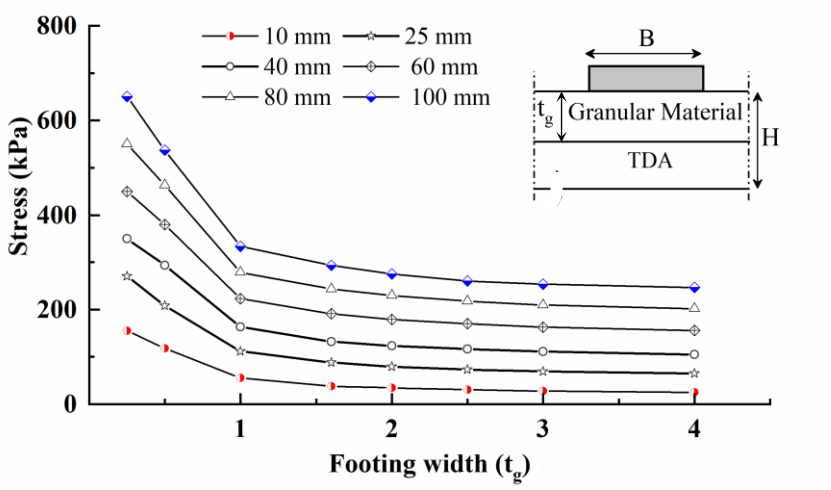

Figure 4-8 Effect on footing performance of changing the footing width as a function of the thickness of the top granular layer.

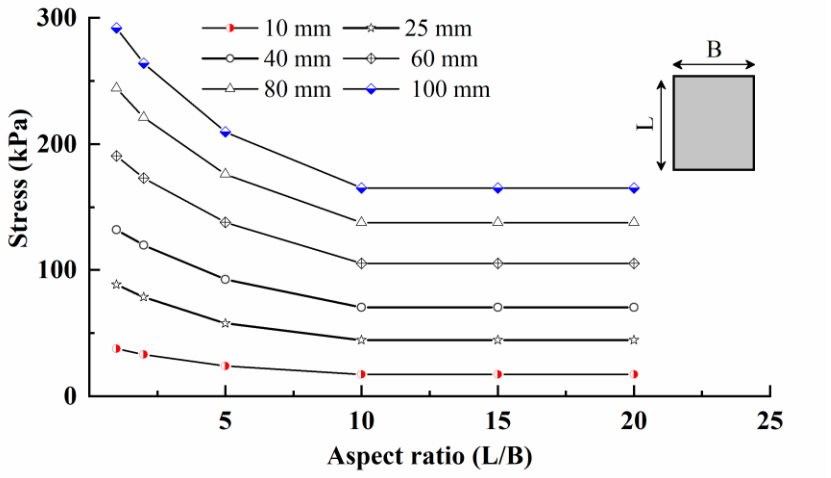

Figure 4-9 Effect of footing geometry on the footing performance.

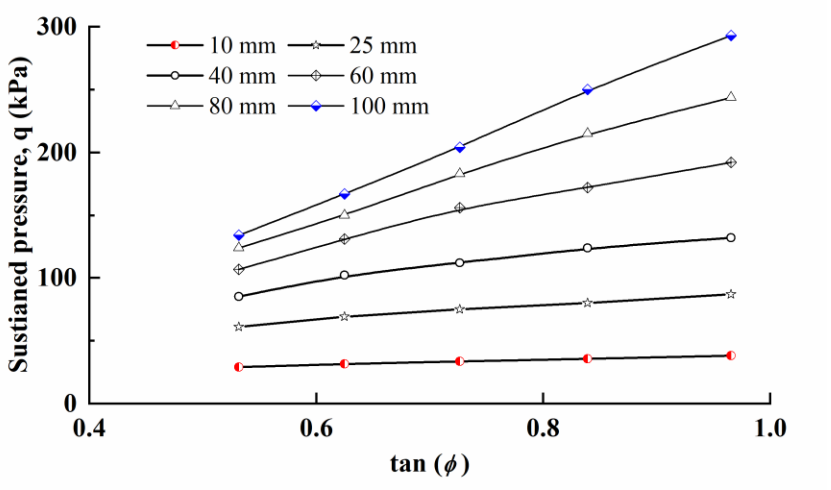

Figure 4-10 Effect on footing performance of changing the angle of internal friction of the granular material.

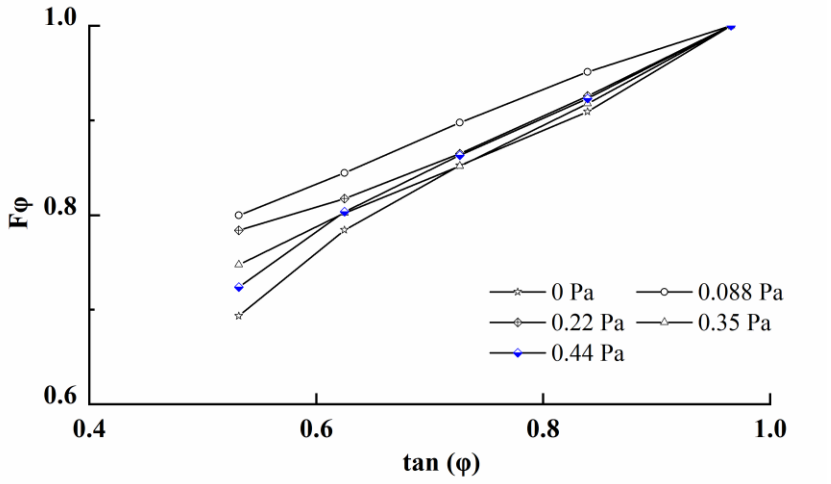

Figure 4-11 Effect on Fφ of changing the effective pressure at the foundation level.

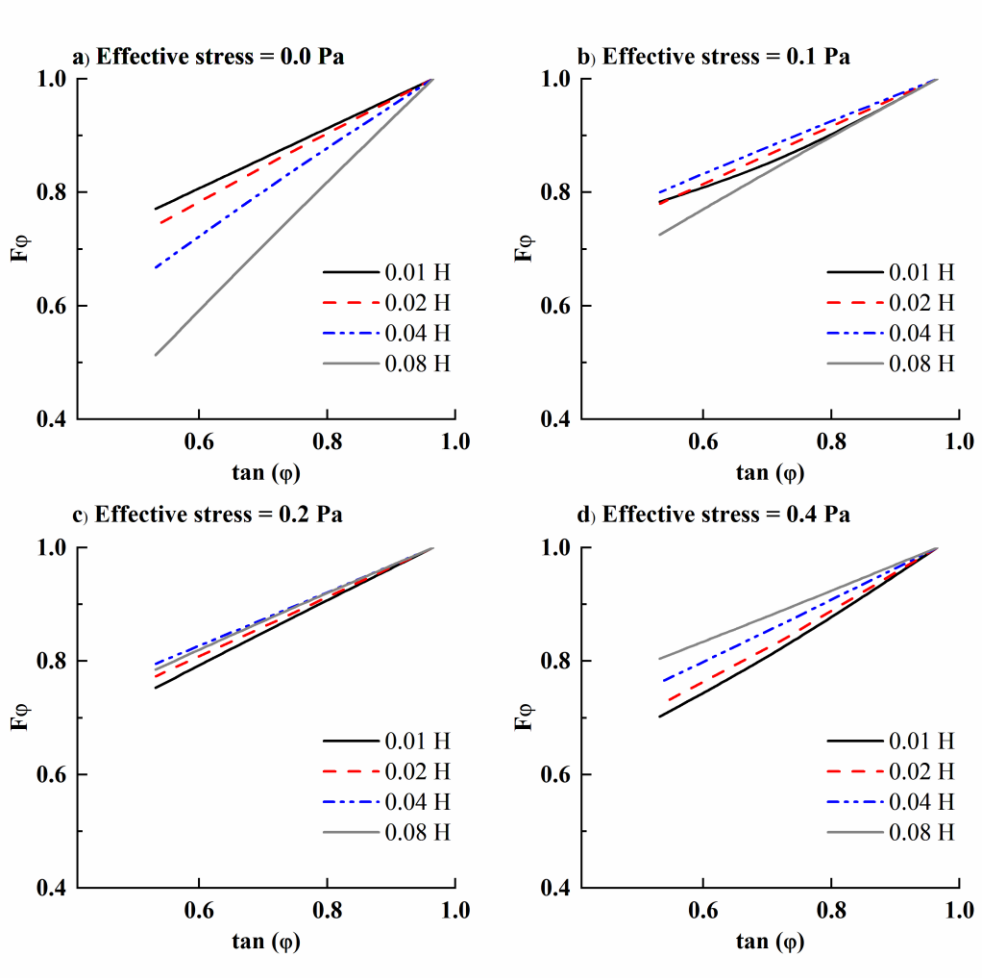

Figure 4-12 Charts for Fφ.

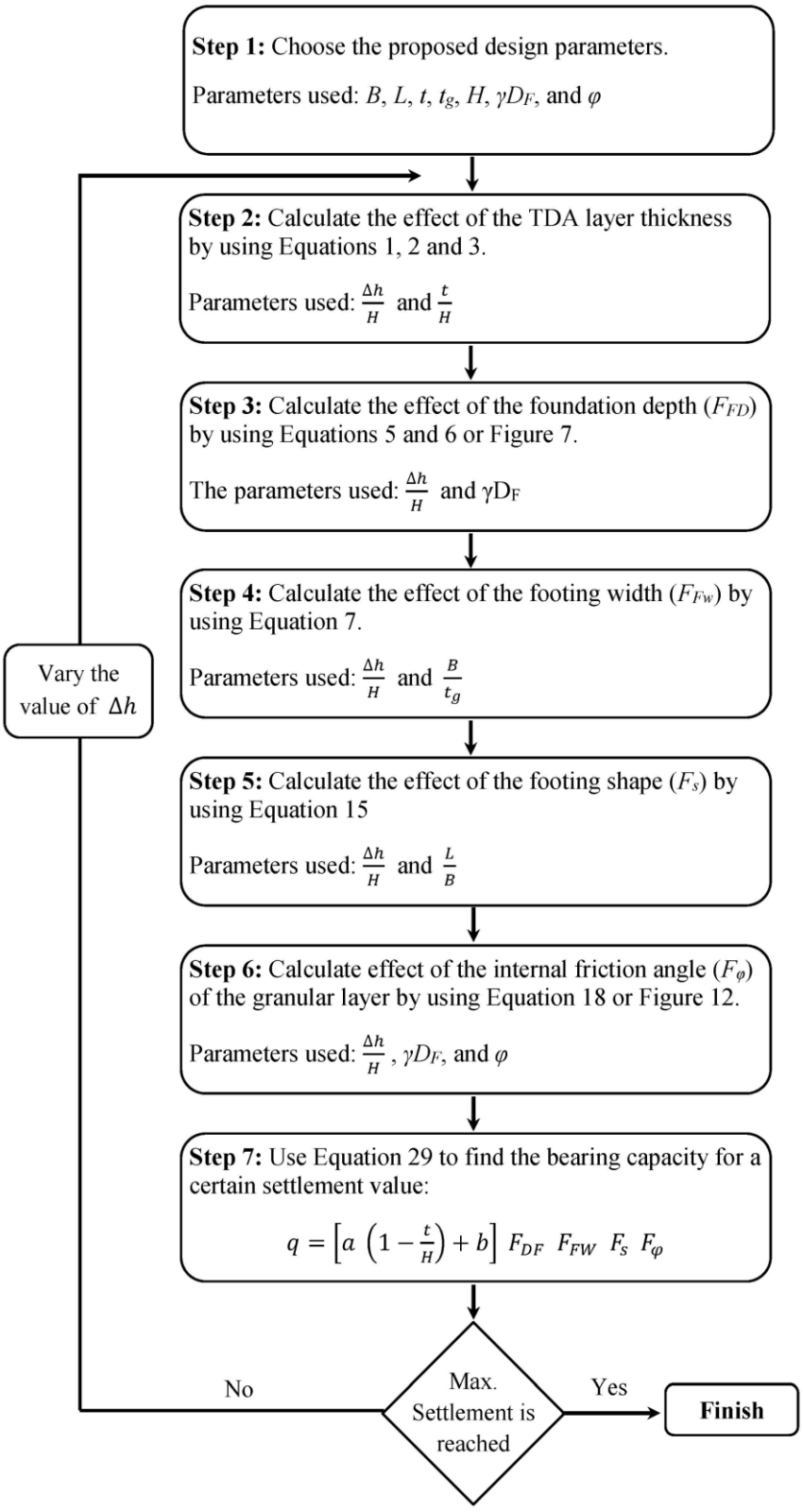

Figure 4-13 Design procedures flowchart.

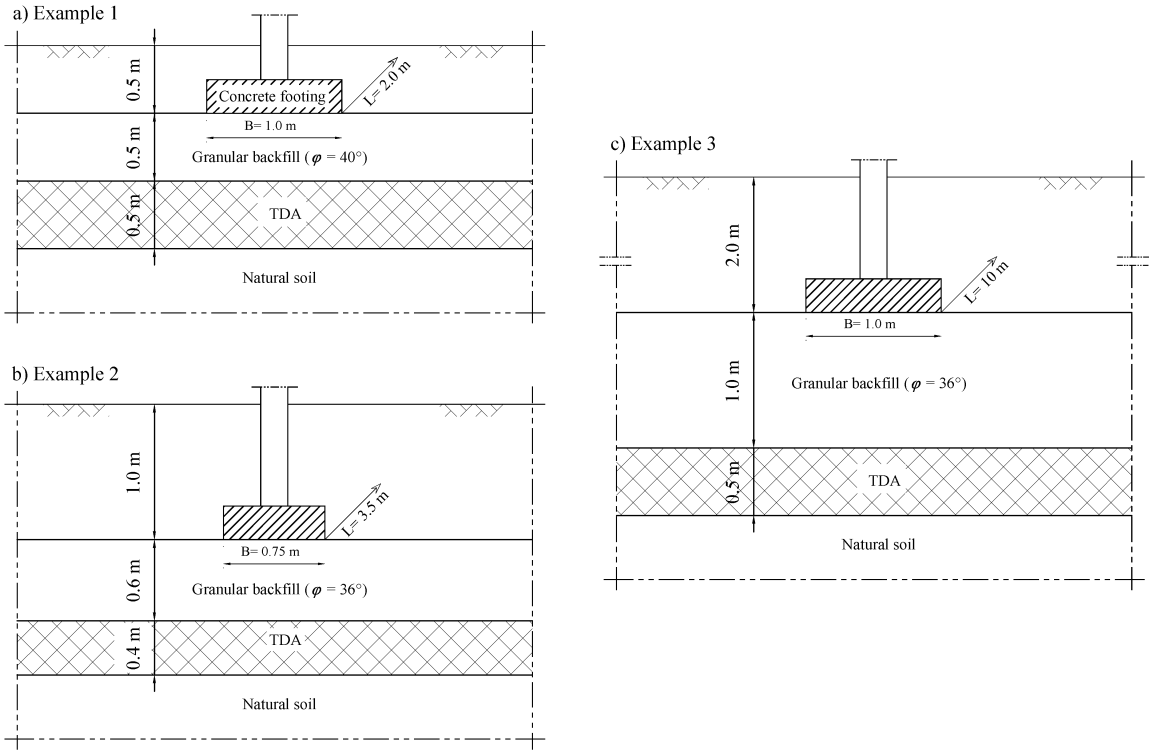

Figure 4-14 Schematic illustration of the three design examples considered.

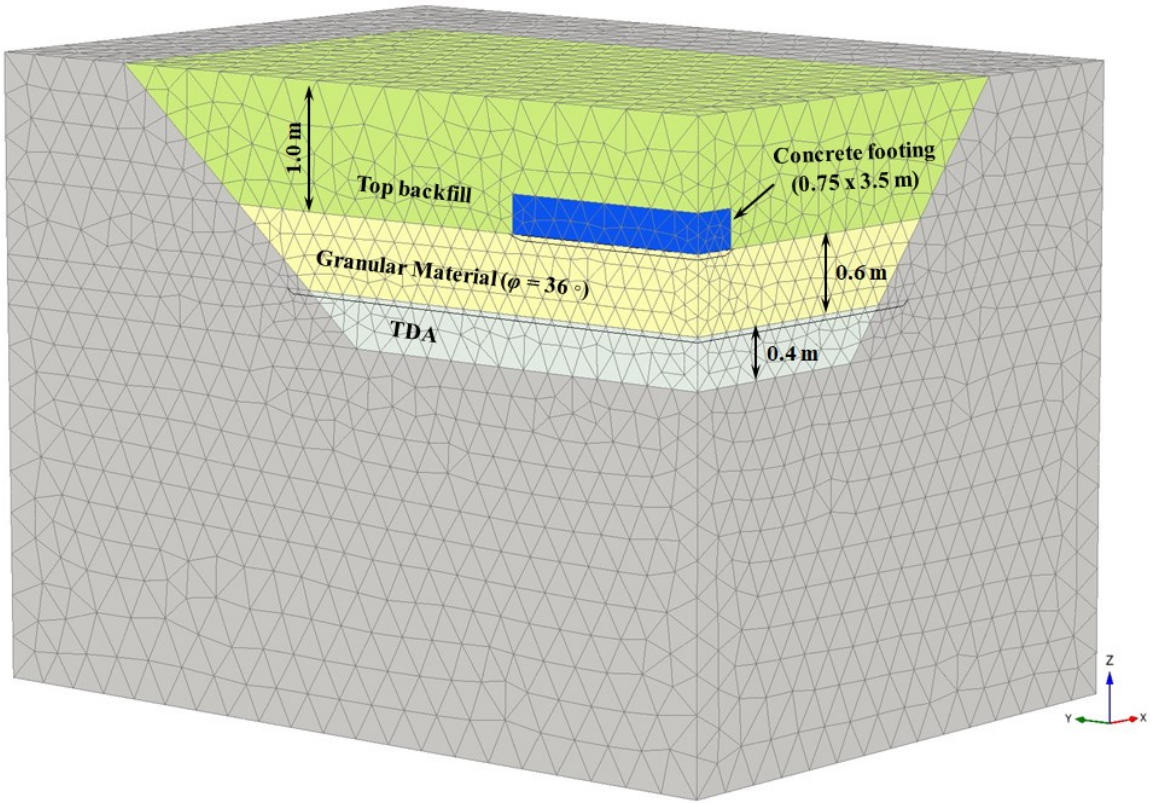

Figure 4-15 Mesh formulation of the FE model for example 2.

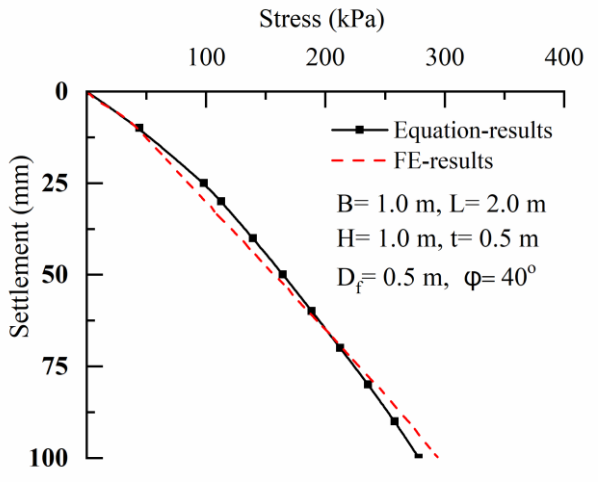

Figure 4-16 Comparison between the FE model and design equation results for example 1.

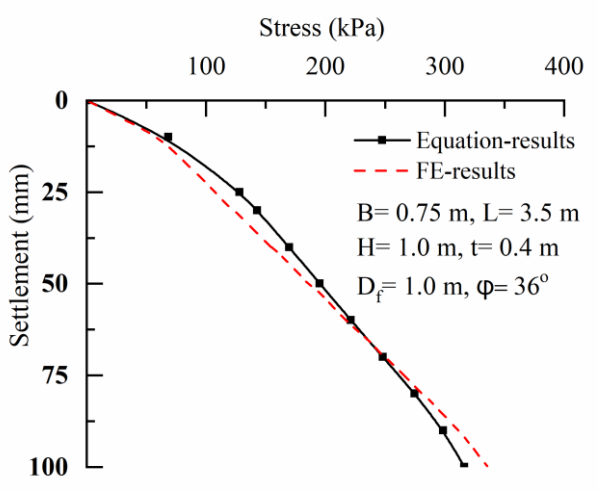

Figure 4-17 Comparison between the FE model and design equation results for example 2.

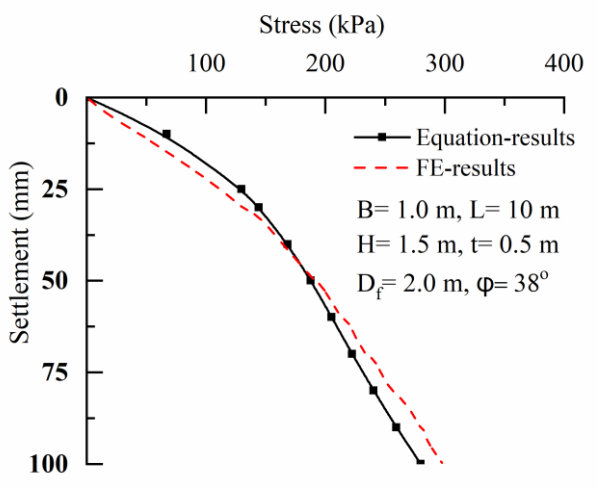

Figure 4-18 Comparison between the FE model and design equation results for example 3.

4.7 REFERENCES

ASTM (2012) D 6270-12: Standard practice for use of scrap tires in civil engineering applications. ASTM International, West Conshohocken, PA, USA.

Bosscher PJ, Edil TB and Eldin NN (1992) Construction and performance of shredded waste-tire test embankment. Transportation Research Record 1345: 44–52.

Bowels, J. E. (2001). Handbook of foundation analysis and design, (international edition).

Das BM and Sivakugan N (2016) Fundamentals of geotechnical engineering Cengage Learning. Cengage Learning.

Dickson T, Dwyer D, and Humphrey D, (2001) Prototype tire-shred embankment construction. Transp. Res. Rec. 1755: 160–167. https://doi.org/10.3141/1755-17.

Elias V, Welsh J, Warren J, Lukas R, Collin JG, and Berg RR (2006) Ground Improvement Methods, Volumes I and II, Publication No.'s FHWA NHI-06-019 and FHWA NHI-06-020, US Dept. of Transportation, Federal Highway Administration.

Engstrom, G M, and Lamb R (1994) Using shredded waste tires as a lightweight fill material for road surfaces. Rep. No. MN-RD-94-10. Minnesota, US: Dept. of Transportation.

Humphrey DN (2005) Tire Derived Aggregate – A New Road Building Material. In Seventh International Conference on the Bearing Capacity of Roads, Railways and Airfields, Trondheim, Norway, ARRB Group Limited, Vermont South, Australia.

Humphrey DN (2008) Tire derived aggregate as lightweight fill for embankments and retaining walls. In *Scrap Tire Derived Geomaterials — Opportunities and Challenges* (Hazarika H and Yasuhara K (eds)). Taylor & Francis Group, London, UK, pp. 59–81.

Humphrey DN and Eaton RA (1995) Field performance of tire chips as subgrade insulation for rural roads. In Sixth International Conference on Low-Volume Roads, Minneapolis, MN, Transportation Research Board, Washington, DC, USA, pp. 77–86.

Humphrey D and Blumenthal M (2010) The use of tire-derived aggregate in road construction applications. In *Green Streets and Highways 2010: An Interactive Conference on the State of the Art and How to Achieve Sustainable Outcomes*. ASCE, Reston, VA, USA, pp. 299–313.

El Naggar H, Soleimani P, and Fakhroo A (2016) Strength and stiffness properties of green lightweight fill mixtures. Geotech. Geol. Eng. 34 (3): 867–876. https://doi.org/10.1007/s10706-016-0010-1.

Lefebvre G (1981) Fourth Canadian Geotechnical Colloquium: Strength and slope stability in Canadian soft clay deposits. Canadian Geotechnical Journal, 18(3), pp.420-442.

Lefebvre G, Ladd CC and Pare JJ (1988) Comparison of field vane and laboratory undrained shear strength in soft sensitive clays. In Vane shear strength testing in soils: Field and laboratory studies. ASTM International.

Mahgoub A and El Naggar H (2019a) Using TDA as an engineered stress-reduction fill over preexisting buried pipes. Journal of Pipeline Systems Engineering and Practice 10(1), https://doi.org/10.1061/(ASCE)PS.1949-1204.0000362.

Mahgoub A and El Naggar H (2019b) Using TDA underneath shallow foundations: field tests and numerical modelling. Geotechnique (under review)

Mills B, El Naggar H, and Valsangkar AJ (2015) North American overview and Canadian perspective on the use of tire derived aggregate in highway embankment construction. Chap. 22 in Vol. 2 of Ground improvement case histories, edited by Indraratna and Chu. New York: Elsevier.

Plaxis B (2017) Reference manual for PLAXIS 2D. Delft, Netherlands.

Quigley RM (1980) Geology, mineralogy, and geochemistry of Canadian soft soils: a geotechnical perspective. Canadian Geotechnical Journal, 17(2), pp.261-285.

Rashwan S and Charette P (2015) Demonstration of the Viability of Using Tire Derived Aggregate (TDA) to Replace Natural Material (NM) in Residential Home Basement Construction. Summary report of the demonstration project at 263 Waverly Street, Winnipeg, Manitoba, Canada.

Shalaby A, and Khan RA (2002) Temperature monitoring and compressibility measurement of a tire shred embankment: Winnipeg, Manitoba, Canada. In Transportation research record 1808, 67–75. Washington, DC: National Research Council, Transportation Research Board.

Sparkes J, El Naggar H and Valsangkar A (2019) Compressibility and shear strength properties of tire-derived aggregate mixed with lightweight aggregate. Journal of Pipeline Systems Engineering and Practice 10(1), https://doi.org/10.1061/(ASCE)PS.1949-1204.0000354.

Stark TD, Arellano D, Horvath JS and Leshchinsky D (2004) Geofoam applications in the design and construction of highway embankments. NCHRP Web Document 65 (project 24-11), National Cooperative Highway Research Program, Washington, DC.

Upton, R. J., and G. Machan. (1993) Use of shredded tires for lightweight fill. Transp. Res. Rec. 1422: 36–45.

CHAPTER 5 INNOVATIVE APPLICATION OF TDA AROUND CORRUGATED STEEL PLATE (CSP) CULVERTS

Ahmed Mahgoub and Hany El Naggar

5.1 INTRODUCTION

According to the Rubber Manufacturers Association report of 2017, rapid developments in the automotive industry have caused the volume of scrap tires to increase significantly. Consequently, providing safe disposal for these tires has become a critical issue worldwide. Tire rubber that is stockpiled in landfills threatens the environment and human health (Cetin et al. 2012). The best way to reduce the number of tires in landfills is to promote tire recycling. For instance, scrap tires are burned for fuel, used as construction materials, and utilized in several other ground rubber applications (Pierre 2013). The Rubber Manufacturers Association 2017 report states that only 7.9% of the scrap tires in the USA are recycled in civil engineering applications. The excellent geotechnical properties of tire-derived aggregate (TDA) should help increasing its future market share and promoting its use in many other civil applications providing an innovative alternative to conventional backfilling materials. In this paper a new application of TDA backfill around CSP culverts is proposed and its feasibility is explored experimentally and numerically as discussed later.

According to ASTM D6270-08, for civil engineering applications tires are generally shredded to form two types of TDAs to replace natural aggregates: type A with a maximum particle size of 75 mm, and type B with maximum particle size of 305 mm. Since the 1990s, comprehensive studies have been carried out to investigate the material properties of TDA

(e.g., Eaton et al. 1994; Benson et al. 1996; Edil 2005; Wartman et al. 2007; Humphrey 2008; Moo-Young et al. 2003; Xiao et al. 2013; Meles et al. 2014; El Naggar et al. 2016; Ashari and El Naggar 2017; Sparkes et al. 2019). These studies demonstrate that TDA has outstanding geotechnical properties. It weighs 60% less than conventional backfill (Sparkes et al. 2019). In addition, it is more porous and is a better thermal insulator than conventional backfill (Eaton et al. 1994; Benson et al. 1996; Warith and Rao 2006). Many full-scale tests have been performed by using TDA as a lightweight backfill material in embankments and behind retaining walls (e.g., Hoppe 1998; Tweedie et al. 1998; Humphrey 2005; Humphrey 2008; Humphrey and Blumenthal 2010; Mills et al. 2015). In addition, many studies have been conducted on the use of TDA as a dampening material that is placed behind retaining structures to protect them from earthquake damage (e.g., Xiao et al. 2012; Ahn and Cheng 2014).

Thanks to its compressibility and light weight, TDA has also been successfully utilized in buried pipe and culvert applications to enhance the arching mechanism above these structures (Tafreshi et al. 2012; Meguid and Youssef 2017; Mahgoub and El Naggar 2019). The pressure distribution around pipes and culverts depends upon the relative stiffness of the structure and the surrounding backfill (Anderson 1913; Marston 1930; Spangler 1950a, b; Spangler and Handy 1973). For instance, the induced earth pressure around buried pipes and culverts can be reduced by installing a layer of compressible material such as TDA above them. This causes the soil above buried pipes and culverts to settle more than the surrounding soils. Consequently, a positive arching mechanism is achieved, causing the earth pressure above the pipes to be less than the theoretical value of the weight of the soil prism above them, as the shear resistance along the sides of the prism balances the weight

of the soil. This approach is referred to as an induced trench installation. In contrast, if the soil prism above the pipes settles less than the surrounding soil, such as in the case of well compacted granular backfill over rigid pipes, negative arching mechanism will develop causing the vertical earth pressure above the pipes to be greater than the theoretical value. Many studies have been carried out to eliminate the skepticism associated with the induced trench installation method, through full-scale tests and numerical modelling (e.g., Spangler and Handy 1973; McAffee and Valsangkar 2008; McGuigan and Valsangkar 2010 and 2011; Turan et al. 2013; El Naggar et al. 2015; Mahgoub and El Naggar 2019; Al-Naddaf et al. 2019).

Meguid and Youssef (2018) performed a small-scale test to investigate the effectiveness of using a layer of TDA material above a 150 mm PVC pipe to decrease pipe stresses under embankment loads. The study showed that the use of TDA above buried pipes under embankment loads decreased pipe crown stresses by 30%. Ni et al. (2018) developed finite element (FE) modelling to explore the utility of a compressible layer above rigid buried pipes beneath a high embankment. The study also included a comparison between the behaviour of pipes with TDA and with expanded polystyrene (EPS) foam.

Mahgoub and El Naggar (2019) performed two full-scale tests to investigate the feasibility of protecting pre-existing pipes located beneath shallow foundations by using TDA as an engineered stress reduction fill above the pipes and below a concrete footing. The study, which was followed by comprehensive FE analyses using PLAXIS 3D, showed that in comparison to using conventional backfill, the use of a layer of TDA above a pipe significantly reduces pipe stresses and the magnitude of transferred pressures.

In a study in northwestern Spain, Rodríguez et al. (2018) used 2.0 m of TDA as a stress reduction layer above the crown of a cut-and-cover concrete rail tunnel with a diameter of 13 m. Their research included a numerical study that used the commercial code the Fast Lagrangian Analysis of Continua (FLAC-3D) to simulate the case study. A parametric study was then conducted to investigate different TDA configurations above the tunnel. The study found that using TDA above a cut-and-cover tunnel significantly reduced the stresses in tunnel liners.

This chapter presents the results of four full-scale tests that were conducted to evaluate the effectiveness of using a layer of TDA material in three different configurations around 600 mm corrugated steel plate (CSP) culverts. Moreover, three-dimensional (3D) finite element models (FEM) of the tests were developed to study the interaction mechanisms in the problem considered. After the finite element models were validated against the results of the full-scale tests, intensive parametric study was then conducted to examine the effect of the TDA backfill envelope configuration around the culvert, the influence of the stiffness of the top granular backfill, the performance of the proposed system under the rigid pavement, the effect of burial depth above the culvert, and the performance of the proposed system under embankment loads.

5.2 EXPERIMENTAL SETUP

Four full-scale tests, with setups 1, 2, 3 and 4, were conducted in a steel tank with rigid walls in the heavy structure laboratory at Dalhousie University, Halifax, Canada. Four corrugated steel plate culverts with a diameter of 600 mm were tested to evaluate the effectiveness of using a layer of TDA around the culverts. Figure 5-1 shows the layouts for the different test configurations considered. Setup 1, which served as a reference case, was

designed to examine the behaviour of a CSP culvert in conventional backfill conditions, where the backfill material was poorly graded sand. Setups 2 to 4 examined the effect of changing the geometry of the TDA backfill envelope around the culvert. In setup 2, the TDA layer above the culvert crown had a thickness of 150 mm (1/4 of the culvert diameter). In setup 3, in addition to the 150 mm TDA layer above the culvert crown, TDA was placed around the upper part of the culvert as far as the springline (the middle of the culvert). As shown in Figure 5-1, in setup 4 the TDA layer was continued to the invert of the culvert (but not underneath it). In all setups, the total cover height above the culvert crown was 600 mm. For each test, a steel plate with the dimensions of the wheel pair at one end of a single axle of the design truck CL-625-(ONT) (CSA, 2014) was utilized for loading.

5.2.1 Steel Tank

The steel soil tank used in the experiments is shown in Figure 5-2. The tank was 2.75 m long, 2.25 m wide, and 1.80 m deep. The walls of the steel tank were designed to be sufficiently rigid to prevent any lateral movement due to the loads applied inside the tank. As shown in Figure 5-2, prior to filling the tank, the tank boundary conditions were prepared by greasing the tank walls and covering them with high density polyethylene sheets, to ensure free movement in the vertical direction between the tank and the filling soils (in order to have a free boundary in vertical direction).

5.2.2 Experimental Specimens

The culverts tested had a length of 2.0 m, a diameter of 0.6 m, and a wall thickness of 1.6 mm. The spiral corrugation was shallow, with an amplitude of 13 mm and a period of 67 mm (see Figure 5-3). In accordance with ASTM A653 (2011b), typical steel was used with a minimum strength (F_y) of 230 MPa, a minimum tensile strength (F_u) of 310 MPa, and a

Young's modulus (E) of 200,000 MPa. The intact section had a bending stiffness (EI) value of 6.2×10^6 Nmm^2/mm and a hoop stiffness (EA) value of 3.28×10^5 N/mm.

5.2.3 Material Properties

The TDA material used in the experiments was obtained from the Halifax C&D Recycling company in Nova Scotia, Canada. The material is categorized as type A, with particles ranging in size from 13 mm to 63 mm. The size distribution of the TDA particles is shown in Figure 5-4. The shear strength parameters of the TDA were determined by using large-scale triaxial tests. Proctor tests and sieve analyses were also performed to classify the material and to determine the maximum capacity. A more detailed description of the laboratory testing program is provided in (Ashari Ghomi 2018; Ashari et al. 2017). Ashari Ghomi (2018) performed large-scale triaxial tests to identify the TDA material failure envelope and used the test results to develop a constitutive material model of the TDA; the triaxial test results for different confinement pressures are shown in Figure 5-5. For the TDA used, the drained internal friction angle *(φ')* was found to be 26.5° and the cohesion *(c')* was 24 kPa.

Poorly graded sand (SP), in accordance with ASTM D 2487-17, was used as a conventional backfill in the different setups. Sieve analyses were performed to obtain the particle size distribution of the sandy material, as shown in Figure 5-4. Proctor testing was carried out to determine the optimum water content and maximum dry density of the granular backfill used. The maximum dry density was 17.75 kN/m^3 and the optimum water content (W_c) was equalized to 13.8%. Triaxial tests were performed to obtain the shear strength parameter ($\varphi' = 39°$) and the modulus of elasticity E.

5.2.4 Instrumentation

As shown in Figure 5-2c, the culverts were instrumented with 16 strain gauges at 8 locations around the culvert circumference: at the crown, the invert, the two opposite haunches, the two opposite springlines, and the two opposite shoulders. Two strain gauges for each location (at the valley and the crest) were mounted to measure the change in pipe thrust forces and bending moments associated with the backfill lifts and external live loads. The strain gauges were installed on the inner surface of the culvert to protect them during the backfill process (Figure 5-2c). Moreover, they were placed at the middle cross-section of the culvert (i.e., beneath the area to be loaded at the backfill surface). The strain gauges were also installed along the spiral angle of the culvert. The strain gauges used were F series foil strain gauges manufactured by the OMEGA company, with operating temperatures from -10° to 45° C and a grid resistance of 350 ohms.

In addition, two linear variable differential transformers (LVDTs) manufactured by TE Connectivity were installed on the vertical and horizontal diagonals of the middle cross-section of the culvert to measure the change in culvert diameter caused by backfilling and loading (Figure 5-2c). Two additional LVDTs were installed at diagonal corners of the loading plate at the backfill surface to measure the plate settlement during loading. These compact string potentiometer LVDTs with voltage driver outputs provide measurements with an accuracy of 0.25%.

A Canon Rebel T4i Digital SLR camera was also set up at an opening in the steel tank to take photographs of the culvert along its longitudinal axis for use with digital image correlation (DIC) (Figure 5-2a). Subsequently, culvert deformations were determined for different loading conditions by using the Ncorr MATLAB coding for photo processing. As

shown in Figure 5-2c, eight cubes (25 mm×25 mm×25 mm) were installed at the crown, the shoulders, the springlines, the haunches, and the invert of the culverts to monitor the deformation during external loading.

5.2.5 Loading

As shown in Figure 5-1, the wheel pad was a thick steel plate 50 mm thick, 600 mm long and 250 mm wide that was placed on the soil surface and aligned with the middle cross-section of the steel culvert. A double acting hydraulic jack connected to a loaded frame was used to apply vertical loads to the loading plate.

5.2.6 Test procedures

After the walls of the steel tank were greased, sand was placed in the tank by using heavy duty bulk bags with a bottom spout (see Figure 5-6a). The sand was then tamped in layers 150 mm thick to form a dense base bedding material below the culvert. The backfill layers were tested by using a sand cone test to ensure that every layer attained at least 95% of the standard Proctor density. Compaction was achieved by using a vibrating plate tamper. After the bedding layer was compacted to a thickness of 600 mm, the instrumented culvert was placed at the designated level. Figure 5-6 illustrates the backfill placement procedures for each layer. The culvert was aligned with the hydraulic jack, so that the instrumented cross-section of the culvert crown was directly below the hydraulic jack. For setup 1, the sandy backfill material was placed around and above the culvert, as illustrated in Figure 5-1a. Compaction near the culvert was carried out by using a steel plate tamper, to protect the culvert from any damage. For setups 2, 3 and 4, TDA was placed as shown in Figures 5-1b, c, and d, respectively. A thin polymeric membrane was placed between the TDA and the surrounding sand backfill to segregate the TDA and to prevent any mixing between the

two materials during compaction. An overbuild layer of TDA was added to compensate for settlement occurring after the placement of cover materials. The top surface of the backfill in the steel tank was levelled at the designated level, then the thick steel plate was positioned so that the center of the plate was directly above the center of the instrumented cross-section of the culvert to be tested. The hydraulic jack was positioned over the steel plate (see Figure 5-1). As shown in Figure 5-7, a framework of two rigid beams was installed above the steel plate so that if the plate was loaded and settled, the position of the framework would remain stationary. From the framework, two LVDTs were then attached at two corners of the plate. A load cell was placed between the hydraulic jack and the steel plate. The load was applied incrementally with the hydraulic jack and was maintained manually with an electric pump. For every setup, loading was applied until failure, or until excessive settlement occurred (60 mm). The results of the full-scale tests (i.e., culvert strains, load cell readings, and loaded plate settlements) were then used to investigate the soil-structure interaction (SSI) of the systems investigated and the effectiveness of these systems in reducing the stresses received by the buried culverts.

5.3 NUMERICAL ANALYSIS

3D finite element analyses (FEA) were conducted to simulate the full-scale test results and to investigate the feasibility of using a TDA backfill envelope around buried culverts. The analyses were performed by using the PLAXIS 3D 2018 software package. The verified FE modelling was then used to generate intensive parametric study to investigate influential parameters on the behaviour of the proposed system. The following sections present the details of the numerical modelling.

5.3.1 FE Mesh

The soil volume was modelled by using the 10-noded tetrahedral FE element included in the element library of the FE package PLAXIS 3D-2018. Figure 5-8 shows the FE mesh for one of the numerical models used in the verification. The verification models comprised around 50,000 elements, with an average element size of approximately 20 mm in the zone between the culvert and the loading plate.

5.3.2 Boundary Conditions

One-quarter of the geometry was modelled, to take advantage of the test setup symmetry in the two horizontal directions. This reduced the extent of the computations and the number of elements (see Figure 5-8). A fully fixed boundary condition was assumed at the base of the models. The lateral boundary conditions were assigned to be free in the vertical direction and fixed in the horizontal direction. Only the perpendicular lateral boundary conditions along the model axes of symmetry were restrained.

5.3.3 TDA Material and Soil Properties

The hyperbolic hardening soil model (HSM) from the PLAXIS 3D library was used to model the stress-dependent variation in stiffness of the cohesionless materials and the TDA materials that were used to backfill the culverts. This double stiffness model is used to model the stress-dependent variation of soil stiffness due to different loading conditions (Schanz et al., 1999). The hyperbolic hardening soil model adopted belongs to the family of double stiffness models, a development of the Duncan and Chang (1970) hyperbolic model. To examine the effectiveness of using the HSM to simulate TDA behaviour, Mahgoub and El Naggar (2019) developed FE models to simulate the triaxial results obtained by Ashari and El Naggar (2017). The study demonstrated that using the HSM in

the FE analysis provided excellent agreement with the TDA behaviour. Table 5.1 shows the parameters used for the TDA and granular materials.

5.3.4 CSP Culvert and the Loading Plate

The spiral CSP culvert and the steel loading plate were simulated by using plate elements, assuming elastic behaviour and axial and flexural rigidities. PLAXIS 3D treats the plate elements in the same manner as conventional beam elements, where the shear, bending and normal forces are considered in the element formulation. The modulus of elasticity of the steel used was 200 x 10^3 MPa, the loading plate thickness was 50 mm, and the culvert thickness was 1.6 mm. The culvert plate was simulated in the FE models by using the actual shape of the culvert corrugations shown in Figure 5-3, with a spiral angle of 17° relative to the vertical axis. As shown in Figure 5-9, the local axes of the culvert plate elements were assigned to be aligned with and perpendicular to the culvert spiral angle, in order to ensure correct distribution of the stress around the culvert.

To simulate the smooth thin polymeric membrane between the TDA layer and the upper granular material, five-node interface elements were added with a reduction factor (R_{inter}) of 0.30. In addition, an interface element with R_{inter} equal to 0.5 was added around the CSP culvert and between the steel plate and the soil to simulate the soil-structure interaction (SSI) between them.

5.3.5 Construction Sequence

The construction sequence used in the full-scale tests was simulated in the 3D modelling. The initial in-situ stresses were established by using the K_0 procedure, where vertical stresses increase linearly with depth. The backfill was then placed in 150 mm lifts until the

designated upper level of the bedding layer was reached (see Figure 5-1). The CSP culvert was then activated. Subsequently, the backfill material was placed, and the interface elements around the culvert and between the TDA and the surrounding granular backfill were activated. Finally, the loading plate was placed, and progressive vertical loads were applied until failure.

5.3.6 Parametric Study

This section describes the developed parametric study to investigate crucial parameters affecting the stress arching mechanism of the proposed setups. Five sets of models were developed in the parametric study.

The first set of models (set1) discusses the effect of the TDA backfill envelop shape around the culvert. In addition to the three configurations that were tested (i.e., TDA was above the crown, above the springlines, and around the culvert till the invert), another two configurations were modeled (Figure 5-10): 1) TDA was placed above the culvert shoulders, 2) TDA was around the culvert till the haunch.

The second set (set 2) examines the effect of changing the stiffness of the top layer over TDA. The top layer was changed to medium dense sand, very dense sand, A1-gravel, and crushed stone. Setups 2 and 4 were utilized in this set of models. Table 5.2 shows the parameters used in set2. Furthermore, the performance of the proposed setups (1, 2, 3, and 4) under rigid pavement was investigated in the third set of models (set3). In this set, the top 200 mm in the granular layer over TDA was replaced by a concrete slab.

The fourth set of models (set4) discusses the effect of changing the burial depth over the culverts (d). The burial depth over the culvert crown changed to 0.6 m (1D), 0.9 m (1.5D),

1.2 m (2*D*), 1.8 m (3*D*), 2.4 m (4*D*) and 4.8 m (8*D*); where *D* is the culvert diameter. The TDA layer thickness was kept 150 mm above the crown (i.e., 0.25*D*). Setup 2 was utilized in this set of models. For the comparison purposes, an applied load of 50 kN (which corresponds to 333.33 kPa) was selected to calculate the surface settlement and the transferred stresses to the culvert in this set of models.

Finally, the fifth set of models (set5) studied the effectiveness of the proposed setups (using a TDA backfilled envelope around the culverts) under embankment loads. Embankments with 3 m, 5 m, 10 m height were used in the analysis for the four considered setups. The unit weight of the used embankment backfilling material was 20 kN/m^3.

5.4 RESULTS AND DISCUSSION

In this section, the results of the full-scale tests are presented, together with the FE model validations conducted for the tests to investigate the soil-structure interaction (SSI) between the buried CSP culverts and the surrounding TDA backfill. In addition, this section contains the results of the parametric study to examine the effectiveness of the proposed system.

5.4.1 Culvert Response During Backfilling

Changes in the vertical and horizontal culvert diameters with increasing backfill height (the height of the soil above the base) are plotted in Figure 5-11. From this figure it can be seen that for setup 1, when the backfill reached the crown the culvert experienced a vertical diameter change of 1.6 mm (as the crown moved upward) and a horizontal diameter change of -1.55 mm (as the springlines moved inward). As a result of further increasing the backfill height, over the culvert crown, the vertical diameter contracted by 0.3 mm (as the crown

moved downward) and the diameter at the springlines expanded by 0.25 mm (as the springlines moved outward). For setup 2, it can be seen from Figure 5-11 that the culvert experienced the same behaviour as in setup 1 when the backfill height reached the culvert crown. Because the backfill over the culvert crown in setup 2 contained a layer of TDA and was lighter than the backfill in setup 1, in the final step the vertical and horizontal diameters in setup 2 changed equally by only about 0.1 mm (i.e., the vertical diameter contracted, and the horizontal diameter expanded). In setup 3, where there was a layer of TDA around the culvert down to the springline (see Figure 5-1c), the vertical diameter expanded by 0.65 mm and the horizontal diameter contracted by approximately the same amount when the backfill reached the crown. However, upon completion of backfilling above the culvert crown, the vertical and horizontal diameters in setup 3 exhibited a slight, equal change of 0.1 mm. Finally, in setup 4, where a TDA backfill envelope surrounded the culvert sides (see Figure 5-1d), the change in the horizontal and vertical diameters when the backfill reached the crown was only around 0.35 mm (as the crown moved upward and the springlines moved inward). However, the diameters changed by only around 0.2 mm (as the crown moved downward and the springlines moved outward) once the backfill was completely filled to the top level above the crown. In essence, it can be seen from Figure 5-11 that when the backfill reached the culvert springline, in setups 1, 2, and 3 the culvert experienced a vertical diameter change of around 0.5 mm (with the crown moving upward) and a horizontal diameter change of -0.5 mm (with the springlines moved inward); in contrast, almost no deformation was encountered in the culvert in setup 4. In conclusion, the existence of a TDA layer around the culvert significantly reduces the deformation. In setup 4 the culvert deformation decreased by approximately 80% during backfilling, in

comparison to setup 1 (where the culvert was surrounded with granular material). This effect could be more pronounced in deeply buried culverts, where the backfill load has a more significant effect on culvert behaviour; such behaviour will be examined later in the discussion of the results of the parametric study.

5.4.2 Response due to Live Loading

5.4.2.1 Surface Settlement and Culvert Deformations

As described in the section on test procedures, the load was applied progressively for every setup until surface failure or excessive settlement (60 mm) occurred. Figure 5-12 shows the load-settlement curve for each test together with the FE results. It can be seen from Figure 5-12 that there is good agreement between the results of the full-scale tests and the FE models; thus, it is evident that the FE modelling is able to capture the observed behaviour. Furthermore, Figure 5-13a illustrates the local bearing capacity failure that occurred beneath the loading plate for setup 1, whereas Figure 5-13b shows the typical punching shear failure that occurred for setups 2, 3, and 4. Similar conclusions were reached in the study by Mahgoub and El Naggar (2019), where punching shear failure was encountered in the granular stiff layer above the TDA layer during loading. However, Mahgoub and El Naggar (2019) studied the effectiveness of using a TDA layer over a pre-existing small metal pipe with a diameter of 200 mm, beneath a footing with a width of 800 mm (4 times the pipe diameter). In contrast, in the present study a metal culvert 600 mm in diameter was positioned beneath a loading plate with a width of 250 mm (~0.42 times the culvert diameter). The main objectives of the current study are therefore: 1) to explore the effect of changing the TDA backfill envelope around a metal culvert on the SSI between the buried culvert and the surrounding backfill material; 2) to investigate the stress

bridging/arching mechanism over buried culverts that are larger than the loaded area; and 3) to determine the minimum depth of material above the culvert crown required to achieve an optimal effect when using a TDA layer above/around the culvert.

It can be seen from Figure 5-12 that the load-settlement relationships for setups 2, 3, and 4 were nonlinear until a certain load value was reached (i.e., the punching shear failure load), and then the relationships behaved linearly until the end of the test. In addition, the figure shows that the punching shear failure load varied as a result of changing the TDA backfill envelope around the culvert. The punching shear failure loads for setups 2, 3, and 4 were approximately 22 kN (146 kPa), 12 kN (80 kPa), and 8 kN (53.3 kPa), respectively.

Figure 5-14 shows the horizontal and vertical diameter changes of the culverts in different setups during the application of surface loading. In general, as external loads were applied progressively, the culvert vertical diameter contracted (as the crown moved downward) and the horizontal diameter expanded (as the springlines moved outward) until the occurrence of surface failure. Furthermore, it can be seen from Figure 5-14 that the culverts in the setups with TDA (setups 2, 3, and 4) experienced less deformation (at the horizontal and the vertical culvert diameters) than the culvert in setup 1 (with granular backfill), at load increments less than the punching shear failure load for each setup (22 kN (146 kPa) for setup 2, 12 kN (80 kPa) for setup 3, and 8 kN (53.3 kPa) for setup 4). In setups 2, 3, and 4, the deformation increased dramatically after the occurrence of punching shear failure, in comparison to the increase observed for setup 1. This is due to the fact that when the shear failure occurred, the TDA accommodated greater settlement and the stress was concentrated in a small area above the culvert. On the other hand, the increase in culvert deformation in setup 4 following punching shear failure was greater than in setups 2 and

3, because in setup 4 the TDA layer extended around the whole culvert to the invert, providing less confinement for the culvert. In contrast, in setup 2 granular backfill material surrounded the whole culvert, and thus less culvert deformation resulted. Likewise, the culvert deformation induced in setup 3 was less than in setup 4, because in setup 3 granular material surrounded the lower part of the culvert up to the springlines. To permit comparison of culvert deformation shapes in the different setups as determined by digital image correlation (DIC) and FE analysis, Figure 5-15 plots the shapes at the maximum applied loads for each test setup. It can be seen from this figure that there is excellent agreement between the FE results and the culvert deformations determined by DIC. The deformation values determined by the DIC method were first compared with LVDT readings at the maximum loads, in order to confirm the accuracy of the DIC results. The figure illustrates that setup 4 experienced the maximum deformation values (9 mm) with the lowest failure load (24 kN, which is 160 kPa), that was attributed to the existence of the compressible media (TDA) around the culvert sides.

In conclusion, even though setup 4 exhibited better performance during backfilling than is the case with the other setups, it resulted in lower punching shear failure loads and greater settlement than setups 2 and 3. Therefore, in applications where the culvert is not exposed to concentrated heavy external live loads (i.e., in the case of deeply buried culverts), and the backfilling loads are the main loading conditions, setup 4 can be recommended. In order to optimize the effectiveness of using TDA around buried culverts, the applied loads should not exceed the punching failure capacity of the proposed system, which is governed by the strength and stiffness of the top granular layer. The section describing the parametric study

will therefore discuss many alternatives for increasing the punching failure capacity of the top granular layer.

5.4.2.2 Culvert Stresses

The internal forces (i.e., the bending moment and thrust) in the culvert cross-section during the application of wheel pair loads were calculated by using the readings of the installed strain gauges. The strains on the culvert were measured at the inside corrugation valley (ε_1) and the inside crest (ε_2). Equations 1 to 4 were then used to calculate the internal forces as follows:

$$\varepsilon_{ave} = \varepsilon_1 - \left(\frac{h+t}{2h}\right)(\varepsilon_1 - \varepsilon_2) \quad (1)$$

$$N = \varepsilon_{ave}\, EA \quad (2)$$

$$K = (\varepsilon_1 - \varepsilon_2)/h \quad (3)$$

$$M = EI\, K\, x\, 10^{-3} \quad (4)$$

where ε_{ave} is the average strain; h = the distance between the gauges (mm); t = the wall thickness (mm); N = the thrust force per unit length (kN/m); E = Young's modulus (MPa); A = the cross-sectional area of the wall per unit length (mm^2/mm); K = the curvature (10^{-6}/mm); M = the bending moment (kN·m/m); and I = the second-moment of area per unit length (mm^4/mm).

The stresses at each point can then be calculated by using Equation 5:

$$\sigma = \frac{N}{A} + \frac{M}{I}\, y\ 10^3 \quad (5)$$

where σ = the stress at any point (MPa); and y = the vertical distance from the neutral axis (mm).

Figure 5-16 illustrates the change in the circumferential internal forces and the stresses in the culvert crown (the point exposed to the maximum stress) for the four setups. The same trends observed in the change in culvert diameter during external loading (Figure 5-14) are displayed in Figure 5-16 for the culvert internal forces and stresses. Before the occurrence of punching shear failure, the internal forces and the stresses at the culvert crown in setups 2, 3, and 4 (utilizing TDA) were less than in setup 1 (utilizing only conventional backfill). For greater clarity, Figure 5-17 plots the stresses measured at different locations around the culvert circumference (i.e., at the crown, shoulder, springline, haunch, and invert) for certain load values (6 kN/ 40 kPa, 10 kN/ 66.67 kPa, and 20 kN/ 133.3 kPa). These loads were selected to represent the situation before punching shear failure occurred; as stated in Section 5.4.2.1, the punching load failure for setups 2, 3, and 4 occurred at around 22 kN (146.67 kPa), 12 kN (80 kPa), and 8 kN (53.3 kPa), respectively. The stresses presented in Figure 5-17 are normalized relative to the stresses in the control case (setup 1). It can be seen in Figure 5-17a that at an applied load of 6 kN, the culvert in setup 2 experienced stresses that were approximately 10% to 22% lower than those in setup 1 at the different locations. Similarly, in setup 3 the stress reduction was between 25% and 80%, and in setup 4 the stress reduction around the culvert was between 55% and 82%, in comparison to setup 1. Figure 5-17a shows that in setup 2 the stress was less than in setups 3 and 4; for setup 2 the applied load of 6 kN was around 27% of the punching load failure, while for setups 3 and 4 the applied load of 6 kN amounted to 50% and 75% of the punching load failure, respectively. In addition, setup 2 had conventional backfill surrounding the culvert

(providing strong confinement) that supported the culvert laterally and decreased springline deformation, thus reducing culvert stresses. In particular, the culvert was subject to a small loaded area at the surface; this aspect will be clarified in more detail later by the results of the parametric study. It can also be seen that in setup 3, where the conventional backfill extended only up to the springlines, the stress was more than in setup 2, since setup 3 provided less confinement. Likewise, Figure 5-17b shows the reduction in stresses for setups 2 and 3 at an applied load of 10 kN (66.67 kPa). Setup 4 is excluded from this figure, since the applied load of 10 kN (66.67 kPa) exceeds that of the punching shear failure for this setup. The stress around the culvert was reduced by around 10% to 50% in setup 2 and by around 30% to 70% in setup 3, in comparison to setup 1. In Figure 5-17c, at an applied load of 20 kN (133.3 kPa), the stresses decreased by around 15% to 25% in setup 2.

For comparison sake between the tests measurement and the FE results for the culvert stresses, Figure 5-18 was plotted for the circumferential stresses around the culvert (i.e., crown, shoulder, springline, haunch, and invert) at the maximum applied loads of each test. The culvert showed that there is a good match between the test measurements and the FE results.

Overall, it may be concluded that placing TDA around the buried flexible culverts at shallow depths decreases the punching shear failure load of the top granular layer, as it limits the thickness of the top layer, and consequently increases the induced stresses and the deformations of the culverts. However, using TDA around the culverts in other circumstances could be considerable alternative. For example, it could be a good alternative for the cold regions in North America and Western Europe, where TDA is a good thermal insulator and a compressible material to resist thawing and frosting forces.

In addition, as TDA has excellent dampening properties, it could be used around the culverts in zones of high seismicity and/or near earthquake faults locations. Furthermore, using a compressible material like TDA around the culverts could be a beneficial option in the case of swelling soils, that usually causes destructive loads to the infrastructures.

5.4.3 Results of the Parametric Study

This section presents the results of the parametric study. The developed models of the parametric study were created after extending the model boundaries to 10 times the culvert diameter in each horizontal direction to eliminate any effect of changing the model geometry. In addition, the bottom boundary was placed 5 times the culvert diameter below the invert.

5.4.3.1 Effect of the TDA Backfill Envelop Shape around the Culvert

Figure 5-19 shows the effect of changing the TDA backfill envelope geometry on the stress-settlement relationship and the transferred pressure over the crown. The presented transferred pressure for the different configurations (C1-C5; the different considered configurations are shown in Figure 5-10) was normalized to the applied pressure. It can be observed from Figure 5-19 that when the TDA backfill envelope covered more area around the culvert, the sustained pressures by the loading plate decreased at the same settlement value. It also can be observed from the same figure that the relationship between the transferred pressure over the crown and the applied surface pressure started linearly and continued nonlinear at a certain value. The transferred pressure to the culvert crown was approximately within the same range for all considered configurations. While the corresponding settlement varied notably as it can seen from the figure. For example, at an applied pressure of 100 kPa the corresponding settlement was 8 mm, 12 mm, 16 mm, 21

mm, and 27.5 mm for C1, C2, C3, C4 and C5 respectively; whereas the percentage of the transferred pressure hovered over a limited range from 39% to 43%. In addition, it can be observed that the nonlinear behaviour in C1 (TDA above the crown) started earlier than C5 (TDA around the culvert). That is because the TDA layer in C1 was contained (and confined) by a rigid medium compared to C5, where the culvert in C5 was surrounded by TDA that made the culvert experienced more deformations, and subsequently the base of the top TDA layer above the crown became weaker.

5.4.3.2 Effect of the Stiffness of the Top Layer

Replacing the top granular layer above the TDA with stiffer materials increases the punching shear capacity, and thus enhances the performance of the proposed system. Figure 5-20 shows the effect of changing the sandy granular layer above TDA to a medium dense sand, a very dense sand, an A1 gravel layer and a crushed stone layer, in setups 2 and 4. For setup 2, Figure 5-20a shows that the punching shear failure stresses (the end value of the nonlinear behaviour) for the different top granular layers was approximately 80 kPa for medium sand, 145 kPa for dense sand, 215 kPa for A1 gravel, and 300 kPa for crushed stone. Likewise, Figure 5-20b illustrates that for setup 4, the punching shear failure load was approximately 37 kPa for medium sand, 53 kPa for dense sand, 95 kPa for A1 gravel, and 125 kPa for crushed stone. In addition, it is also worth to note from Figure 5-20 that, the percentage of the transferred pressure through the weaker material increased sharply and became milder in the considered stiffer materials. In addition, the figure illustrates that using stiffer material in the top layer decreased the transferred pressures to the culvert crown notably. For example, at an applied pressure of 100 kPa in setup2 (Figure 5-20a), the transferred pressure over the crown was 44% for medium dense sand, 39% for

very dense sand, 18% for A1 gravel, and only 14.5% for crushed stone. While for setup4 (Figure 5-20b), it was 50% for medium dense sand, 44% for very dense sand, 30% for A1 gravel, and 25% for crushed stone. It can thus be concluded from Figure 5-20 that the type of backfill material used in the top layer significantly affects the stress arching mechanism over the buried culvert and consequently the transferred stresses.

5.4.3.3 Effect of Using Rigid Pavement

For certain applications, the use of rigid (concrete) pavement offers considerable advantages, for instance in parking lots for heavy trucks, and at weigh-scale stations. To examine this effect, the upper 200 mm of the top granular layer was replaced by a reinforced concrete slab for setups 1, 2, 3, and 4. The normalized results (for maximum culvert stresses, crown deformation, and surface settlement) are presented in Figure 5-21. The values are normalized relative to the results for the control case (where TDA is not used). A load of 110 kN, equivalent to the static load of the heaviest wheel pair of the 625 kN truck, was applied in the FE models. The rigid concrete slab distributed the stresses over a wider area above the culvert trench and consequently prevented the incidence of punching shear failure in the top layer above the TDA (via stress bridging). It can be seen from Figure 5-21 that the use of TDA enhances stress arching and significantly reduces the culvert stresses and deformation. In comparison to the control case, the deformation of the culvert crown in setups 2, 3 and 4 was reduced by approximately 55%, 35% and 20%, respectively; while the maximum culvert stresses were reduced by approximately 40%, 35%, and 22%, respectively. Figure 5-21 also shows that the top surface settlement increased by 14%, 35%, and 50% more than the control case when TDA utilized in setup

2, 3 and 4 respectively; however, it should be noted that the maximum surface settlement of the control case is only 2.5 mm.

5.4.3.4 Effect of the Burial Depth above the Culvert Crown

Figure 5-22 shows the effect of changing the culvert embedment depth on the transferred pressure above the culvert crown and the surface settlement. The reported transferred pressure and settlement were corresponding to an applied load of 50 kN (333.33 kPa). The transferred pressure was normalized to the effective pressure, σ_{eff}, above the culvert crown of each model. Figure 5-22 illustrated that the pressure over the crown was approximately $17.5\ \sigma_{eff}$ when the cover height *(d)* was only 1*D* (i.e., very shallow), and decreased sharply to $7.5\ \sigma_{eff}$ for a cover height of 1.5*D*. Then, the pressure over the culvert crown decreased mildly until the backfill cover reached *3D.* In addition, it can be seen from Figure 5-22 that when the backfill height *(d)* was more than 3*D*, the transferred pressure to the culvert crown was less than the weight of the soil prism above the culvert crown, it was attributed to the positive arching mechanism that developed due to the existing of the compressible material (TDA) above the crown. Therefore, it can be concluded from Figure 5-22 that after the cover height reached *3D*, the effect of the surface loading was eliminated and the weight of the backfill controlled the behaviour.

5.4.3.5 Culvert Behaviour under Embankment Loads

The distribution of stresses induced over buried culverts beneath high embankments differs from the stresses resulting from surface loads at shallow depths. Figure 5-23 provides a schematic representation of stress distributions over buried culverts due to surface and embankment loads. It can be observed from this figure that where there is no concentration of applied loads over a small, limited area, punching shear failure is not to be expected.

Moreover, embankment loads are distributed over a large area and are transferred to buried culverts vertically (to the crown) and laterally (to the sides). Therefore, the use of TDA around a culvert can assist in reducing culvert stresses. Figure 5-24 illustrates the effects of 3 m, 5 m, and 10 m embankments on the configurations tested (setups 1, 2, 3 and 4). The maximum culvert stresses, the culvert crown deformation, and the maximum settlement at the top surface of the embankment are presented in Figure 5-24 as values that have been normalized relative to the control case (setup 1, where only granular backfill was used).

As can be seen from Figure 5-24a, the same behaviour was found for the three embankment heights. The maximum culvert stresses in setup 2 (with TDA above the crown) were approximately 45% of the maximum stresses in setup 1. In setup 3, where the TDA layer extended down around the culvert to the springlines, the maximum stresses were around 38% of those in the control case. Figure 5-24b shows that in setups 2 and 3, the culvert crown deformations were around 60% and 78% less than in the control case (setup 1), respectively. Thus, in setups 2 and 3, the use of TDA resulted in greater reduction of culvert stresses and deformations, due to the positive arching effect in the trench backfill. However, in setup 4 (with TDA extending down around the culvert to the invert), the induced stresses and deformation were greater than in setups 2 and 3. In setup 4, the maximum stress and the crown deformation of the culvert were around 70% and 80% of those in the control case, respectively. The reason for the poorer performance of setup 4 is that setups 2 and 3 provided greater confinement around the lower part of the culvert. It should also be noted that the culvert crown deformed downward in setups 1 and 4, and

upward in setups 2 and 3, where there was TDA above the crown and granular sand around the springlines.

Finally, Figure 5-24c shows that for an embankment 3.0 m in height, the surface settlement increased by 8%, 9.2%, and 12% for setups 2, 3 and 4, respectively, in comparison to the control case (setup 1). For a 5.0 m embankment the surface settlement increased slightly by 5%, 6.3%, and 7.5%; and for a 10 m embankment, the surface settlement increased by only 1.5%, 2%, and 2.35% for setups 2, 3, and 4, respectively. Thus, as the embankment height increased, the amount of surface settlement decreased.

5.5 SUMMARY AND CONCLUSION

In this study, the results of four full-scale tests were presented to evaluate the effectiveness of using a layer of TDA material in three different configurations around CSP culverts. The experimental work was followed by 3D finite element models of the tests to explore the complex SSI between the culverts and the proposed backfill. Then, intensive parametric study was conducted to examine the effect of the culvert burial depth, the envelope shape of the backfill area around the culvert, the granular backfill stiffness, the use of rigid pavement, and the performance of the proposed system under embankment loads. The conclusions drawn from the study can be summarized as follows:

- During backfilling, the existence of a TDA layer around the culvert significantly reduced the culvert deformation by around 80% of that observed with conventional backfill materials.

- Due to the external surface loading, before the punching shear failure occurred beneath the loaded area, there was a significant decrease in the culvert stresses and deformations.
- At shallow depths, using TDA around the whole culvert down to the invert resulted in greater deformation and stresses than was the case for culverts with a layer of TDA only above the crown or down to the springlines. This was because the utilization of a TDA layer around the whole culvert resulted in less confinement, thus allowing greater deformations that cause higher stresses.
- Using stiffer material in the top layer increased the punching shear capacity of the proposed system and consequently enhanced the developed arching mechanism.
- Using rigid pavement above buried culverts with a TDA layer distributed the stresses over a wider area above the culvert trench (stress bridging) and prevented the incidence of punching shear failure of the top layer above the TDA, notably improving the culvert performance.
- The pressure over the crown was approximately $17.5\,\sigma_{eff}$ for shallower culverts (cover =1D) and decreased sharply to $7.5\,\sigma_{eff}$ for a cover height of 1.5D. Then, the pressure over the culvert crown decreased mildly until the backfill cover reached *3D.*
- When the backfill height above the culvert crown was more than $3D$, the transferred pressure to the culvert crown was less than the weight of the soil prism above the culvert crown, it was attributed to the positive arching mechanism due to the existing of the compressible material (TDA) above the crown.
- Using a layer of TDA around the culvert under embankment load conditions enhanced the culvert behaviour significantly in comparison to using only conventional backfill

Table 5.1: Parameters used in the FEA

Layers	Constitutive model	Unit weight (kN/m^3)	E_{50} (MPa)	E_{oed} (MPa)	c' (kPa)	φ' (°)
*The granular material (SP)	HSM	17.75	58	46.5	-	39
**TDA	HSM	7	2.75	2.2	24	26.5

Note: E = modulus of elasticity; E_{oed} = tangent stiffness from odometer test; E_{50} = secant modulus; HSM= hardening soil model;
*The properties at P_{ref} = 100 kPa and R_f=0.65.
**The properties at P_{ref} = 25 kPa and R_f=0.95.

Table 5.2: Parameters used for models in set 2

Layers	Constitutive model	Unit weight (kN/m^3)	E_{50} (MPa)	E_{oed} (MPa)	c' (kPa)	φ' (°)
Medium silty sand (SP-SM)	HSM	15.5	35	28	-	34
A1- gravel	HSM	21	110	88	-	44
Crushed stone	HSM	24	200	160	-	50

Note: E = modulus of elasticity; E_{oed} = tangent stiffness from odometer test; E_{50} = secant modulus; HSM= hardening soil model; the properties at P_{ref} = 100 kPa and R_f=0.65.

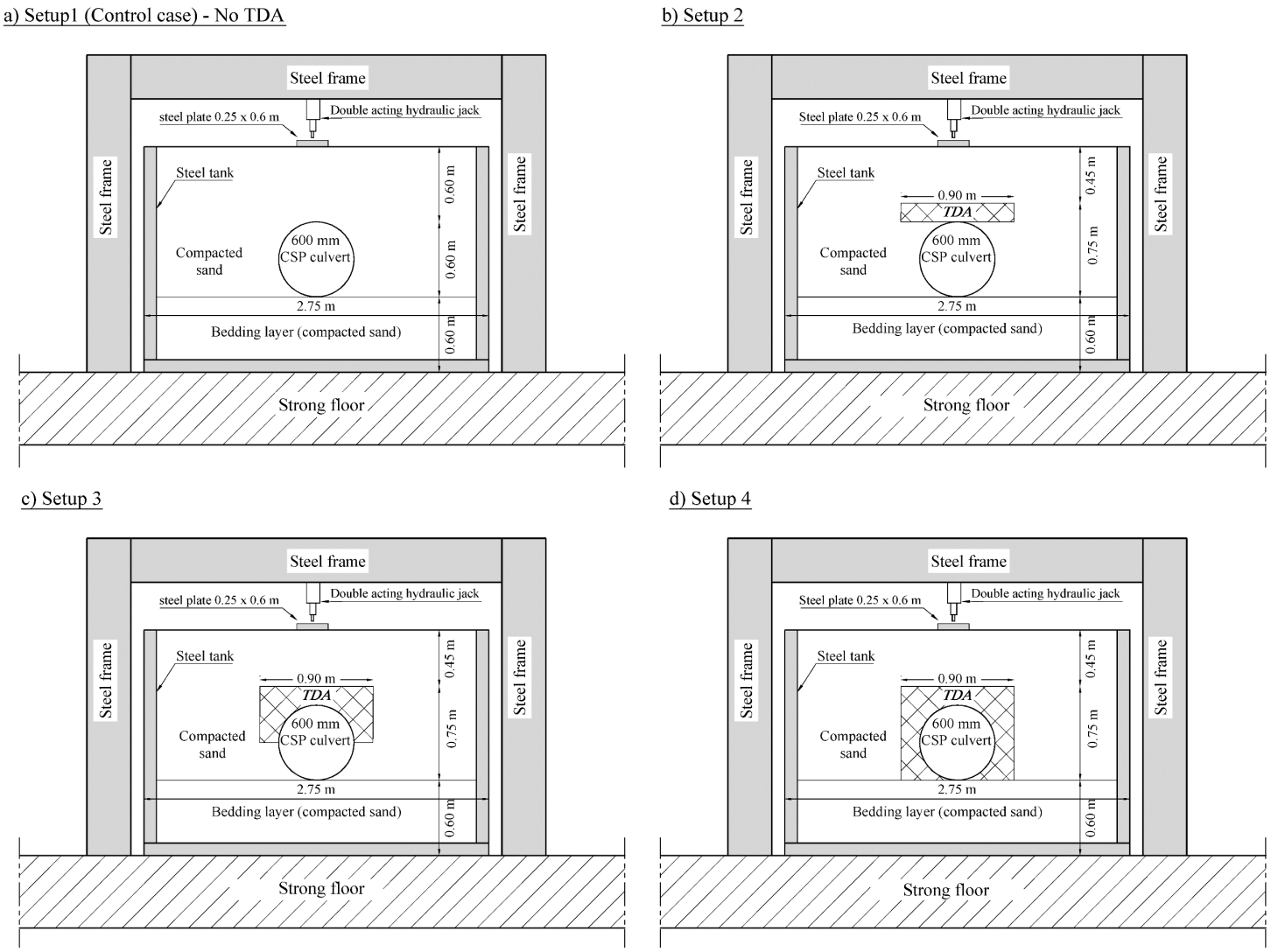

Figure 5-1 Test setups

Figure 5-2 Test components: a) steel tank, b) corrugated culvert, and c) culvert instrumentations

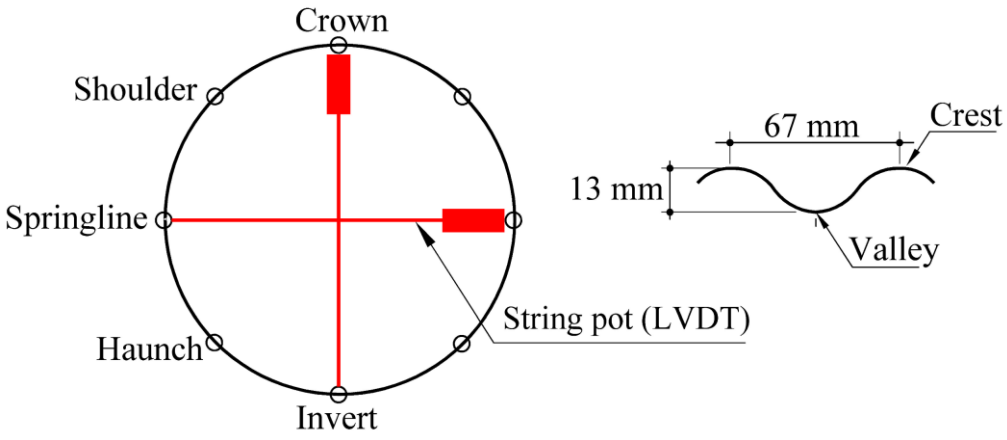

Figure 5-3 Culvert instrumentation locations

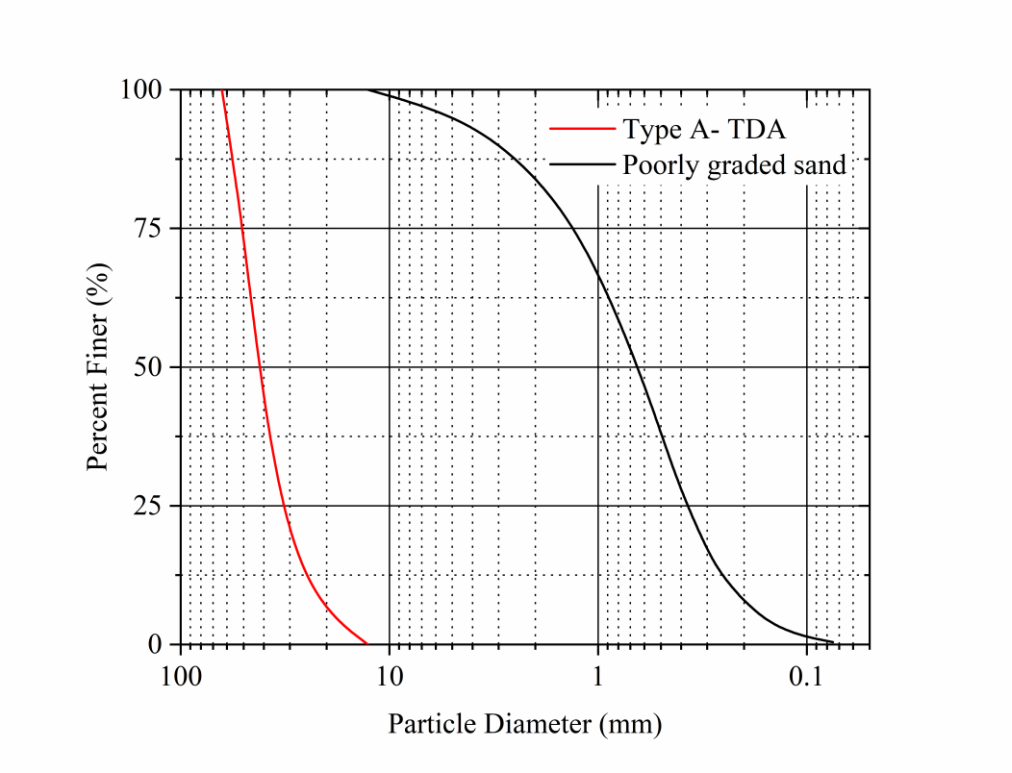

Figure 5-4 Particles size distribution of backfill materials

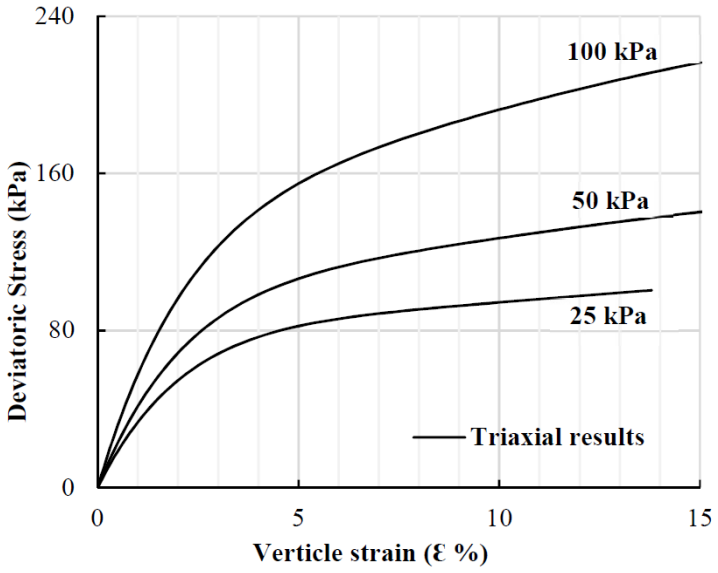

Figure 5-5 Triaxial test results of the TDA material (Ashari and El Naggar 2017)

Figure 5-6 Backfill compaction procedures

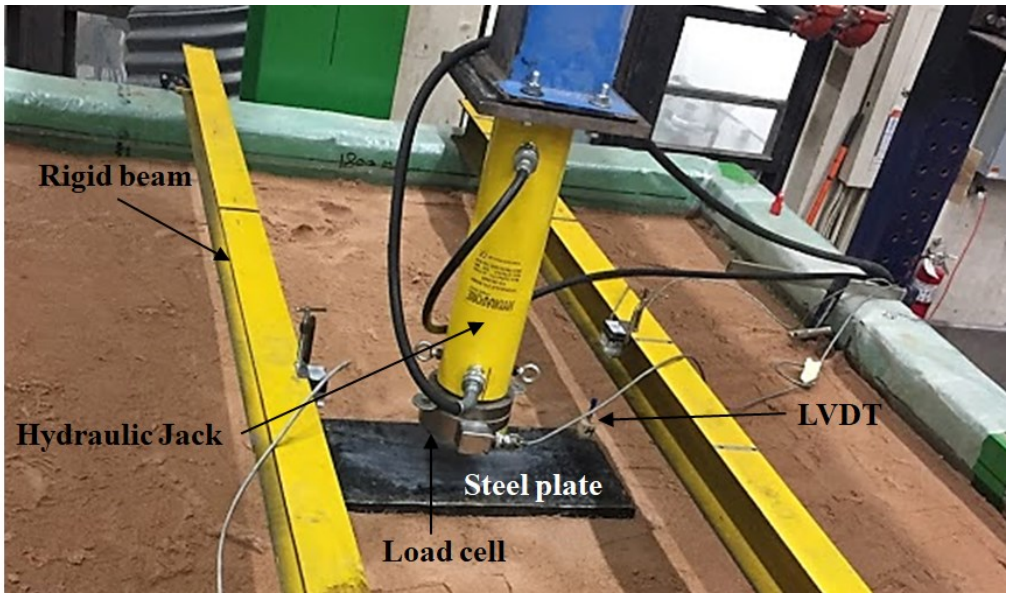

Figure 5-7 Loading plate layout

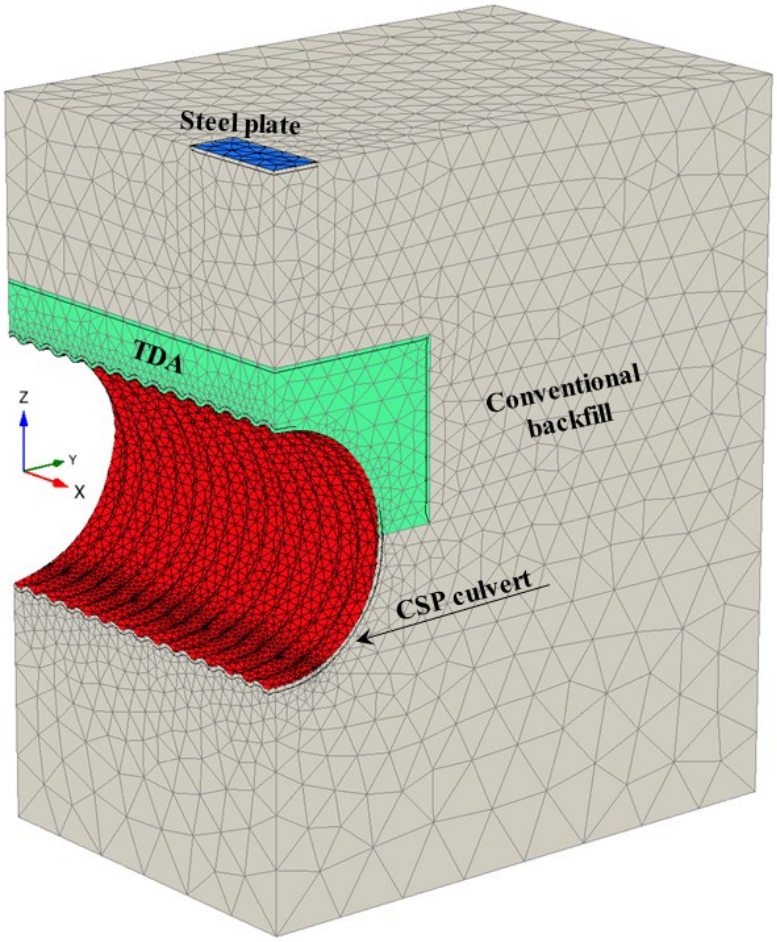

Figure 5-8 Numerical modelling for setup 3

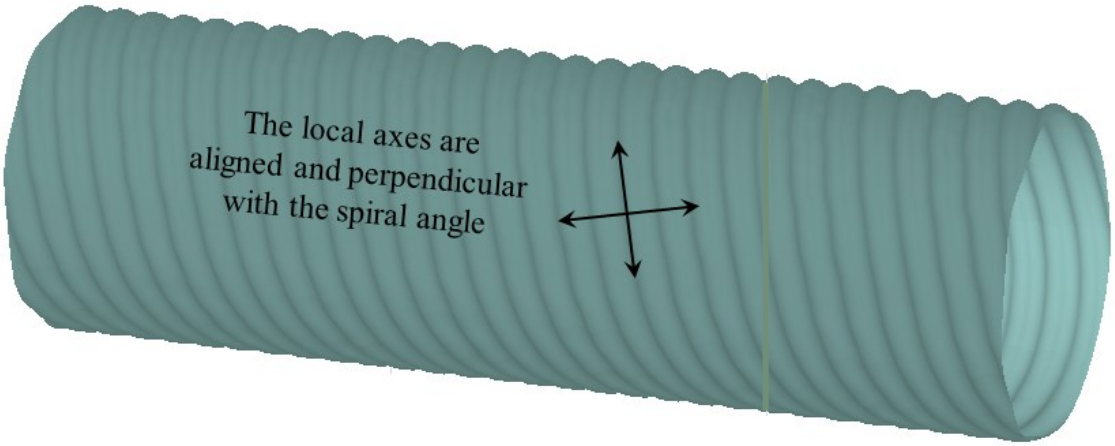

Figure 5-9 Culvert local axes for numerical modelling

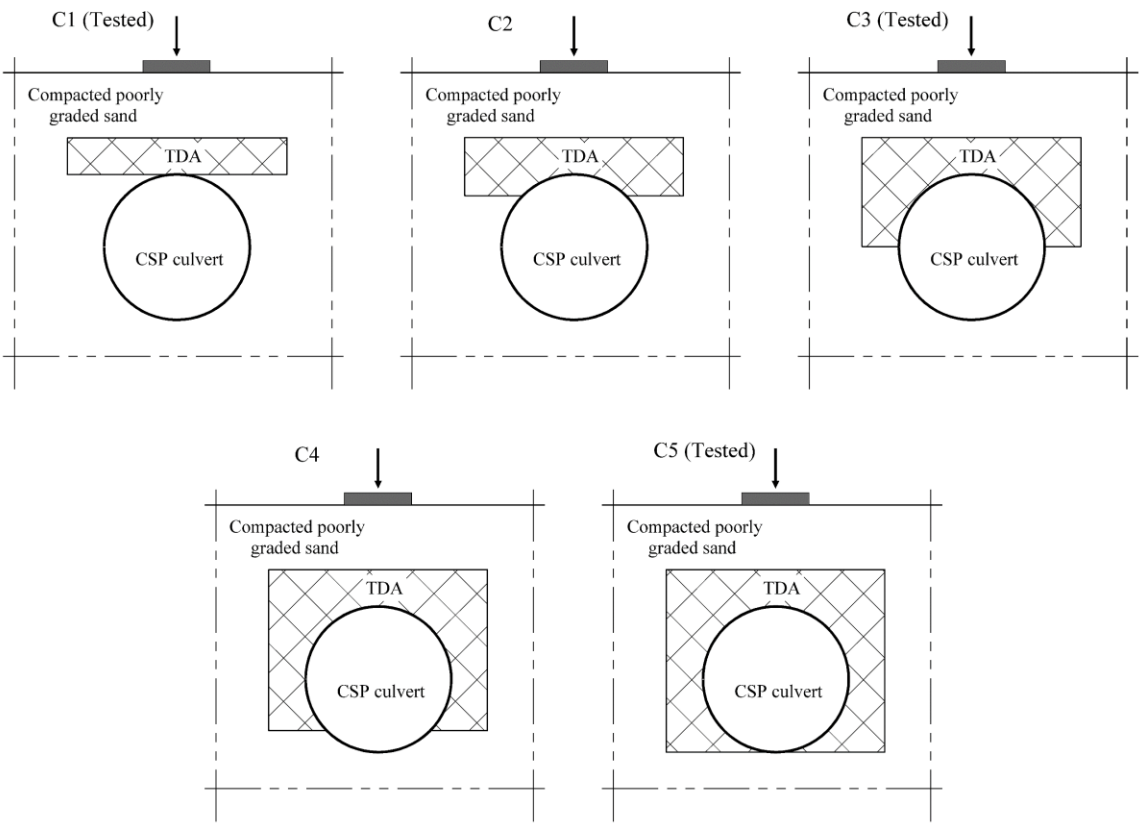

Figure 5-10 Configuratons tested for the first set of models in the parametric study

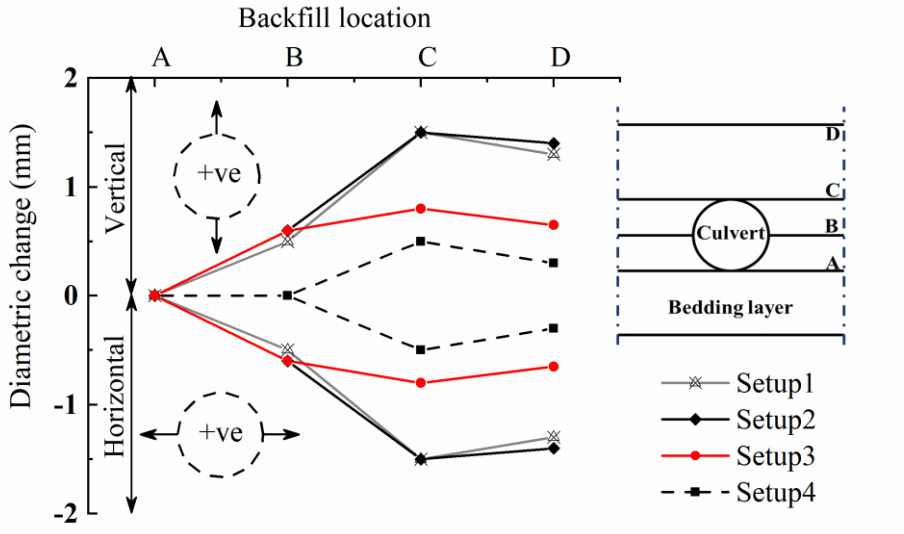

Figure 5-11 Culvert response during backfilling

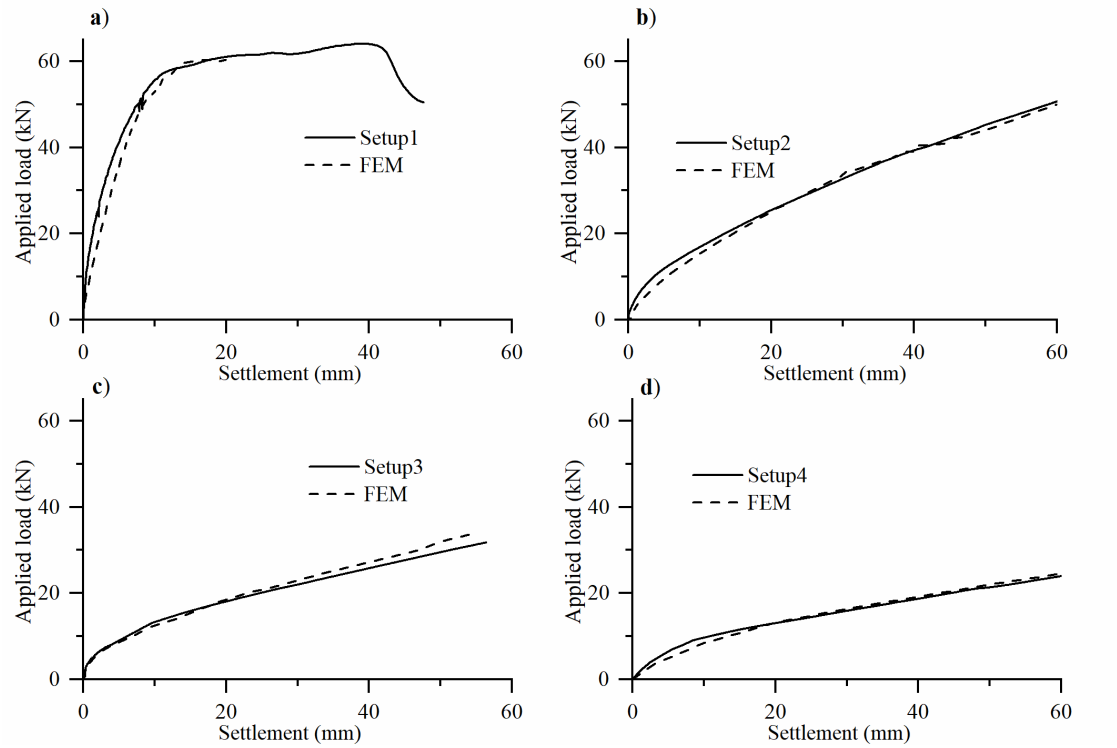

Figure 5-12 Load-settlement curves for the four test setups

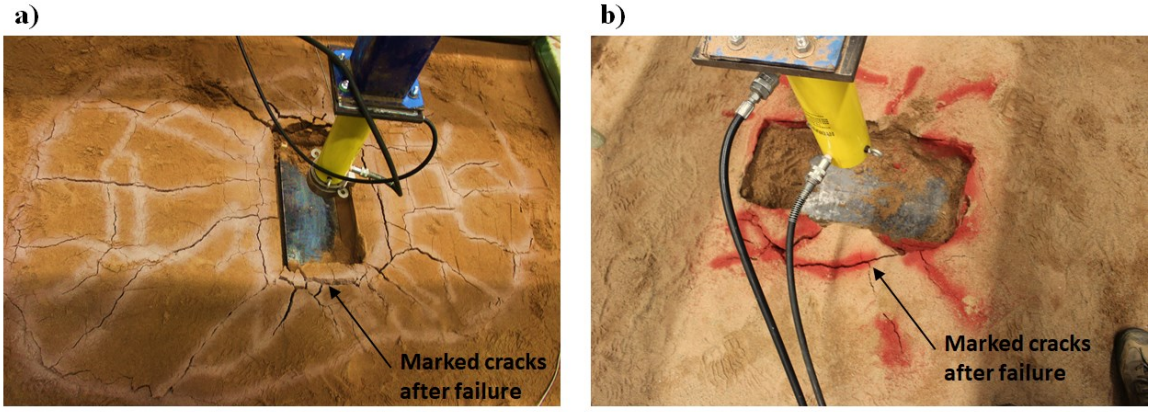

Figure 5-13 Modes of failure: a) Local bearing capacity failure, and b) Punching shear failure

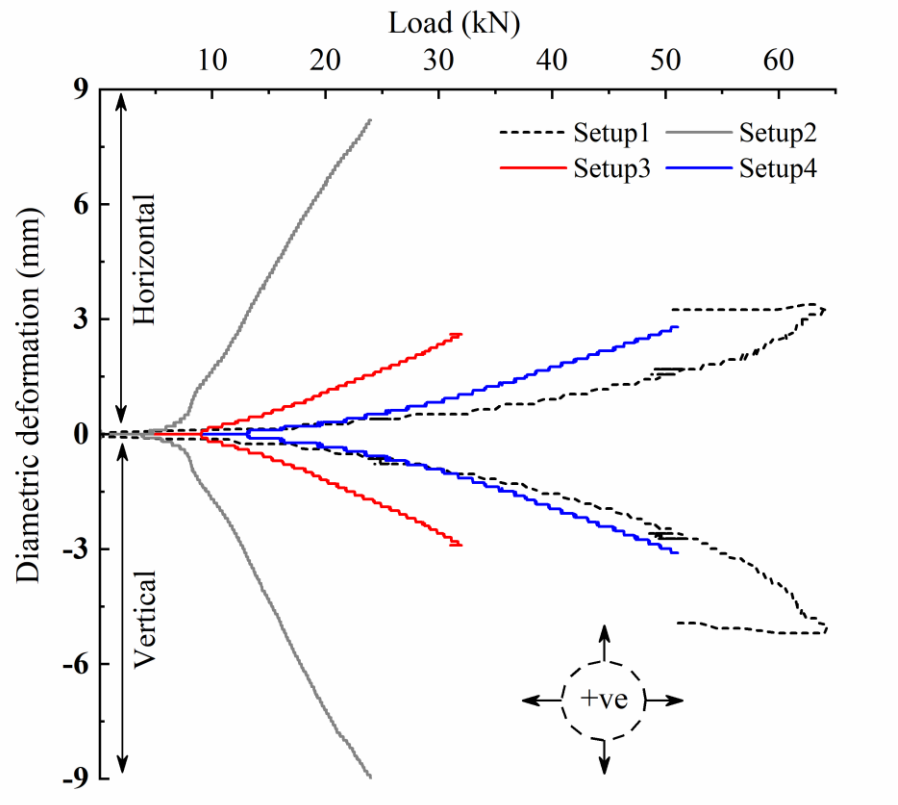

Figure 5-14 Diametric deformation of the culverts tested

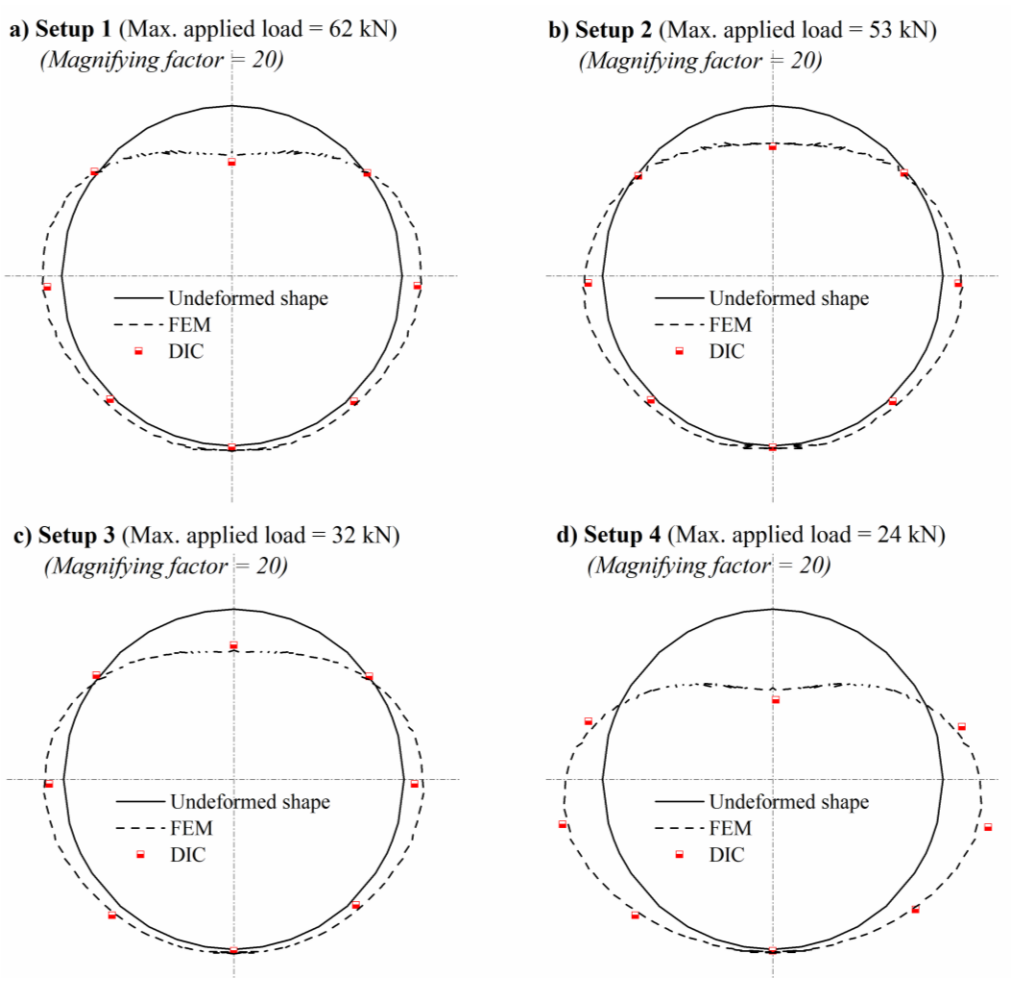

Figure 5-15 Culvert deformation at the maximum applied load for each test

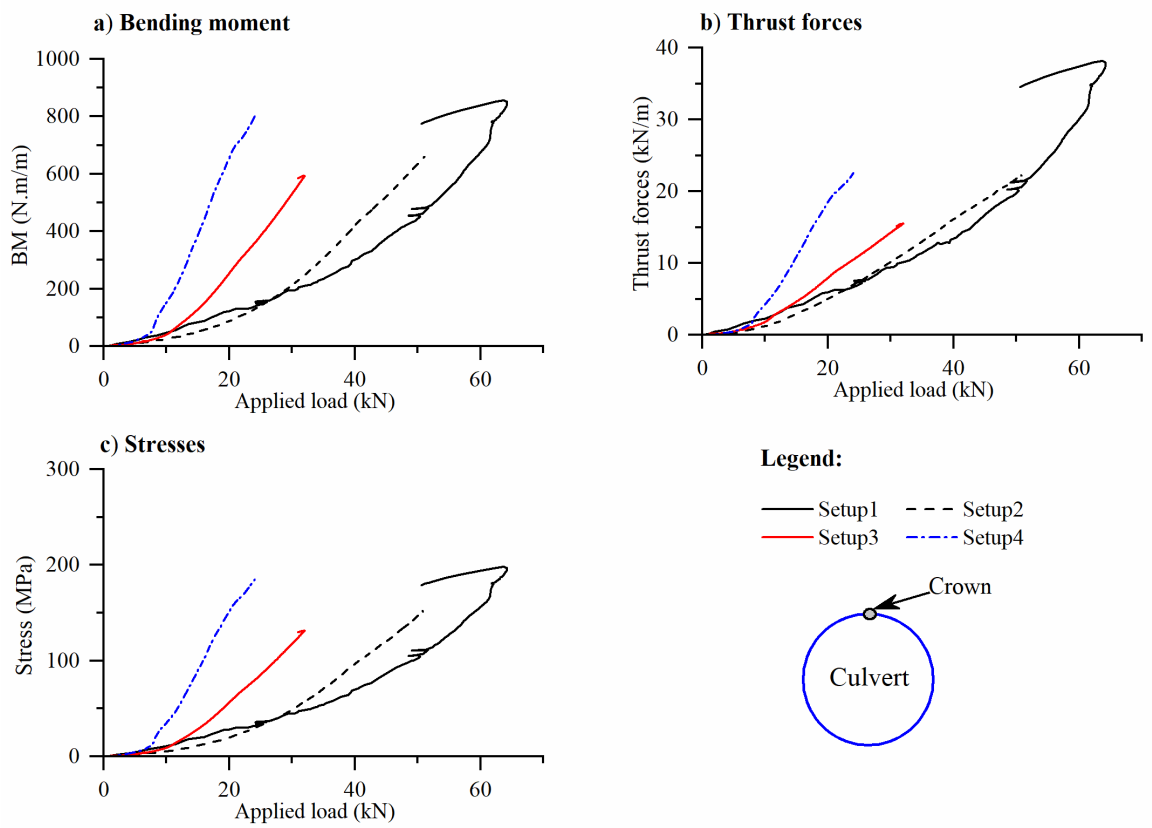

Figure 5-16 Internal forces and stesses at the culvert crown

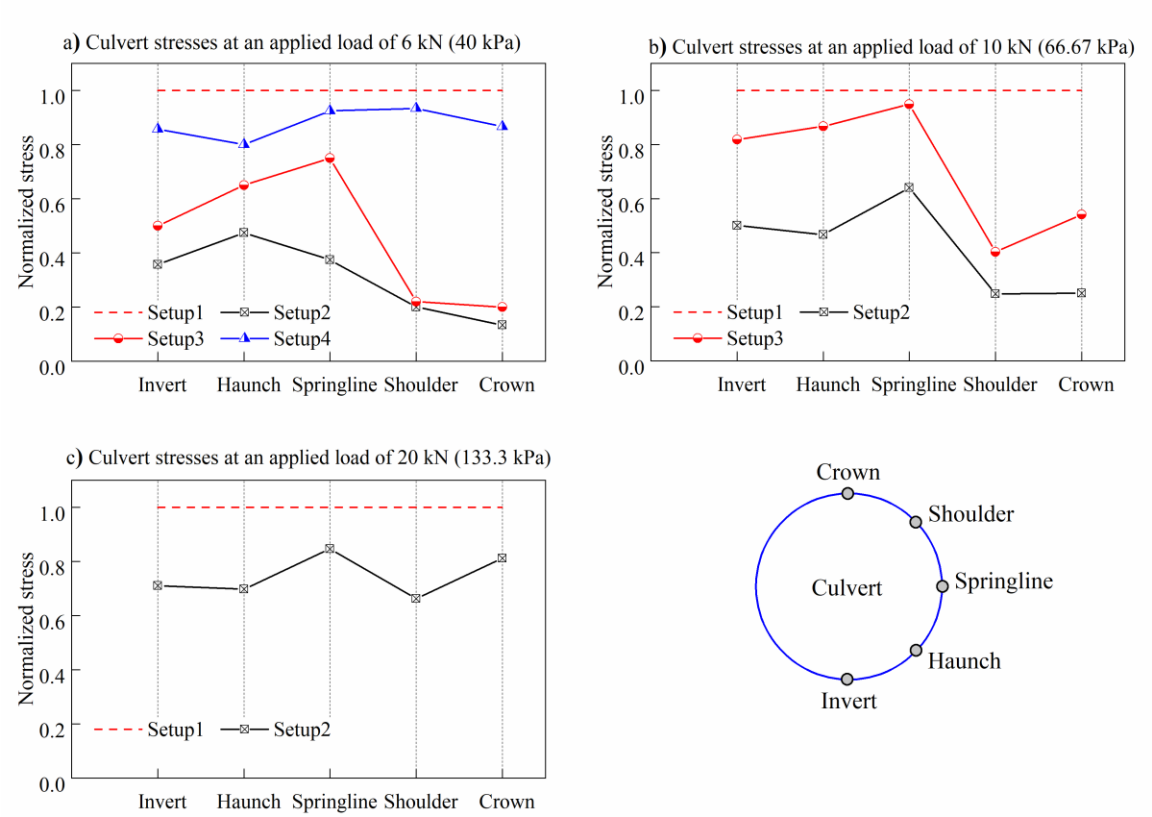

Figure 5-17 Culverts stresses at applied loads that were less than the punching failure loads

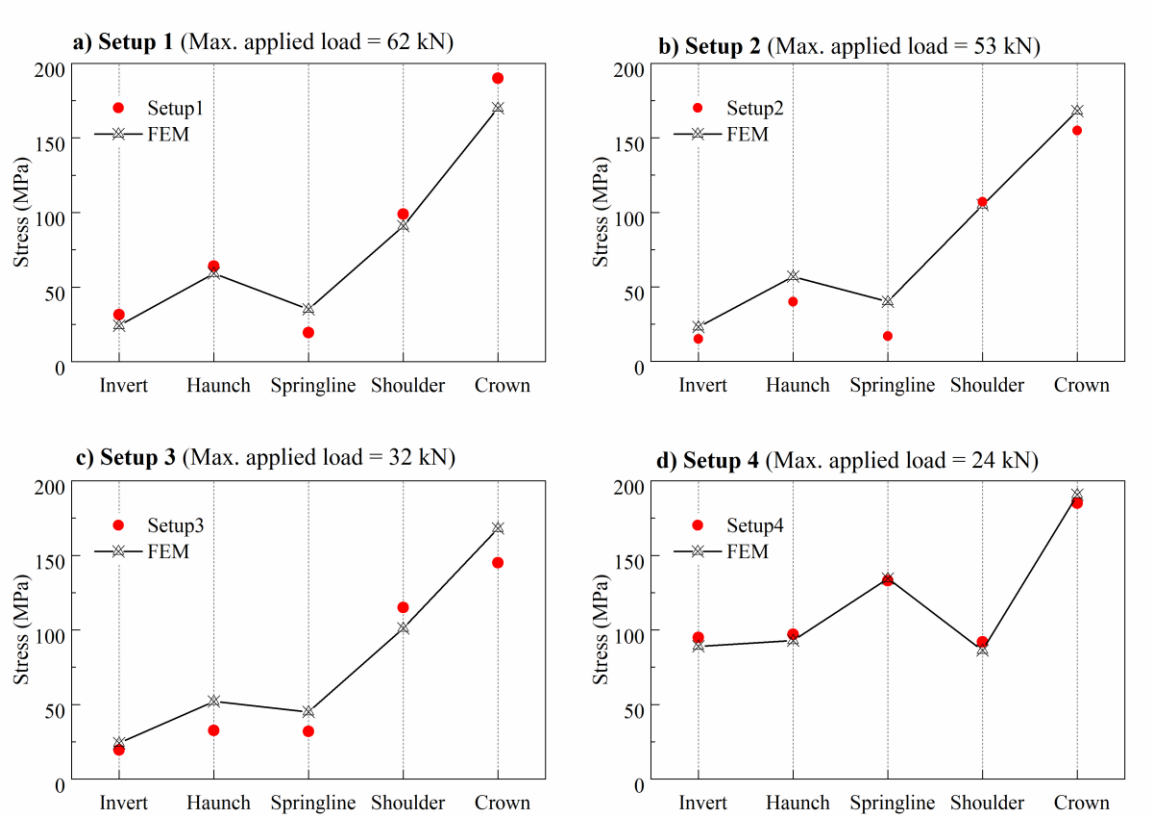

Figure 5-18 Culvert stresses at the maximum applied loads

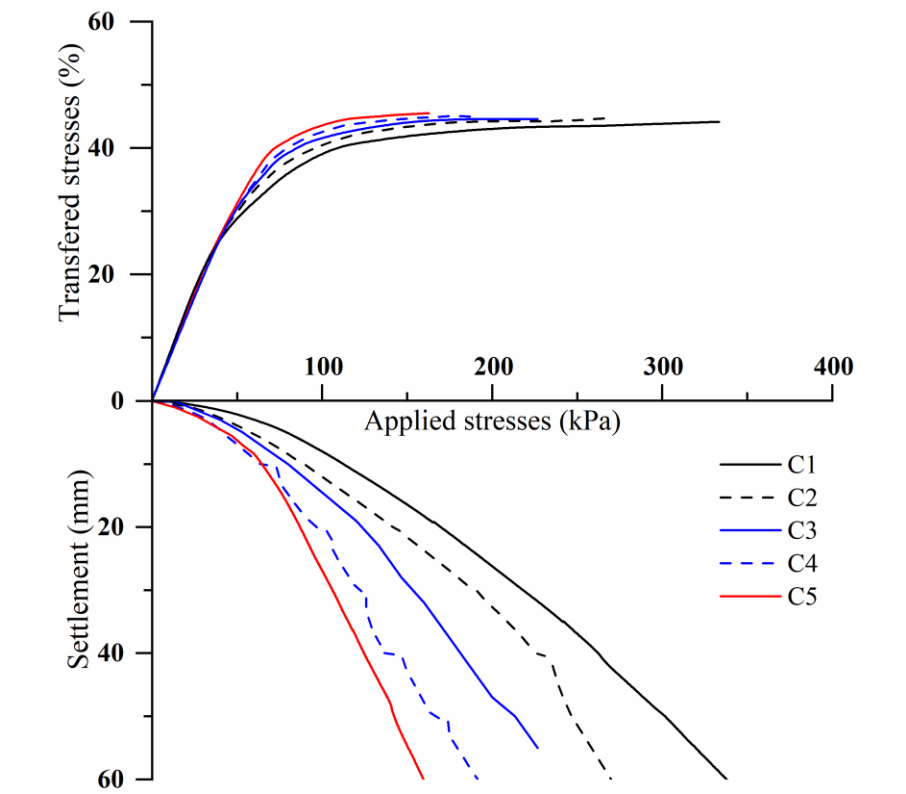

Figure 5-19 Effect of envelope shape of the TDA backfill around the culvert

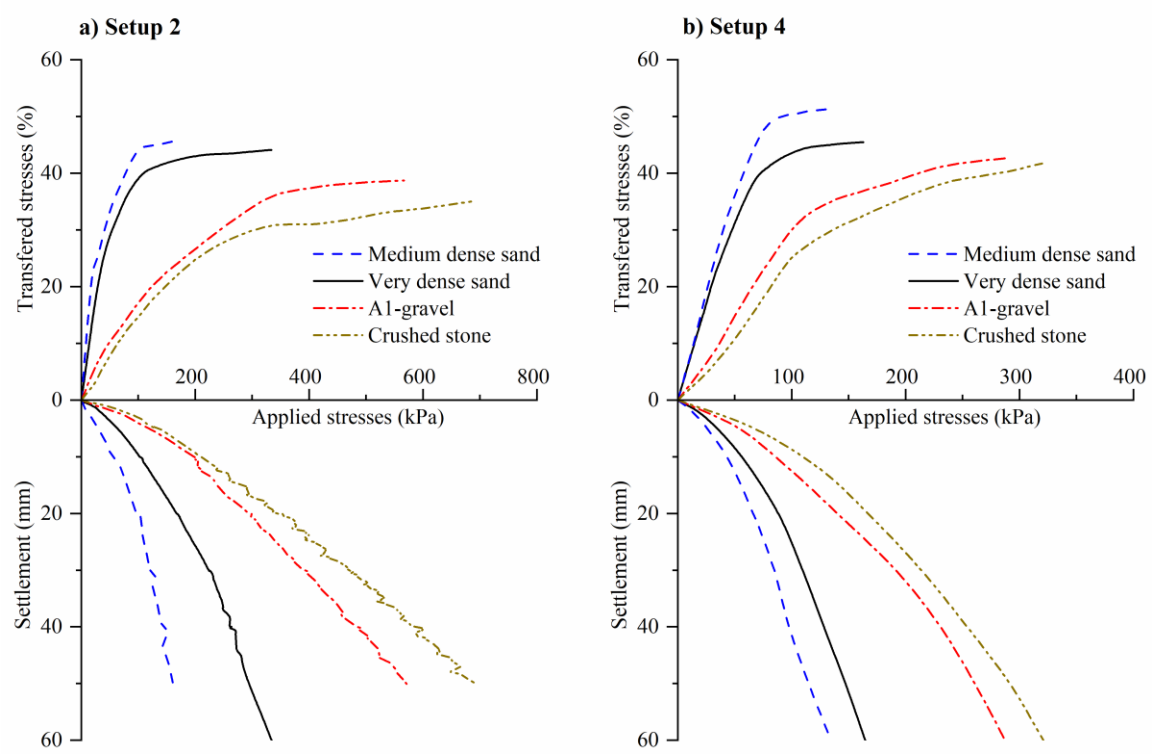

Figure 5-20 Effect of changing the top ganular layer

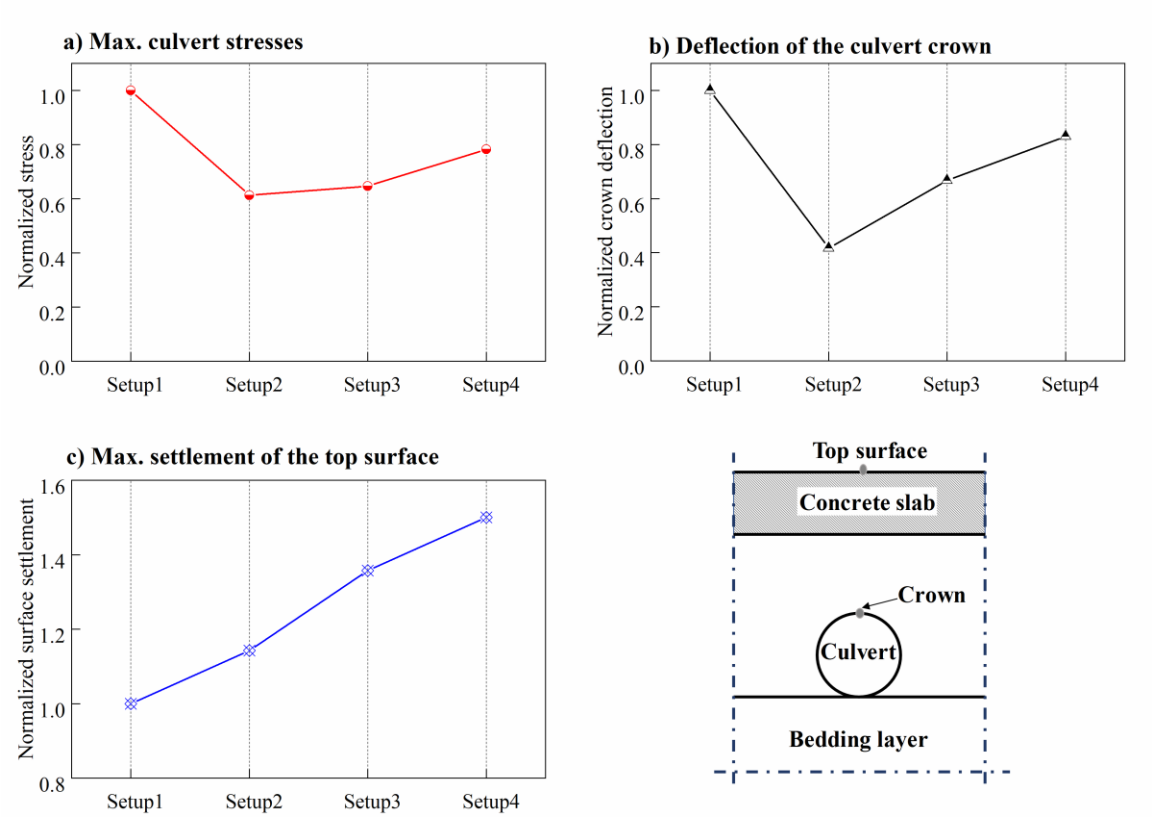

Figure 5-21 Culvert behaviour beneath rigid pavement

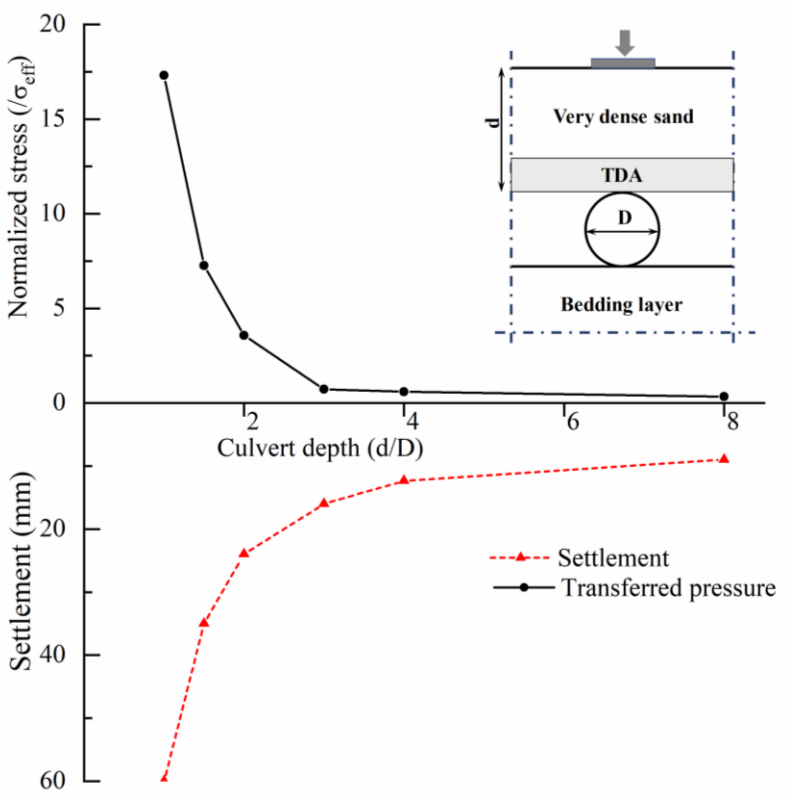

Figure 5-22 Effect of changing the backfill cover height above the culvert crown

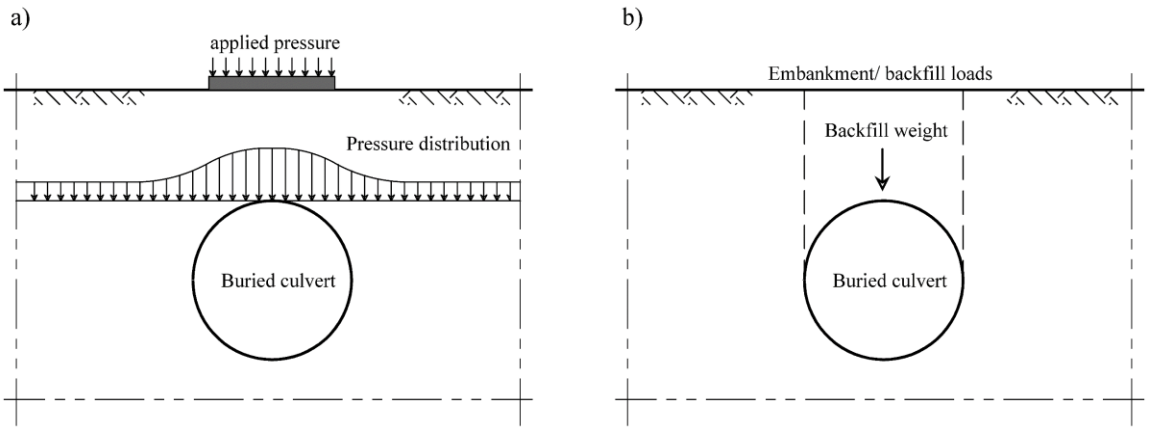

Figure 5-23 Schematic representation of pipe loads: a) surface loading; b) backfill loading

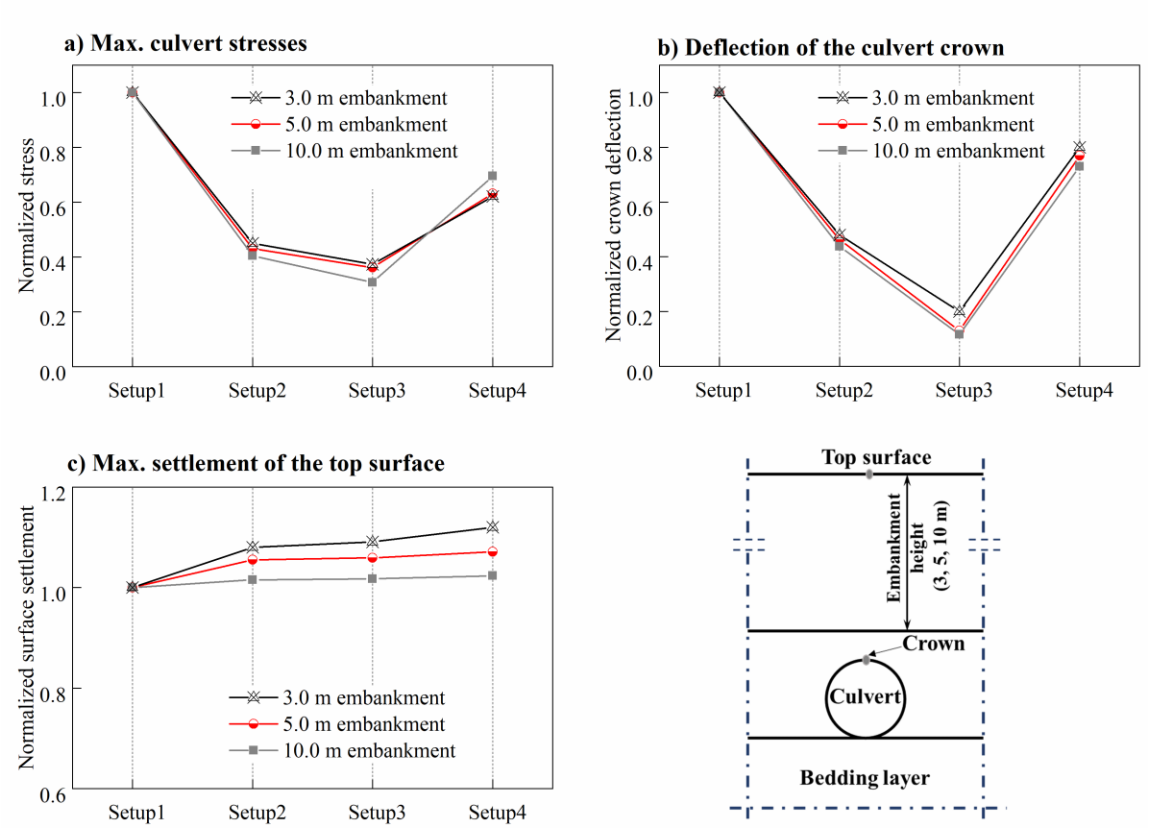

Figure 5-24 Effect of embankment loads on buried culverts

5.6 REFERENCES

Ahn I-S and Cheng L (2014) Tire derived aggregate for retaining wall backfill under earthquake loading. Construction and Building Materials **57**: 105–116, https://doi.org/10.1016/ j. conbuildmat.2014.01.091.

Al-Naddaf M, Han J, Xu C, Rahmaninezhad SM (2019) Effect of geofoam on vertical stress distribution on buried structures subjected to static and cyclic footing loads. Journal of Pipeline Systems Engineering and Practice, 10(1):04018027.

Anderson AO (1913) Vol. 31 of the theory of loads on pipes in ditches: And tests of cement and clay drain tile and sewer pipe. Ames, IA: Iowa State College of Agriculture and Mechanic Arts.

ASTM (2012) D 6270-12: Standard practice for use of scrap tires in civil engineering applications. ASTM International, West Conshohocken, PA, USA.

Ashari M and El Naggar H (2017) Evaluation of the physical properties of TDA-sand mixtures. In GeoOttawa, the 70th Canadian Geotechnical Conference Ottawa. Canadian Geotechnical Society.

Ashari Ghomi M (2018) Large-scale triaxial testing of sustainable TDA backfilling alternatives. Master's thesis. Dalhousie University.

Benson CH, Olson MA and Bergstrom WR (1996) Temperatures of insulated landfill liner. Transportation Research Record **1534(1)**: 24–31, https://doi.org/10.3141/1534-05

Canadian Standards Association (CSA) (2014). CAN/CSA-S6-14 – Canadian Highway Bridge Design Code. Mississauga, Ontario.

Cetin H, Fener M, and Gunaydin O (2006) Geotechnical properties of tire-cohesive clayey soil mixtures as a fill material. Engineering Geology, 88(1–2), 110–120. https://doi.org/10.1016/j.enggeo.2006.09.002

Eaton RA, Roberts RJ and Humphrey DN (1994) Gravel Road Test Sections Insulated with Scrap Tire Chips: Construction and First Year's Results. US Army Corps of Engineers, Cold Regions Research and Engineering Laboratory, Hanover, NH, USA. Special Report 94-21.

Edil TB, and Bosscher P J (1992) Development of engineering criteria for shredded or whole tires in highway applications. Report No. WI 14-92, Department of Civil and Environmental Engineering, University of Wisconsin, Madison, Wisconsin.

El Naggar H, Turan A. and Valsangkar A. (2015) Earth pressure reduction system using geogrid-reinforced platform bridging for buried utilities. Journal of Geotechnical and Geoenvironmental Engineering, 141, No. 6, 04015024.

El Naggar H, Soleimani P, and Fakhroo A (2016) Strength and stiffness properties of green lightweight fill mixtures. Geotech. Geol. Eng. 34 (3): 867–876. https://doi.org/10.1007/s10706-016-0010-1.

Hoppe EJ (1998) Field study of shredded-tire embankment. Transportation Research Record **1619(1)**: 47–54, https://doi.org/10.3141/1619-06.

Humphrey DN (2008) Tire derived aggregate as lightweight fill for embankments and retaining walls. In Scrap Tire Derived Geomaterials — Opportunities and Challenges (Hazarika H and Yasuhara K (eds)). Taylor & Francis Group, London, UK, pp. 59–81.

Humphrey D and Blumenthal M (2010) The use of tire-derived aggregate in road construction applications. In Green Streets and Highways 2010: An Interactive Conference on the State of the Art and How to Achieve Sustainable Outcomes. ASCE, Reston, VA, USA, pp. 299–313.

Mahgoub A, El Naggar H (2019) Using TDA as an Engineered Stress-Reduction Fill over Preexisting Buried Pipes. Journal of Pipeline Systems Engineering and Practice;10(1):04018034.

Marston A (1930) The theory of external loads on closed conduits in the light of the latest experiments. In Vol. 9 of Proc., Highway research board. Washington, DC: Highway Research Board.

McAffee RP, Valsangkar AJ, (2008) Field performance, centrifuge testing, and numerical modelling of an induced trench installation. Can. Geotechnical J. 45 (1), 85e101.

McGuigan B L and Valsangkar AJ (2010) Centrifuge testing and numerical analysis of box culverts installed in induced trenches. Can. Geotech. J. 47 (2): 147–163. https://doi.org/10.1139/T09-085.

McGuigan BL, and Valsangkar AJ (2011) Earth pressures on twin positive projecting and induced trench box culverts under high embankments. Can. Geotech. J. 48 (2): 173–185. https://doi.org/10.1139/T10-058.

Meles D, Bayat A, Hussien Shafiee M, Nassiri S, Gul M (2014) Investigation of tire derived aggregate as a fill material for highway embankment. International Journal of Geotechnical Engineering, 8(2):182-90.

Meguid MA, Youssef TA (2018) Experimental investigation of the earth pressure distribution on buried pipes backfilled with tire-derived aggregate. Transportation Geotechnics, 14:117-25.

Mills B, El Naggar H, and Valsangkar AJ (2015) North American overview and Canadian perspective on the use of tire derived aggregate in highway embankment construction. Chap. 22 in Vol. 2 of Ground improvement case histories, edited by Indraratna and Chu. New York: Elsevier.

Moo-Young, Sellasie K, Zeroka D, and Sabnis G (2003) Physical and chemical properties of recycled tire shreds for use in construction, Journal of Environmental Engineering, 129(10), 921-929.

Ni P, Qin X, Yi Y (2018) Numerical study of earth pressures on rigid pipes with tire-derived aggregate inclusions. Geosynthetics International, 25(5): 494-506.

Plaxis B (2016) Reference manual for PLAXIS 2D. Delft, Netherlands:Plaxis.

Pierre DKS (2013) Canadian waste tire practices and their potential in sustainable construction. Dalhousie Journal of Interdisciplinary Management **9(1)**.

Rodríguez LM, Arroyo M, Cano MM (2018) Use of tire-derived aggregate in tunnel cut-and-cover. Canadian Geotechnical Journal, 55(7):968-78.

Sparkes J, El Naggar H and Valsangkar A (2019) Compressibility and shear strength properties of tire-derived aggregate mixed with lightweight aggregate. Journal of Pipeline Systems Engineering and Practice **10(1)**, https://doi.org/10.1061/(ASCE)PS.1949-1204.0000354.

Spangler MG (1950a) A theory of loads on negative projecting conduits. In Vol. 30 of Proc., Highway Research Board, 153–161. Washington, DC: Transportation Research Board.

Spangler MG (1950b) Field measurements of the settlement ratios of various highway culverts. Bulletin 171. Ames, IA: Iowa Engineering Experiment Station.

Spangler MG, and Handy RL (1973) Soil engineering. New York: Intext Educational.

Tafreshi SM, Mehrjardi GT, Dawson AR (2012) Buried pipes in rubber-soil backfilled trenches under cyclic loading. Journal of Geotechnical and Geoenvironmental Engineering;138(11):1346-56.

Tweedie JJ, Humphrey DN and Sandford TC (1998) Full-scale field trials of tire shreds as lightweight retaining wall backfill under at-rest conditions. Transportation Research Record **1619**: 64–71, https://doi.org/10.3141/1619-08.

Turan A, El Naggar MH, and Dundas D (2013) Investigation of induced trench method using a full-scale test embankment. Geotech. Geol. Eng. 31 (2): 557–568. https://doi.org/10.1007/s10706-012-9608-0.

Wartman J, Natale M and Strenk P (2007) Immediate and time-dependent compression of tire derived aggregate. Journal of geotechnical and geoenvironmental engineering, 133(3), pp.245-256.

Xiao M, Bowen J, Graham M and Larralde J (2012) Comparison of seismic responses of geosynthetically reinforced walls with tire-derived aggregates and granular backfills. Journal of Materials in Civil Engineering **24(11)**: 1368–1377, https://doi.org/10.1061/(ASCE)MT.1943- 5533.0000514.

CHAPTER 6 COUPLED TDA-GEOCELL STRESS BRIDGING SYSTEM FOR METAL PIPES

Ahmed Mahgoub and Hany El Naggar

6.1 INTRODUCTION

Many new and pre-existing pipeline networks will have to share space with other infrastructure and be subjected to traffic and construction loads in addition to the dead weight of the soil. In urban areas such networks are usually buried beneath roads at shallow depths by using conventional trenching and backfilling techniques. Unfortunately, it is not uncommon for buried pipelines, conduits, and utilities to fail due to heavy traffic loading. This can result in deaths, injuries, reduced functionality and significant economic losses.

Geosynthetics have been used for many years to protect buried pipes and underground utilities (Moghaddas and Khalaj 2008; Palmeira and Andrade 2010). Several field and laboratory studies have been conducted to examine the response of conduits buried beneath geogrid reinforced backfill and subjected to cyclic loads. These studies found a significant reduction in deformation in the presence of geogrid reinforcement (Moghaddas and Khalaj 2008; Palmeira and Andrade 2010).

In recent years, geocells have demonstrated their effectiveness in various geotechnical engineering applications, exhibiting their potential to surpass the performance of other soil reinforcement alternatives. Geocells are three-dimensional (3D) panels manufactured from welded high-strength polymers or polymeric alloys such as polyethylene, polyolefin, etc. (Hegde and Sitharam 2015). The geocell reinforcing mechanism provides confinement for surrounding materials via its interconnected cells, thus preventing the lateral spreading of

soils as loads are applied. Therefore, geocells serve as a stiffer mattress that redistributes applied loads over a wider area (Dash et al. 2007). Geocell reinforcement behaviour depends upon factors such as geometric characteristics, the tensile strength of the material from which the geocell is made, subgrade and fill aggregate compaction, and soil cover thickness (Kargar and Hosseini 2016; Zhang et al. 2018).

Many studies have shown the efficacy of using geocells to enhance road construction by reducing road deformation and rutting characteristics (Cuelho and Perkins 2009; Madhavi et al. 2010; Pokharel et al. 2011). For instance, Al-qadi and Hughes (2000) conducted a field test by using geocells to stabilize the subgrade beneath flexible pavement. The study demonstrated that using a combined geocell and geogrid system significantly improved the performance of flexible pavement over a weak subgrade. In addition, many studies have utilized geocells in soil layers beneath foundations, to increase the bearing capacity and decrease settlement (Dash et al. 2003; Hedge and Sitharam 2017; Thakur et al. 2012). Many researchers have highlighted the benefits of using geocells as a type of reinforcement above buried pipes, to reduce both pipe deformation and soil settlement (Mehrjardi et al. 2012; Mehrjardi et al. 2013; Mehrjardi et al. 2015). Hegde and Sitharamth (2015) investigated a geocell-geogrid combination to protect underground utilities and buried pipelines by performing small-scale laboratory tests with 75 mm polyvinyl chloride (PVC) pipes. The study also included 3D numerical analyses to simulate the problem. The study concluded that a 40% reduction in buried pipe stresses was achieved when soil reinforcement was used above the pipe.

The increasing utilization of vehicles worldwide generates large quantities of used tires. Around one billion scrap tires have been discarded globally, with over 250 million in the

USA and 30 million in Canada (El Naggar et al. 2016). Promotion of the re-use and recycling of rubber tires has increased progressively since 1990, because of the environmental hazards associated with uncontrolled landfill disposal (Rubber Manufacturers Association 2017). Stockpiled waste tires are flammable and may produce toxic fumes that can result in serious health hazards for human beings (Pierre, 2013). Scrap rubber tires can be recycled via tire-derived fuel (TDF), ground rubber applications, rubberized asphalt-concrete mixtures, and tire-derived aggregate (TDA) in civil engineering applications (Rubber Manufacturers Association 2017).

Tire-derived aggregate is generally used in civil engineering applications as a lightweight backfill material. It is commonly produced by cutting waste tires into relatively small pieces (12 mm to 300 mm). ASTM D6270 classifies TDA into two types: Type A has a smaller particle size and is usually used as an insulation material for road projects or a fill material behind retaining walls; whereas type B, which consists mainly of larger particles, is primarily used as an embankment fill. Shredded tire products have several desirable geotechnical properties that can enhance the overall performance of civil engineering infrastructure. Such products weigh only one-third to half as much as conventional granular backfill materials. The specific gravity of TDA ranges from 1.15 to 1.21, while the specific gravity of conventional backfill ranges from 2.55 to 2.75 (Edil 2005; Sparkes et al. 2019). Moreover, TDA is considered to be a durable material that resists degradation in a severe operating environment. TDA has been utilized as a drainage material beneath perforated leachate collection pipes (Rowe and McIsaac 2005). Edil et al. (2005) showed that, in drainage applications, the permeability of TDA is ten times that of gravel. In addition, TDA is regarded as a good thermal insulator and is eight times more effective than regular soil

in this respect (Eaton et al. 1994; Benson et al. 1996; Rezaei et al. 2012). The use of TDA as a lightweight backfill material in embankments and retaining wall projects has been examined by many researchers (Bosscher et al. 1992; Tweedie et al. 1998; Hoppe 1998; Humphrey et al. 2000; Salgado et al. 2003; Yoon et al. 2006; Humphrey, 2008; Humphrey and Blumenthal 2010; Xiao et al. 2012; Meles et al. 2014; Mills et al. 2015).

TDA has been used in trench fill projects above buried pipes, culverts, and cut-and-cover tunnels to enhance the arching mechanism. Because TDA has high deformability, it can be advantageous for inducing an increased settlement differential between the soil prism above the pipe and the adjacent soil. Consequently, a positive arching effect can be achieved that reduces earth pressures and decreases the stresses of buried structures (Meguid and Youssef 2018; Ni et al. 2018; Rodríguez et al. 2018; Mahgoub and El Naggar 2019).

Mehrjardi et al. (2012) conducted small-scale tests to investigate the combined use of geocell reinforcement and rubber-soil mixtures (with rubber contents of 5%, 10%, and 20%) around buried 160-mm PVC pipes. The study concluded that the use of geocell reinforcement with a backfill material that included 5% shredded rubber provided the best performance in terms of reducing pipe deformation and backfill settlement.

This chapter presents the results of six full-scale tests to investigate the efficacy of using a coupled TDA-geocell stress bridging system to enhance the performance of buried metal culverts. Previous studies in the literature conclude that although TDA exhibits an outstanding performance in enhancing the arching mechanism over buried infrastructure, the corresponding settlement of the loaded surface increases significantly when the TDA

is located at a shallow depth. Therefore, geocells were used in this study to mitigate some of the serviceability issues associated with surface settlement, and to explore the benefits of using geocells to enhance stress bridging over culverts. Subsequently, three-dimensional finite element models (FEM) of the tests were developed for validation against the test results, and for investigation of the infrastructure-soil interaction mechanism of the problem under consideration. An extensive parametric study was then conducted to examine the effect of some important parameters on the performance of the system investigated (i.e., the geocell width, geocell installation depth, granular backfill stiffness, number of geocell layers, and culvert embedment depth).

6.2 EXPERIMENTAL SETUP

Six full-scale tests were carried out to investigate the effect of using geocell reinforcement to reduce the stresses in buried corrugated steel plate (CSP) culverts and to decrease the settlement of the backfill surface over the culverts. Three test configurations, C1, C2, and C3 were used, as illustrated in Figure 6-1. Each of the configurations considered had two test setups, one without geocell reinforcement, to act as a basis for comparison, and the other with the proposed geocell bridging system. For ease of reference, a naming scheme for the tests was adopted. The first part of each test name refers to the configuration (i.e., C1, C2, or C3). The second part indicates whether the test setup uses TDA only (T0), geocell only (0G), the TDA-geocell coupled system (TG), or neither TDA nor geocell (00). Thus, the test setups for the six tests conducted are referred to as: C1-00 and C1-0G; C2-T0 and C2-TG; and C3-T0 and C3-TG. For example, the C2 configuration test setup with the proposed TDA-geocell coupled system is referred to as C2-TG, whereas the C2 test setup with no geocell reinforcement is referred to as C2-T0. Configuration C1 examined

the behaviour of a CSP culvert in conventional backfill (poorly graded sand) with no TDA. Configuration C2 had the same layout as C1, except that C2 included a layer of TDA (with a thickness of 150 mm, i.e.1/4 of the culvert diameter) above the culvert crown. Configuration C3 had the same layout as C2, except that in addition to the layer of TDA above the culvert crown, C3 included TDA surrounding the upper part of the culvert down to the springline. The cover height above the culvert crown for all the configurations tested was 600 mm (1D, where D is the culvert diameter).

The spiral CSP culverts tested had a diameter of 0.6 m, a length of 2.0 m, and a spiral angle of 17°. The corrugation amplitude (h) was 13 mm, with a period of 67 mm and a wall thickness (t) of 1.6 mm (see Figure 6-2). The corrugated steel plate had an area per unit length A = 1.64 mm^2/mm and a second moment of area per unit length I = 31 mm^4/mm. The steel had a yield strength (F_y) of 230MPa, a tensile strength (F_u) of 310 MPa, and a Young's modulus of 200,000 MPa.

The tests were conducted in a steel tank with rigid walls. The tank had a length of 2.75 m, a width of 2.2 m, and a depth of 1.8 m. The tank walls were designed to be self-contained and sufficiently rigid to prevent any lateral movement caused by the high loads applied inside the tank (Figure 6-2). It can be seen from Figure 6-5 that a rigid frame was positioned over the tank for loading purposes. In each test, a steel plate with the dimensions of the wheel pair at one end of a single axle of the design truck CL-625-(ONT) (CSA, 2014) was used for loading. As shown in Figure 6-5, a steel plate 50 mm thick, with a length of 600 mm and a width of 250 mm was utilized to simulate the wheel pad on the backfill surface.

6.2.1 Backfill

The conventional backfill used in this study was classified as poorly graded sand (SP) in accordance with ASTM D 2487-17. The soil grading is shown in Figure 6-3. The optimum water content (W_c) and maximum dry density of the granular backfill were determined by using a Proctor test and were found to be 13.8% and 17.75 kN/m^3, respectively. The drained shear strength parameters and modulus of elasticity, obtained by using triaxial tests, are presented in Table 6.1.

The TDA material used in the tests was classified as type A, with particles ranging in size from 13 mm to 63 mm. The grading of the TDA material used is shown in Figure 6-3a. The average dry density of the TDA used was approximately 7 kN/m^3. A full laboratory test program was performed by Ashari Ghomi (2018) and Ashari et al. (2017) to determine the TDA material characterization and shear strength parameters. A series of large-scale triaxial tests, Proctor tests and sieve analyses were performed to find the shear strength parameters, classify the material, and determine the maximum dry density. A more detailed description of the laboratory testing program is provided in (Ashari Ghomi 2018; Ashari et al. 2017). For the TDA used, the drained internal friction angle (φ') was found to be 26.5° and the cohesion (c') was 24 kPa. Figure 6-3b shows the relationship between the deviatoric stress and axial strain of the TDA at different confinement pressures.

6.2.2 Geocell Reinforcement

Geocell type GF30 manufactured by Gridforce was used in this study to assess its performance as a soil reinforcing element. Figure 6-1d shows the typical geometry and configuration of the geocell product used in this study. The geocells are manufactured from low-density polyethylene (LDPE) in the form of three-dimensional interconnected cells.

Each cell is 70 mm wide, 70 mm long, and 30 mm deep. The cell wall thickness is 3 mm. The geocells were manufactured in the form of square tiles having a width of 500 mm. The geocells were installed by laying them on a level base, then the tiles were interlocked with one another to spread to the required dimensions. Finally, a layer of backfill material was added to cover the geocells before compaction. The LDPE had a tensile strength (F_u) of 20 MPa, and a Young's modulus of 300 MPa.

6.2.3 Instrumentation

The vertical and horizontal diameter changes of the culvert during loading were measured by using two linear variable differential transformers (LVDTs) manufactured by TE Connectivity. The voltage driver outputs provided measurements with an accuracy of 0.25% (see Figure 6-2). They were installed at the middle cross-section of the test culvert, directly below the loaded area at the top surface of the soil. Two additional LVDTs were installed at diagonal corners of the loading plate at the top surface of the soil, to measure the plate settlement during loading (see Figure 6-5).

A camera was set up just outside the culvert to take pictures along its longitudinal axis during loading for use with digital image correlation (DIC). A Canon Rebel T4i digital SLR camera was positioned at an opening in the steel tank at the culvert location. Subsequently, the culvert deformations were obtained by using the Ncorr MATLAB code for photo processing. As shown in Figure 6-1b, white target cubes were glued to the inner circumference of the culvert at the middle cross-section.

Sixteen strain gauges were mounted on the inner surface of the culvert with a half bridge circuit arrangement. At each gauge location (i.e., the crown, shoulders, springlines,

haunches, and invert), the culvert surface was rubbed with sandpaper; then it was wiped and dried before the strain gauges were attached by using liquid adhesive. At each location two strain gauges were mounted (at the valley and the crest), parallel to the corrugation spiral angle (see Figure 6-2d). The strain gauges measured changes in the culvert thrust forces and bending moments during loading. The strain gauges used were F series foil gauges manufactured by the OMEGA company, with operating temperatures from $-10°$ to $45°$ C and a grid resistance of 350 ohms. In addition, the loads applied to the steel plate were measured by using a load cell, as shown in Figure 6-5, and a hydraulic jack was fixed on a rigid steel frame. All the data were acquired by using a computerized data acquisition system.

6.2.4 Test Procedures

Prior to conducting the test, the walls of the steel tank were greased, then they were covered with high-density polyethylene sheets to ensure movement in the vertical direction between the tank and the fill soils (see Figure 6-2a). Backfill was placed in the tank by using heavy duty bulk bags with a bottom spout. The backfill was compacted in lifts 150 mm thick by using a vibrating plate tamper and tested by using a sand cone test to ensure that it reached the desired compaction level (95% of the standard Proctor dry density). After the first 600 mm of the granular layer (the bedding layer) was compacted, the instrumented culvert was placed at the designated level. With the aid of a laser level, the center of the culvert to be tested was aligned directly beneath the hydraulic jack. For the C1 configuration test setups (C1-00, and C1-0G), the sandy backfill material was placed and compacted around and above the culvert in 150 mm lifts until the top level (600 mm above the culvert crown) was reached. Hand tamping with a steel plate tamper was used to compact the backfill near the

culvert to protect the culvert from any damage. For test setups C1-0G, C2-TG, and C3-TG, a geocell layer was placed at 550 mm above the culvert crown (see Figure 6-1) to allow for a 25-mm granular layer above the geocell panels.

For the C2 configuration, a 150-mm layer of TDA was placed and compacted above the culvert crown. For the C3 configuration. additional TDA was also placed around the upper part of the culvert down to the springlines (see Figures 6-1b and c). In order to separate the TDA from the surrounding granular backfill, a thin polymeric membrane was placed between the TDA and the backfill. After backfilling was complete and the designated top level had been reached, loading was applied to the surface through a steel plate designed to simulate a wheel pair measuring 250 mm x 600 mm. The steel plate was positioned directly above the center (the instrumented cross-section) of the culvert to be tested and below the hydraulic jack (see Figure 6-1). As shown in Figure 6-5, two rigid steel beams were placed above the steel plate and supported so as to be stationary during application of the loads. Two LVDTs were then fixed to the framework and attached to diagonal corners of the plate. As illustrated in Figure 6-5, a load cell was placed between the hydraulic jack and the steel plate. For every test, progressive loading was applied until failure or until excessive settlement occurred (60 mm). The measurements taken during each test (i.e., culvert strains, load cell readings, and loaded plate settlement) were then utilized to examine the soil-structure interaction (SSI) of the systems investigated and to explore the effectiveness of the systems in reducing the surface settlement and the stresses received by the culvert.

6.3 NUMERICAL ANALYSIS

Three-dimensional numerical simulations for analysis of the coupled TDA-geocell stress bridging system for metal culverts were performed by using the finite element code PLAXIS 3D 2018. Model geometry, model calibration and verification, and a parametric study are discussed in the following sections. The FE analysis was developed in two stages. The first stage comprised the verification of the conducted full-scale tests. The second stage then included the parametric study.

6.3.1 Model Geometry

The tests executed with different configurations (as presented in Figure 6-1) were simulated to validate the FE models by comparing the FE results with the results of the tests. The 3D modelling therefore adhered to the dimensions, material properties and construction sequence used in the full-scale tests. One-quarter of the problem was modelled, to benefit from the test setup symmetry in the two horizontal directions. Thus, the extent of the computations and the number of elements were reduced. Figure 6-6 illustrates the FE model developed for setup C3-TG and includes the different elements used in the analysis.

A high order 10-noded tetrahedral FE element from the element library of PLAXIS 3D-2018 was utilized for the soil elements. Figure 6-6 shows the FE mesh of one of the numerical models used for the verification (C3-TG). The verification models comprised around 70,000 elements, with an average element size of approximately 20 mm in the zone between the culvert and the loading plate. The large number of small elements assured a high level of accuracy, especially at locations where nonlinear behaviour was anticipated.

The spiral CSP culvert was modelled by using a plate element from the PLAXIS library. The actual corrugation shape was simulated, with a spiral angle 17° from the vertical axis, as shown in Figure 6-6. The plate elements in PLAXIS have the same element formulations as conventional beam elements, where the shear, bending and normal forces are considered. In addition, the local axes were aligned with the corrugation angle and hence with the strain gauges. Moreover, the 50-mm steel loading plate was simulated by using the same plate element. The loading plate has a modulus of elasticity of 200 GPa. In addition, to simulate the interaction between the culvert and the soil, interface elements were used with R_{inter} equal to 0.5.

The geocell layer was modelled by using full three-dimensional elements simulating the true 3D geometry of the used geocells, employing the plate elements from the PLAXIS 3D library (as shown in Figure 6-6). Interface elements were placed around the sides of each geocell to model the interaction between the geocell and the fill soil. The roughness of the interaction was modelled by utilizing a strength reduction factor at the interface, R_{inter} = 0.5.

With regard to the model boundary conditions, at the model centerlines only perpendicular lateral boundary conditions were restrained. The lateral boundary conditions at the outer sides were free in the vertical direction and fixed in the horizontal direction. Finally, the model base was fixed in both directions (horizontal and vertical). Once the full-scale tests were verified, the model was extended to 10D (where D is the culvert diameter) in the two lateral directions for the purpose of the parametric study.

6.3.2 Soil Model

An elastoplastic hardening soil model (HSM) from the PLAXIS 3D library was used to model the stress-dependent variation in stiffness of the granular materials and the TDA materials. In contrast to the Mohr-Coulomb model, the yield surface of the HSM is changed according to plastic straining and is not fixed to the principal stress space. Many features are incorporated in the HSM. First, it simulates the stress-dependent stiffness of the soil. In the simulation, it also accounts for the loading history (e.g., the construction sequence, compaction effect, etc.). Furthermore, it has independent behaviour for unloading/ reloading simulations (Schanz et al., 1999). Many studies have demonstrated the effectiveness of using the HSM model to simulate TDA behaviour (Bernal et al. 1996; Ashari Ghomi 2018; Mahgoub and El Naggar 2019). Table 6.1 shows the parameters used for the TDA and granular materials in drained conditions. In addition, five-node interface elements were added with a reduction factor (R_{inter}) of 0.30 to simulate the smooth thin polymeric membrane between the TDA layer and the granular material.

6.3.3 Parametric Study

Five groups of models (referred to as group G1 to group G5) were developed in the parametric study to examine the effect of changing crucial parameters on the behaviour of the coupled TDA-geocell bridging system over buried culverts. A summary of the parameters examined in the different model groups is provided in Table 6.2 and the parameters are illustrated in Figure 6-7. The layout of configuration C2 was used for the FE analysis in the parametric study. The first group of models (G1) examines the effect of changing the geocell width on the system performance. The geocell width (W) was changed to 0.4D, 0.8D, 1.5D, 2D, 2.5D, 3D, and 4D, where D is the culvert diameter.

The second group of models (G2) explores the effect of the geocell embedment depth (d_g) on the behavior of the proposed system. The geocell embedment depth was varied from $0.1t_g$ to $1.0t_g$; where t_g is the thickness of the top granular layer above the layer of TDA. In the third group of models (G3), different numbers of geocell layers (N) were considered in the FE analysis, which used one, two, or three geocell layers. The distance between the geocell layers was designated as 50 mm.

The fourth group of models (G4) investigates how the surface settlement and culvert stresses are affected by changes in the stiffness of the top granular layer above the TDA. Four types of backfill were introduced for the FE analysis (i.e., medium dense sand, very dense sand, A1 gravel, and crushed stone). The parameters of the backfill materials used are shown in Table 6.3.

Finally, the fifth group of models (G5) examines the effect of the culvert embedment depth. The cover depth (d) over the culvert crown was varied from 1.0D to 8D, where D is the culvert diameter. For purposes of comparison, an applied load of 50 kN (333.33 kPa, the maximum applied load for setup C2-T0) was selected to calculate the surface settlement and stresses transferred to the culvert for this group of models.

6.4 RESULTS AND DISCUSSION

This section presents the results of the full-scale tests, together with the validation of the FE models. It also includes the results of the parametric study to investigate the performance of the proposed TDA-geocell bridging system for buried culverts.

6.4.1 Tests Results and FE Model Validation

6.4.1.1 Surface Settlement and Culvert Deformation

The efficacy of using a coupled bridging system of TDA with geocell reinforcement to address surface settlement and culvert deformation is discussed in this section. As illustrated in Figure 6-8, after application of loads incrementally on the steel plate for different test setups, punching shear failure was observed for the configurations containing TDA (C2 and C3). This is due to the presence of a strong granular layer over a compressible layer of TDA. In contrast, local shear failure occurred in the test setups that did not contain TDA (C1-00 and C1-0G). Figure 6-9 shows the load-settlement curves for all six test setups. (Each of the three configurations has two test setups). In addition, the FE results for each test are presented, together with the test results to be validated. It can be seen from Figure 6-9 that the FE models exhibited excellent agreement with the test results. Furthermore, it can be observed from Figure 6-9a that the utilization of geocell reinforcement increased the ultimate load by approximately 40%. Moreover, it can be seen in Figure 6-8b that the use of geocell reinforcement prevented extended soil failure, since the geocell layer acted as a stress mattress with the ability to sustain tension forces and to enhance the stress distribution beneath the loaded area. Similarly, as shown in Figures 6-9b and c, in configurations C2 and C3 the presence of a geocell layer increased the sustained load by approximately 45%.

The load-settlement curves in Figures 6-9a and b first exhibit a nonlinear behaviour and then continue linearly. This change in behaviour corresponds to the incidence of punching shear failure in the strong layer overlying the TDA layer. Punching shear failure occurred at around 22 kN (146.6 kPa) in test setup C2-T0. In contrast, punching shear failure

occurred at around only 12 kN (80 kPa) in test setup C3-T0, due to the more extensive use of TDA. The installation of geocell reinforcement in configurations C2 and C3 increased the punching failure load capacity to approximately 30 kN (200 kPa) and 20 kN (133.3 kPa) for test setups C2-TG and C3-TG, respectively.

Figure 6-10 illustrates culvert vertical and horizontal diameter changes caused by external surface loading. The figure shows that during loading, the vertical diameter contracted (the crown moved downward) and the horizontal diameter expanded (the springlines moved outward). It can be seen from Figure 6-10a that the use of geocell reinforcement in configuration C1 significantly enhanced the culvert performance. In test setup C1-00, where no geocell reinforcement was used, the vertical culvert diameter contracted by 5.0 mm at the maximum applied load of 62 kN. However, in test setup C1-0G, with geocell reinforcement, the change in vertical culvert diameter was only 2.8 mm at the same load value.

Figures 6-10b and c present culvert diameter changes in configurations C2 and C3, respectively (with TDA), together with the culvert deformation in the reference case (setup C1-00). In test setup C2-T0 (with a TDA layer but no geocell layer), the culvert exhibited less deformation than in the reference case until the punching shear failure load (22 kN) was reached. The culvert then deformed dramatically until failure. In contrast, when a geocell layer was added to reinforce the top granular layer, the vertical and horizontal culvert diameters deformed less than in the reference case, even after the punching shear failure load was reached. It can also be seen from Figure 6-10b that the increased rate of culvert deformation which occurred following punching shear failure was less pronounced in test setup C2-TG than in setup C2-T0. Consequently, it is evident that even though test

setup C1-00 exhibited less settlement at the ultimate applied load, utilization of the coupled TDA-geocell system (setup C2-TG) above the buried culvert crown enhanced the culvert performance. Furthermore, it can be observed from Figure 6-8 that the use of this stress bridging system prevented the extended failure of the top surface that occurred in the reference case (C1-00, illustrated in Figure 6-8a), and resulted in contained soil failure (as illustrated in Figure 6-8d for setup C2-TG). More details will be discussed in the presentation of the results of the parametric study.

Similarly, Figure 6-10c presents vertical and horizontal culvert diameter changes for configuration C3, together with culvert diameter changes for the reference case (setup C1-00). The same trend can be observed here: The culvert deformations occurring prior to reaching the punching shear failure loads 12 kN and 20 kN for test setups C3-T0 and C3-TG, respectively, were less than the deformation in the reference case. However, it is noticeable that even with the use of geocell reinforcement in setup C3-TG, the culvert deformation increased more than in the reference case, in contrast to what was observed for setup C2-TG. This is probably due to the fact that configuration C3 used more extensive TDA envelope than in configuration C2, with the result that the bridging system in configuration C3 had to accommodate more settlement and consequently a greater concentration of stress above the culvert was transferred.

Figure 6-11 shows the culvert deformation shapes at the maximum applied load for each test setup. The figure compares the FE results and the deformations determined via digital image correlation (DIC). The DIC results were first calibrated by using measurements of the LVDTs that were installed on the horizontal and vertical diameters of the culverts. It can be seen from Figure 6-11 that even though there was convergence of the maximum

value of culvert deformation, the maximum applied loads varied. For each configuration, when a geocell layer was used (in setups C1-0G, C2-TG, and C3-TG), the maximum applied load increased significantly. For example, in setup C1-0G (with a geocell layer), the maximum applied load was 88 kN and the crown deflection was around 4.5 mm; whereas in setup C1-00 (with no geocell layer), the maximum applied load was 62 kN and the resulting crown deflection was approximately 5.0 mm.

6.4.1.2 Culvert Stresses

The culvert internal forces and stresses were calculated by using measurements of the strain gauges installed inside the culvert at the corrugation valley and crest, ε_1 and ε_2, respectively (refer to Figure 6-2 for details). The following equations (Equations 1 to 4) were used to calculate the internal forces:

$$\varepsilon_{ave} = \varepsilon_1 - \left(\frac{h+t}{2h}\right)(\varepsilon_1 - \varepsilon_2) \quad (1)$$

$$N = \varepsilon_{ave}\, EA \quad (2)$$

$$K = (\varepsilon_1 - \varepsilon_2)/h \quad (3)$$

$$M = EI\, K\, x\, 10^{-3} \quad (4)$$

where ε_{ave} is the average strain; h = the distance between gauges (mm); t = the wall thickness (in mm); N = the thrust force per unit length (kN/m); E = Young's modulus (MPa); A = the cross-sectional area of the wall per unit length (mm^2/mm); K = the curvature (10^{-6}/mm); M = the bending moment (kN·m/m); and I = the second moment of area per unit length (mm^4/mm).

Consequently, the stresses at each point can be calculated using the following equation:

$$\sigma = \frac{N}{A} + \frac{M}{I}\, y\ 10^3 \qquad (5)$$

where σ = the stress at any point (MPa); and y = the vertical distance from the neutral axis (mm).

Figure 6-12 shows the maximum circumferential stresses measured around the culverts (i.e., crown, shoulder, springline, haunch, and invert) at the maximum applied load for each test setup. It can be seen from this figure that the culvert crown experienced the maximum culvert stress in each test setup. For this reason, to compare the performance of the different configurations, Figures 6-13 and 6-14 present the internal forces and maximum stresses at the culvert crown during loading. In addition, Figure 6-12 also demonstrates the ability of the FEM numerical modelling to capture the system performance.

Figures 6-13a and 6-14a show the effect of using geocell reinforcement in configuration C1 (with no TDA). The figures present changes in the bending moment, thrust forces, and culvert crown stresses during the progressive application of external loading. It can be seen that the use of geocell reinforcement results in considerable enhancement of the culvert performance. For instance, at an applied load of 62 kN, in test setup C1-0G (with a geocell layer), the culvert crown experienced approximately 50% of the stresses occurring in test setup C1-00 (the reference case, with no geocell layer).

The effectiveness of using a coupled stress bridging system of TDA and geocell reinforcement can be seen in Figures 6-13b and 6-14b. These figures show the changes in internal forces and stresses at the culvert crown in configuration C2. For comparison purposes, the results are presented together with the internal forces and stresses of the reference case (setup C1-00). The same trend can be observed as discussed in the previous

section: Prior to the occurrence of punching shear failure in test setup C2-T0 (with a TDA layer above the crown), the internal forces and stresses induced were less than in the reference case (setup C1-00, with no TDA or geocell layer). In test setup C2-TG (with a TDA layer and a geocell layer), the top granular layer was stiffer due to the geocell reinforcement, and consequently the stress bridging over the culvert was significantly enhanced. It can be observed from Figure 6-14b that in setup C2-TG, the crown stresses at an applied load of 62 kN were around 30% lower than the stresses in the reference case (setup C1-00). Thus, it can be concluded that using a layer of TDA above the buried culverts reduces the culvert stresses prior to the occurrence of punching shear failure. Furthermore, the use of geocell reinforcement in the top granular layer increases the layer stiffness, which enhances stress arching.

Likewise, Figures 6-13c and 6-14c illustrate the internal forces of the test setups in configuration C3. These figures show that the presence of a geocell layer in setup C3-TG increased the punching failure capacity in comparison to that of setup C3-T0, where only TDA (and no geocell) was used above the culvert springlines. However, the enhancement of culvert performance occurred only until the punching failure capacity of the top layer was reached, then the culvert stresses increased more than in the reference case (C1-00). Additional parameters that can increase the punching failure capacity and hence enhance the performance of the proposed system will be discussed when the results of the parametric study are considered.

Figure 6-15 plots the stresses measured at different locations around the culvert circumference (i.e., the crown, shoulder, springline, haunch, and invert) at certain applied load values (10 kN, 20 kN, and 50 kN). The stresses shown are normalized to the stresses

in the reference case (setup C1-00). At an applied load of 10 kN, the stress reduction achieved in configuration C2 by using a TDA layer located only above the culvert crown was more pronounced than that achieved in configuration C3, where TDA was used down to the springlines. This was due to the fact that the culvert sides were confined by a stronger material in configuration C2. In test setup C3-T0, at an applied load of 20 kN, which exceeded the punching shear failure load for this setup, the culvert stresses at all locations were greater than in the reference case. In contrast, at an applied load of 20 kN, in setup C3-TG the stresses were similar to the stresses in the reference case, since this load was close to the punching shear failure load for setup C3-TG. Furthermore, it can be seen from Figure 6-15b that the stress reduction achieved by using only a TDA layer (with no geocell) above the crown (setup C2-T0) was approximately equivalent to the reduction achieved by setup C1-0G (with a geocell layer but no TDA layer). Setup C2-TG thus achieved the best bridging system for an applied load of 20 kN. Finally, Figure 6-15c shows the culvert stresses at an applied load of 50 kN. Here no data is presented for configuration C3, since 50 kN exceeded the loads applied to the test setups for this configuration. At an applied load of 50 kN, the stresses induced in setup C2-T0 exceeded those in the reference case, since the applied load was greater than the punching failure capacity of this setup. Thus, in contrast to the findings for an applied load of 20 kN, for an applied load of 50 kN the stress bridging system in setup C2-TG was less efficient than that of setup C1-0G. This is probably due to the fact that setup C2-TG accommodated more settlement and that the applied stresses were concentrated over a small area above the buried culvert. The following section discusses additional alternatives to enhance the performance of the proposed coupled TDA-geocell stress bridging system.

6.4.2 Results of the Parametric Study

A detailed interpretation of the FE models developed for the parametric study is presented in this section.

6.4.2.1 Width of the Geocell Layer

Figure 6-16 illustrates the load-settlement relationships for the various models developed. In the models the width of the geocell layer was varied from 0.4D (the loading plate test width) to 4D. The figure shows that widening the geocell layer has no effect on the system performance when the width of the geocell layer exceeds 0.8D (2 times the loading plate width). This is because when $W \geq 0.8\,D$, the loading area has sufficient protrusion to interact with the surrounding soil. In addition, Figure 6-16 also demonstrates that the use of a geocell layer with a width of 0.4D (0.25 m) improves system performance and decreases surface settlement, in comparison to the same configuration without a geocell layer (C2-T0). This is probably attributable to the extension of the geocell layer in the other direction, which helped to distribute the stresses widely beneath the loaded area, and consequently resulted in decreased settlement. From the results presented, it can be recommended that when the location of moving loads is variable, the width of the geocell used should exceed the trench width by 0.5 m, which is two times the width of the loaded area.

6.4.2.2 Effect of the Geocell Embedment Depth

Figure 6-17 illustrates the effect of changing the placement depth (d_g) of the geocell layer. This group of models (group G2) investigates the effect of varying the geocell location from 0.1 t_g (directly below the loading plate) to 1 t_g (at the bottom of the upper granular layer, directly above the TDA layer). It can be seen from Figure 6-17 that placing the

geocell layer near the loading plate resulted in the best performance. The surface settlement increased markedly when the geocell layer was positioned further below the loading surface. This could be explained by the fact that since the presence of a TDA layer resulted in excessive settlement, causing punching shear failure beneath the loaded area, locating the geocell layer directly beneath the loading plate expanded the exposed settlement surface and consequently increased the failure load capacity. On the other hand, Figure 6-17 shows that placing the geocell layer directly above the TDA layer (at 1 t_g), farther from the stress influence zone beneath the loaded area, slightly enhanced the performance in comparison to the case without geocell reinforcement (setup C2-T0). It can thus be concluded that in order to obtain optimum benefits from the use of geocell reinforcement, the geocell layer should be placed close to the loaded surface (just beneath).

6.4.2.3 Effect of the Number of Geocell Layers Used

Figure 6-18 shows how the use of multiple geocell layers beneath the loaded area affects the surface settlement and the pressure transferred to the culvert crown. In this figure, the transferred pressures for the different cases are normalized to the applied pressure. It should be noted that increasing the number of geocell layers used increased the stiffness of the top granular layer, thus enhancing the stress bridging over the buried culvert and decreasing the surface settlement. It can be observed from Figure 6-18 that the pressure transferred through the backfill system increased nonlinearly. The percentage of the pressure transferred increased progressively until it reached a certain value; this phenomenon may be attributed to backfill stiffening. For instance, at an applied pressure of 250 kPa, the pressure transferred to the culvert crown was 32%, 29%, and 26% for the models with one, two, or three geocell layers, respectively. Hence, from an economic point of view using

one layer of geocell provides the best return on the investment. The following section therefore discusses the effect of increasing the stiffness of the top layer by using stiffer granular materials on the performance of the proposed system.

6.4.2.4 Effect of the Stiffness of the Top Granular Layer

In the fourth group of models (group G4), four different granular materials (i.e., medium dense sand, very dense sand, A1 gravel, and crushed stone) were utilized in the analysis to examine the effect of changing the stiffness of the top granular layer on the performance of the proposed coupled TDA-geocell stress bridging system. Figure 6-19 shows the load-settlement relationships for the different models, together with the percentage of stresses transferred to the culvert crown. In this figure, the dashed lines represent the results for FE models with only a TDA layer (and no geocell) above the culvert crown, while the solid lines represent models with the coupled TDA-geocell system. Figure 6-19 demonstrates that using stiff materials in the top layer significantly enhanced the system performance. Moreover, in some cases the use of geocell with a weaker granular layer matched the behaviour of a stronger layer with no geocell. For example, it can be seen from Figure 6-19 that using a geocell layer with A1 gravel material was equivalent to using crushed stone with no geocell. In addition, it should also be noted that the percentage of transferred stresses increased sharply for weaker materials and more gradually for stiffer materials, showing that the stiffer materials significantly enhanced the stress arching mechanism over the buried culvert.

6.4.2.5 Effect of the Culvert Embedment Depth

Figure 6-20 shows how changing the culvert embedment depth affects the surface settlement and the pressures transferred above the culvert crown. The pressures and

settlement reported correspond to an applied load of 50 kN (333.33 kPa). For each model, the transferred pressure was normalized to the effective pressure above the culvert crown. It can be seen from Figure 6-20 that for culverts located at shallow depths ($d < 2D$), the use of geocell reinforcement resulted in significant enhancement of the transferred pressure and surface settlement. However, the use of geocell improved the system behaviour only moderately when the depth of the backfill cover ranged from 2D to 3D. Moreover, the presence of a geocell layer affected the system behaviour only slightly when the culvert placement depth exceeded 3D. It is also worth noting from Figure 6-20 that the pressure transferred to the culvert crown was less than the weight of the soil prism above the culvert crown. This could be attributed to the positive arching mechanism resulting from the presence of compressible (TDA) material above the crown. Hence, it can be concluded that if the culvert is buried deeper than three times its diameter, the effect of the geocell on the culvert performance is marginal and consequently is discouraged from an economic point of view.

6.5 SUMMARY AND CONCLUSIONS

Six full-scale tests were conducted to evaluate the benefits of using a coupled stress bridging system of TDA and geocell over buried metal culverts. The system developed uses a geocell-reinforced top granular backfill layer over a TDA layer to induce a stress arching mechanism capable of controlling the surface settlement and reducing the stresses imposed on the culvert beneath. The complex soil-structure interaction was examined by monitoring changes in the culvert stresses, culvert deformation, and surface settlement during service loading. Furthermore, 3D finite element models of the tests were developed to study the interaction mechanisms of the problem under consideration. Finally, an

extensive parametric study was conducted to examine the effect of important parameters on the performance of the system investigated. The following conclusions can be drawn based on the results of the research:

- The use of TDA above culverts reduces culvert stresses significantly until the occurrence of punching shear failure in the top layer.
- In the first test configuration (C1), the use of geocell reinforcement increased the ultimate load capacity by approximately 40% and prevented extended soil failure. The geocell layer acted as a stress mattress capable of sustaining tension forces and enhancing the stress distribution beneath the loaded area.
- Performance is not affected by the geocell width when the width of the geocell layer exceeds 0.8D (twice the width of the loading plate). Therefore, in light of the results presented, it is recommended that the width of the geocell layer should be 0.5 m more than the trench width (i.e., two times the width of the loaded area, one width from each direction), when the location of moving loads is variable.
- Placing the geocell layer directly below the loaded area yielded the best performance. The surface settlement increased markedly when the geocell layer was positioned at a greater depth beneath the loading surface.
- The study demonstrated that increasing the number of geocell layers used increased the stiffness of the top granular layer, thus enhancing stress bridging over the buried culvert and decreasing the surface settlement.
- The use of stiff granular materials in the top layer above the TDA significantly enhanced the stress arching mechanism over the buried culverts. Moreover, in some cases a geocell layer coupled with weaker materials matched the behaviour of stronger

materials with no geocell layer. For example, the use of a geocell layer with A1 gravel was equivalent to using crushed stone (which is stiffer than A gravel) without a geocell layer.

- The use of geocell reinforcement with culverts located at shallow depths ($d < 2D$) resulted in significant enhancement in terms of the transferred pressure and surface settlement. However, when the depth of the backfill cover ranged from 2D to 3D, the use of geocell reinforcement resulted in only a moderate improvement in the system behaviour. Moreover, the presence of a geocell layer affected the system behaviour only slightly when the culvert placement depth exceeded 3D, where D is the culvert diameter.

Table 6.1: Parameters used in the FEA

Layers	Constitutive model	Unit weight (kN/m^3)	E_{50} (MPa)	E_{oed} (MPa)	c' (kPa)	φ' (°)
*The granular material (SP)	HSM	17.75	58	46.5	-	39
**TDA	HSM	7	2.75	2.2	24	26.5

Note: E = modulus of elasticity; E_{oed} = tangent stiffness from odometer test; E_{50} = secant modulus; HSM= hardening soil model;
*The properties at P_{ref} = 100 kPa and R_f=0.65.
**The properties at P_{ref} = 25 kPa and R_f=0.95.

Table 6.2: Parametric study

Model group	Variable	Values
G1	W	(0.4, 0.8, 1.5, 2.0, 2.5, 3.0, 4.0) D
G2	d_g	(0.1, 0.25, 0.5, 1.0) D
G3	N	(1, 2, 3) layers of the geocell
G4	Top granular layer	Medium dense sand, very dense sand, A1-gravel, and crushed stone
G5	d	(1, 1.5, 2.0, 3.0, 4.0, 8.0) D

Note: the table should be read with Figure 6-7

Table 6.3: Parameters used for model group G4

Layers	Constitutive model	Unit weight (kN/m^3)	E_{50} (MPa)	E_{oed} (MPa)	c' (kPa)	φ' (°)
Medium silty sand (SP-SM)	HSM	15.5	35	28	-	34
A1- gravel	HSM	21	110	88	-	44
Crushed stone	HSM	24	200	160	-	50

Note: E = modulus of elasticity; E_{oed} = tangent stiffness from odometer test; E_{50} = secant modulus; HSM= hardening soil model; the properties at P_{ref} = 100 kPa and R_f=0.65.

a) Configuration1 (C1-0G)

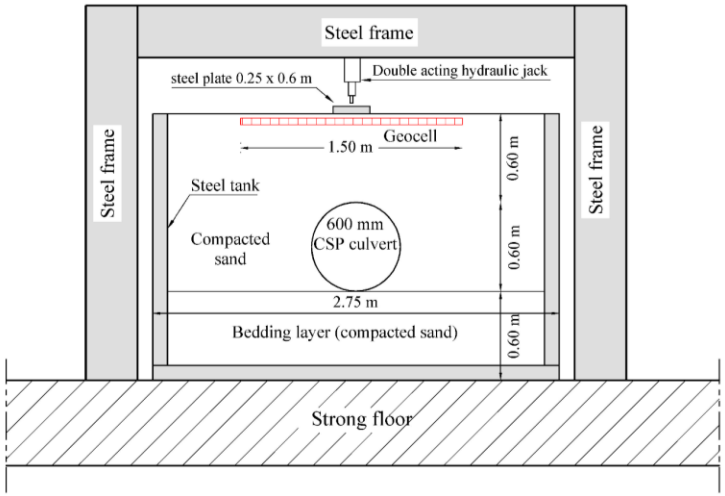

b) Configuration2 (C2-TG)

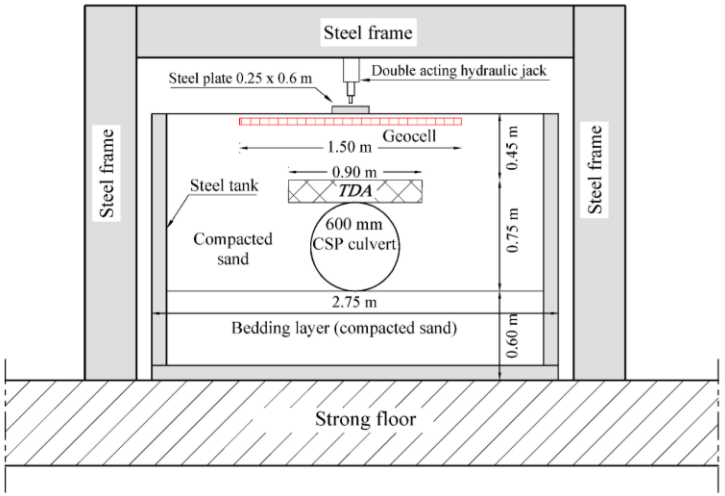

c) Configuration3 (C3-TG)

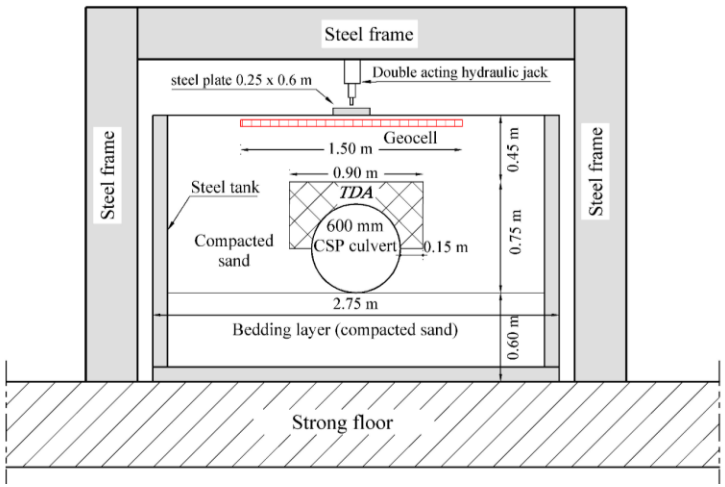

d) Geocell panel

Naming scheme:

C3-TG

- C3 represents configuration No. 3
- T represents TDA
- G represents Geocells

Figure 6-1 Tests layouts

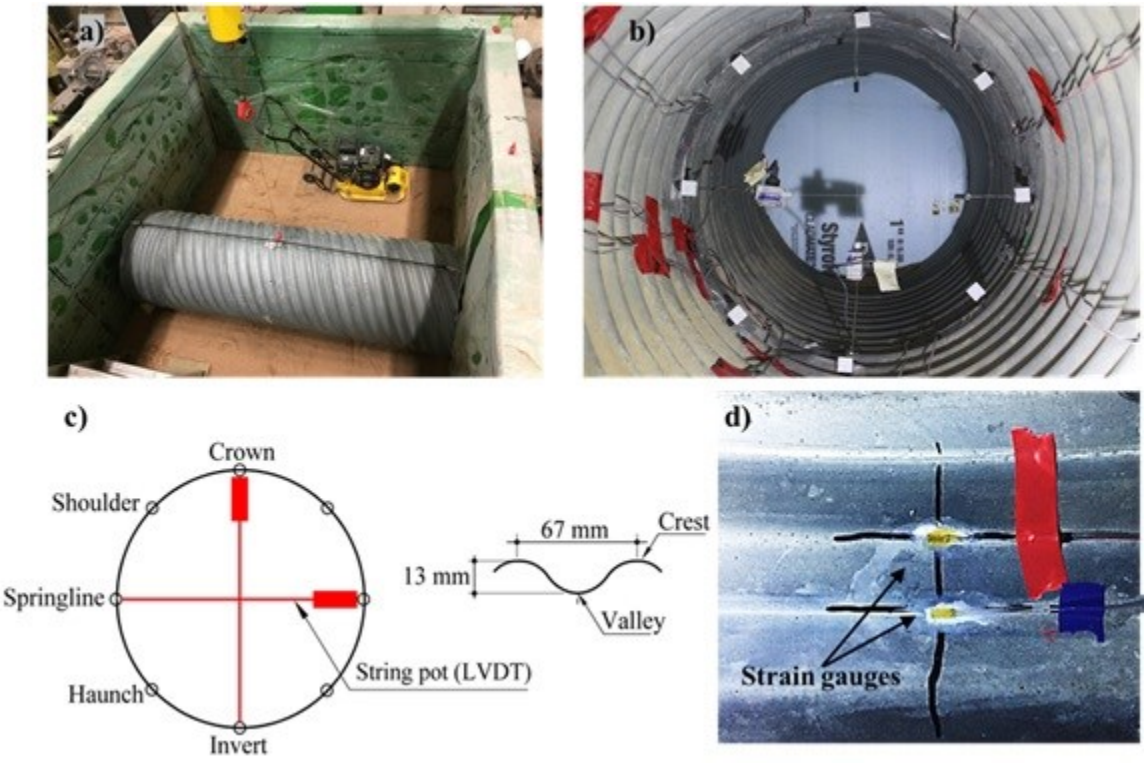

Figure 6-2 Tests instrumentation

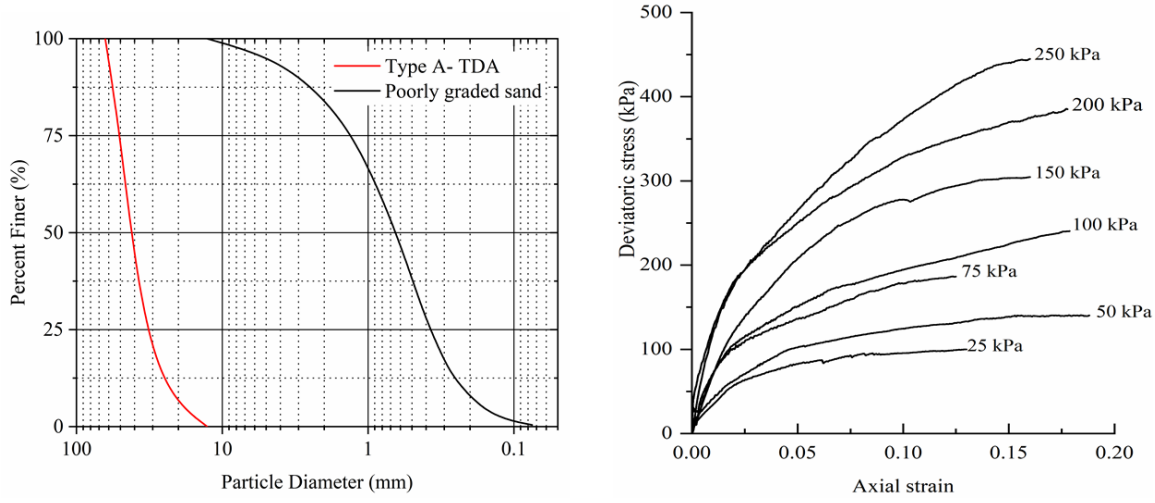

a) Backfill gradation

b) Triaxial results of TDA

Figure 6-3 Laboratory test results for backfill materials, a) Backfill gradation; b) TDA triaxial test results (Ashari Ghomi 2018)

Figure 6-4 Geocell installation

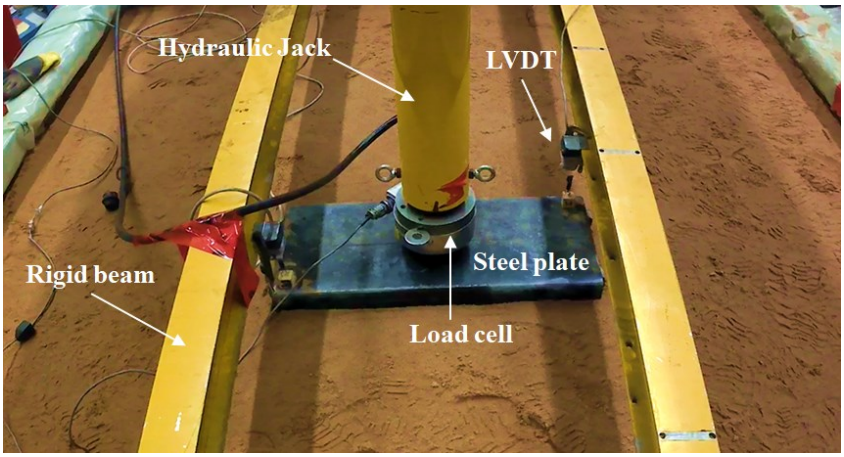

Figure 6-5 Loading plate layout

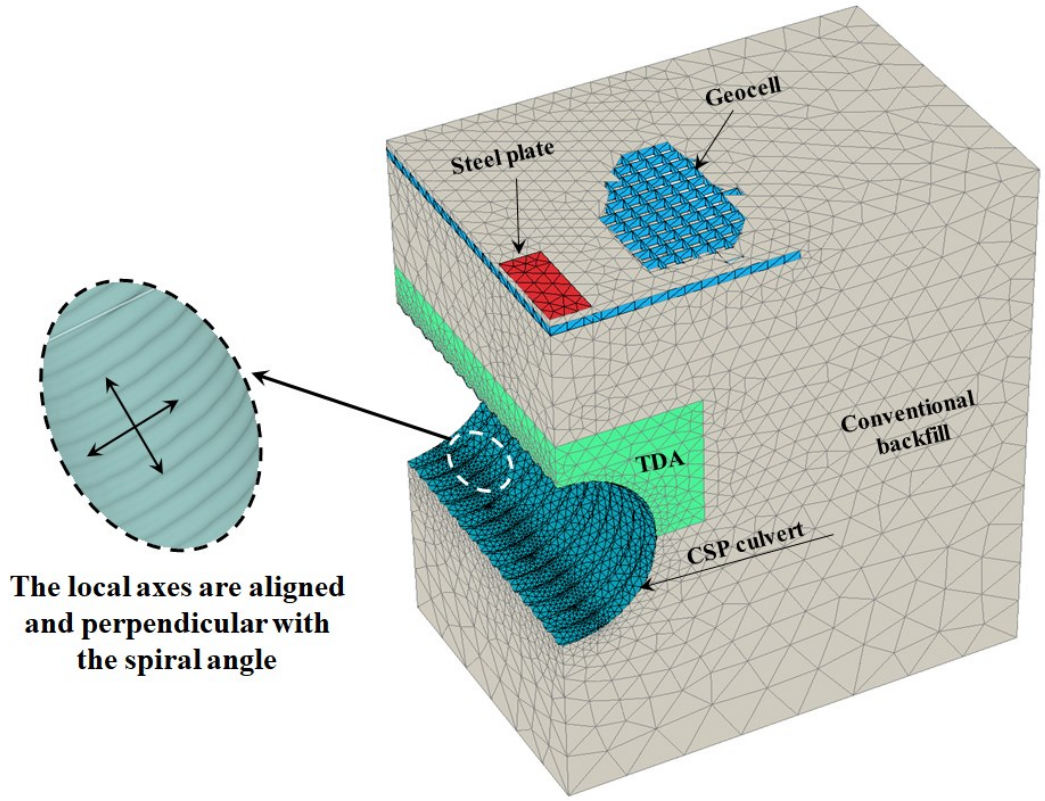

Figure 6-6 Numerical modelling of setup C3-TG

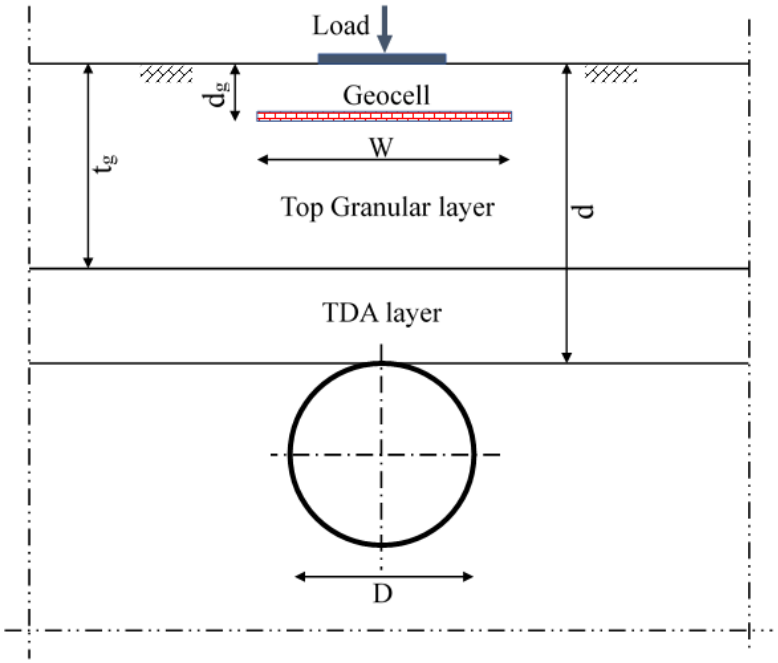

Figure 6-7 Parameters examined in the parametric study

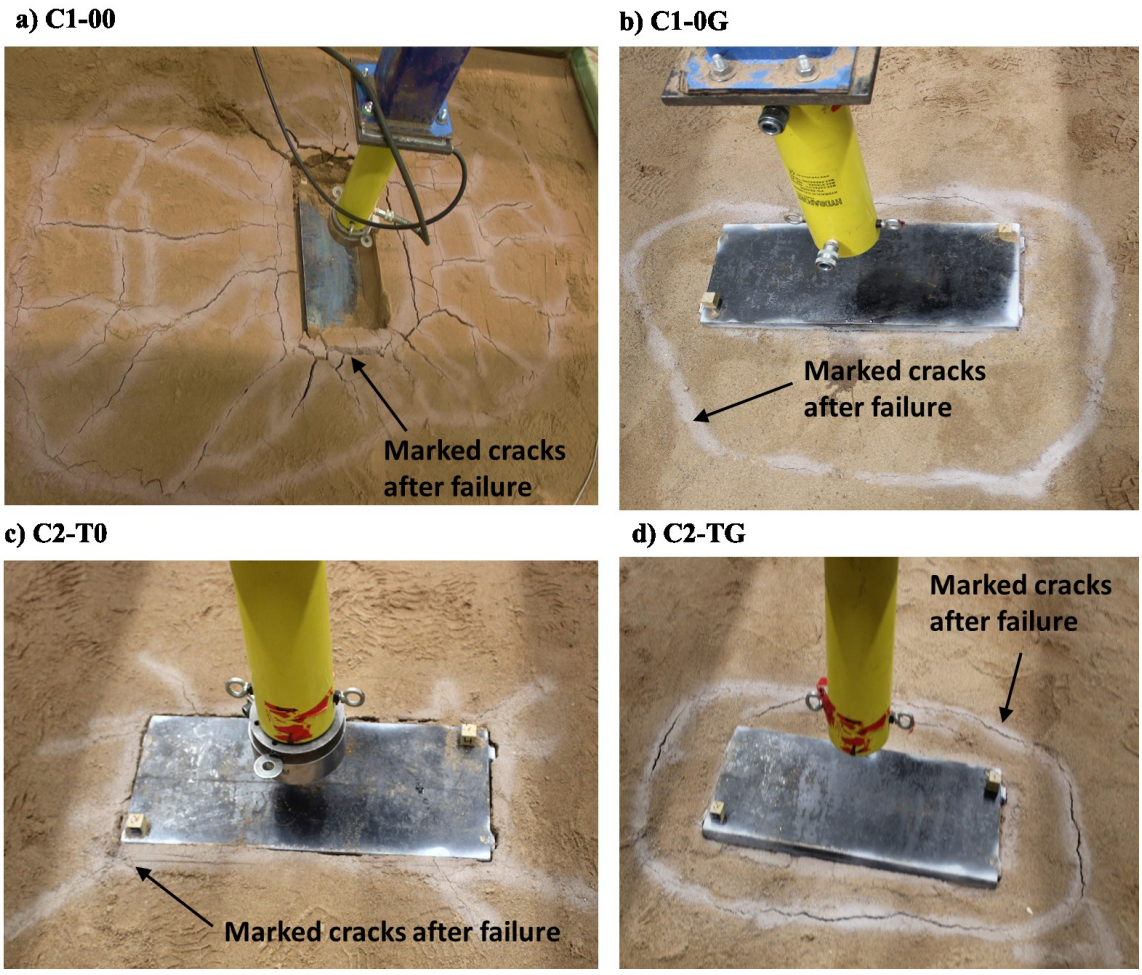

Figure 6-8 Failure mechanism for tests configurations 1 and 2

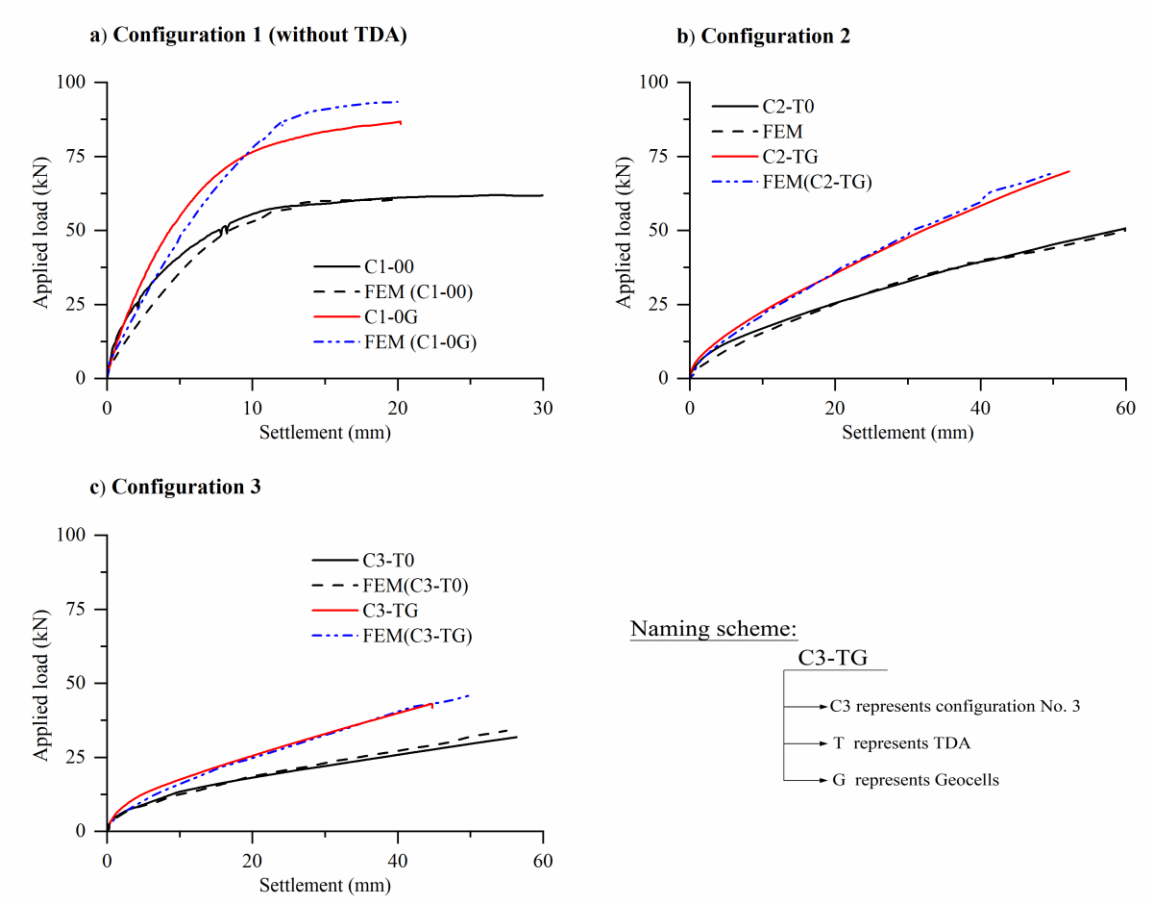

Figure 6-9 Load-settlemnt curve for different configurations (FE results versus tests results)

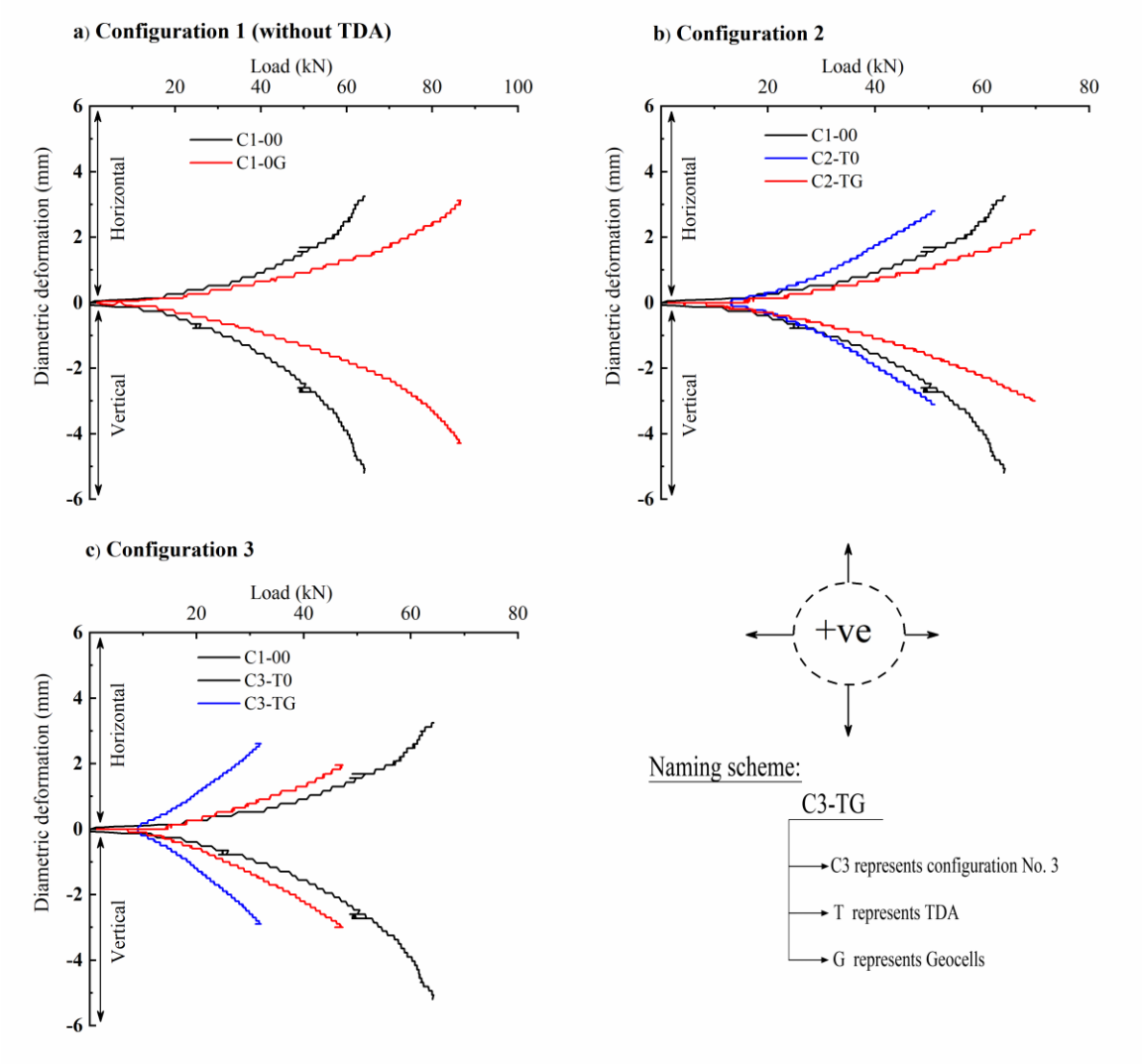

Figure 6-10 Culvert diameter changes during the loading, for test configuration a) C1; b) C2; c) C3

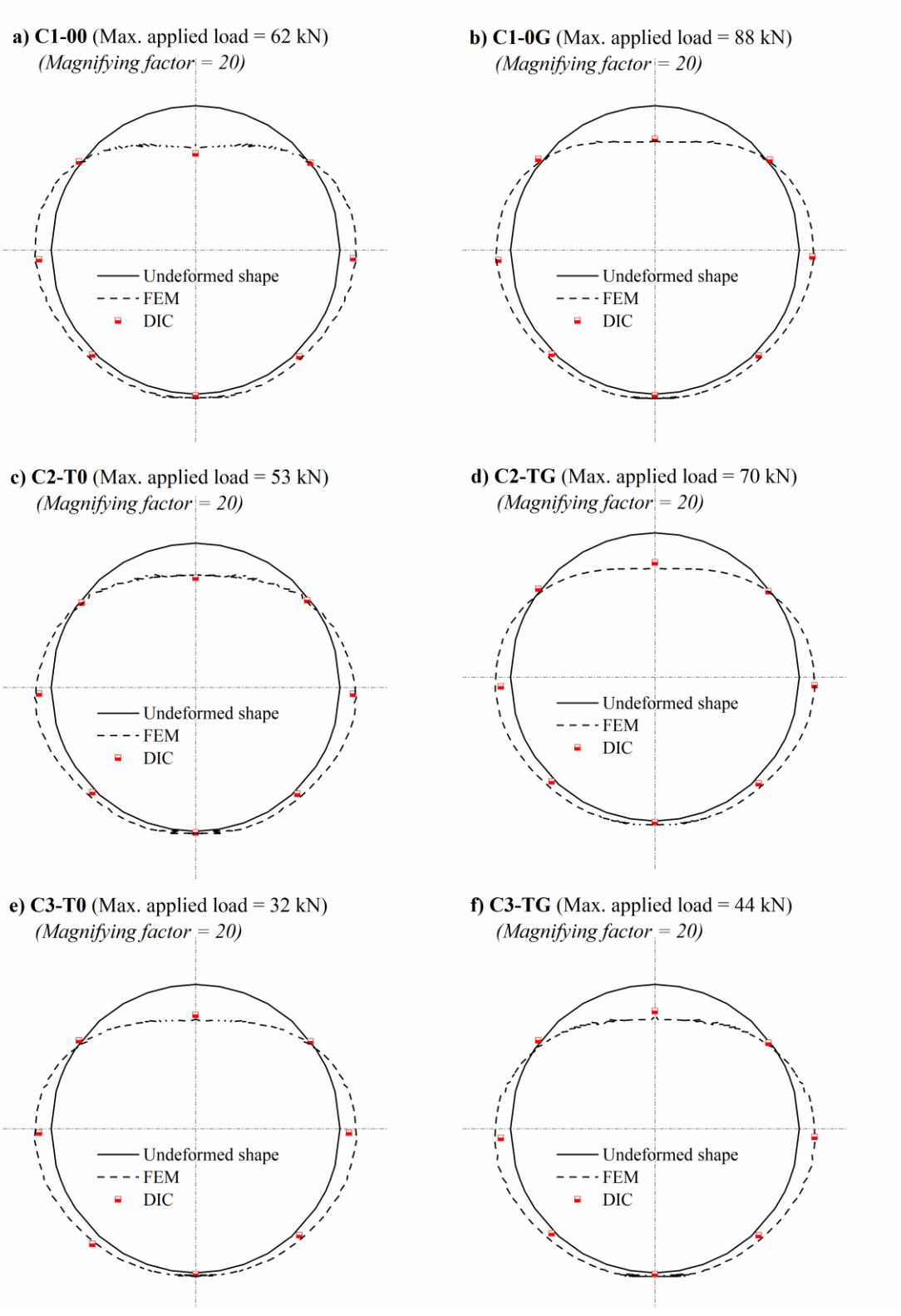

Figure 6-11 Culverts deformations at the maximum applied load for each test setup

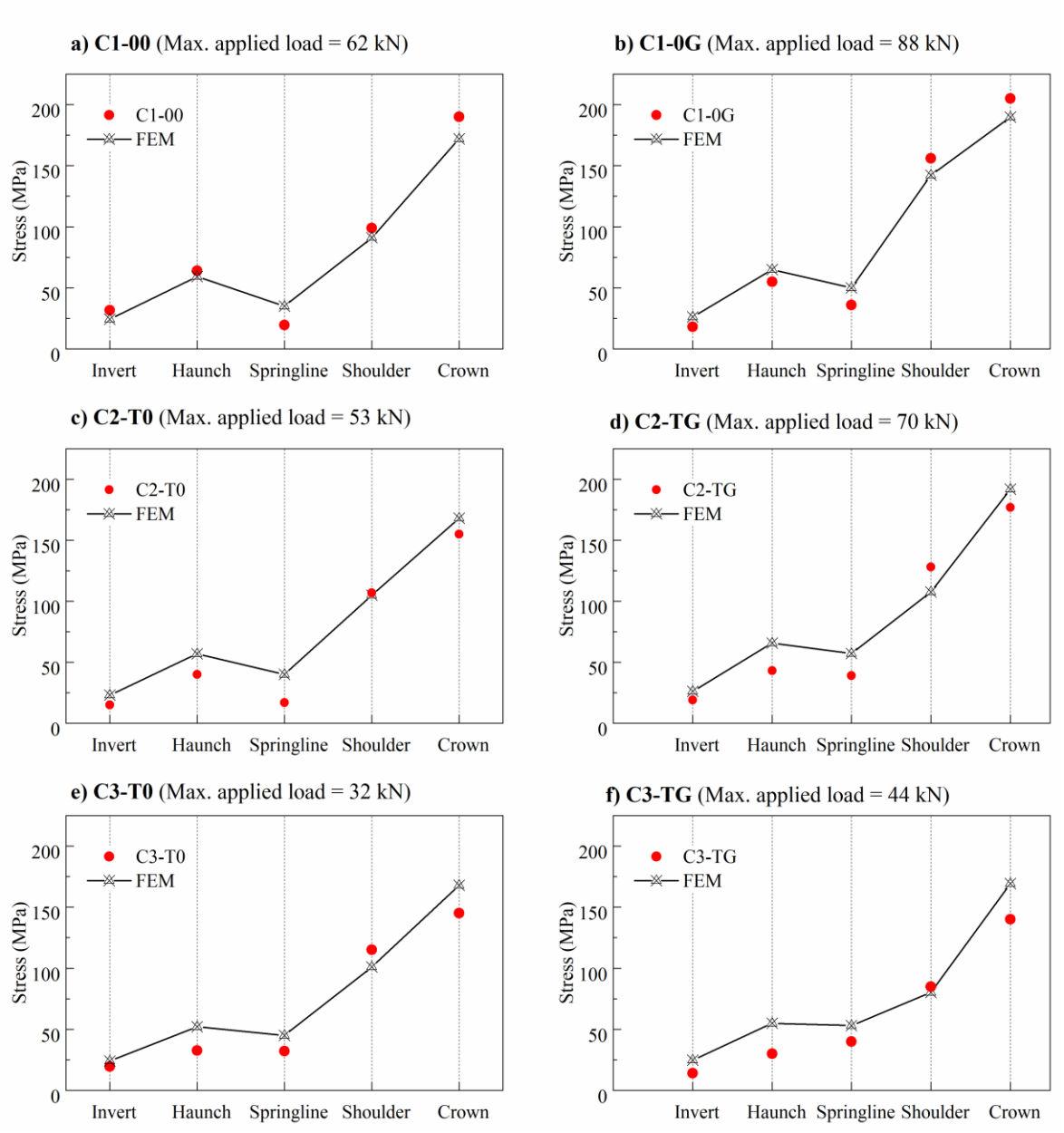

Figure 6-12 Maximum circumferential stresses around the culverts at the maximum applied loads of each test setup

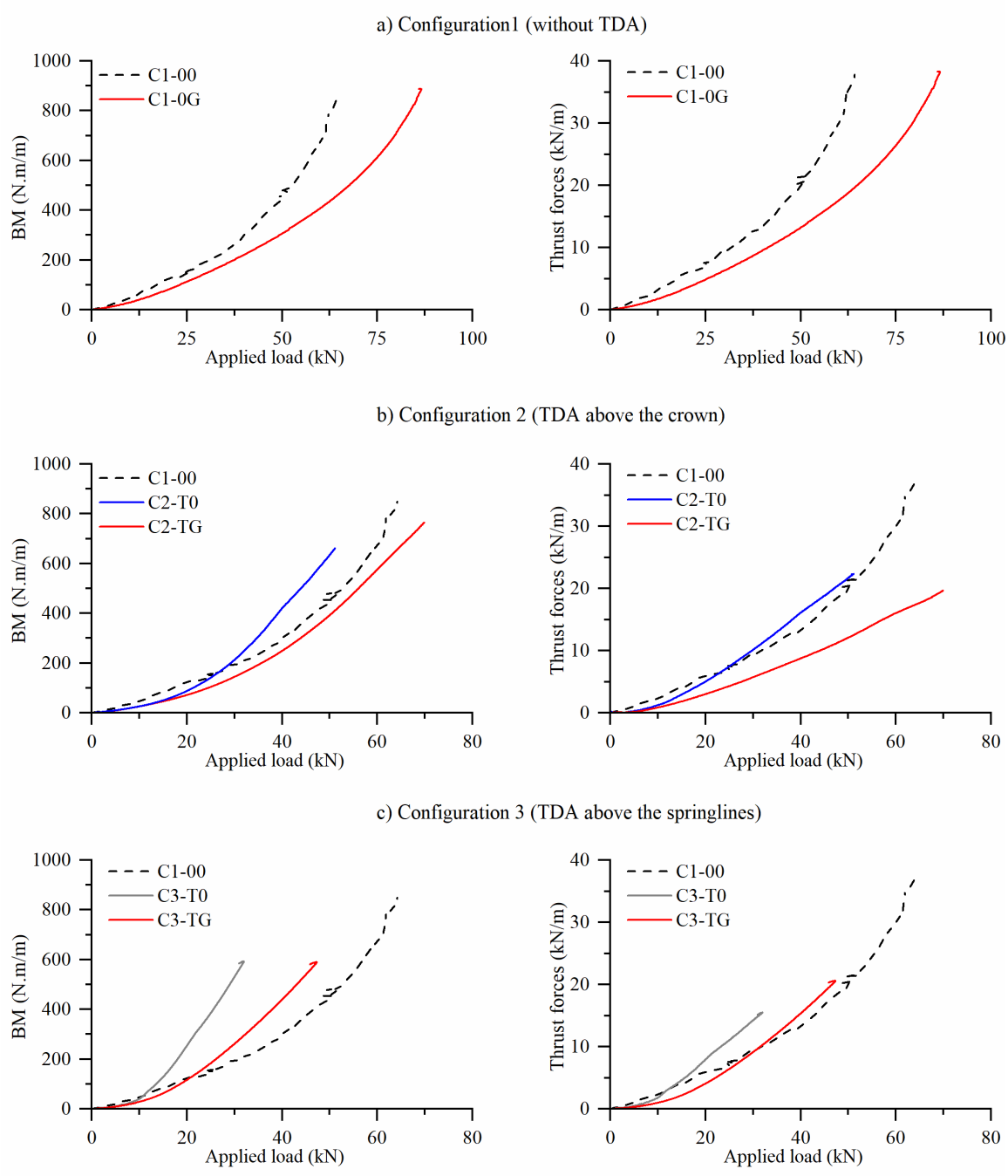

Figure 6-13 Circumferential internal forces at the culvert crown during loading, for test confugrations a) C1; b) C2; c) C3

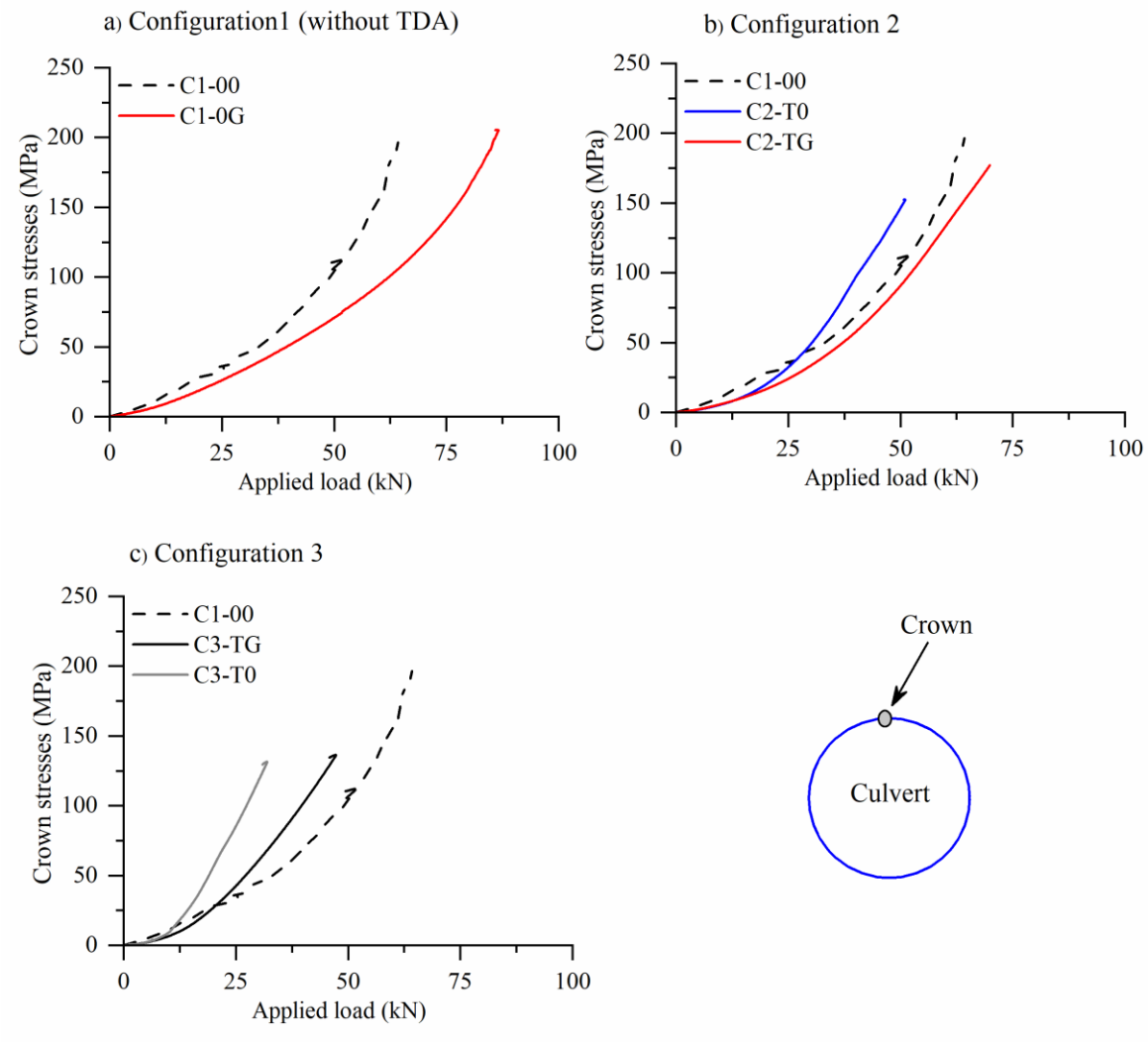

Figure 6-14 Circumferential stress changes at the culvert crown during loading, for test confugrations a) C1; b) C2; c) C3

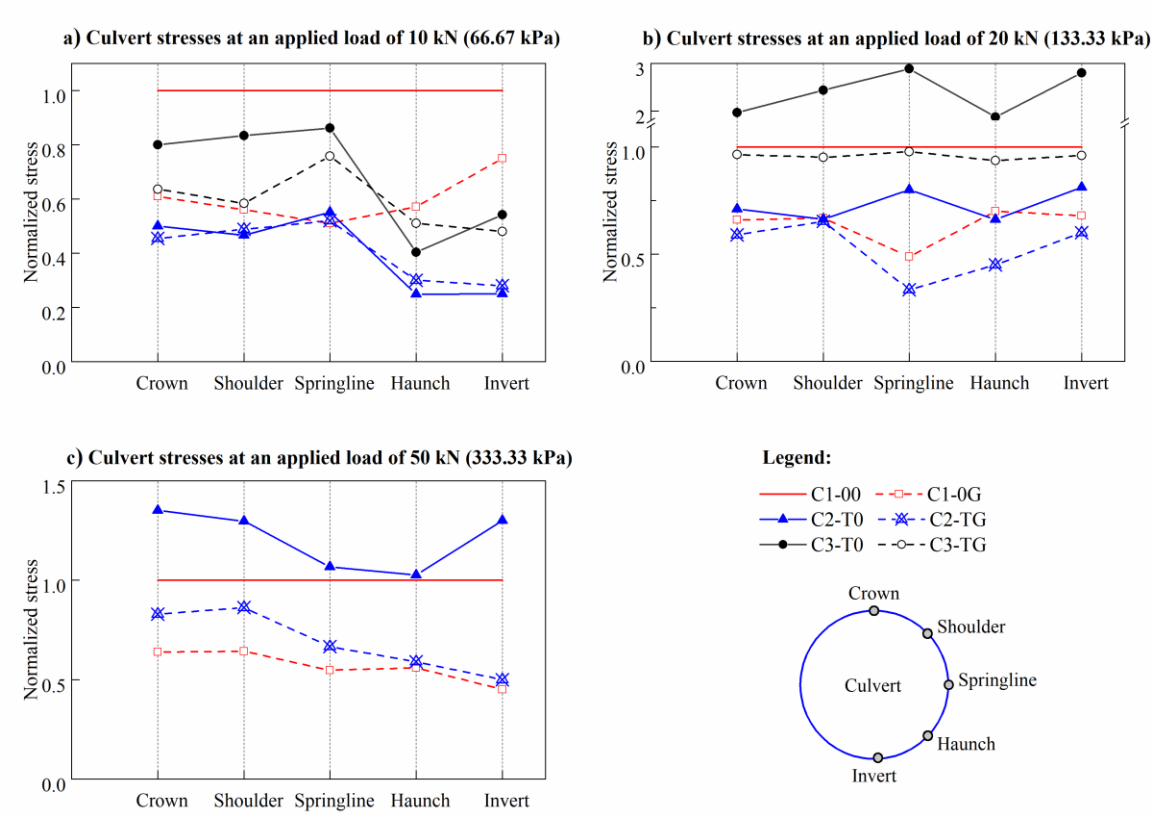

Figure 6-15 Normalized stresses around the culverts at applied loads of 10 kN (66.67 kPa), 20 kN (133.33 kPa) and 50 kN (333.33 kPa)

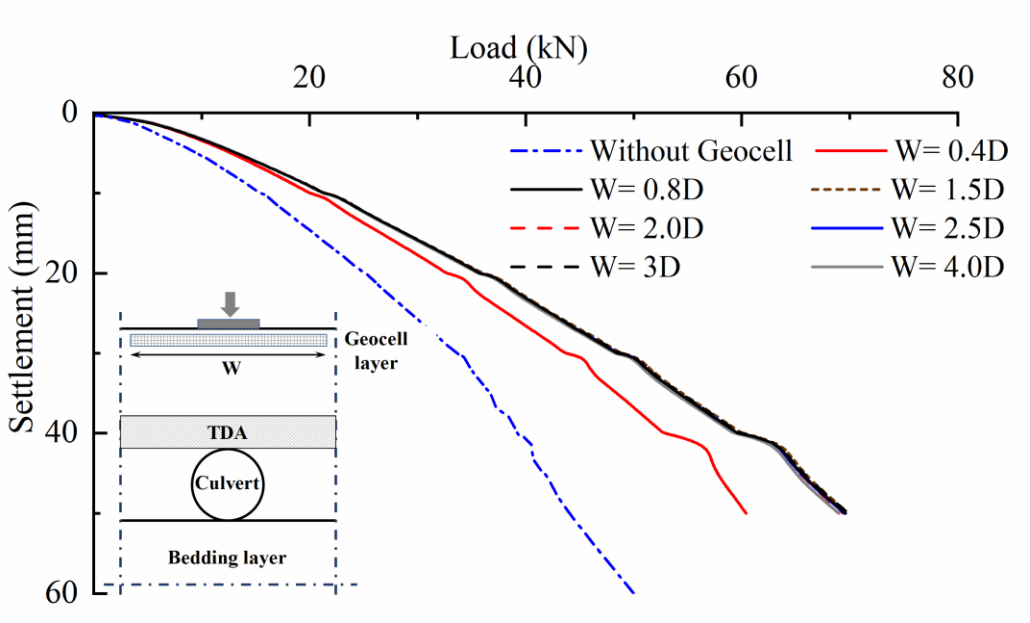

Figure 6-16 Effect of changing the geocell width (G1 results)

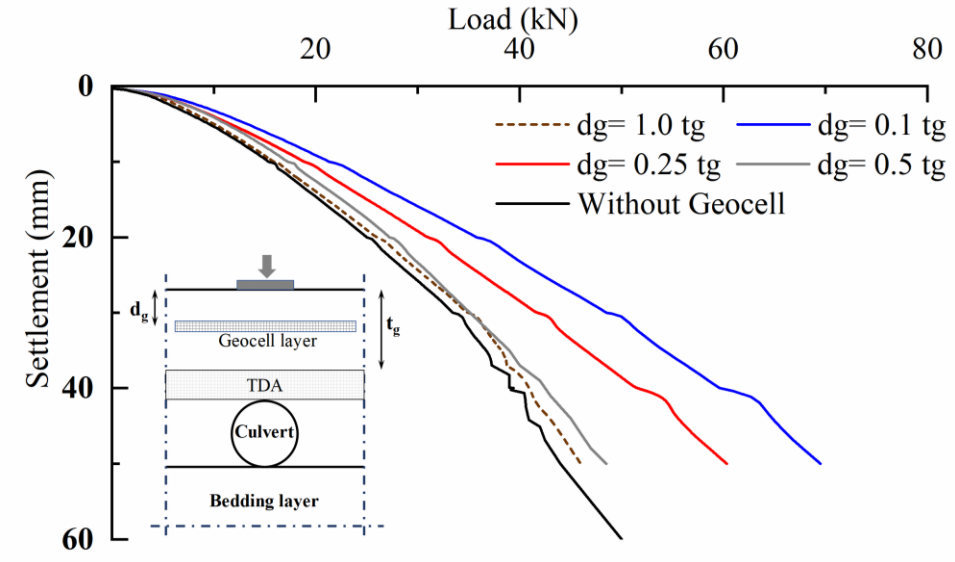

Figure 6-17 Effect of changing the embedment depth of the geocell layer (G2 results)

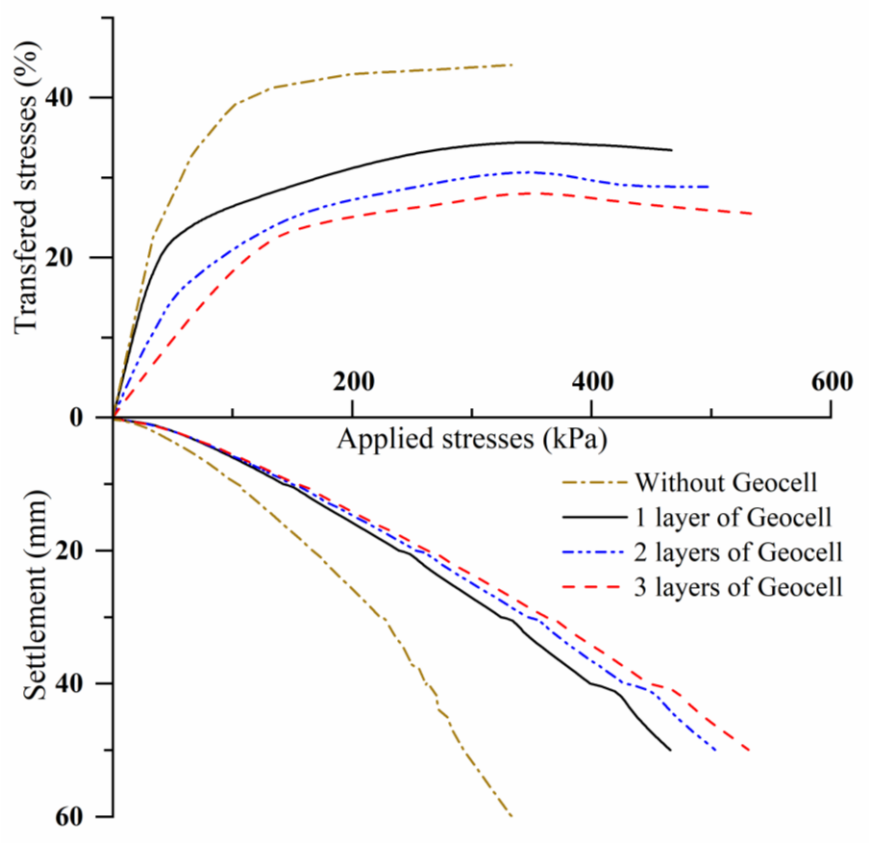

Figure 6-18 Effect of changing the number of geocell layers (G3 results)

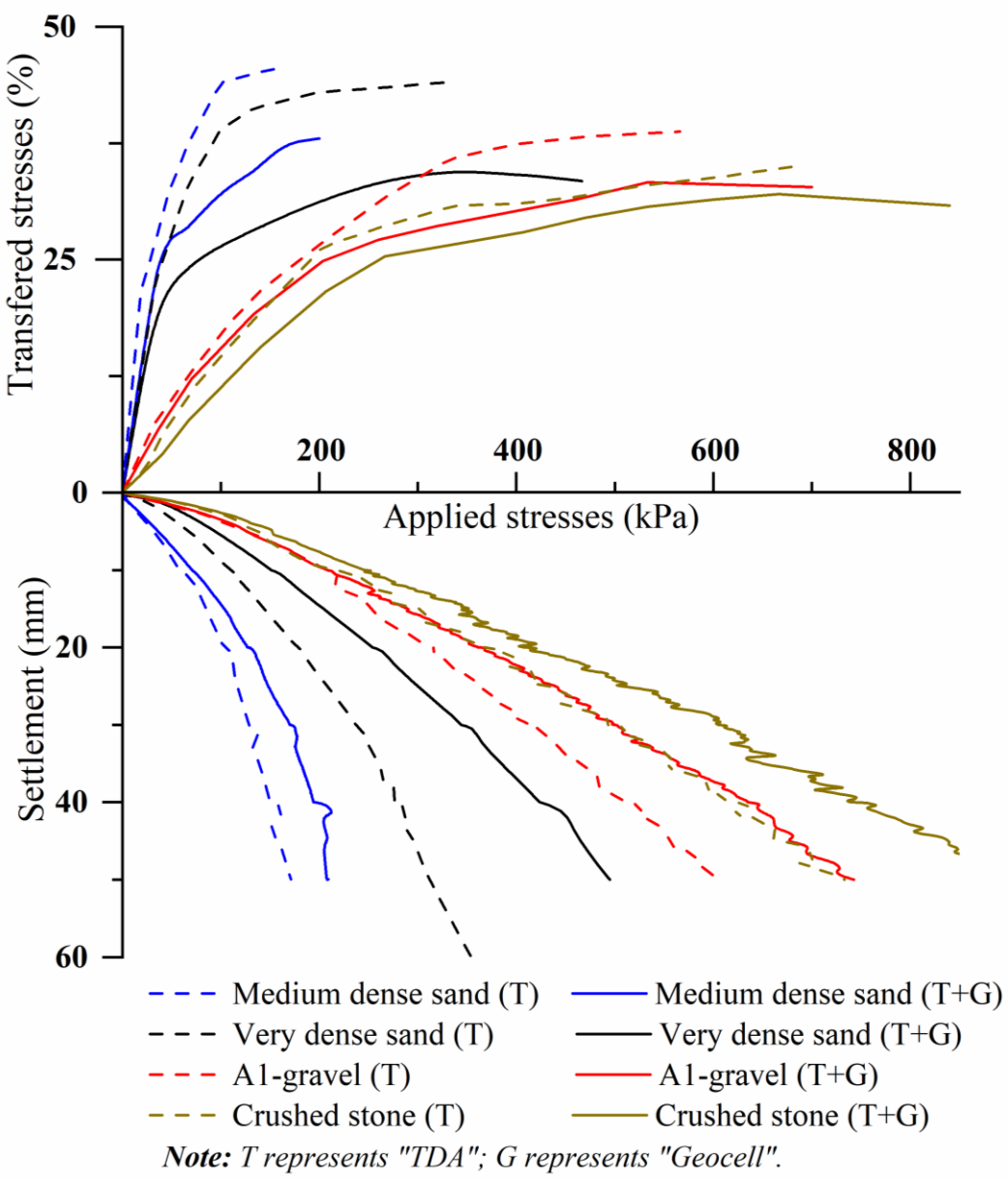

Figure 6-19 Effect of changing the top granular layer (G4 results)

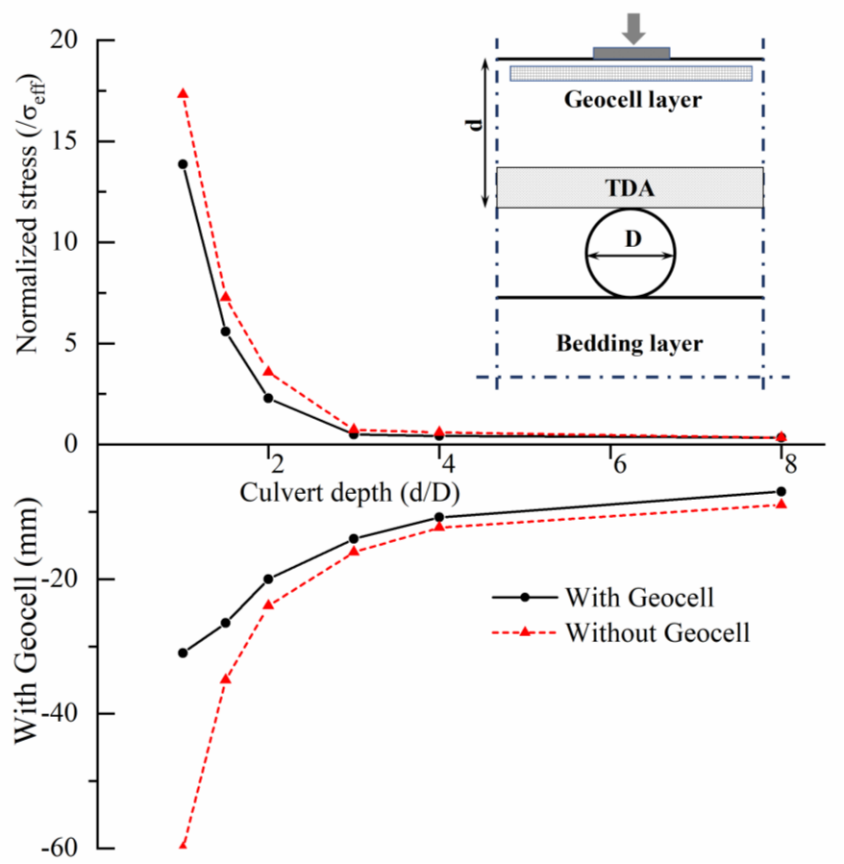

Figure 6-20 Effect of changing the backfill cover above the culvert crown (G5 results)

6.6 REFERENCES

Al-Qadi IL, Hughes JJ (2000) Field evaluation of geocell use in flexible pavements. Transportation research record;1709(1):26-35.

ASTM (2012) D 6270-12: Standard practice for use of scrap tires in civil engineering applications. ASTM International, West Conshohocken, PA, USA.

Ashari M and El Naggar H (2017) Evaluation of the physical properties of TDA-sand mixtures. In GeoOttawa, the 70th Canadian Geotechnical Conference Ottawa. Canadian Geotechnical Society.

Ashari Ghomi M (2018) Large-scale triaxial testing of sustainable TDA backfilling alternatives. Master's thesis. Dalhousie University.

Benson CH, Olson MA and Bergstrom WR (1996) Temperatures of insulated landfill liner. Transportation Research Record 1534(1): 24–31, https://doi.org/10.3141/1534-05.

Bosscher PJ, Edil TB and Eldin NN (1992) Construction and performance of shredded waste-tire test embankment. Transportation Research Record 1345: 44–52.

Cuelho E, Perkins S (2009) Field investigation of geosynthetics used for subgrade stabilization. Montana. Dept. of Transportation. Research Programs.

Dash SK, Sireesh S, Sitharam TG (2003) Model studies on circular footing supported on geocell reinforced sand underlain by soft clay. Geotextiles and Geomembranes.21(4):197-219.

Edil TB, and Bosscher P J (1992) Development of engineering criteria for shredded or whole tires in highway applications. Report No. WI 14-92, Department of Civil and Environmental Engineering, University of Wisconsin, Madison, Wisconsin.

Edil TB (2005) A review of mechanical and chemical properties of shredded tires and soil mixtures. InRecycled Materials in Geotechnics (pp. 1-21).

El Naggar H, Soleimani P, and Fakhroo A (2016) Strength and stiffness properties of green lightweight fill mixtures. Geotech. Geol. Eng. 34 (3): 867–876. https://doi.org/10.1007/s10706-016-0010-1.

Hegde A, Sitharam TG (2017) Experiment and 3D-numerical studies on soft clay bed reinforced with different types of cellular confinement systems. Transportation Geotechnics.10:73-84.

Hegde A, Sitharam TG (2015) 3-Dimensional numerical modelling of geocell reinforced sand beds. Geotextiles and Geomembranes ;43(2):171-81.

Hoppe EJ (1998) Field study of shredded-tire embankment. Transportation Research Record 1619(1): 47–54, https://doi.org/10.3141/1619-06.

Humphrey DN, Whetten N, Weaver J, and Recker K (2000) Tire shreds as lightweight fill for construction on weak marine clay. Proceeding International Symposium on Coastal Geotechnical Engineering in Practice, Balkema, Rotterdam, The Netherlands, 611–616.

Humphrey DN (2008) Tire derived aggregate as lightweight fill for embankments and retaining walls. In Scrap Tire Derived Geomaterials — Opportunities and Challenges (Hazarika H and Yasuhara K (eds)). Taylor & Francis Group, London, UK, pp. 59–81.

Humphrey D and Blumenthal M (2010) The use of tire-derived aggregate in road construction applications. In Green Streets and Highways 2010: An Interactive Conference on the State of the Art and How to Achieve Sustainable Outcomes. ASCE, Reston, VA, USA, pp. 299–313.

Kargar M, Mir Mohammad Hosseini SM (2016) Influence of reinforcement stiffness and strength on load settlement response of geocell-reinforced sand bases. Eur. J. Environ. Civ. Eng. 8189, https://doi.org/10.1080/19648189.2016.1214181.

Latha G, Nair A, Hemalatha M (2010) Performance of geosynthetics in unpaved roads. International journal of geotechnical engineering;4(3):337-49.

Mahgoub A, El Naggar H (2019) Using TDA as an Engineered Stress-Reduction Fill over Preexisting Buried Pipes. Journal of Pipeline Systems Engineering and Practice; 10(1):04018034.

Mills, B., H. El Naggar, and A. J. Valsangkar. 2015. “North American overview and Canadian perspective on the use of tire derived aggregate in highway embankment construction.” Chap. 22 in Vol. 2 of Ground improvement case histories, edited by Indraratna and Chu. New York: Elsevier.

Meguid MA, Youssef TA (2018) Experimental investigation of the earth pressure distribution on buried pipes backfilled with tire-derived aggregate. Transportation Geotechnics, 14:117-25.

Mehrjardi GT, Tafreshi SM, Dawson AR (2012) Combined use of geocell reinforcement and rubber–soil mixtures to improve performance of buried pipes. Geotextiles and Geomembranes; 34:116-30.

Mehrjardi GT, Tafreshi SM, Dawson AR (2013) Pipe response in a geocell-reinforced trench and compaction considerations. Geosynthetics International; 20(2):105-18.

Mehrjardi GT, Tafreshi SM, Dawson A (2015) Numerical analysis on Buried pipes protected by combination of geocell reinforcement and rubber-soil mixture. International Journal of Civil Engineering ;13(2):90-104.

Meles D, Bayat A, Hussien Shafiee M, Nassiri S, Gul M (2014) Investigation of tire derived aggregate as a fill material for highway embankment. International Journal of Geotechnical Engineering, 8(2):182-90.

National Research Council of Canada. Associate Committee on the National Building Code. (2015) National building code of Canada associate committee on the national building code, National Research Council.

Ni P, Qin X, Yi Y (2018) Numerical study of earth pressures on rigid pipes with tire-derived aggregate inclusions. Geosynthetics International, 25(5): 494-506.

Plaxis, B. (2017) Reference Manual for PLAXIS 2D, PLAXIS bv, Delft, Netherlands.

Pokharel SK, Han J, Manandhar C, Yang X, Leshchinsky D, Halahmi I, Parsons RL (2011) Accelerated pavement testing of geocell-reinforced unpaved roads over weak subgrade. Transportation Research Record;2204(1):67-75.

Palmeira EM, Andrade HK (2010) Protection of buried pipes against accidental damage using geosynthetics. Geosynthetics International; 17(4):228-41.

Pierre DKS (2013) Canadian waste tire practices and their potential in sustainable construction. Dalhousie Journal of Interdisciplinary Management 9(1).

Rezaei A, Kolahdouz EM, Dargush, GF and Weber AS (2012) Ground source heat pump pipe performance with tire derived aggregate. International Journal of Heat and Mass Transfer, 55, No. 11, 2844–2853.

Rowe RK and McIsaac R (2005) Clogging of tire shreds and gravel permeated with landfill leachate. Journal of Geotechnical and Geoenvironmental Engineering, 131(6):682-93.

Rubber Manufacturers Association (2017) US scrap tire management summary 2005–2009. Rubber Manufacturers Association, Washington, DC, USA.

Salgado R, Yoon S and Siddiki NZ (2003) Construction of Tire Shreds Test Embankment. FHWA/IN/JTRP-2002/35, Joint Transportation Research Program, Indiana Department of Transportation and Purdue University, West Lafayette, IN, USA https://doi.org/10.1520/JAI103711.

Sparkes J, El Naggar H and Valsangkar A (2019) Compressibility and shear strength properties of tire-derived aggregate mixed with lightweight aggregate. Journal of

Pipeline Systems Engineering and Practice 10(1), https://doi.org/10.1061/(ASCE)PS.1949-1204.0000354.

Rodríguez LM, Arroyo M, Cano MM (2018) Use of tire-derived aggregate in tunnel cut-and-cover. Canadian Geotechnical Journal, 55(7):968-78.

Tweedie JJ, Humphrey DN and Sandford TC (1998) Full-scale field trials of tire shreds as lightweight retaining wall backfill under at-rest conditions. Transportation Research Record 1619: 64–71, https://doi.org/10.3141/1619-08.

Tafreshi SM, Khalaj O (2008) Laboratory tests of small-diameter HDPE pipes buried in reinforced sand under repeated-load. Geotextiles and Geomembranes ;26(2):145-63.

Thakur JK, Han J, Pokharel SK, Parsons RL (2012) Performance of geocell-reinforced recycled asphalt pavement (RAP) bases over weak subgrade under cyclic plate loading. Geotextiles and Geomembranes 35:14-24.

Xiao M, Bowen J, Graham M and Larralde J (2012) Comparison of seismic responses of geosynthetically reinforced walls with tire-derived aggregates and granular backfills. Journal of Materials in Civil Engineering 24(11): 1368–1377, https://doi.org/10.1061/(ASCE)MT.1943- 5533.0000514.

Yoon S, Prezzi M, Siddiki NZ and Kim B (2006) Construction of a test embankment using a sand-tire shred mixture as fill material. Waste Management 26(9): 1033–1044, https://doi.org/10.1016/j.wasman.2005.10.009.

Zhang L, Ou Q, Zhao M (2018) Double-beam model to analyze the performance of a pavement structure on geocell-reinforced embankment. Journal of Engineering Mechanics ;144(8):06018002

CHAPTER 7 SEISMIC DESIGN OF METAL ARCH CULVERTS: DESIGN CODES VS. FULL DYNAMIC ANALYSIS

Ahmed Mahgoub and Hany El Naggar

Published in Journal of Earthquake Engineering, Volume 23, 9

https://doi.org/10.1080/13632469.2019.1625830

7.1 INTRODUCTION

Corrugated steel plate (CSP) culverts have proved to be an outstanding substitute for short-span bridges due to their lightweight, low cost, simplicity of construction, and durability (Hurd et al., 1994). Since 1896, countless CSP culvert applications have provided to be feasible and effective solutions in highway systems, water crossings, and railways throughout North America, Europe and worldwide (Mirza & Porter 1981; Kolymbas 2005). CSP culverts are flexible soil-metal structures which combine the use of structural steel plates and the surrounding engineered backfilling soil. They are designed and constructed to induce an interaction between the two elements to serve the ultimate purpose of carrying significant overburden and vehicular loads (Abdel Sayed et al. 1993). These structures are constructed by bolting together corrugated metal plates to form different configurations (i.e., a large pipe shape, an arch shape, or a box shape). Many studies have been performed to investigate the static behaviour of buried CSP culverts by utilizing the ring compression theory (e.g., Meyerhof & Fisher 1963; and White & Layer 1960), and the finite element (FE) analysis (e.g., Brown et al. 1968; Duncan 1976; and Katona et al. 1976; Elshimi et al. 2013). In addition, many full-scale tests have been carried out to gain a comprehensive

understanding of CSP culvert behaviour (e.g., McGrath et al. 2002; Elshimi et al. 2013; Vallée 2015; and Regier et al. 2018).

Although many design codes and standards adopted detailed design procedures for arch metal culverts under static loading conditions (e.g. AASHTO LRFD Bridge Design Specifications; NCHRP 473; Australian/New Zealand standards; and the Canadian Highway Bridge Design Code (CHBDC)), there is a lack of design procedures in these codes regarding the seismic design of these structures. For instance, neither the AASHTO LRFD Bridge Design Specifications nor the NCHRP 473 include any seismic design recommendations for arch metal structures. While, the Canadian Highway Bridge Design Code includes seismic loading requirements for long span arch metal culverts, however, it relies on the study by Byrne et al. (1996) which considered several different conditions not compatible with the flexible nature of CSP metal culverts as will be discussed in detail in the next section. Moreover, the Australian/New Zealand standards recommended the seismic design to be conducted as per the CHBDC. Hence, it has become vital to understand and include the effects of seismic loading in the design of CSP culverts.

Byrne et al. (1996) proposed a well-documented finite element (FE) dynamic analysis which forms the basis of the seismic design guidelines in a number of design codes as mentioned above. However, this study examined the seismic behaviour of precast concrete arch culverts only which is much stiffer than metal culverts. The dynamic analyses were developed using a FE code (FLUSH) for a circular arch concrete culvert with a span of 10.8 m and a rise of 5.5 m. The study showed that the seismic loading resulted in a notable increase in culvert thrust forces and bending moments, particularly for a peak ground acceleration (PGA) greater than 0.3 g. Furthermore, the study highlighted the strong impact

of the soil-structure interaction (SSI) occurring between the culvert and the surrounding backfill, where the dynamic forces are “attracted to” the stiffer medium. Thus, during earthquakes the induced horizontal forces are concentrated at the backfill, which represents the stiffer medium; whereas the vertical forces are resisted by the culvert (the stiffer body in the vertical direction). Figure 7-1 shows the mesh formulation and the FE model developed by Byrne et al. (1996). Here it can be seen that the model does not include the effect of the subsurface materials below the foundation. Because the SSI is significantly affected by the low cross-sectional stiffness of a CSP culvert in comparison to reinforced concrete, the study thus has limitations when utilized for the seismic design of CSP culverts. Moreover, the concrete arches used in the study provide greater foundation stability than is the case with CSP culverts, where the metal arches have only hinged connections with the concrete footings. The study of Byrne et al. (1996) was reviewed and extended by Wood and Jenkins (2000), who used the same culvert geometry and materials, but enhanced the model by adding a layer with a thickness of 8 m beneath the foundation, to account for the effect of the subsurface materials. Moreover, Wood and Jenkins (2000) simulated the earthquake load as a uniform horizontal body force in four equal increments, to model a total inertia load corresponding to an acceleration of 0.2 g. Only half of the culvert was utilized in the model, an approach which was suitable for the analysis because the earthquake loads were simulated by applying equivalent horizontal forces to all the elements. The subsequent degradation in soil shear strength was not simulated, due to the simplicity of the dynamic load applications. However, the foundation layer was modelled using two moduli of elasticity, 20 GPa and 100 MPa, to represent a rigid and flexible foundation, respectively. Nevertheless, these values do not sufficiently represent soft and

loose soils. The researchers concluded that the effect of seismic loads decreased with an increasing depth of the soil cover.

Another numerical study using the Fast Lagrangian Analysis of Continua (FLAC) was performed by the New Zealand Transport Agency (2008) to examine the seismic performance of long-span CSP culverts. A detailed parametric study was utilized to investigate the performance of a high-profile arch culvert with a span of 11.66 m and a rise of 7.29 m, under seismic loading conditions. The parametric study examined soil shear strength, dilation angle, the cover over the culvert, and the presence and size of concrete stiffening beams. The study showed a significant increase in thrust forces at the culvert base, ranging from 40% to 65% for different foundation layer types (from stiff to soft soils) due to seismic loading. The bending moment at the culvert springline likewise exhibited an increase of up to 200% in soft soils. In the analysis, the Mohr-Coulomb (MC) soil model was used to simulate soil behaviour. However, the MC model is not capable of simulating the stress dependency of soil stiffness or its variation with the strain magnitude, which is significant for the dynamic analysis. Moreover, no sensitivity analyses were conducted to calibrate the boundary conditions and model dimensions that are a focus of discussion in this paper.

Arai et al. (2011) carried out a centrifuge test and FE study to investigate the behaviour of buried arched concrete culverts with a closed base, during earthquakes. The study confirmed that buried arch culverts exhibit an outstanding performance in withstanding earthquake loads. This study was extended by Sawamura et al. (2013) to include centrifuge model tests and FE analysis to investigate the dynamic interactive behaviour between concrete multi-arch culverts and the surrounding backfill. These two studies examine

concrete culverts with a closed base. Thus, they cannot accurately predict the seismic behaviour of CSP culverts with an open base.

On the other hand, many other studies have also been conducted on the seismic design of underground culverts and pipelines but not the long-span metal open base culverts investigated in this study (e.g. Hindy and Novak 1979; Youd & Beckman 1996 1997 and 2003; Davis & Bardet 2000; Hashash et al. 2001; NCHRP 611 2008; Debiasi et al. 2013; El Naggar 2014 and Abuhajar et al. 2015). One of the recent studies was by Katona (2010), that used the FE program CANDE-2007 to develop a comprehensive study to investigate the seismic behaviour of buried culverts. In the study, seismic loads were applied as an equivalent horizontal displacement to the horizontal model boundaries (racking or deformation displacement method), an approach that was developed by Wood and Lower (2007) and Wang (1993) for tunnels with a length greater than the width/diameter. Katona's analysis was applied to a CSP pipe 10 ft in diameter and to a concrete box culvert 10 ft high and 20 ft wide. The study found that there is a good agreement between the CANDE-2007 software results and the simplified closed-form solutions for the cases concerned. Simplified analyses (i.e., simplified linear and pseudo-static models) usually neglect the degradation of the soil stiffness with increasing cyclic strain amplitude and the impact of the soil-structure interaction between buried structures and the surrounding soil (Huo et al., 2006 and Bobet et al. 2008). Moreover, these simplified methods may yield misleading results, particularly when the structure is more flexible than the surrounding soil (Huo et al. 2006). Furthermore, as an initial phase of the comprehensive study presented in this paper, Mahgoub and El Naggar (2017) studied the seismic performance of CSP culverts in the city of Victoria, Canada, for different earthquake magnitudes. The

2017 study showed that for low-profile culverts, internal forces at the springline exhibited notable changes during earthquakes, a determining factor for the design in this case. These findings are discussed further below.

It can be concluded that most of the seismic studies have focused on buried pipes or closed concrete culverts and cannot be relied upon for the design of long-span CSP arch culverts. The present study utilized PLAXIS 2D for full dynamic finite element (FE) analyses after verifying the static results of the developed models against a well documented case study. In the development of the FE models, an advanced soil model was used with different cross-sectional stiffnesses, seismic records, and subsurface conditions under the CSP culverts. In addition, the effects of changing the foundation, backfill height and culvert configuration on CSP culvert behaviour were examined. Finally, the results were compared with the results of the simplified seismic equations in the CHBDC, as these equations considered to be the commonly used simplified equations for these structures. Moreover, Canada has different seismic hazard zones which ranging from low to medium to high and very high seismicity across the country that gave this study more reliability to cover different levels of seismicity.

7.2 VERIFIED FIELD TEST

A full-scale field test of a large-span culvert was performed by Webb et al. (1999) as part of the project referred to as Recommended Specifications for Large-Span Culverts (NCHRP Report 473). The CSP culvert tested was a non-galvanized corrugated steel low-profile arch with a span of 9.50 m and a rise of 3.7 m. The cross-section comprised corrugated steel plate with a pitch of 152 mm, depth of 51 mm, and plate thickness of 5.5 mm (with shallow corrugations). Figure 7- 2 shows the geometry of the culvert tested. Two

concrete footings, each 1.50 m wide and 0.60 m thick were constructed with an elastic modulus of 30 GPa and a Poisson ratio of 0.15. The granular backfill was placed and compacted in 0.3 m lifts, up to 4.57 m (15 ft) in height (i.e., providing a cover of 0.90 m above the crown). As reported in the study, the in-situ material was well-graded sand with gravel (SW), in accordance with ASTM (i.e., site type C).

A full monitoring system was installed to monitor the structure during different construction stages. The culvert was monitored during the backfill placement until the backfill reached 0.9 m above the crown. Strain gauges and deformation monitoring instruments were positioned at the crown, shoulders and springlines of the culvert. Figure 7- 2 shows the locations of the monitoring instruments around the culvert that were used to verify the FE model under static conditions during backfilling. The data monitored included bending moments and vertical deformations at the middle station for the crown and shoulder (curvature change). Additional details are provided in Webb et al., (1999); NCHRP Report 473, and in Mahgoub and El Naggar (2017).

7.3 METHODOLOGY

Site response analyses using 1D-FE models were carried out to scale and select simulated time histories proposed by Atkinson (2009, 2012) and Atkinson and Boore (2006), in order to represent seismic hazards in the cities chosen to represent different levels of seismicity (i.e., Victoria, Vancouver, Montreal and Toronto). A 2D-FE model of a CSP long-span culvert was then developed and verified against a well-documented case study of a culvert under static loading condition. Full dynamic analyses were subsequently completed by incorporating the scaled time history records into the verified FE model. In addition, sensitivity analyses were performed to calibrate the model boundary conditions and

dimensions. Finally, the investigation was extended by including a detailed parametric study to examine the effect of site subsurface conditions, foundation settings, culvert spans and cross-sections, and culvert configurations on CSP culvert performance under earthquake loading conditions.

7.4 SITE RESPONSE ANALYSIS

To conduct the site response analysis, simulated records were selected and scaled from large data sets that were developed by Atkinson and Boore (2006), Macias et al. (2008), Boore and Atkinson (2008), and Atkinson (2009 and 2012). In these data sets, Western Canada is represented as having moderate to high earthquake hazards, while Eastern Canada has low to moderate hazards. As described in Atkinson (2009), for each site class (i.e., site type A (hard rock), site type C (soft rock and very dense soil), site type D (stiff clay), and site type E (soft soil)), five sets of records were generated for Western Canada, representing three different earthquake magnitudes (i.e., M6.5, M7.5 and M8.6); and four sets were created for Eastern Canada, representing two earthquake magnitudes (M6.0 and M7.0). As explained by Atkinson (2009), each data set has 45 random records at different fault locations for every site condition, to represent earthquakes in specific regions and site types. In the present study, only short period earthquakes (M6 and M6.5) are incorporated in the analyses. Table 7.1 summarizes the simulated records for Eastern and Western Canada. Figure 7- 3 displays two different signals for Eastern and Western Canada, with their characteristics, and compares between them. It can be seen that, before any scaling factors are applied, the Western record has a higher Fourier amplitude (0.062) and PGA (0.48) than the Eastern record, which has a Fourier amplitude of 0.027 and a PGA of 0.41.

Fourier spectrum analyses were utilized for all records to obtain the signal characteristics (i.e., the maximum and fundamental frequency) applied in the FE models.

This section discusses the method used to scale and match the compatible time histories to the target uniform hazard spectrum (UHS) in the National Building Code of Canada (NBCC 2015). Even though the target UHS (with a probability level of 2% in 50 years) is available for site type C only, it can be generated for other site types by scaling the targeted records by means of amplifying or deamplifying factors given in NBCC 2015. The NBCC site types are classified according to the shear wave velocity for each site type (see Table 7.2).

As recommended by Atkinson (2009), time history records were selected and scaled by defining the target UHS for the selected cities with different seismic hazard levels and site types in accordance with NBCC (2015). The proposed sets of records were specified according to the region studied (e.g., Eastern or Western Canada) and the site type. Subsequently, 1D finite element models were developed to obtain the resulting response spectrum for unscaled records to match the target UHS for the period of interest, ranging from 0.1 to 1 second, as well as the peak ground acceleration (PGA). Next, the records were compared by calculating the ratio between the targeted spectrum acceleration (PSA_{targ}) and the simulated spectrum acceleration (PSA_{sim}) at every point within the relevant period of interest, and the mean and standard deviation values were determined. As suggested by Atkinson, only records with scaling factors (PSA_{targ} / PSA_{sim}) between 0.5 and 2.0 were considered. The appropriate record was subsequently scaled by multiplying it by the mean value of (PSA_{targ} / PSA_{sim}).

7.4.1 Free-Field Site Response Analysis With 1-D FE Modelling

1D finite element analyses were conducted using PLAXIS-2D. Sets 1 and 2 for Eastern and Western Canada were utilized to find the most appropriate records for the cities concerned. For each site type, the data from 90 records were applied to the bottom of the soil column (which was considered to be the bedrock level). In the model, seismic waves were propagated from the source up to the ground level to produce the response spectrum, with varying soil deposits (types A, C, D, and E) acting as a filter. In addition, the resulting response spectrum and the PGA were matched and compared with the targeted NBCC 2015 values.

7.4.1.1 Geometry

The soil column was simulated by a column of homogeneous soil 40.0 m high and 1.6 m wide, corresponding to the required site type (A, C, D, or E). Figure 7- 4 shows the model geometry and mesh formulation. The element sizes were chosen based on the wave propagation and velocity, as discussed in the following section.

7.4.1.2 Finite Element Mesh

The soil was modelled using the 15-noded triangular plane strain element. This element provides more accurate results because it follows a higher order interpolation function (PLAXIS Manual, 2017). The mesh generation in PLAXIS was adjusted in order to comply with equation (1) of Kuhlemeyer and Lysmer (1973), to make the element length less than or equal to one-eighth of the wavelength, so as to prevent any error during the wave propagation:

$$\lambda/8 = V_{S\,min}/(8 \times f_{max}) \qquad (1)$$

where $V_{S\,min}$ is the lowest shear wave velocity in the soil profile and f_{max} is the maximum frequency component of the inserted wave that can be calculated from Fourier spectrum analysis.

7.4.1.3 Boundary Conditions

For the simulation of one-dimensional wave propagation, the PLAXIS library option of a tied degree of freedom was assigned to the lateral boundary conditions of the model, to simulate the soil column for the site response analysis. The mesh was generated so as to distribute the nodes identically (with the same elevation) along the vertical boundaries of the model. Thus, the nodes at the same elevation are connected and will experience the same horizontal and vertical displacement (PLAXIS manual 2017).

7.4.1.4 Soil Model

The Hardening Soil with Small Strain (HS-Small) model from the PLAXIS library was used to model the soil behaviour. The model was formulated by Benz (2006) to simulate the soil stress-strain behaviour of nonlinear and stress-dependent soils. In the HS-Small model, the unloading/reloading behaviour is assumed to be linearly elastic within the first small strain range. The relationship of unloading/reloading then decreases nonlinearly according to the strain value. The small-strain stiffness was described with the hyperbolic curve developed by Hardin and Drnevich (1972), where the soil stiffness decays with increasing strain according to the modulus reduction curve, with shear modulus, *G*, and shear strain, γ. The relationship between *G* and γ can be identified through cyclic triaxial tests or by various other empirical relationships reported by researchers in the literature, e.g., Seed and Idriss (1970) for cohesionless soil, Vucetic and Dobry (1991) for cohesive soils, and Schnabel (1973) for rock materials. Table 7.3 shows the soil parameters used in

the analyses, representing the various site types: rock (A), very dense sand (C), stiff clay (D), and soft clay (E) in a drained condition. The parameters of site type C were selected according to the natural ground surface found in the case study (Webb, 1999), while the parameters for other soil types were chosen according to reasonable ranges given in the literature (e.g., Bowels 1997; Das and Sivakugan 2016). Table 7.4 shows the utilized degradation curves for each of the different considered subsurface conditions. Cyclic and dynamic loading can be appropriately simulated by the HS-Small model, because the maximum small strain stiffness is recovered when the loading cycle reverses (hysteretic behaviour). The correlations proposed by Black and Hardin (1969), Biazer and Hicher (1994), and Alpan (1970) were used in calculating the maximum shear modulus G_0.

7.4.1.5 Damping

In PLAXIS, the damping matrix (C) = $\alpha M + \beta K$ is used, where M is the mass matrix, and K is the stiffness matrix. In addition, Rayleigh Damping scalers (α, β) were added for target frequencies 1 and 2 to define the damping behaviour of the soil.

$$\alpha + \beta \omega^2 = 2\omega\xi \quad and \quad \omega = 2\pi F \tag{2}$$

Two targeted frequencies (F_1 and F_2) were identified. F_1 is the fundamental frequency of the soil layer which is given by:

$$F_1 = \frac{V_s}{4H} \tag{3}$$

where Vs is the average soil shear velocity according to the site type (see Table 7.1). F_2 is the closest integral odd number given by the ratio between the fundamental frequency of

the input signal (according to the Fourier Spectrum) and the fundamental frequency of the soil layer (Hudson et al., 1994).

7.4.1.6 Results and Discussion of The Site Response Analyses

Table 7.5 shows which records were selected according to the site type and earthquake magnitudes, with the estimated amplification or scale factors. Figures 7-5, 7-6, 7-7 and 8 show the simulated response spectrum for the scaled records for site types A, C, D, and E, as compared with the targeted NBCC 2015 spectrum within the various periods of interest for the cities concerned. It should be noted that the records used were named and numbered in accordance with Atkinson (2009), as given on www.seismotoolbox.ca.

7.5 DEVELOPMENT OF FE MODEL FOR CSP CULVERTS

Figure 7-9(a) is a schematic drawing of the geometry of the adopted two-dimensional finite element model, while Figure 7-9(b) illustrates the mesh formulation and the different parts simulated, i.e., the CSP culvert, backfill, interface, and concrete footings. The detailed parametric study is described below in Section 7.5.3.

The natural ground and the backfilling envelope were modelled using higher order 15-noded triangular elements. The model comprised approximately 12,000 elements, with an average element size of 180 mm around the culvert. The large number of small-sized elements ensured high accuracy, especially at locations where nonlinear behaviour was anticipated (e.g., close to the culvert). The HS-Small model was used to simulate the material behaviour of the soil. The backfill material properties, shown in Table 7.6, were selected according to the results of the hyperbolic model developed by Webb (1999). In addition, the same considerations as those described in Section 7.4.1.2 for generating the

mesh were utilized in the complete 2D FE model. The reinforced concrete footings were modelled as volume elements using an elastic material model. The steel plates were also modelled as an isotropic elastic material using the PLAXIS 2D plate element, which allows for orthotropic elastic material behaviour and uses axial and flexural rigidities. PLAXIS 2D treats the plate elements in the same way as conventional beam elements, where the shear, bending and normal forces are considered in the element formulation. The steel plate properties used in the model were obtained from Webb (1999), as shown in Table 7.7. The base plate, used to fix the steel arches to the concrete footing, was a horizontal steel plate 300 mm wide and 5 mm thick. The base plate was anchored to the concrete footing and joined to the culvert as a simple connection. A hinged connection between the culvert and the base plate could therefore be considered, due to the reasonable relative stiffness between them.

The friction behaviour at the culvert-soil interface was modelled using five-noded interface elements from the PLAXIS library. The roughness of the interaction was modelled by utilizing a strength-reduction factor at the interface, R_{inter} = 0.67. Interface elements were likewise applied between the concrete footings and the soil layers, with R_{inter}= 0.67. The compaction of the soil placed around the culverts was also simulated, to capture the behaviour of CSP culverts with an adequate degree of accuracy. Soil compaction has a significant effect on the behaviour of flexible and rigid structures. In this study, the compaction effect was considered by using the procedure described in Taleb and Moore (1999), and Elshimi and Moore (2013). The main concept of the procedure is to apply the high horizontal earth pressure remaining in the soil after compaction. While compacting each layer, the compaction effort induces horizontal stresses against the culvert wall that

reaches to its passive resistance (i.e., the maximum horizontal stress that can be attained by cohesionless soil). After the compaction of the layer finishes, all or part of these induced horizontal stresses will be released depending on the soil stiffness and the culvert rigidity. Flexible culverts will experience a lateral movement during the compaction and the majority of the resulting stresses from the compaction will be released. However, rigid culverts will deform slightly then most of the compaction stresses will be constrained in the adjacent backfill resulting in an increase in the culvert internal forces. Additional details regarding the experimental and numerical proof of this method of accounting for the compaction effects on CSP culverts are presented in Taleb and Moore (1999), and Elshimi and Moore (2013).

7.5.1 Calibration of the Boundary Conditions

For static analyses, in the model a fully fixed boundary condition (BC) was assumed at the base. However, the lateral boundaries were set to be free in the vertical direction and fixed in the horizontal direction. Once the construction of the culvert and backfilling were completed, the boundary conditions were changed to the dynamic conditions. PLAXIS 2D has three types of dynamic boundary condition: 1D with tied degrees of freedom, 2D viscous (or absorbent) boundaries, and 2D free-field boundaries (FFBC). A sensitivity analysis was carried out to investigate the effect of changing the model width on the predicted response spectrum at the ground surface in the middle of the model. Figure 7-10(a) shows the different response spectra simulated by using a model width of 120 m (~12 times the culvert span) with viscous boundary conditions and free-field boundary conditions, in comparison to the results of the 1D study for the selected record for Victoria, with site type C as an example.

Figure 7-10(a) shows that free-field boundary conditions achieve a better match with 1D analyses than is the case with viscous boundary conditions. The sensitivity analysis illustrates that in order to use viscous boundary conditions, the model should be extended to a width of 250 m. The use of larger boundary distances (for viscous BCs) thus leads to computational inconvenience. Many trials were carried out with 2D free-field boundaries to find the minimum width required for every earthquake record selected. Figure 7-10(b) illustrates the effect of changing the model width on the estimated spectrum for Victoria, for site type C. Accordingly, free-field boundary conditions were used in the analyses, with a minimum width of 120 m for the dynamic analyses.

7.5.2 Simulation of the Construction Sequence

The construction sequence stages utilized in the full-scale test were simulated in the 2D modelling as follows:

7. The initial in-situ stress state was applied using the K_o where initial geostatic stresses were established, assuming increasing vertical stress with depth ($\sigma_v = \gamma\, z$) and horizontal stresses based on $\sigma_h = K_o\, \sigma_v$. The groundwater table was assumed to be below the profile being considered.
8. Excavation of the ground to the proposed foundation level was simulated by deactivating the soil elements inside the culvert trench.
9. The reinforced concrete footings were activated.
10. Construction of the culvert was then simulated by activating the steel arch culvert and the base plate.

11. The granular backfill was added in 0.3 m lifts up to the proposed height (0.90 m above the crown). Meanwhile, the compaction effect was applied with each lift and then deactivated in a separate stage immediately after.
12. Finally, the selected scaled signals were applied to the bottom model boundary (rock base), for the different models.

7.5.3 Parametric Study and Work Plan

Table 7.8 and Figure 7-11 illustrate the parametric study and work plan parameters that were investigated in this research. Six sets of numerical models for full dynamic analyses were developed. The first set (set 1) focused on the effect of different seismic hazards on a low-profile culvert. Four scaled records representing four cities across Canada, with different hazard levels (i.e. Victoria, Vancouver, Montreal, and Toronto), were utilized for site type A. The effect of changing the site conditions on culvert performance was examined in set 2. In this set, culvert performance was investigated for site types C, D and E for the cities concerned.

Set 3 was developed to examine the effect of culvert rigidity on culvert seismic performance. In this set, three culvert spans (i.e., 9.55 m, 15.0 m, and 20.0 m) were used, and the backfill height above the crown (h_c) was 0.90 m. The culvert aspect ratio (height/span) was 0.37. Shallow, deep and deeper corrugated plates were utilized in this set for a culvert with a span of 9.55 m. In the simulation, plates with deep and deeper corrugations were utilized for a culvert span of 15 m (as the shallow corrugation is not suitable of such span), and only plates with deeper corrugations were used for a culvert span of 20 m. The footing width was also changed in order to keep the pressure beneath the footings constant.

The effect of changing the backfill height above the culvert crown (h_c) was investigated in set 4. Cover heights (h_c) of 1.5, 3.0, 4.5, 6.0, 7.5, and 9.0 m were considered. The culvert simulated in this set had deep corrugations and a span of 9.55 m. As in the case of set 3, the pressure beneath the footings was kept constant by changing their width.

In set 5, the effect of increasing the footing stability on culvert behaviour was studied by increasing the footing width (B). The considered culvert had a shallow corrugation and a span of 9.55 m. Footings width varying between 2 to 4 m was used for the models located in Vancouver. While, the culvert located in Montreal were developed using footing width of 2.5 and 3.0 m. It should be noted that even though a footing width of 4.0 m could not be used in a practical application (since the footing width would be almost 41% of the culvert span), it was considered here in order to gain a better understanding of the culvert behaviour.

Set 6 focuses on the effects of different culvert configurations (i.e., low-profile, semi-circular and high-profile) on the seismic behaviour. It can be seen from Figure 7-11(b) that a constant culvert span of 9.55 m was used, however, different aspect ratios (height/span) were adopted. The aspect ratios used for low-profile, semi-circular, and high-profile culverts were 0.387, 0.50, and 0.565, respectively. The backfill height above the crown (h_c) was 0.9 m and the footing width (B) was 1.5 m. The scaled records for Vancouver (high seismic hazard) for site type C were incorporated in sets 3, 4 and 6, and the records for Vancouver and Montreal (i.e., high and medium seismic hazards) for site type C were used in set 5. Then, all the results from the FE models in all the sets were compared with the results of the simplified design equations of the CHBDC.

7.6 RESULTS AND DISCUSSION

This section presents the results of the finite element study for the different sets of models and compares the results with those of the CHBDC equations. The CHBDC code provides for the seismic design of large-span metal culverts in Section 7.5.5, with the following equations:

$$M_E = M_D A_V \qquad (4)$$

$$T_E = T_D A_V \qquad (5)$$

where M_D, and T_D are the moment and thrust force resulting from the dead load (backfill), and A_V is the vertical acceleration ratio, which is equal to two-thirds of the peak ground acceleration (PGA). M_E and T_E represent the maximum bending moment and thrust force resulting from seismic loading at the culvert crown and base, respectively. More details on the calculation of M_D and T_D are presented in CHBDC (CAN/CSA-S6-14, 2014).

7.6.1 CSP Culvert Static Behaviour

The results of the FE model developed in this study were verified against the measured results of a case study of a CSP culvert under static loading conditions. Detailed results are provided in Mahgoub and El Naggar (2017). Figure 7-12 compares the results for the maximum thrust forces and bending moments obtained from the FE model, CHBDC equations and field test. It can be seen from the figure that there was good correspondence among the results. For the FE model, the CHBDC equations, and the field test case study, the maximum bending moment at the crown was found to be 7.95 kN.m/m, 7.65 kN.m/m, and 7.45 kN.m/m, respectively. As reported in Webb (1999), the thrust forces measured in the case study were inaccurate; they were therefore not included. As shown in Figure 7-12,

the maximum thrust force at the culvert base was 159 kN/m for the FE analysis and 156 kN/m for the CHBDC equations. Moreover, for footing settlement, an excellent match was achieved between the FE results and the case study measurements. Webb (1999) reported that the footings exhibited approximately 4.0 mm settlement after completion of the backfill, and the FE results yielded 3.87 mm. In addition, the maximum vertical deformation at the crown was 80 mm in the FE model, as compared to 72 mm in the case study measurements.

Figure 7-13 shows the culvert static internal forces and footing movements obtained from the FE models for different site conditions (i.e., the thrust forces, bending moments, footing settlement and lateral movement), in comparison to the results of the CHBDC equations. These results illustrate the effect of different site types on the static behaviour of CSP culverts. As mentioned in the CHBDC commentary, subsurface conditions, i.e., bedrock or other relatively incompressible materials, need to be encountered at a shallow depth to prevent excessive settlement that could give rise to additional internal forces on the culvert. It should also be kept in mind that the CHBDC does not propose considerations for calculating the different internal forces in various locations around the culvert (only the maximum thrust forces at the base and the bending moment at the crown). The thrust forces and bending moments were obtained from the FE models for the culvert base and crown, respectively. It can be seen from Figure 7-13 that regardless of the site type, the CHBDC equations yielded constant values of -155.65 kN/m for the base thrust forces and 7.65 kN.m/m for the crown bending moments. In contrast, the thrust forces obtained from the FE analyses were -156, -159.5, -168.4, and -187.8 kN/m and the crown bending moments were 7.75, 7.9, 8.3, and 7.13 kN.m/m for site types A, C, D and E, respectively. Moreover,

the FE model indicated footing settlements of 0.0, 3.87, 8.9, and 17.0 mm for site types A, C, D and E, respectively. Although the FE model found no notable horizontal movement for footings laid in site types A, C and D, footings in site type E were shown to move 3.6 mm laterally, toward the outer side of the culvert. Therefore, it is evident that in weak subsurface conditions, the CHBDC equations underestimate the thrust forces. In addition, while the bending moments obtained from the CHBDC equations corresponded closely to the FE results for site type A, the FE results indicated greater bending moments for weaker soils, in site types C and D. The FE model also predicted a smaller crown bending moment for site type E in comparison to the CHBDC equations. This is due to a lateral movement of 3.6 mm and settlement of 17 mm for site type E, in contrast to settlements of 0, 3.87, and 8.9 mm found for site types A, C, and D, respectively.

The selected scaled signals were applied to the different FE models for different site types. The following sections discuss the seismic performance of CSP long-span culverts in more detail.

7.6.2 Culvert Seismic Performance for Site Type A (Set 1)

Figure 7-14 illustrates the effect of an earthquake on CSP culvert internal forces (thrust forces and bending moments) for the four cities Toronto, Montreal, Vancouver and Victoria for site type A, throughout the duration of the earthquake. This set was based on the assumption incorporated in Byrne et al. (1996) and subsequently in the CHBDC equations, that the footings rest on and are anchored to rock.

Figure 7-14 shows that during the earthquake, the thrust forces at the base increased from about -156 kN/m at the beginning (static conditions) to -158 kN/m at 21.5 seconds for

Toronto, and to -161 kN/m at 21.4 seconds for Montreal. Moreover, the base thrust forces increased to -165 kN/m at 22.2 seconds for Vancouver, and to -175 kN/m at 24.2 seconds for Victoria.

Figure 7-15 shows an example of the change in the soil pressure distribution under static and seismic loading conditions for the culvert located in Vancouver. The figure also presents the culvert deformed shape under the static loading condition (i.e., before the earthquake incident), at the maximum encountered thrust forces (at the 22.2 seconds of the earthquake), and at the end of the earthquake with the corresponding changes of the soil pressure distribution around the culvert. Under the static condition, there is a concentration of the soil pressure at the culvert springline due to the backfill placement accompanied by a decrease of the soil pressure at the culvert crown due to the upward movement of the crown (i.e., peaking). On the other hand, at the 22.2 seconds of the earthquake, the culvert moved to the left. Consequently, a concentration of the soil pressure was observed at the culvert left side (in the movement direction) and relief in the stresses was exhibited on the right side. At the end of the earthquake, no footing distortion occurred, and the residual deformed shape of the culvert was formed. Consequently, the corresponding soil pressure changed as shown in Figure 7-15. In addition, Figure 7-16 shows the bending moments and the thrust forces envelopes of the discussed culvert example. It can be noticed from Figure 7-16 that the base, the springline, the shoulder and the crown locations are the key-locations where changes in the internal forces occurs. Therefore, theses selected locations (see Figure 7-11a) were monitored throughout the earthquake and considered in the discussion to determine the maximum bending moments and the corresponding thrust forces.

In Figure 7-17, the maximum thrust forces at the culvert base obtained from the FE analyses are plotted against the response spectrum (SPA) at 0.2 seconds, as given in NBCC 2015, and are compared to the results of the CHBDC equations. It can be seen from Figure 7-17 that while the maximum thrust forces obtained from the FE analysis increase directly with increasing SPA, the values generated by the CHBDC equations are approximately the same for culverts located in Montreal and Vancouver. This is because the CHBDC equations depend upon PGA values, which are approximately the same for the two cities (≈ 0.33). In contrast, the SPA for Montreal is 0.41 g, while the SPA for Vancouver is 0.585 g. It is therefore evident that earthquakes with the same PGA may be associated with different effects and hazards, as illustrated in Figure 7-17(b). Moreover, Figure 7-17 shows that the CHBDC equations overestimated the thrust forces, yielding values of -170, -189, -190, and -210 kN/m for Toronto, Montreal, Vancouver, and Victoria, respectively. In comparison, FE analyses obtained values of -158, -161, -165, and -175 kN/m for the same cities. The CHBDC equations are based on Byrne et al. (1996), who used a concrete culvert that was more rigid than the surrounding backfill, to attract loads. In contrast, CSP culverts are more flexible than the culvert used by Byrne et al. (1996).

On the other hand, Figure 7-14 shows that the maximum bending moments (BM) at the culvert crown for all the FE models in set 1 were 8.2, 9.4, 10.7, and 12.2 kN.m/m for Toronto, Montreal, Vancouver, and Victoria, respectively. As shown in Figure 7-17, the bending moments at the crown calculated by CHBDC equations were 8.25, 9.16, 9.21, and 10.16 kN.m/m for Toronto, Montreal, Vancouver, and Victoria, respectively. No difference was found between calculated force values for Montreal and Vancouver. However, the FE values increased proportionally with the value of SPA at 0.2 seconds. It can be concluded

that for site type A, the CSP culvert internal forces are more accurately predicted by using values of the response spectrum at 0.2 seconds, rather than PGA values.

7.6.3 Culvert Seismic Performance in Different Site Conditions (Set 2)

7.6.3.1 Site Type C

Figure 7-18 illustrates changes in the culvert internal forces throughout the duration of an earthquake for the cities Toronto, Montreal, Vancouver, and Victoria, for site type C. The figure shows that the culvert base was permanently affected by the maximum thrust forces, which were calculated as -158 (at 22.8 seconds), -190 (at 22.2 seconds), -220 (at 26.2 seconds), and -232 kN/m (at 28.1 seconds) for Toronto, Montreal, Vancouver, and Victoria, respectively. In addition, it can be seen that although for Toronto the maximum bending moments were encountered at the culvert crown (8.63 kN.m/m at 23.76 seconds), the maximum bending moments were found at the culvert springline for Montreal (13.73 kN.m/m at 21.8 seconds), Vancouver (28 kN.m/m at 25.636 seconds), and Victoria (39 kN.m/m at 26.13 seconds).

For a better understanding of culvert seismic behaviour, and in order to evaluate the CHBDC equations, Figure 7-19 compares the FE and CHBDC results for the maximum thrust forces at the culvert base, and the corresponding bending moments. In addition, the figure compares the maximum bending moments at the culvert crown and springline with the corresponding thrust forces, using SPA at 0.2 seconds. Moreover, the footing deformation (i.e., settlement, lateral movement, and footing tilting) is presented to clarify the soil-structure interaction between the culvert and the surrounding backfill. It can be seen from Figure 7-19(a) that there is good agreement between the crown bending moments obtained by the FE analyses and the CHBDC equations. The crown bending moments were

8.63, 9.25, 9.35, and 9.40 kN.m/m in the FE analyses for Toronto, Montreal, Vancouver, and Victoria, respectively, as compared with 8.33, 9.4, 9.41, and 10.45 kN.m/m obtained by the CHBDC equations. Furthermore, the FE analyses showed an acceptable match between the estimated thrust forces at the culvert base and those calculated by the CHBDC equations. The culvert base thrust forces obtained by the FE models were -180, -190, -220, and -230 kN/m, while those calculated by the CHBDC equations were -172, -194, -194.5, and -216 kN/m for Toronto, Montreal, Vancouver, and Victoria, respectively. For Montreal, Vancouver, and Victoria, Figure 7-19(a) also shows a significant increase in the springline bending moments, which were 13.73, 28, and 39 kN.m/m, respectively. This phenomenon is likewise illustrated in Figure 7-19(b), which shows that culvert footings subjected to earthquakes exhibited differential settlement, tilting and lateral movement, which affected culvert behaviour.

The culvert footing settlement indicated in Figure 7-19(b) was approximately uniform (-5.8 mm at point 1, and -5.4 mm at point 2) for Toronto. Subsequently, the footing tilting was insignificant (about 0.02°). Moreover, the footing moved 1.7 mm laterally. Therefore, there is no notable effect on the culvert seismic behaviour, and the previous conclusion for culverts located in sites of type A is applicable. In contrast, the culvert footing behaviour was subject to notable distortion for culverts located in Montreal, Vancouver, and Victoria, as shown in Figure 7-19(b).

It can be seen that the maximum settlement was -14, -47.5, and -79.5 mm, respectively, for these cities. Moreover, the corresponding lateral movements were 13, 17, and 24 mm, and the footing tilting due to differential settlement amounted to 0.15°, 0.98°, and 2.08°, respectively. As shown in Figure 7-19(b), for these three cities an approximately linear

increase of the bending moments and thrust forces at the culvert springline, as well as footing settlement, horizontal movement and tilting, were observed with an increasing response spectrum (SPA).

7.6.3.2 Site Type D

The FE results for culverts in site type D were similar to those found for site type C. Figure 7-20 shows the calculated internal forces for the four cities throughout the duration of an earthquake. A similar trend was found for the models developed for site type D, as the maximum thrust forces were encountered at the culvert base in all the models. These forces were -191, -230, -240, and -274 kN/m, for Toronto, Montreal, Vancouver, and Victoria, respectively. On average, these thrust forces were approximately 17% greater than the thrust forces calculated for culverts located in sites of type C. In addition, the maximum bending moments were found at the crown for culverts located in Toronto, while they were found at the springline for culverts in Montreal, Vancouver, and Victoria. The maximum bending moment for a culvert located in Toronto in site type D was found to be around 7% greater than that for a comparable culvert located in site type C. In contrast, the average increase in maximum bending moments for site type D culverts in Montreal, Vancouver, and Victoria was found to be around 20% higher than that for culverts located in sites of type C. The increased internal forces were due to the increase in the response spectrum and footing distortion (i.e., settlement, lateral movement, and tilting), as shown in Figure 7-21.

As illustrated in Figure 7-21(a), the CHBDC equations underestimated the culvert base thrust forces, obtaining values of -176, -194, -197, and -209 kN/m for Toronto, Montreal, Vancouver, and Victoria, respectively. In comparison, FE analyses yielded -191, -230, -245, and -274 kN/m for the same cities. In addition, the FE results show crown bending

moments for culverts in Montreal, Vancouver, and Victoria (5.9, 3.0, and 5.4 kN.m/m, respectively) that are considerably lower than the results obtained by CHBDC equations (9.4, 9.5, and 10.1 kN.m/m, respectively). The culvert springline bending moments found by FE analyses were 16.3, 34.5, and 46 kN.m/m for Montreal, Vancouver, and Victoria, respectively. Changing the subsurface conditions thus affected the culvert footing behaviour, and consequently the culvert internal forces.

It can be seen from Figure 7-21 that the culvert springline bending moments, base thrust forces and footing distortion (i.e., settlement, horizontal displacement, and tilting) increased with increasing SPA in Montreal, Vancouver, and Victoria (similarly to the situation for site type C). For Toronto, the settlement was calculated to be approximately uniform (similarly to site type C); settlement was -10.2 mm at point 1, and -8.7 mm at point 2. Thus, the footing tilting was 0.06°, which can be considered to be negligible. Likewise, the horizontal displacement was 4.4 mm. However, for Montreal, Vancouver, and Victoria, the maximum footing settlement was -24, -52, and -109 mm, respectively, and the tilting was 0.5°, 1.8°, and 4.1°. The horizontal footing displacements were 14, 21, and 35 mm, respectively, in these cities.

7.6.3.3 Site Type E

Site type E is characterized by soft weak soil. Therefore, severe distortion and settlement in the culvert foundations were expected. Similarly to the results for site types A, C, and D, Figure 7-22 shows the change in culvert internal forces throughout the duration of an earthquake. For all four cities, the maximum bending moments calculated in the FE models were found at the culvert springline. The maximum bending moments were 12.7, 20.9, 47, and 65 kN.m/m for Toronto, Montreal, Vancouver, and Victoria, respectively, while the

maximum thrust forces at the culvert base were -215, -238, -261, and -290 kN/m, respectively. Figure 7-23 shows that maximum settlement of the culvert footing was found to be -30, -67, -217, and -317 mm for Toronto, Montreal, Vancouver, and Victoria, respectively, with tilting of 0.98°, 2.44°, 8.19°, and 11.92°. Likewise, the horizontal displacement values were 16.5, 33.5, 123.5, and 203.5 mm, respectively. It can be seen that these severe footing deformations were associated with an increase in springline bending moments of 19%, 36%, and 41% for culverts located in Montreal, Vancouver, and Victoria, respectively, as compared to culverts in site type D. Similarly, the culvert base thrust forces increased by 12%, 4%, 8%, and 6%. Moreover, the CHBDC equations underestimated the maximum thrust forces at the culvert base by 19%, 15%, 36%, and 46%, in comparison to the FE results for Toronto, Montreal, Vancouver, and Victoria, respectively. The maximum bending moments calculated by the CHBDC equations for the four cities were 8.86, 9.41, 9.18, and 9.70 kN.m/m at the culvert crown; these results did not match the FE results (in terms of either location or value).

Figure 7-24 presents the maximum bending moments obtained from the FE models, plotted against footing tilting, for different cities and site types. When the footing tilting was less than 0.1°, the maximum bending moments were found at the culvert crown; hence, the CHBDC equations were applicable. When the footing tilting exceeded 0.1°, the maximum bending moments were at the springline, with the result that the CHBDC equations were inaccurate. For site type A, where the footing tilting was negligible (≈ 0.0), the maximum bending moments increased only due to changes in the SPA of the different signals. In addition, an approximately linear increase in the culvert springline bending moments was found in the FE models that were developed for the same site type (C, D or E).

7.6.4 Effect of Culvert Rigidity (Set 3)

In set 3, the culvert rigidity was changed by using different spans and cross-sections. *NF* (the flexibility number) was used to express the culvert cross-sectional rigidity according to Equation 6 as described in the CHBDC:

$$NF = \frac{E_s\,(1000\,D^3)}{E\,I} \qquad (6)$$

where, E_s is the elastic modulus of the backfill used, D is the culvert span, E is the steel modulus of elasticity and I is the culvert cross-section moment of inertia.

Figure 7-25 shows the effect of changing the *NF* on the value of the maximum bending moment divided by the culvert span. As mentioned in Section (7.5.3), seismic records for the city of Vancouver for site type C were used in the analyses. Moreover, all of the FE models found that the maximum bending moments were in the culvert springline.

It can be seen from Figure 7-25(a) that linear fitting was an appropriate tool for representing the relationship between the decrease in the maximum bending moment with increasing culvert NF. Figure7-25(b) shows that as the stiffness of the cross-sections decreased, the deformations increased, and consequently the internal forces (thrust forces and bending moments) decreased. For example, three different cross-sections, with shallow, deep and deeper corrugations, were utilized for a culvert with a span of 9.5 m; the maximum bending moments obtained for them were 28, 85, and 124 kN.m/m, respectively. The maximum thrust forces at the base were 220, 244, and 249 kN/m, and the crown deformations were 48.5, 14.2, and 6.9 mm, respectively.

7.6.5 Effects of Changing the Backfill Height (Set 4)

Set 4 was designed to study the effect of increasing the backfill height above the culvert crown on the culvert maximum internal forces. In Figure 7-26, normalized maximum thrust forces and bending moments are plotted against the cover height (h_c). The internal forces were normalized with respect to the field test, where the cover height above the crown was 0.9 m. It can be seen from Figure 7-26 that there is a nonlinear relationship between the maximum bending moment at the culvert springline and the cover height, while the maximum thrust forces at the culvert base increase directly with the cover height. It was also observed that if the backfill height above the crown (h_c) was increased by a factor of 10, the bending moment increased up to 3.7 times and the maximum thrust forces increased up to 4.5 times, in comparison to the reference case. This is related to the arching effect that was mobilized by SSI.

7.6.6 Effect of the Footing Width (Set 5)

As discussed in Section 7.6.3, the behaviour of culvert footings (i.e., settlement, lateral movement, and tilting) has a notable effect on the seismic performance of CSP culverts. Therefore, in this section FE models developed for Vancouver and Montreal, for site type C, were used to investigate enhancing the footing stability by increasing the footing width (B).

7.6.6.1 Vancouver, Site Type C

Figure 7-27 shows the effect of changing the culvert footing width (B) (i.e., to 1.5, 2.0, 2.5, 3.0, and 4.0 m) on the culvert internal forces and footing deformations. In the figure, the footing width is normalized with respect to the culvert span (i.e., yielding ratios of 0.16, 0.21, 0.26, 0.31, and 0.42 of the culvert span). The culvert internal forces were obtained

from the FE models for the culvert crown, springline and base. It can be seen from Figure 7-27(a) that the bending moment at the culvert springline was sensitive to the footing width. It decreased linearly to 28, 25.5, 23, 20, and 16 kN.m/m as the footing width increased to 0.16, 0.21, 0.26, 0.31, and 0.41 of the culvert span, respectively. Meanwhile, the footing tilting decreased to 0.97°, 0.78°, 0.68°, 0.46° and 0.31°, respectively, while the bending moment at the crown was approximately constant (at 9.35 kN.m/m). The maximum thrust forces at the culvert base were less sensitive to the footing width, decreasing to -220, -217, -210, -204, and -201 kN/m as the footing width increased to 0.16, 0.21, 0.26, 0.31, and 0.41 of the culvert span, respectively. Therefore, it can be concluded that when the footing width increased approximately 2.5 times, the maximum bending moment decreased by 43%, the footing tilting decreased by 68%, and the maximum thrust forces decreased by 9%.

7.6.6.2 Montreal, Site Type C

Only three culvert footing widths (i.e., 1.5, 2.5, and 3.5 m) were used for Montreal. It can be seen that the trend described above is repeated in Figure 7-28. The footing tilting decreased to 0.15°, 0.11°, and 0.09° as the footing width increased to 0.16, 0.26, and 0.31 of the culvert span, respectively. Likewise, the bending moments at the culvert springline decreased to 13.7, 7.4, and 4.9 kN.m/m and the thrust forces at the culvert base decreased slightly to -190, -186, and -184 kN/m, respectively. The crown bending moment remained approximately constant (at 9.25 kN.m/m) and became the predominate value for the design. It would therefore be feasible to use the CHBDC equations for the design, where the calculated crown bending moment and base thrust were 9.4 kN.m/m and 192 kN/m, respectively.

7.6.7 Seismic Performance of Different Culvert Configurations (Set 6)

This section compares the seismic performance of three CSP culvert configurations (i.e., low-profile, semi-circular, and high-profile culverts). Four locations around the culverts (i.e., the culvert base, springline, shoulder, and crown) were investigated during the duration of an earthquake. Figure 7-29(a) shows the maximum bending moments at the four locations, with the corresponding thrust forces from the FE analyses. It can be seen from the figure that the distribution of internal forces around the culverts changed according to the culvert configuration. The maximum bending moment in the low-profile culvert was at the springline, while the maximum bending moments in the semi-circular and high-profile culverts were at the shoulder. In addition, the maximum thrust forces were found at the culvert base. Moreover, Figure 7-29(b) shows the footing deformations (i.e., footing settlement and tilting) for the different culvert configurations. The figure shows that the culvert footings tilted and settled in a similar manner, with maximum footing settlements of -45.0, -49.0, and -49.6 mm, and footing tilting of 0.96°, 0.955°, and 1.08° for the low-profile, semi-circular, and high-profile culverts, respectively.

7.6.8 Seismic Mitigation Scheme Utilizing TDA around Large-Span Metal Arch Culverts

In this section an innovative solution by using a lightweight dampening material around large-span metal culverts to reduce the induced stresses due to the seismic loading conditions was introduced to be used in high seismicity regions (e.g., Vancouver).

7.6.8.1 TDA Overview

Tire derived aggregate (TDA) is a lightweight backfill material that has numerous uses in civil applications. It is produced by shredding waste tires into relatively small pieces.

ASTM D6270 classifies TDA into two types: Type A which has a smaller particle size (<70 mm) and is recommended to be used for drainage, vibration dampening and insulation in several civil engineering applications; whereas type B, which consists mainly of larger particles

(up to 300 mm), is primarily used as an embankment fill (El Naggar et al. 2016). TDA has outstanding geotechnical properties, where it weighs (60% of the conventional backfill) and costs less than the conventional backfill material (Sparkes et al. 2019, Yoon et al. 2006). In addition, it is durable material against the variable climatic conditions (Chu 1998). Furthermore, Edil et al. (2005) showed that the permeability of TDA is ten times that of gravel. Moreover, it is considered to be a good thermal insulator and is eight times more effective than regular soil in this regard (Benson et al. 1996).

These outstanding properties qualified TDA to be used in many civil applications. For instance, many researchers explored the feasibility of using TDA in roadway embankments (e.g., Humphrey and Blumenthal 2010; Meles et al. 2014; Mills et al. 2015). In addition, it was used successfully in retaining walls, mechanically stabilized earth (MSE) retaining walls and abutment projects (e.g., Tweedie et al. 1998; Humphrey, 2008; Xiao et al. 2012). TDA has been used in trench fill projects above buried pipes, culverts, and cut and cover tunnels to enhance the arching mechanism (e.g., Meguid and Youssef 2018; Ni et al. 2018; Mahgoub and El Naggar 2019). Moreover, TDA exhibited outstanding performance when used as a dampening material for dynamic loads below rail lines; and behind retaining walls subject to dynamic and/or earthquake loads (Wolfe et al. 2004; Xiao et al. 2012; Ahn and Cheng. 2014).

To study the dynamic performance of TDA as a backfill material for retaining walls, Ahn and Cheng (2014) performed a full-scale shake table test on a retaining wall with TDA backfill and compared the results with those of conventional backfill. They reported that TDA exerted less dynamic pressure on the wall in comparison to conventional soil, while resulting in greater displacement than was the case with conventional soil. Xiao et al. (2012) developed a small-scale shaking table test to investigate the seismic responses of mechanically stabilized earth (MSE) retaining walls with TDA and compares the responses with the traditional granular backfill under the same simulated earthquake excitations. The study concluded that under the same seismic conditions, using TDA in MSE walls resulted in less lateral and vertical displacements, less accelerations, and less static and dynamic stresses compared to using conventional backfill.

Furthermore, Esmaeili et al. (2016) studied the performance of using mixtures of TDA in the railway subgrade (ballast) to reduce the induced vibrations caused by trains passage. The study showed that after mixing TDA with ballast, the damping ratio of the mixtures was increased two times the damping ratio of the pure ballast; and subsequently decreased the rail vibrations impacts on the surrounding structures.

Many studies in the literature investigated the dynamic properties of TDA to get the damping ratio and the shear modulus degradation curve. McCartney et al. (2017) conducted a large scale cyclic simple shear test on type B TDA with a maximum aggregate size of 320 mm. The study showed that there was significant increase in the TDA damping ratio, compared to the granular soils; where the damping ratio range at 0.1% shear strain was found to be in the range of 21 to 26.8%.

In addition, Moussa and El Naggar (2019) conducted a series of large-scale cyclic triaxial tests to determine the dynamic properties of type A TDA (i.e., the damping ratio, and shear modulus reduction curves under different confining pressures). The TDA exhibited outstanding behaviour as a dampening material, with an approximately constant damping ratio ranging from 14% to 24%. Several other studies were carried out that had a good agreement with the conclusions by McCartney et al. (2017) and Moussa and El Naggar (2019) (e.g., Feng and Sutter 2000; and Hazarika et al. 2010; Madhusudhan et al. 2019).

In this study, the properties by Moussa and El Naggar (2019) were used in the analyses. They conducted a series of large-scale cyclic triaxial tests at Dalhousie University, as apart of this research project, to determine the dynamic properties of type A TDA (i.e., the damping ratio, and shear modulus reduction curves under different confining pressures). Figure 7-30 shows the used degradation curve of the TDA shear modulus versus shear strain and the damping ratio versus shear strain at a confinement pressure of 25 kPa.

7.6.8.2 Considered Configurations

Four different configurations (C1-C4) around the arch culvert were suggested to enhance their seismic performance. Figure 7-31 shows the backfill configurations used in the analyses. The considered culvert was a low profile with a shallow corrugation, a span of 9.55 m, and a footing width of 1.5 m (same geometry as the culvert in the verified case study). The scaled records for Vancouver (high seismic hazard) for site type C were incorporated in the analyses. Figure 7-31 illustrates that the first configuration (C1) had a TDA layer around the arch culvert up to the crown. In addition, a 0.5 m of TDA was used at the outer side of the footings and underneath them. The other configurations have the same geometry of C1, however, configuration C2 did not have TDA around or underneath

the footing, and an additional TDA layer surrounded the footing in configuration C3. While in configuration C4, an additional TDA layer of 0.2 m was added above the arch crown. The same considerations as those described in Sections 7.4.1.4 and 7.4.1.5 were utilized to define the material properties in the FE models.

7.6.8.3 Results and Discussions

Figure 7-32 shows the maximum arch internal forces at the base, the crown and the springline locations in each of the different proposed configuration (i.e., configurations C1 to C4) normalized by the internal forces of the reference case that only had a conventional backfill (i.e., without TDA). Moreover, the footing deformation (i.e., settlement, and lateral movements) is presented to clarify the soil-structure interaction between the culvert and the surrounding backfill.

Figure 7-32a shows that the arch culverts in all configurations (without TDA, C1-C4) experienced the maximum bending moment at the springlines, and the maximum thrust at the base. The thrust forces at the base were decreased by approximately 28%, 29%, 30%, and 37%, while the bending moment at the springline was reduced by 28%, 11%, 10%, and 35% for C1, C2, C3, and C4, respectively, relative to the reference case. The bending moment at the base for all considered configurations was almost zero. In addition, it can also be observed from Figure 7-32a that there was a significant decrease in the value of the bending moment at the crown in comparison with the reference case, where it was decreased by 75%, 60%, 65%, and 76% for C1, C2, C3 and C4, respectively. This decrease of the internal forces is attributed to the existence of the dampening lightweight TDA backfill around the culvert. Meanwhile, the decrease in the internal forces in C4 was more than the other configurations, because it had larger area covered by TDA, helped to

decrease the induced stresses and enhancing the arching mechanism around the culvert. In addition, Figure 7-32b shows that there was a relationship between the values of the lateral movements of the footing and the decrease in the bending moments at the crown and the springline, where less lateral movement occurred, more decrease in the bending moment was obtained. For C1, that had TDA around the arch and underneath the footings, the lateral movement were 8 mm compared to 17 mm in the reference case (without TDA). Therefore, the bending moments at the springlines and the crown locations were reduced by 28% and 75%, respectively. While, as there is no TDA in the outer side of the footing in configuration C2, the footing was deformed laterally by a 13 mm. Subsequently, the decrease of the bending moment was less than that of the configuration C1. The footing in configuration C4 was exposed to a lateral movement of 6 mm, consequently, the arch culvert experienced the least bending moments among the different configurations. Even though the TDA configuration around the footing in configurations C2 and C3 was different, configurations C2 and C3 had the same lateral deformations approximately. That was because, configuration C3 had a TDA layer around the footing that decayed the footing support in the inner side which allowed more lateral deformations. Figure 7-32b also shows that due to the existing of TDA underneath the footings in configurations C1, C3 and C4 the maximum settlement underneath the foundation was 67 mm, 68 mm, and 62 mm that was more than the maximum settlement of the reference case that was 51 mm. While the maximum settlement at the footing of configuration C2 was 38 mm (less than the reference case), where the configuration had TDA backfill that decreased the stresses underneath the footing and no compressible material was placed underneath the arch foundations. Therefore, the settlement was decreased. It can be seen from the presented results that using

TDA around arch culverts enhances the seismic performance of CSP arch culvert significantly and hence can provide a practical seismic mitigation alternative.

7.7 DESIGN RECOMMENDATIONS

Based on the results of the conducted study presented above, the following design recommendations can be deduced.

- For site type A, the CHBDC design equations were found to yield reasonable predictions as can be noticed from Figure 7-17, hence, can be used in the seismic design of CSP culverts under different seismic hazards.
- Whereas, for site type C, the CHBDC design equations can be used in cases where the design spectral response acceleration for a period of 0.2 seconds (SPA @ 0.2) is less than 0.6 g based on the results presented in Figure 7-19, where an acceptable agreement between the design equations and the FE results was encountered. For SPA@ 0.2 seconds > 0.6 the predictions of the design equations of the CHBDC started diverging from the FE results and hence it is not recommended in this case.
- For site type D, the CHBDC design equations could be relied on, when the SPA @ 0.2 seconds is less than 0.4 g as shown in Figure 7-21, whereas the estimated stresses by the FE analysis is around 10% or less of the predictions of the CHBDC equations. For cases were the SPA@ 0.2 seconds is greater than 0.4 the CHBDC equations are not recommended.
- For site type E, the simplified equations of the CHBDC are not recommended and a full dynamic finite element analysis is required.

7.8 SUMMARY AND CONCLUSIONS

A detailed two-dimensional finite element study was conducted to investigate the performance of CSP culverts under both static and seismic loading conditions. The study involved developing models that simulated the construction sequence and accounted for the soil-structure interaction, including the effects of compaction of the backfill around the culvert. The seismic component of the study included full dynamic analyses of CPS culverts with different spans and cross-sections, foundations and culvert configurations, buried in different soil conditions, in locations with different seismicity levels. In addition, a seismic mitigation scheme utilizing TDA around and/or under arch culverts was presented and discussed. The following conclusions can be drawn based on the results of the study:

- In static loading conditions, when settlement increased, the CHBDC equations underestimated the thrust forces and were conservative with regard to the bending moments.
- Free-field boundary conditions effectively simulate the propagation of waves into the far field with minimum reflection at the boundary, and consequently can be used in the seismic analysis of CSP culverts.
- The simplified equations do not account for any soil structure interactions arising from different site types. However, this study found that the site type has a significant effect on culvert performance under seismic loading conditions, especially in the case of site types D and E.
- For low-profile culverts, the internal forces at the springlines exhibit a notable change during earthquakes and govern the design in this case.

- Culvert footing movement/distortion is a significant factor that affects the distribution of culvert internal forces resulting from earthquake loading conditions.
- In low-profile culverts, maximum bending moments were found at the culvert crown when the footing tilting was less than 0.1°; consequently, the simplified design equations were applicable. However, when the footing tilting exceeded 0.1°, the maximum bending moments were found at the springline.
- A linearly inverse relationship between the maximum bending moment and the culvert flexibility number (NF) was observed.
- There is a nonlinear relationship between the maximum bending moment at the culvert springline and the cover height, whereas the maximum thrust forces at the culvert base increase directly with the cover height.
- For earthquake loading in Vancouver (site type C in zone of high seismicity), when the culvert footing width was increased approximately 2.5 times, the maximum bending moment decreased by 43%, the footing tilting decreased by 68%, and the maximum thrust forces decreased by 9%.
- For earthquake loading in Montreal, zone of medium seismicity (site type C), when the culvert footing width was increased approximately 1.67 times, the culvert springline bending moment decreased by 46%, and the crown bending moment became the predominate design value. Consequently, it would be feasible to use the simplified equations for the design.
- The internal force distribution around the culvert changed according to the culvert configuration. The maximum bending moment for a low-profile culvert was at the

springline, while the maximum bending moments for semi-circular and high-profile culverts were at the shoulder.

- For arch culverts located in zones of high seismicity, the simplified equations are not recommended, and a full dynamic finite element analysis is required.
- Using TDA around the arch culvert enhances the seismic performance of CSP arch culverts significantly and can provide a suitable mitigation scheme.

Table 7.1: Sets developed for unscaled time history records (Atkinson, 2009)

Set ID.	Earthquake magnitude	R- Fault distance (km)	Area	Hazard type	*No. of records
set 1	M6.5	10 to 15	Western Canada	High	45 for each Set
set 2	M6.5	20 to 30		Moderate	
set 1	M6	10 to 15	Eastern Canada	Moderate	
set 2	M6	20 to 30		Low	

*The records are simulated for every site type (A, C, D and E)

Table 7.2: Site classifications according to NBCC (2015)

Site Type	V_s (m/s)	SPT (N60)	Su (kPa)
A (Rock)	>1500	-	-
C (Very Dense Soils)	360-760	>50	>100
D (Stiff Soils)	180-360	15-50	50-100
E (Soft Soils)	<180	<15	<50

(V_s) is the shear wave velocity, (S_u) is the undrained shear strength

Table 7.3: The soil parameters used

Material	φ'	E_{50}	E_{oed}	E_{ur}	γ	c	G_0
	°	MPa	MPa	MPa	kN/m^3	kPa	MPa
A (Rock)**	45	400	320	1200	24	400	1600
C (Very Dense Soils) *	43	40	32	120	20	0	200
D (Stiff Soils)	25	11	9	33	18	30	55
E (Soft Soils)	15	3.75	3	11	17	15	33

*According to (Webb, 1999)

** Assumed to represent the strong rock behavior with minor and negligible deformations

Table 7.4: Degradation curves defined for different subsurface conditions

Material	Degradation Curve (G/ G_0)
A (Rock)	Schnabel (1973)
C (Very Dense Soils)	Seed and Idriss (1970)
D (Stiff Soils)	Vucetic and Dobry (1991)
E (Soft Soils)	Vucetic and Dobry (1991)

G_0 is the initial or maximum shear modulus

Table 7.5: Summary of the selected records for various site types and earthquake magnitudes

City	Site type	*Record No.	Amplification factor	Set No.
Toronto	A	#3	0.52	2- East Records
	C	#2	0.70	2- East Records
	D	#30	0.50	2- East Records
	E	#28	0.50	2- East Records
Montreal	A	#4	1.20	2- East Records
	C	#2	0.52	1- East Records
	D	#4	1.00	2- East Records
	E	#27	1.30	1- East Records
Vancouver	A	#2	0.785	1- West Records
	C	#34	0.75	1- West Records
	D	#4	0.80	1- West Records
	E	#34	1.00	1- West Records
Victoria	A	#2	1.15	1- West Records
	C	#3	0.69	1- West Records
	D	#2	1.10	1- West Records
	E	#3	1.03	1- West Records

*The numbering is according to the available data in Atkinson (2009)

Table 7.6: The backfill parameters used (Webb,1999)

Parameter	Value	units
φ'	41	°
E_{50}	33	MPa
E_{oed}	26.4	MPa
E_{ur}	99	MPa
γ	18.50	kN/m^3
C	0	kPa
P_{ref}	41	kPa
G_0	125	MPa

Table 7.7: Steel and concrete properties (Webb, 1999)

Material	E (GPa)	Passion's Ratio	Inertia (mm^4/mm)
Concrete (Foundation)	30	0.15	----
*Steel (Shallow Corrugation)	200	0.3	2079.8
**Steel (Deep Corrugation)			24124.5
**Steel (Deeper Corrugation)			97031.45

*cross-section used in the cased study

**cross-sections considered in the parametric study according to ASTM (A796)

Table 7.8: Work plan and parametric study

Set index	Parameters used							No. of models
	Soil cover (*hc*)	CSP used (*XS*)	Culvert span (*S*)	Culvert aspect ratio	Foundation width (*B*)	Site type	Location	
set 1	0.9 m	Shallow corrugation	9.55 m	0.387	1.5 m	A	Victoria, Vancouver, Montreal and Toronto	4
set 2	0.9 m	Shallow corrugation	9.55 m	0.387	1.5 m	C, D and E	Victoria, Vancouver, Montreal and Toronto	12
set 3	0.90 m	Shallow, deep and deeper corrugation	9.55, 15.0 and 20.0 m	0.387	varies	C	Vancouver	6
set 4	0.9, 1.5, 3.0, 4.5, 6.0, 7.5 and 9.0 m	Deep corrugation	9.55 m	0.387	varies	C	Vancouver	7
set 5	0.9 m	Shallow corrugation	9.55 m	0.387	1.5, 2, 2.5, 3, 3.5 and 4.0 m **1.5, 2.5 and 3.0 m***	C	Vancouver **Montreal***	9
set 6	0.9 m	Deep corrugation	9.55 m	0.387, 0.5 and 0.565; refer to Figure (7-11b)	1.50 m	C	Vancouver	3

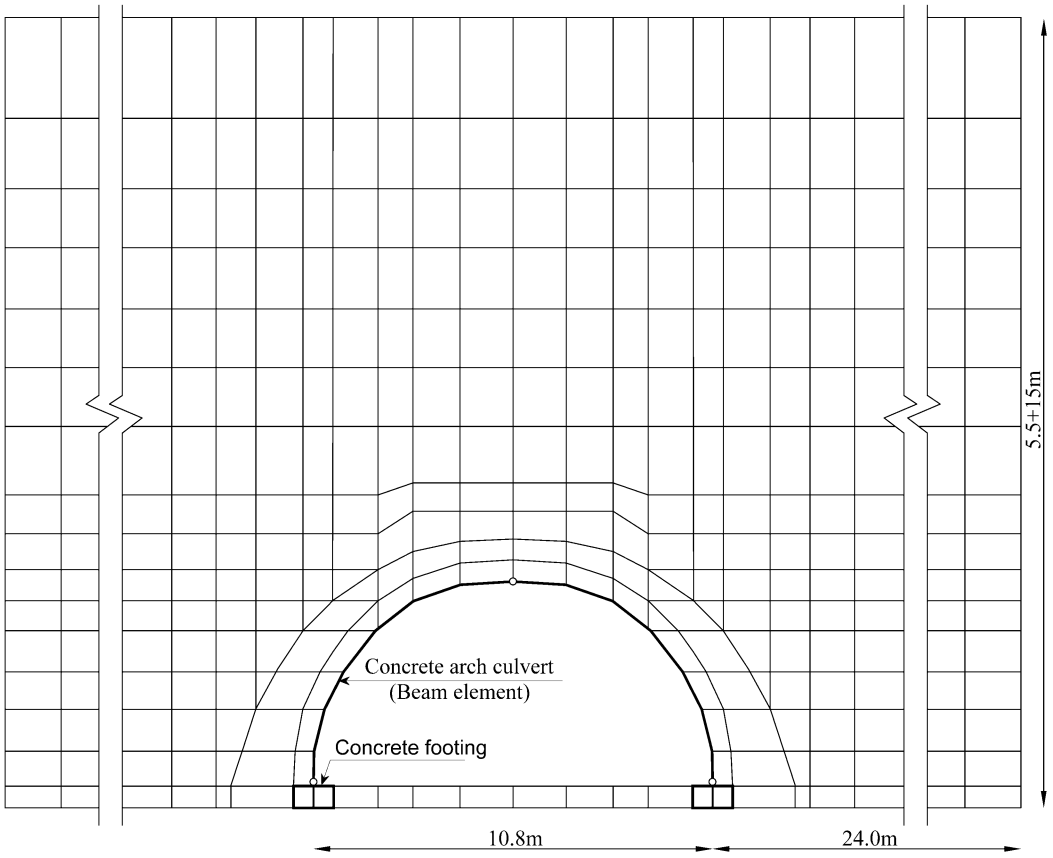

Figure 7-1 The FE model developed by Byrne et al. (1996)

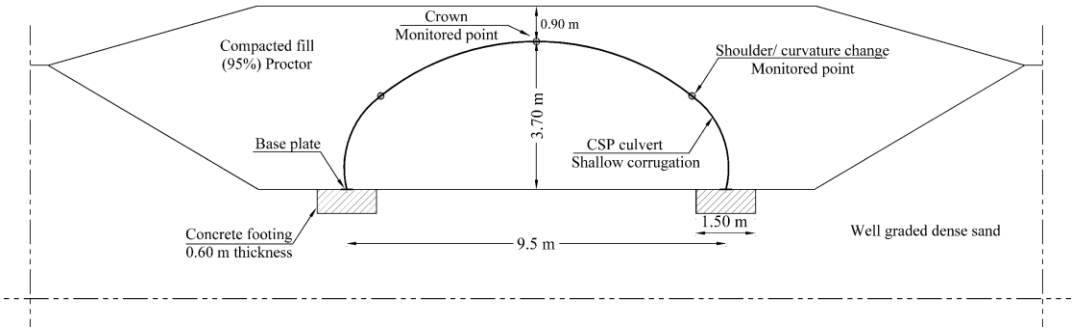

Figure 7-2 Steel arch geometry, reproduced in accordance with Webb et al. (1999)

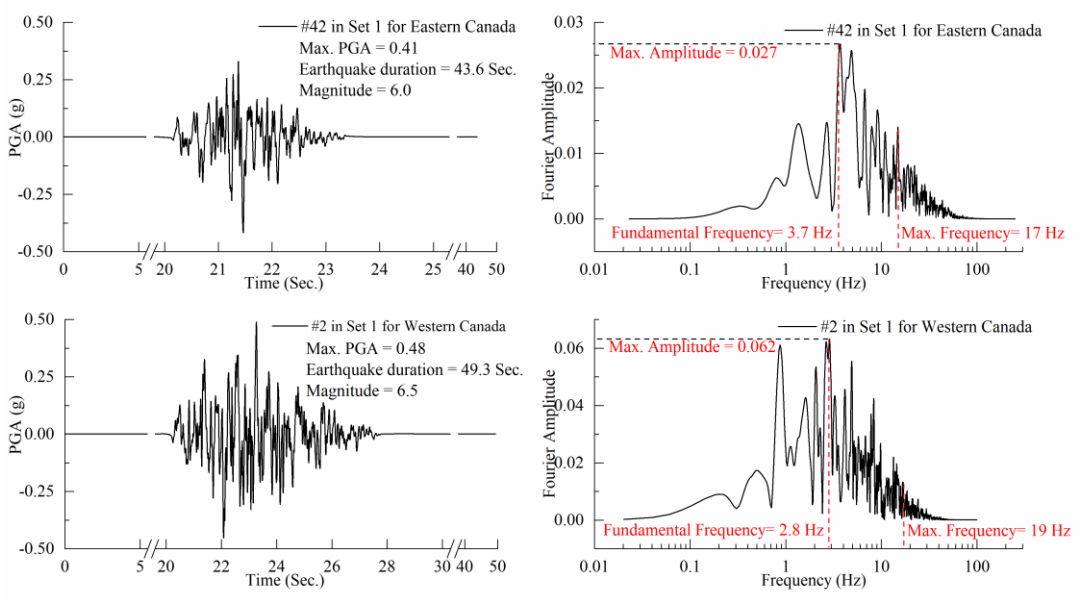

Figure 7-3 Examples of accelerograms for Western and Eastern Canada for site type C (Atkinson 2009)

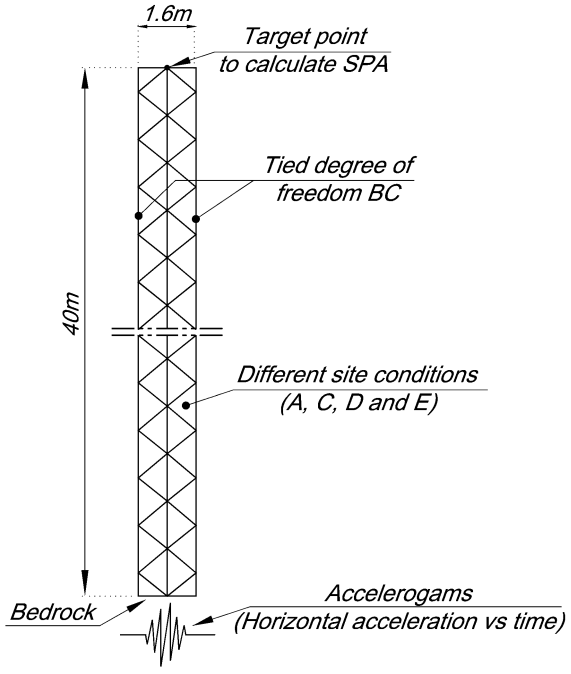

Figure 7-4 Geometry of the 1D FE analysis

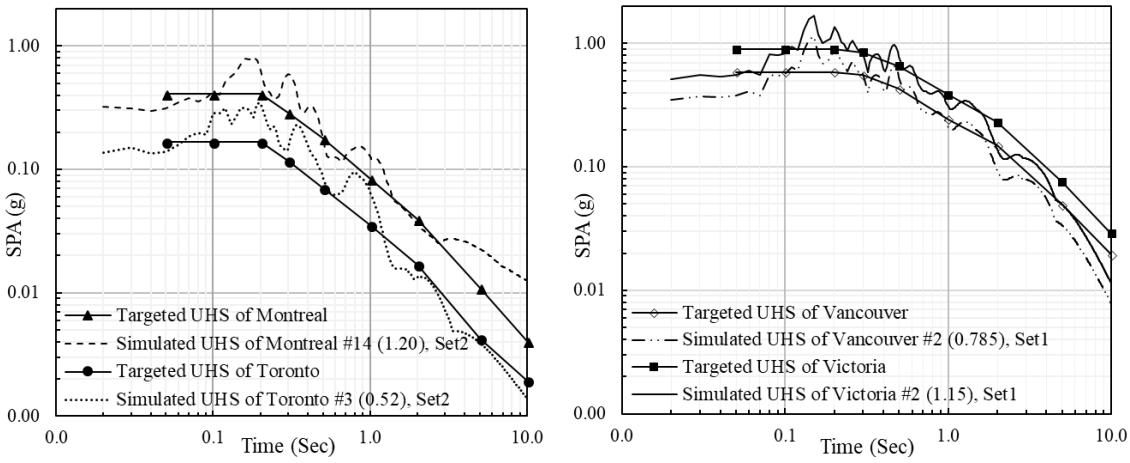

Figure 7-5 Targeted NBCC 2015 spectra compared to selected scaled simulated records, with the estimated amplification factors for site type A

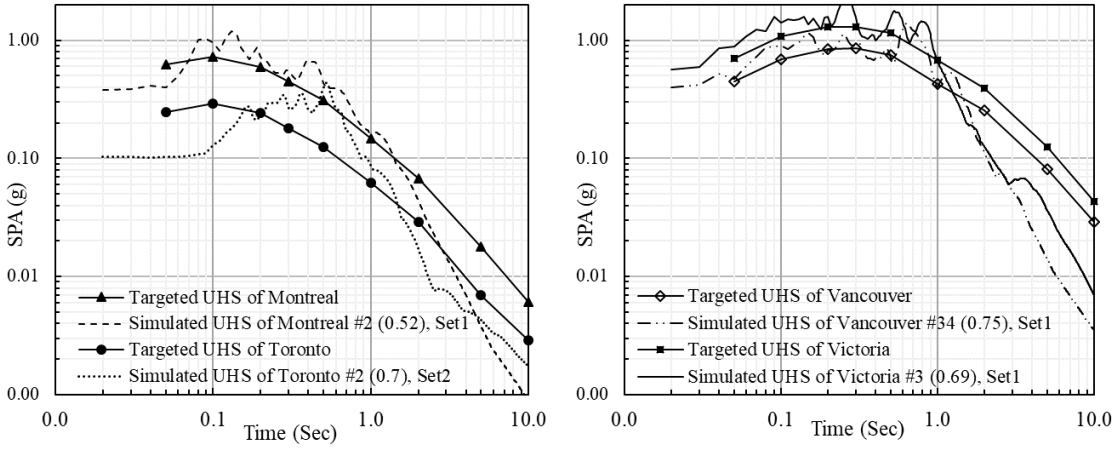

Figure 7-6 Targeted NBCC 2015 spectra compared to selected scaled simulated records, with the estimated amplification factors for site type C

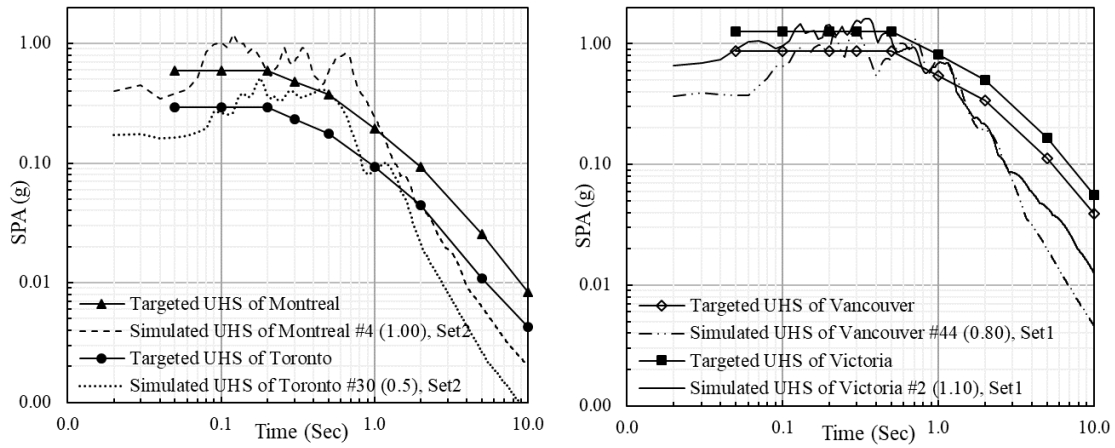

Figure 7-7 Targeted NBCC 2015 spectra compared to selected scaled simulated records, with the estimated amplification factors for site type D

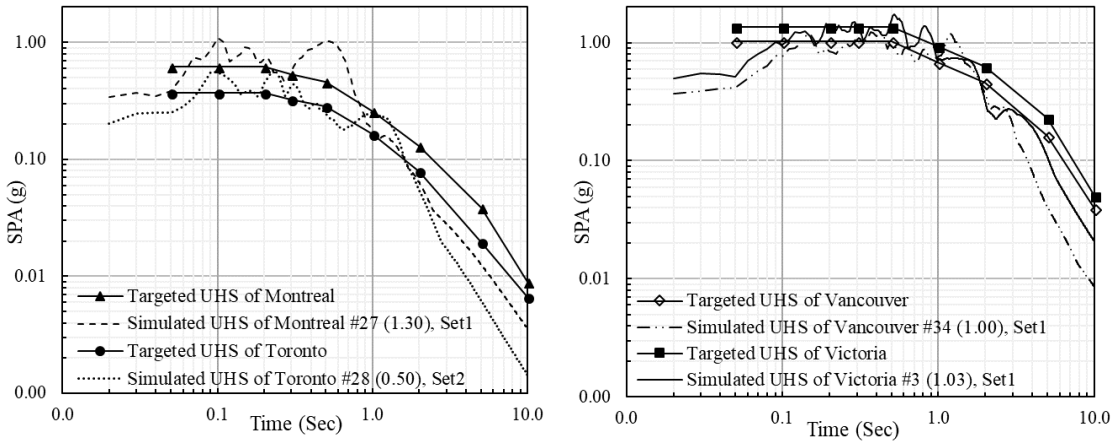

Figure 7-8 Targeted NBCC 2015 spectra compared to selected scaled simulated records, with the estimated amplification factors for site type E

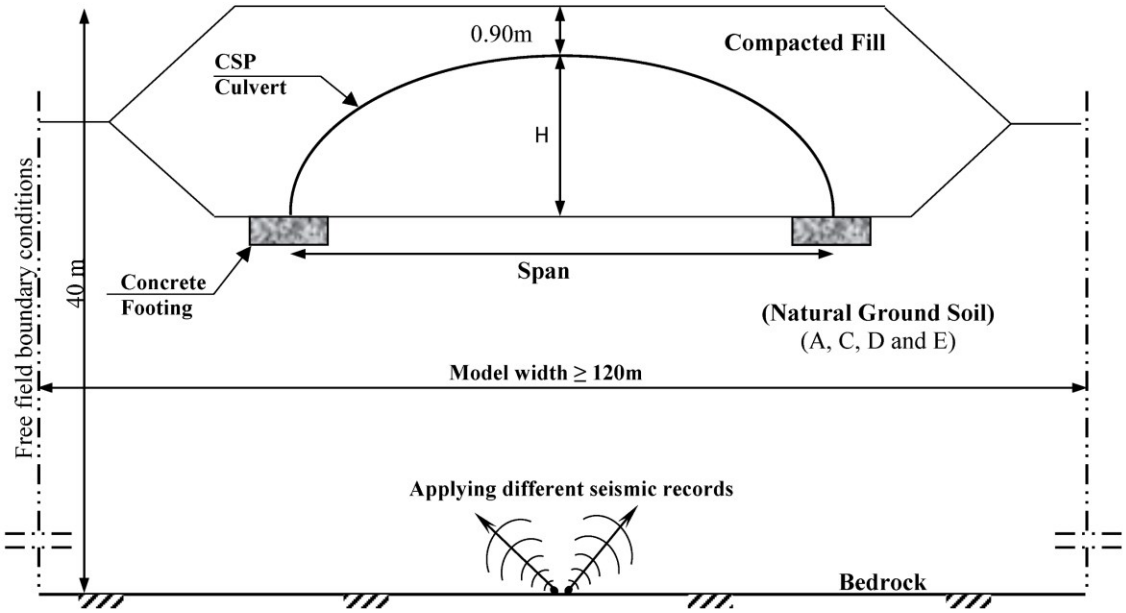

a) The schematic drawing of the simulated problems in seismic

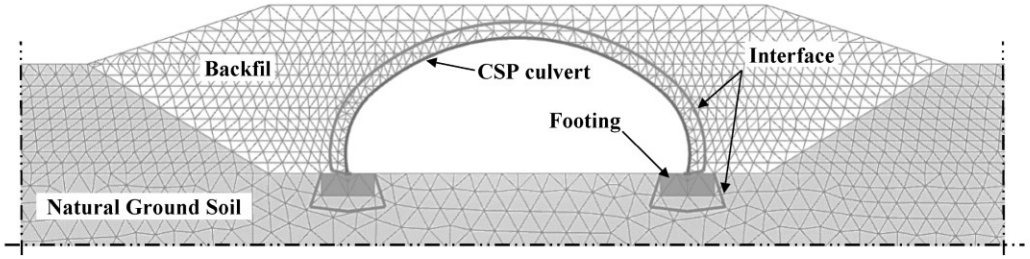

b) FE model with mesh formulation

Figure 7-9 Development of the FE models with mesh formulations

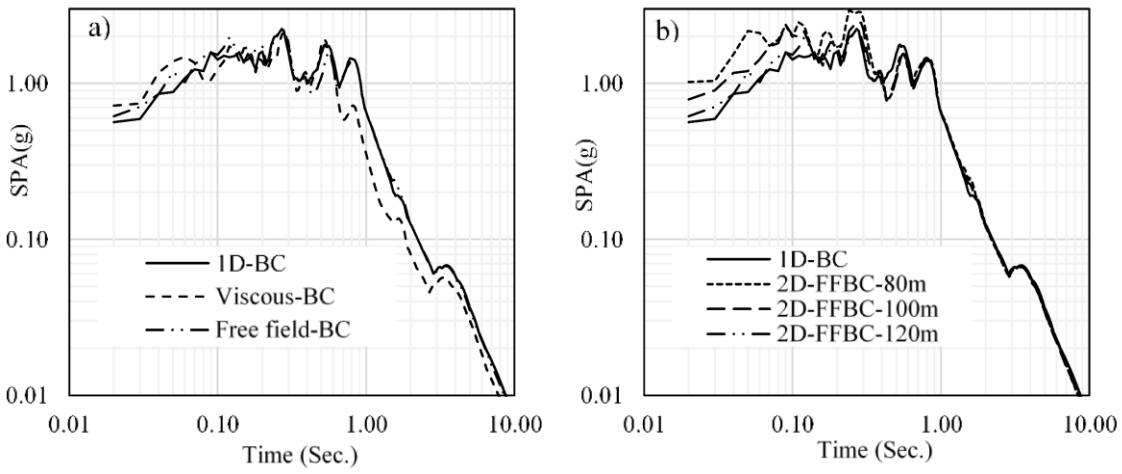

Figure 7-10 The sensitivity analysis conducted for Victoria, for site type C

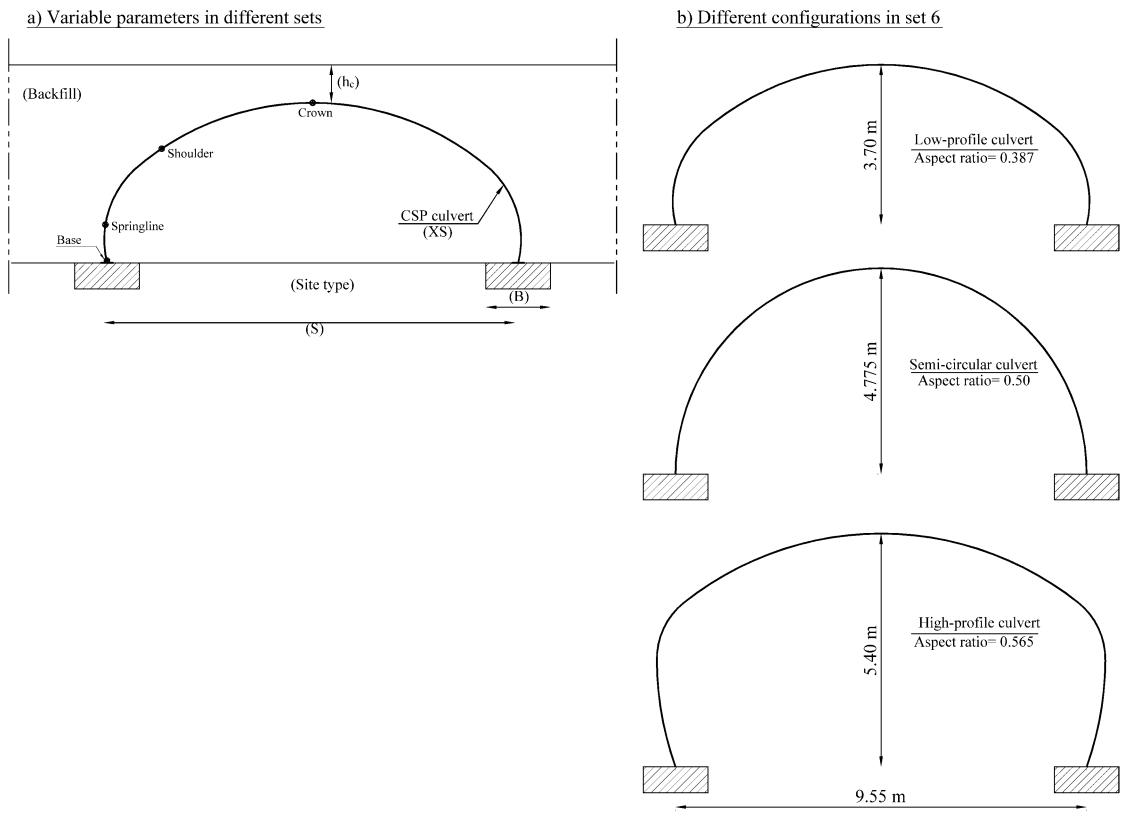

Figure 7-11 Declaration of the parametric study and work plan parameters (refer to Table 8)

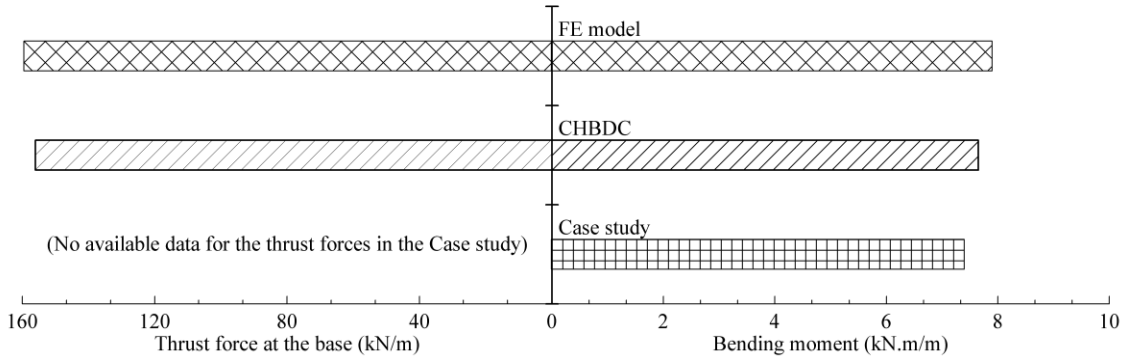

Figure 7-12 Comparison of results of the FE model, CHBDC equations, and field test case study

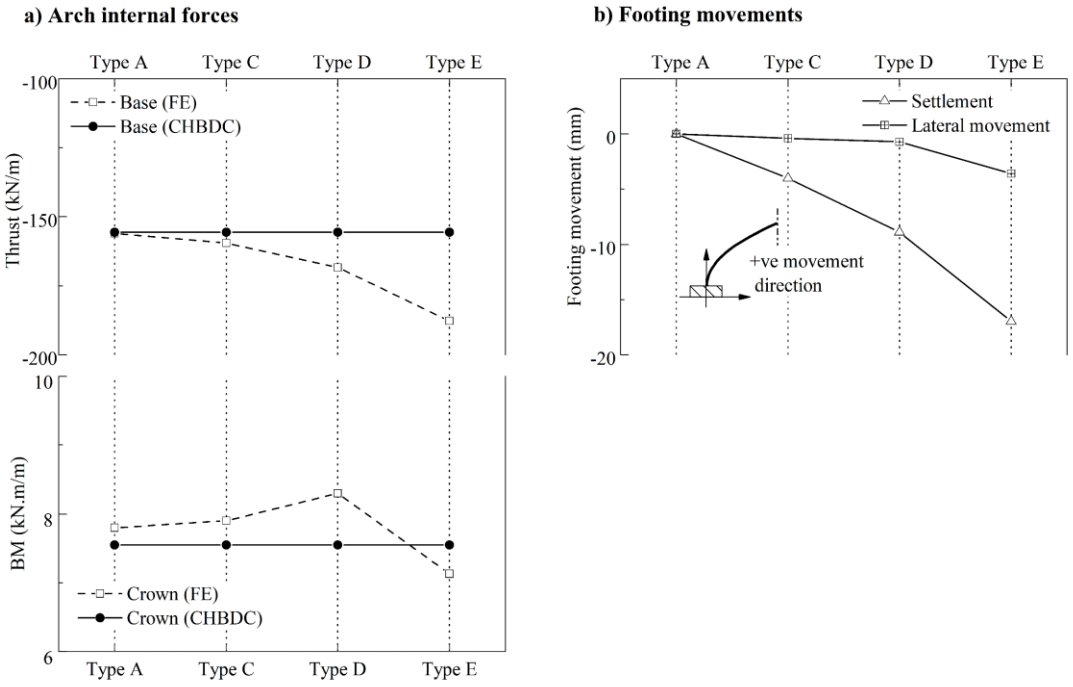

Figure 7-13 Culvert internal forces and footing movements for different site types

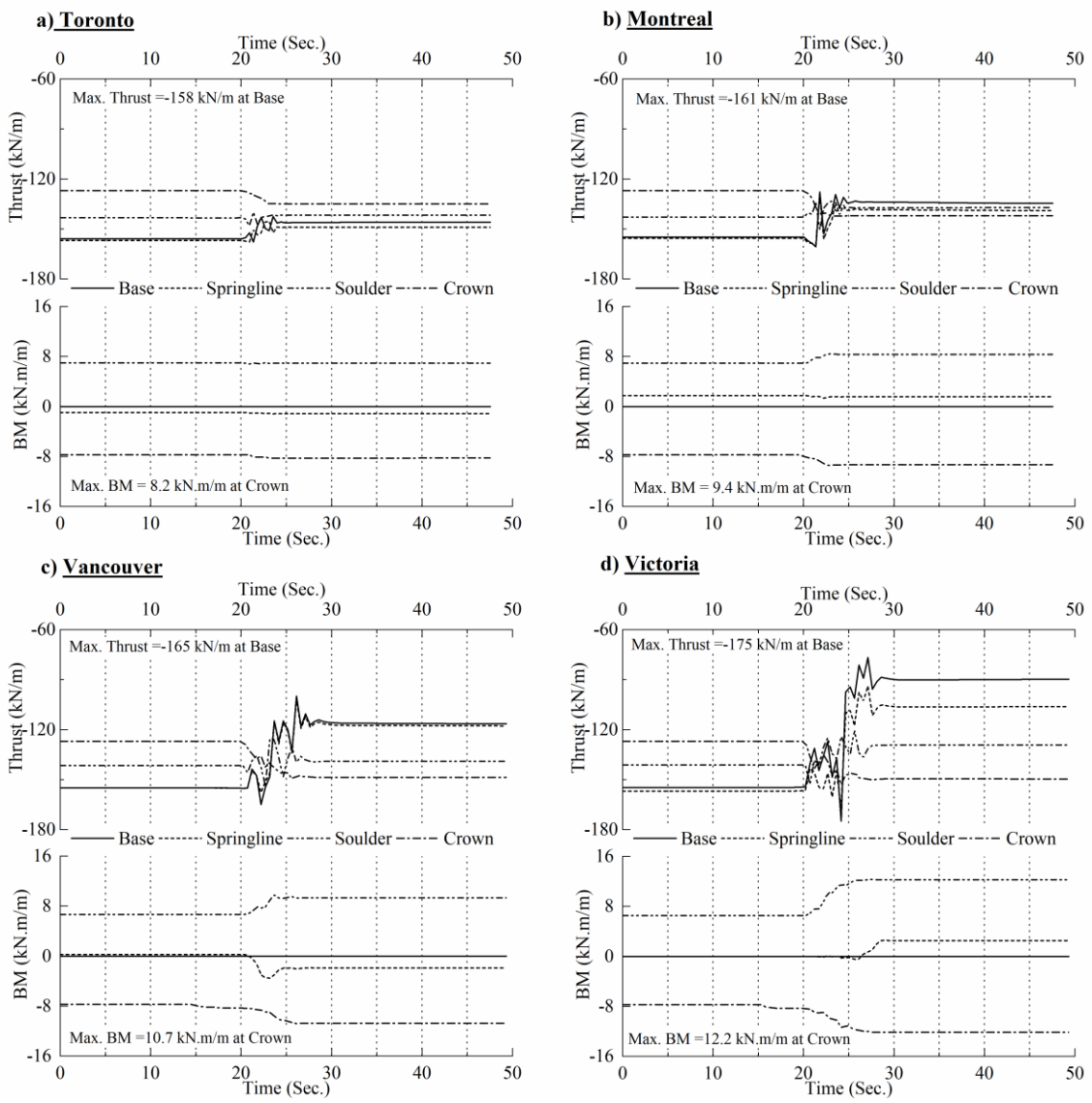

Figure 7-14 Thrust forces and bending moments for different cities throughout the duration of an earthquake, for site type A

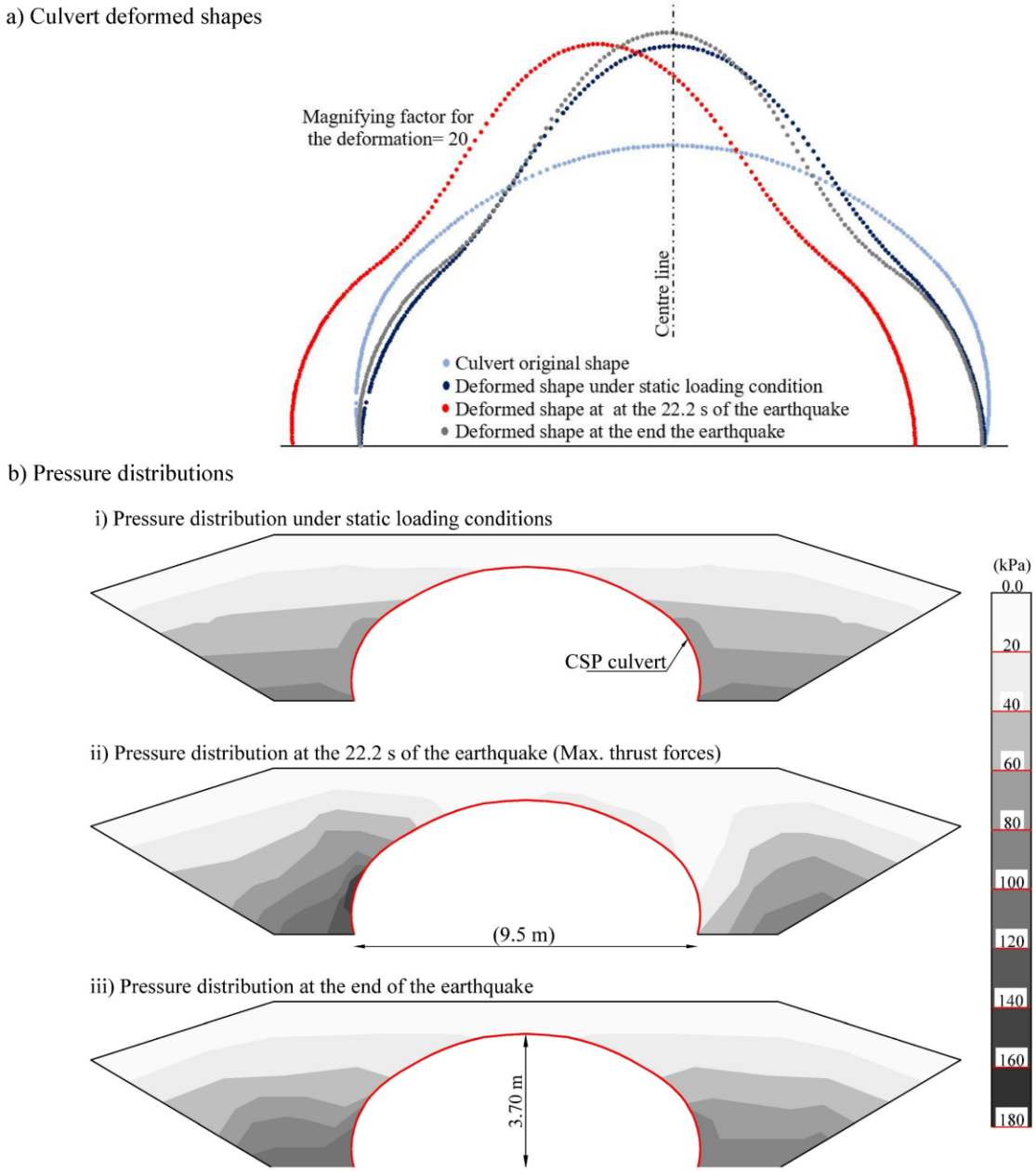

Figure 7-15 Culvert deformed shapes and soil pressure distributions under static and seismic loading conditions

a) Bending moment envelope

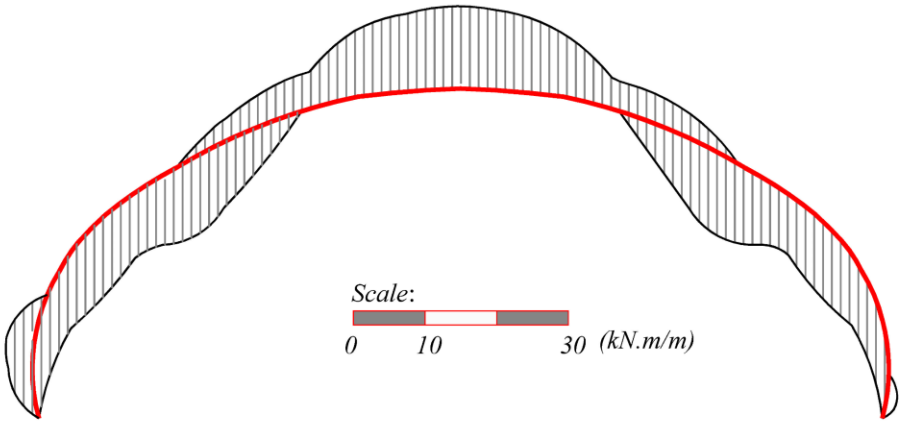

b) Thrust forces envelope

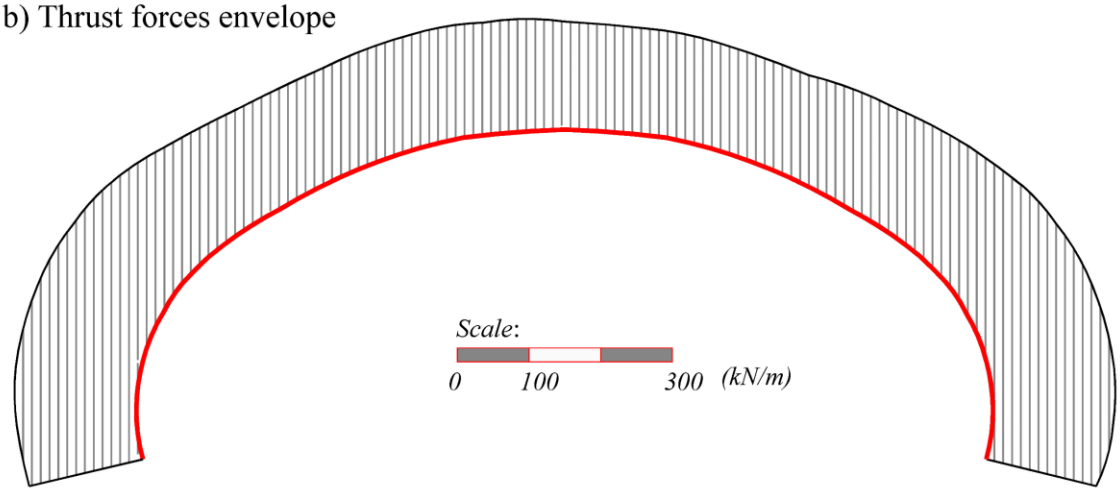

Figure 7-16 Envelopes of Culvert bending moments and thrust forces in Vancouver - site type A

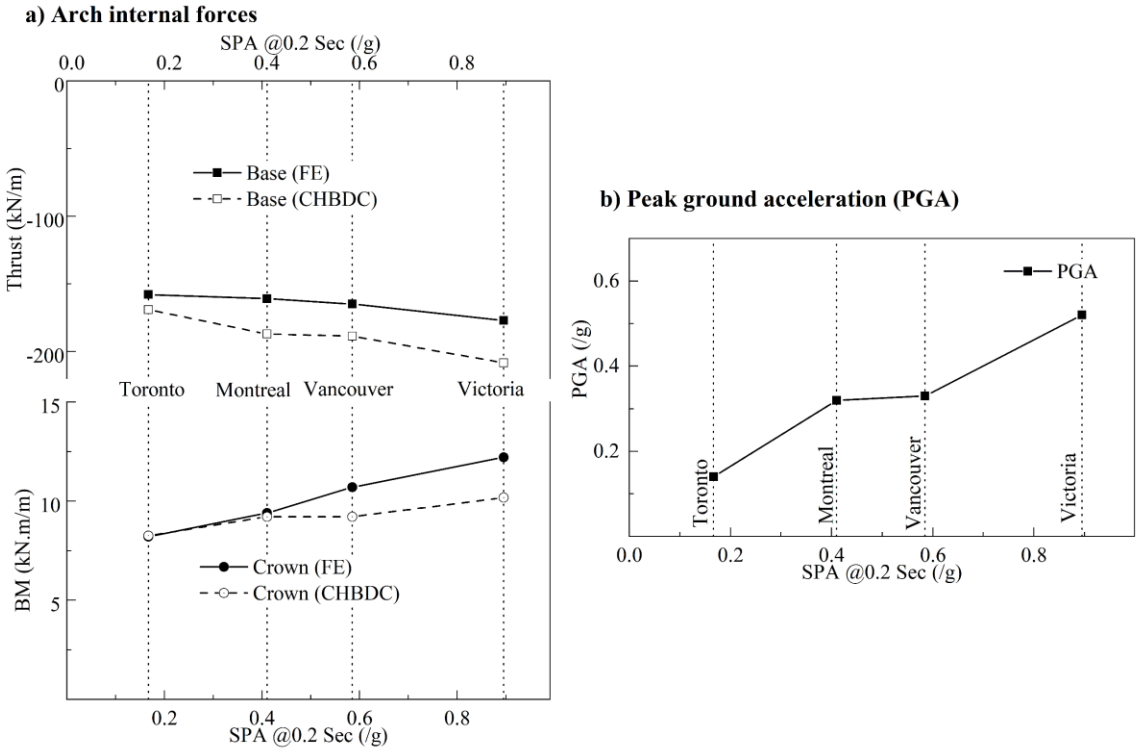

Figure 7-17 Comparison of the results of the FE analysis and CHBDC equations, for site type A

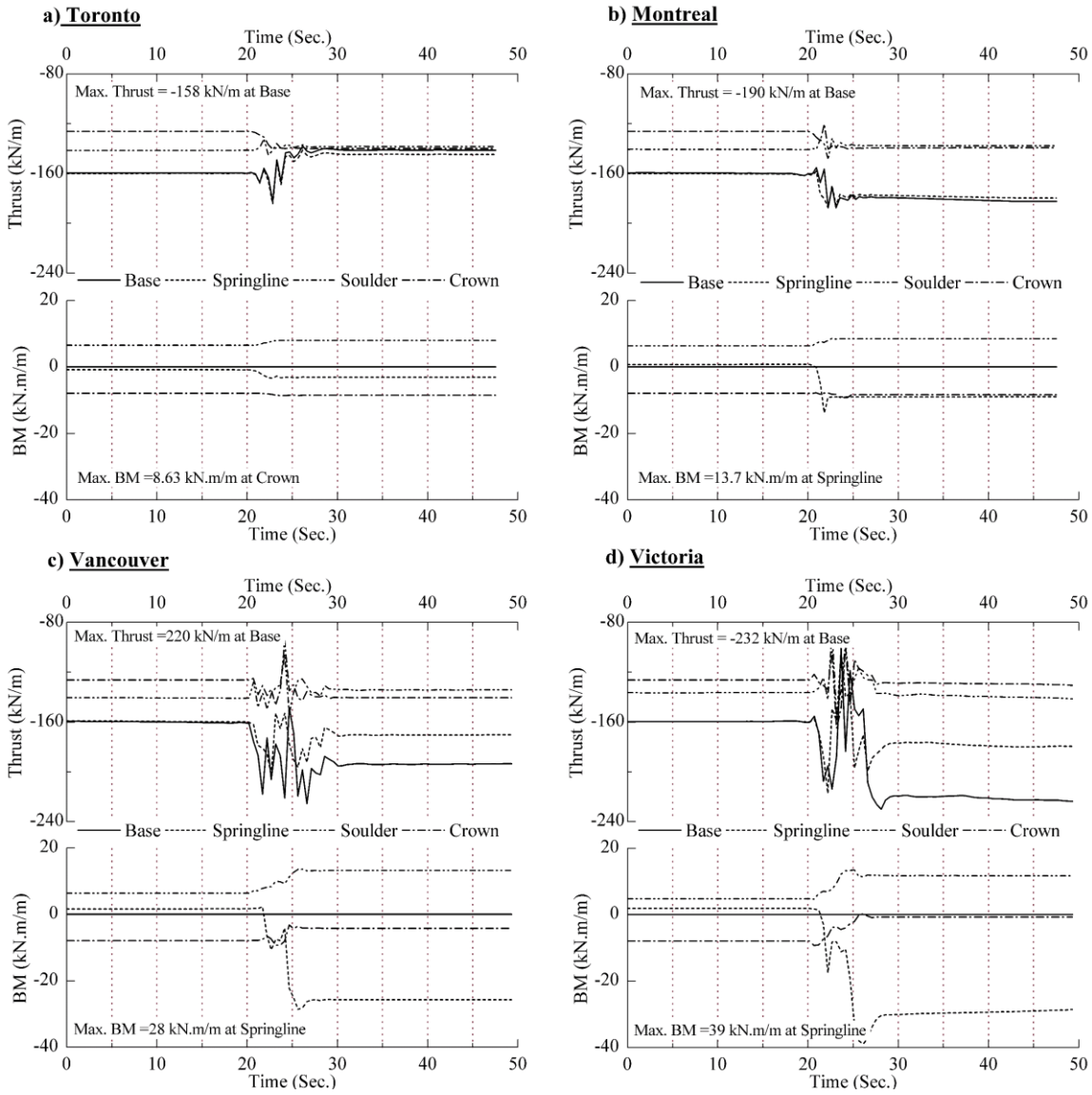

Figure 7-18 Thrust forces and bending moments for different cities throughout the duration of an earthquake, for site type C

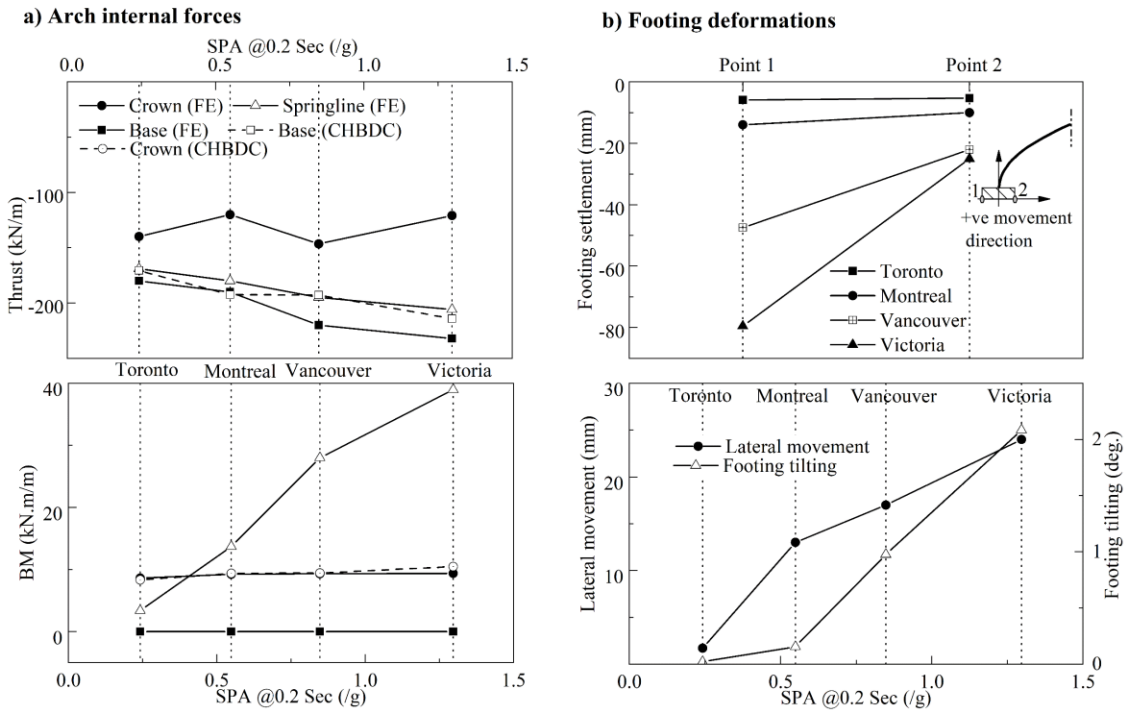

Figure 7-19 Comparison of the results of the FE analysis and CHBDC equations, for site type C

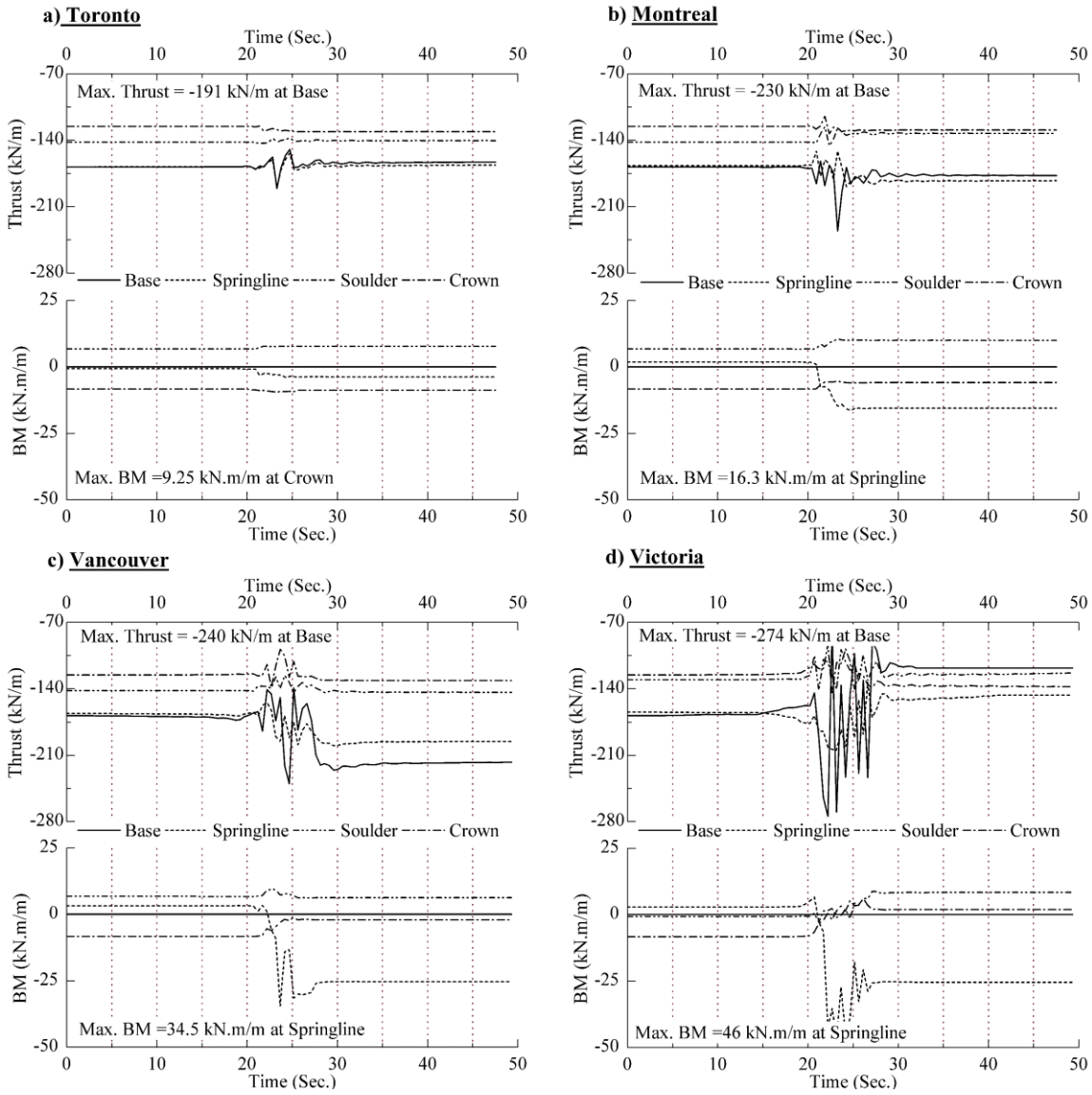

Figure 7-20 Thrust forces and bending moments for different cities throughout the duration of an earthquake, for site type D

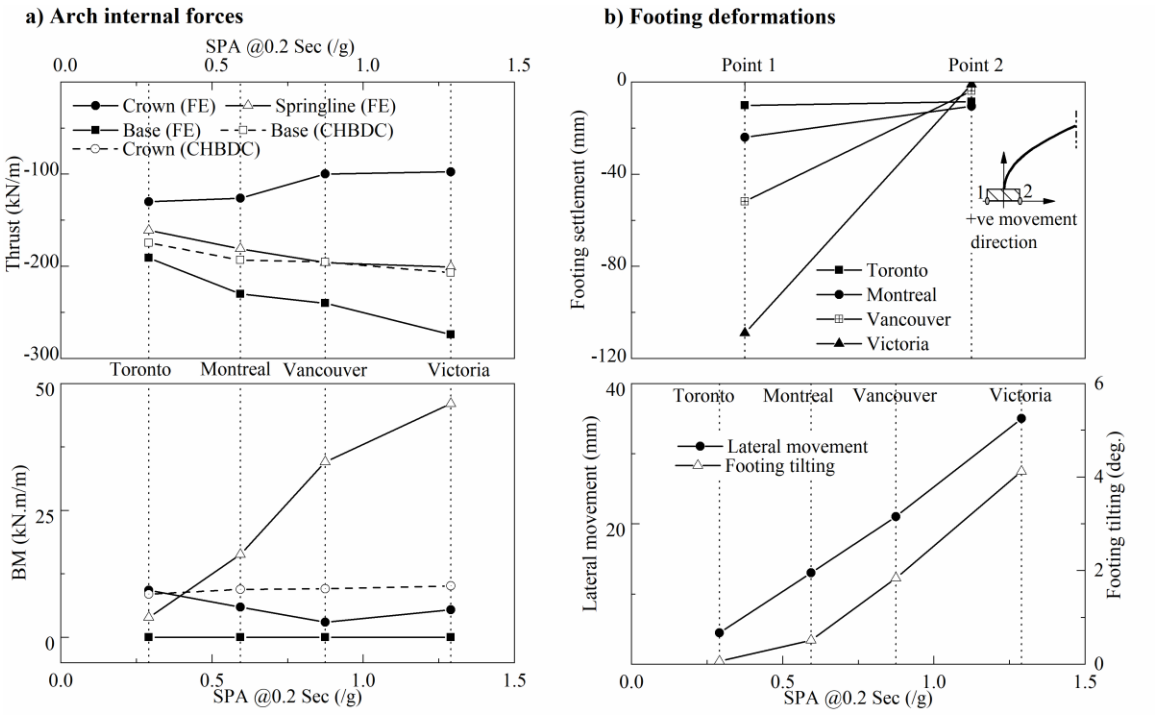

Figure 7-21 Comparison of the results of the FE analysis and CHBDC equations, for site type D

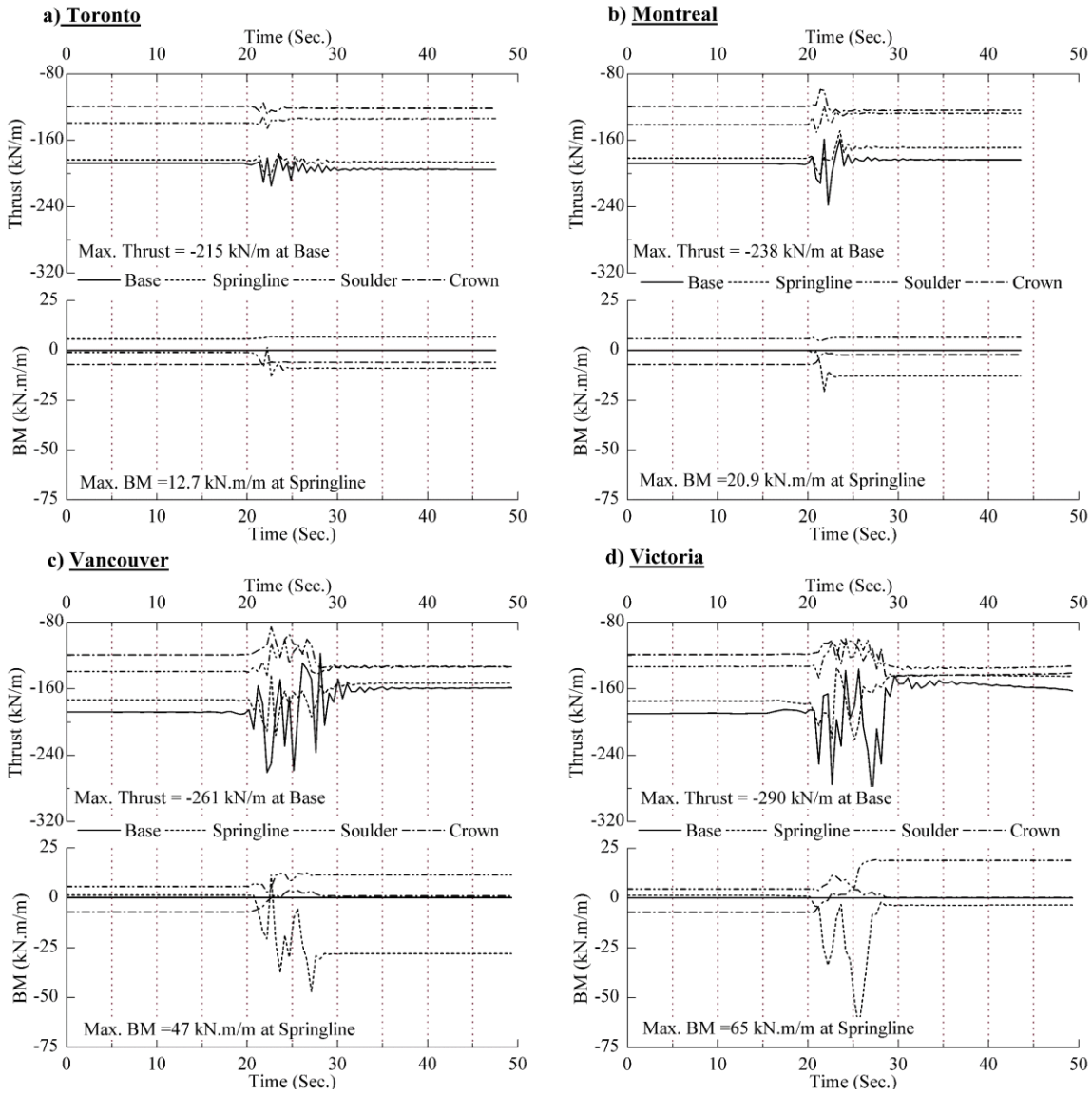

Figure 7-22 Thrust forces and bending moments for different cities throughout the duration of an earthquake, for site type E

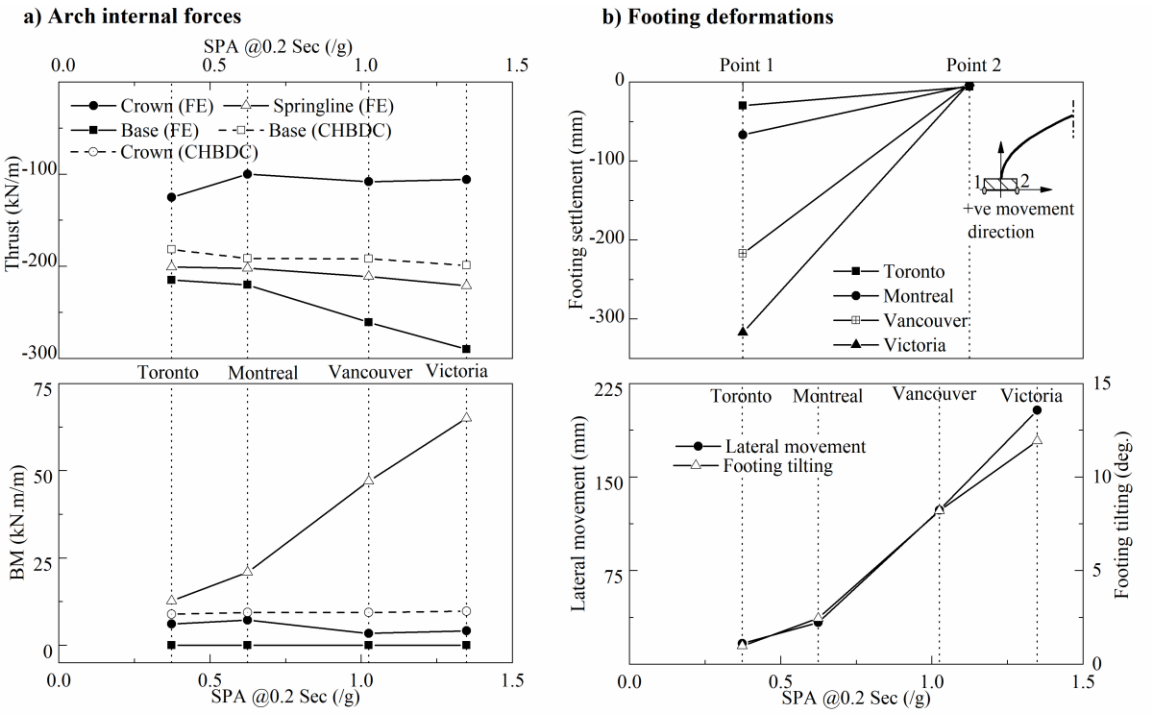

Figure 7-23 Comparison of the results of the FE analysis and CHBDC equations, for site type E

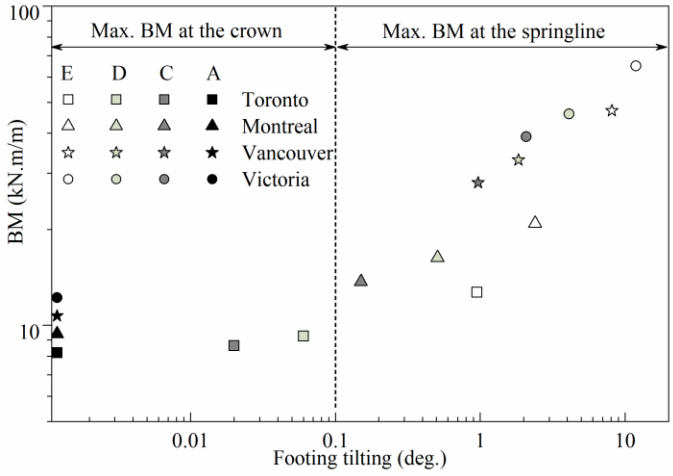

Figure 7-24 Maximum bending moments plotted against footing tilting for different cities and site types

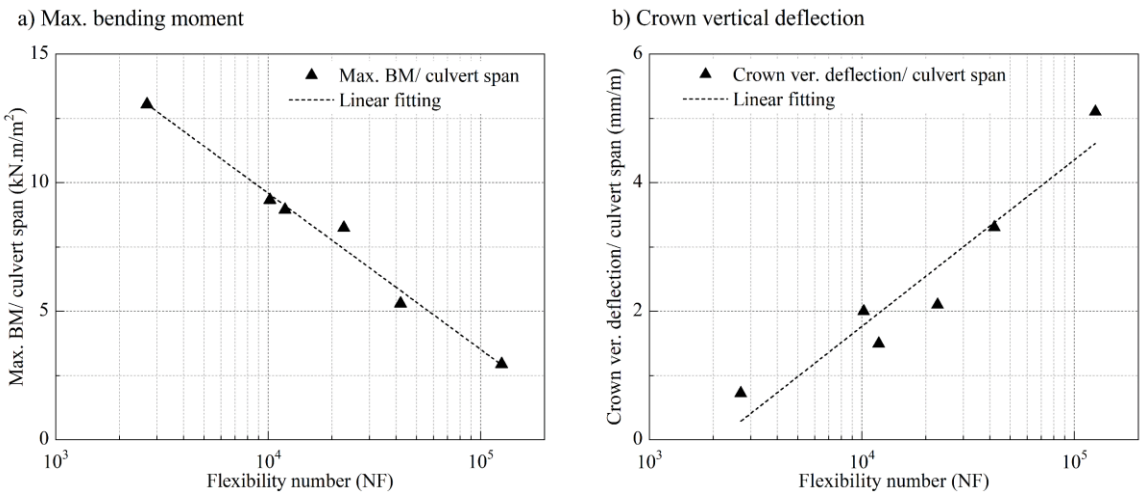

Figure 7-25 Effect of the flexibility number (NF) on the culvert bending moment (BM) and crown deflection

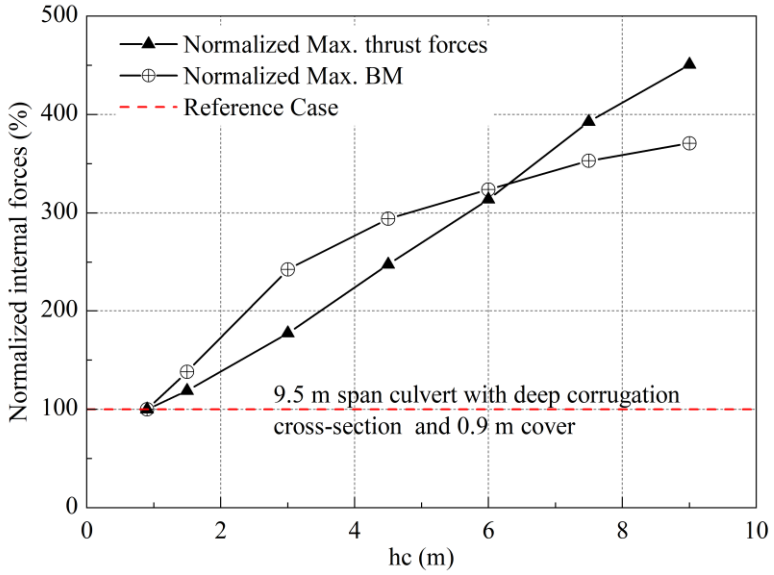

Figure 7-26 Effect of cover height (h_c) on the maximum culvert internal forces

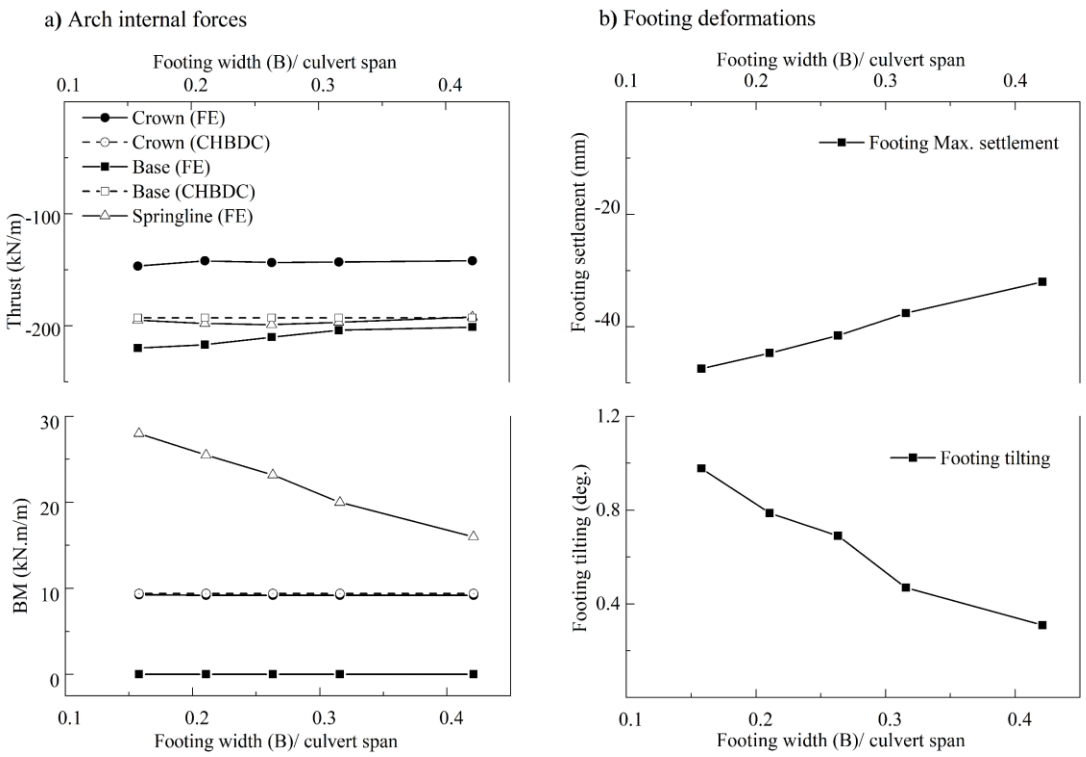

Figure 7-27 Effect of the footing width on culvert behaviour (obtained by using signal data for Vancouver, for site type C)

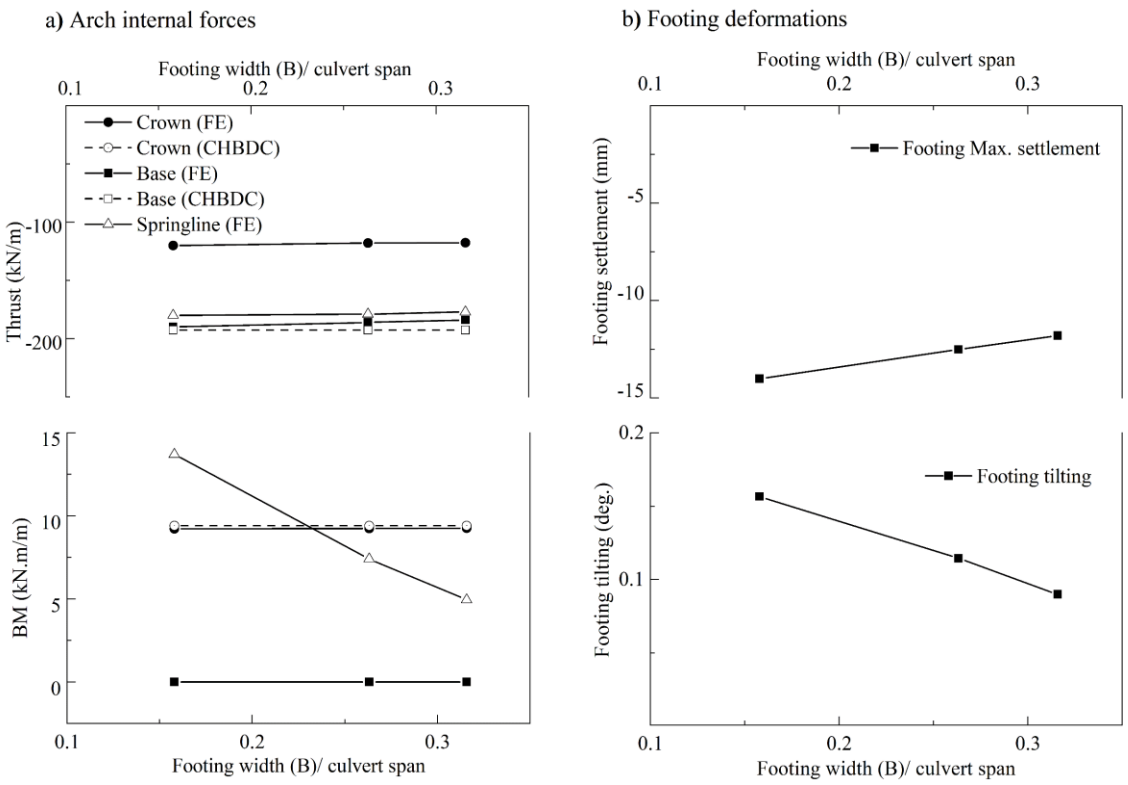

Figure 7-28 Effect of the footing width on culvert behaviour (obtained by using signal data for Montreal, for site type C)

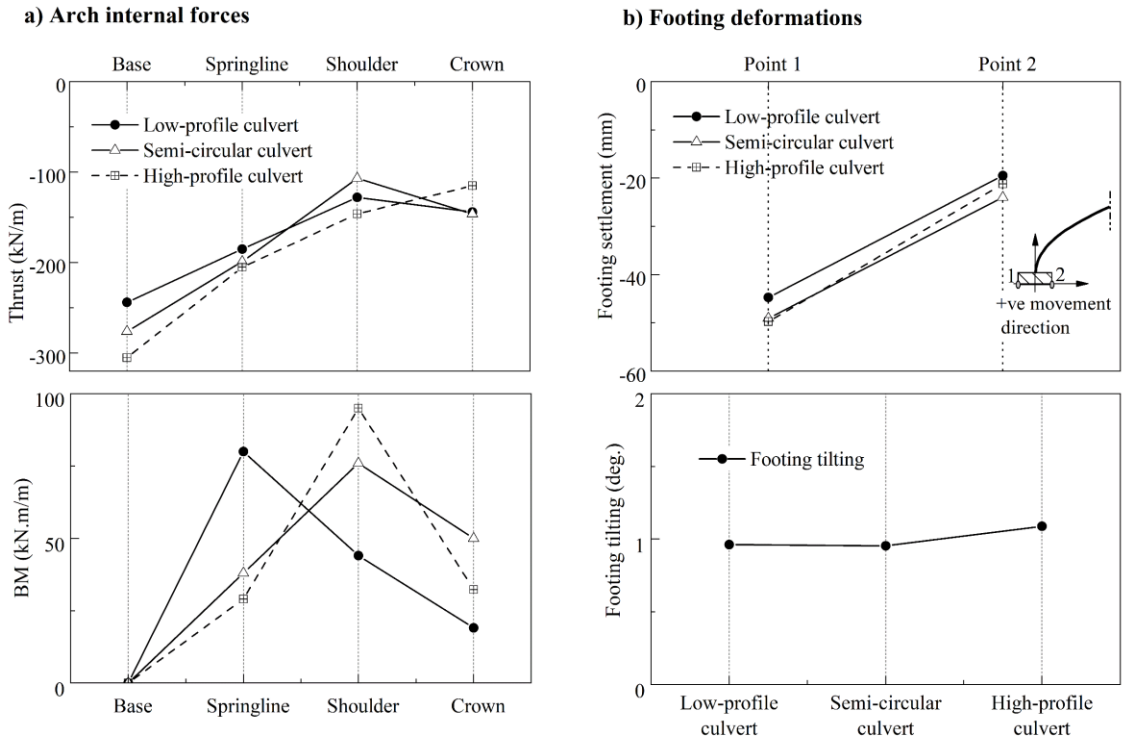

Figure 7-29 Comparison of the seismic performance of different CSP culvert configurations

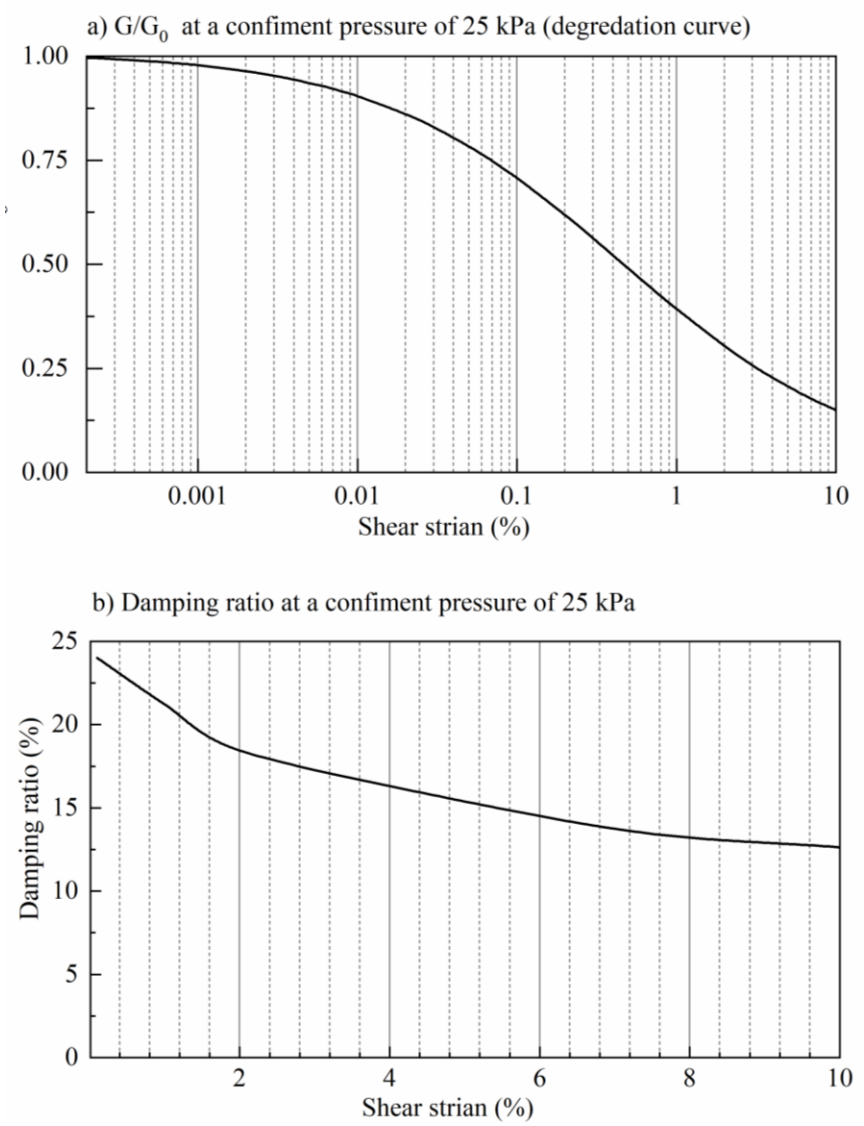

Figure 7-30 TDA dynamic properties (Moussa and Elnaggar 2019)

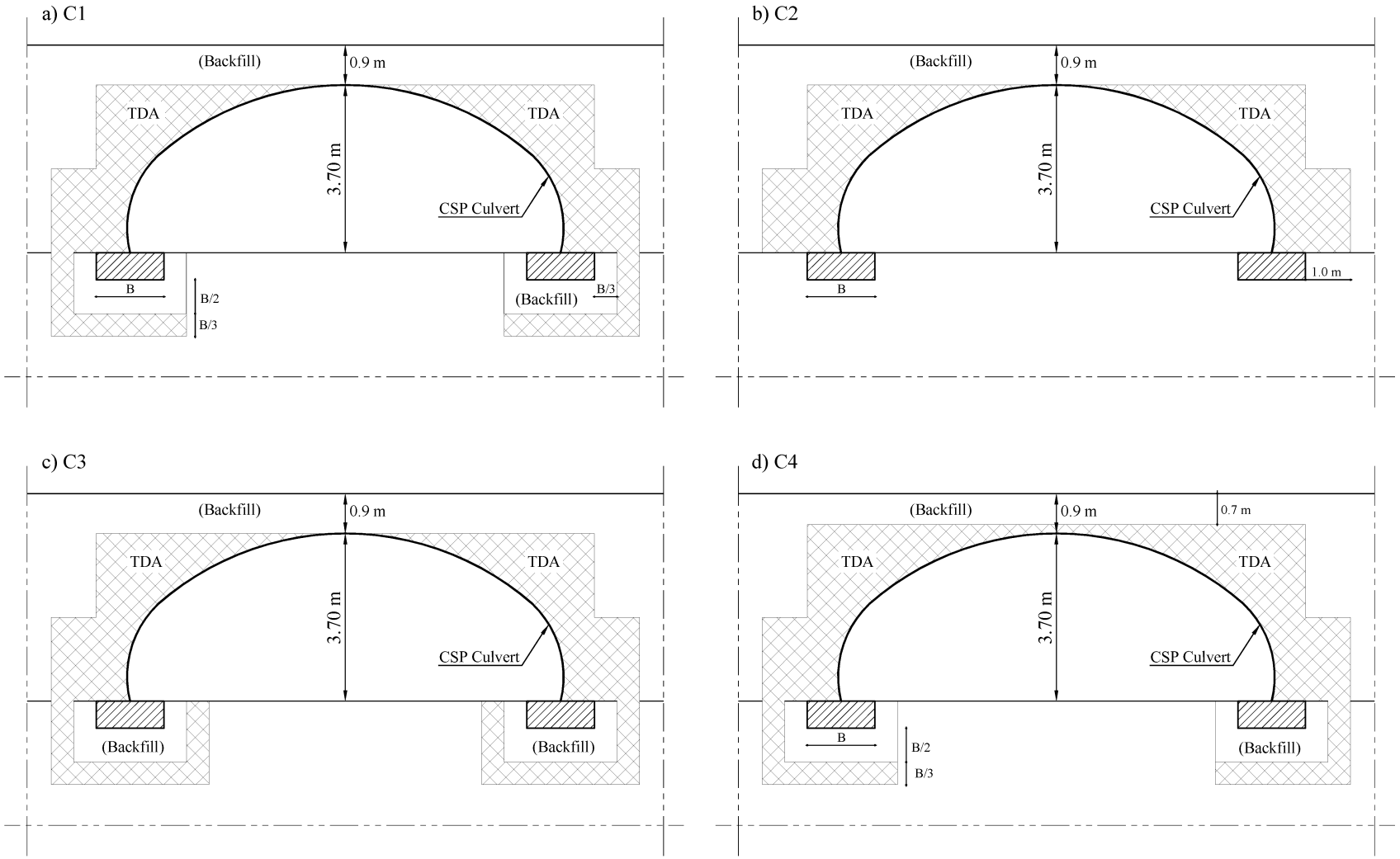

Figure 7-31 TDA configurations around the arch culverts

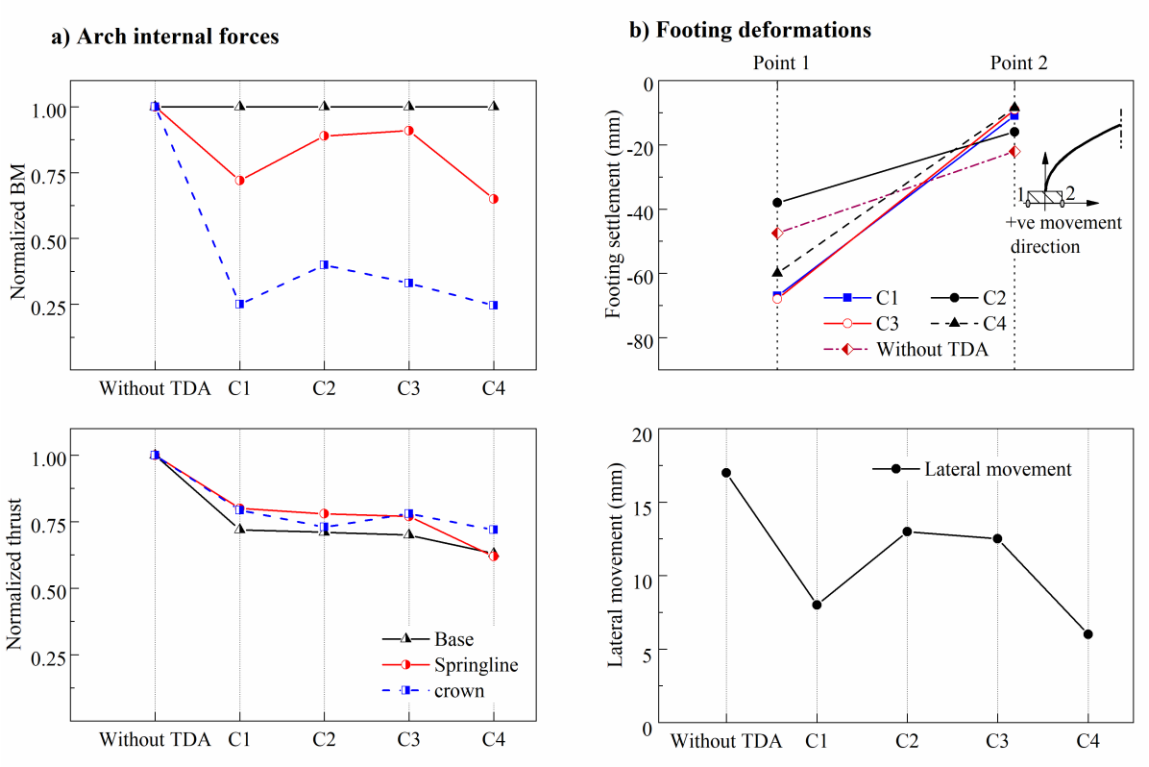

Figure 7-32 TDA effect on large-span arch seismic behaviour

7.9 REFERENCES

AASHTO (2007) LRFD Bridge Design Specifications, 4th ed., American Association of State Highway and Transportation Officials, Washington, DC.

Abdel-Sayed G, Bakht B and Jaeger LG (1993) Soil-Steel Bridges: Design and Construction, McGraw–Hill Inc, New York.

Abuhajar O, El Naggar, H. and Newson, T. (2015) Seismic soil–culvert interaction, Canadian Geotechnical Journal 52(11), 1649–1667. doi:10.1139/cgj-2014-0494.

Ahn I-S and Cheng L (2014) Tire derived aggregate for retaining wall backfill under earthquake loading. Construction and Building Materials **57**: 105–116, https://doi.org/10.1016/ j. conbuildmat.2014.01.091.

Alpan I (1970) The geotechnical properties of soils, Earth-Science Reviews 6(1), 5–49. doi:10.1016/0012-8252(70)90001-2.

Arai T, Sawamura Y, Kishida K. and Kimura M (2011) Behavior of culvert embankment in dynamic centrifuge model test. Paper presented at the 353–356.

ASTM (2012) D 6270-12: Standard practice for use of scrap tires in civil engineering applications. ASTM International, West Conshohocken, PA, USA.

AS/NZS 2041 (1998) Buried Corrugated Metal Structures, Standards Australia & Standards New Zealand, Sydney and Wellington.

Atkinson GM (2009) Earthquake time histories compatible with the 2005 national building code of Canada uniform hazard spectrum, Canadian Journal of Civil Engineering 36(6), 991–1000. doi:10.1139/L09-044.

Atkinson GM (2012) White Paper on Proposed Ground-Motion Prediction Equations (GMPEs) for 2015 National Seismic Hazard Maps. doi:10.1094/PDIS-11-11-0999-PDN

Atkinson GM and Boore DM (2006) Earthquake ground-motion prediction equations for eastern North America, Bulletin of the Seismological Society of America 96(6), 2181–2205. doi:10.1785/0120050245.

Benson CH, Olson MA and Bergstrom WR (1996) Temperatures of insulated landfill liner. Transportation Research Record **1534(1)**: 24–31, https://doi.org/10.3141/1534-05.

Benz T (2006) Small-Strain Stiffness of Soils and Its Numerical Consequences, Mitteilung Des Instituts Für Geotechnik, Der Universität Stuttgart, Stuttgart, Germany.

Biarez J and Hicher P (1994) Elementary Mechanics of Soil Behaviour: Saturated Remoulded Soils, AA Balkema, Rotterdam, Netherlands.

Black WL and Hardin BO (1969) Closure to vibration modulus of normally consolidated clays, Journal of the Soil Mechanics and Foundation Division, 95(6), 1531–1537.

Bobet A, Fernandez G, Huo H and Ramirez J (2008) A practical iterative procedure to estimate seismic-induced deformations of shallow rectangular structures, Canadian Geotechnical Journal 45(7), 923–938. doi:10.1139/T08-026.

Boore DM and Atkinson GM (2008) Ground-motion prediction equations for the average horizontal component of PGA, PGV, and 5%-damped PSA at spectral periods between 0.01 s and 10.0 s, Earthquake Spectra 24(1), 99–138. doi:10.1193/1.2830434.

Bowels JE (1997) Handbook of Foundation Analysis and Design, (International Edition), McGraw- Hill, New York.

Brown CB, Green DR and Powsey S (1968) Flexible culverts under high fills, Journal of the Structural Division 94(4), 905–917.

Byrne P, Anderson D and Jitno H (1996) Seismic analysis of large buried culvert structures, Transportation Research Record: Journal of the Transportation Research Board 1541, 133–139. doi:10.1177/0361198196154100117.

Canadian Standards Association. (2014) Canadian Highway Bridge Design Code, Canadian Standards Association, Ottawa, Canada.

Chu, C-J (1998). A geotechnical investigation of the potential use of shredded scrap tires in soil stabilization. Ph.D. Dissertation, Kent State University, Kent, Ohio.

Das BM and Sivakugan N (2016) Fundamentals of Geotechnical Engineering, CENGAGE Learning, Stamford, CT.

Davis CA and Bardet JP (2000) Responses of buried corrugated metal pipes to earthquakes, Journal of Geotechnology and Geoenvironmental Engineering ASCE 126(1), 28–39.

Debiasi E, Gajo A and Zonta D (2013) On the seismic response of shallow-buried rectangular structures, Tunnelling and Underground Space Technology 38, 99–113. doi:10.1016/j.tust.2013.04.011.

Duncan J M (1976) Finite element analysis of buried flexible metal culvert structures, Laurits Bjerrum Memorial Volume, 213–222.

El Naggar H (2014) Seismic Design of Pipelines. Encyclopedia of Earthquake Engineering, Springer, Berlin, pp. 1–20.

Edil TB (2005) A review of mechanical and chemical properties of shredded tires and soil mixtures. InRecycled Materials in Geotechnics (pp. 1-21).

Elshimi TM, Brachman, RW and Moore I D (2013) Effect of truck position and multiple truck loading on response of long-span metal culverts, Canadian Geotechnical Journal 51(2), 196–207. doi:10.1139/cgj-2013-0176.

Esmaeili M, Zakeri JA, Ebrahimi H, Khadem Sameni M. (2016) Experimental study on dynamic properties of railway ballast mixed with tire derived aggregate by modal shaker test. Advances in Mechanical Engineering; 8(5):1687814016640245.

Fairless G J and Kirkaldie D (2008) Earthquake performance of long-span arch culverts. New Zealand Transport Agency Research Report, (366).

Feng ZY, Sutter KG. (2000) Dynamic properties of granulated rubber/sand mixtures. Geotechnical Testing Journal; 23(3):338-44.

Fortin Vallée JH (2015) Investigation of increased wall stiffness on load effect equations for soil metal structures.

Hazarika H, Hyodo M, Yasuhara K (2010) Investigation of tire chips-sand mixtures as preventive measure against liquefaction. InGround Improvement and Geosynthetics; pp. 338-345.

Hardin BO and Drnevich VP (1972) Shear modulus and damping in soils: design equations and curves, Journal of Soil Mechanics & Foundations Div 98, 667–692.

Hashash, YM, Hook JJ, Schmidt B, John I and Yao C (2001) Seismic design and analysis of underground structures, Tunnelling and Underground Space Technology 16(4), 247–293. doi:10.1016/S0886-7798(01)00051-7.

Hindy A and Novak M (1979) Earthquake response of underground pipelines, Earthquake Engineering & Structural Dynamics 7(5), 451–476. doi:10.1002/eqe.4290070506.

Hudson M, Idriss I M and Beikae M (1994) QUAD4M—A Computer Program to Evaluate the Seismic Response of Soil Structures Using Finite Element Procedures and Incorporating a Compliant Base, Center for Geotechnical Modeling, Dept. of Civil and Environmental Engineering, Univ. of California, Davis, CA.

Huo H, Bobet A, Fernandez G. and Ramirez J (2006) Analytical solution for deep rectangular structures subjected to far-field shear stresses, Tunnelling and Underground Space Technology 21 (6), 613–625. doi:10.1016/j.tust.2005.12.135.

Humphrey DN, Whetten N, Weaver J, and Recker K (2000) Tire shreds as lightweight fill for construction on weak marine clay. Proceeding International Symposium on Coastal Geotechnical Engineering in Practice, Balkema, Rotterdam, The Netherlands, 611–616.

Humphrey D and Blumenthal M (2010) The use of tire-derived aggregate in road construction applications. In Green Streets and Highways 2010: An Interactive Conference on the State of the Art and How to Achieve Sustainable Outcomes. ASCE, Reston, VA, USA, pp. 299–313.

Humphrey DN (2008) Tire derived aggregate as lightweight fill for embankments and retaining walls. In Scrap Tire Derived Geomaterials — Opportunities and Challenges (Hazarika H and Yasuhara K (eds)). Taylor & Francis Group, London, UK, pp. 59–81.

Hurd JO, Hazen GA, Masada T and Sargand SM (1994) Long-term field study of a deep-corrugated metal box type culvert, Canadian Geotechnical Journal 31(2), 175–180.doi:10.1139/t94-023.

Katona MG (2010) Seismic design and analysis of buried culverts and structures, Journal of Pipeline Systems Engineering and Practice 1(3), 111–119. doi:10.1061/(ASCE)PS.1949- 1204.0000057.

Katona MG, Smith JM, Odello RS and Allgood JR (1976) CANDE-A modern approach for the structural design and analysis of buried culverts. Report No. FHWA-RD-77-5, doi:10.1084/jem.143.4.741

Kolymbas D (2005) Tunnelling and Tunnel Mechanics: A Rational Approach to Tunneling, Springer Science & Business Media, Berlin.

Kuhlemeyer RL and Lysmer J (1973) Finite element method accuracy for wave propagation problems, Journal of Soil Mechanics & Foundations Div 99, 289–304.

Macias M, Atkinson GM and Motazedian D (2008) Ground-motion attenuation, source, and site effects for the 26 September 2003 M 8.1 Tokachi-Oki earthquake sequence, Bulletin of the Seismological Society of America 98(4), 1947–1963. doi:10.1785/0120070130.

Mahgoub A and El Naggar H (2017) Assessment of the seismic provisions of the CHBDC for CSP culverts, GeoOttawa 2017, the 70th Canadian Geotechnical Conference, Ottawa, Canada.

Madhusudhan BR, Boominathan A, Banerjee S (2019) Properties of Sand–Rubber Tyre Shreds Mixtures for Seismic Isolation Applications. InSoil Dynamics and Earthquake Geotechnical Engineering; pp. 267-274; Springer, Singapore.

McGrath TJ, Moore ID, Selig ET, Webb MC and Taleb, B (2002) National research council. Recommended specifications for large-span culverts. National Cooperative Highway Research Program (NCHRP) Report 473, Washington, DC: Transportation Research Board.

McCartney JS, Ismaail G, Fox PJ, Sanders MJ, Thielmann, SS and Sander AC (2017) Shearing behavior of tire-derived aggregate with large particle size. II: Cyclic simple

shear. Journal of Geotechnical and Geoenvironmental Engineering, 143(10), 04017079.

Meguid MA, Youssef TA (2018) Experimental investigation of the earth pressure distribution on buried pipes backfilled with tire-derived aggregate. Transportation Geotechnics, 14:117-25.

Meles D, Bayat A, Hussien Shafiee M, Nassiri S, Gul M (2014) Investigation of tire derived aggregate as a fill material for highway embankment. International Journal of Geotechnical Engineering, 8(2):182-90.

Meyerhof GG and Fisher CL (1963) Composite design of underground steel structures, Engineering Journal 46(9), 36–41.

Mills, B., H. El Naggar, and A. J. Valsangkar. 2015. “North American overview and Canadian perspective on the use of tire derived aggregate in highway embankment construction.” Chap. 22 in Vol. 2 of Ground improvement case histories, edited by Indraratna and Chu. New York: Elsevier.

Mirza C and Porter WA (1981) Construction considerations and controls for soil–steel bridge structures, Canadian Journal of Civil Engineering 8(4), 519–534. doi:10.1139/l81-065.

Moussa A and El Naggar H (2019) Dynamic properties of tire derived aggregates. In GeoSt.John's, the 72th Canadian Geotechnical Conference St John’s, Canada. Canadian Geotechnical Society.

National Research Council of Canada. Associate Committee on the National Building Code. (2015) National building code of Canada associate committee on the national building code, National Research Council.

Ni P, Qin X, Yi Y (2018) Numerical study of earth pressures on rigid pipes with tire-derived aggregate inclusions. Geosynthetics International, 25(5): 494-506.

Plaxis B (2017) Reference Manual for PLAXIS 2D, PLAXIS bv, Delft, Netherlands.

Regier C, Moore I D and Hoult NA (2018) Remaining strength of deteriorated corrugated steel culverts, Journal of Pipeline Systems Engineering and Practice 9, 04018002. doi:10.1061/(ASCE)PS.1949-1204.0000309.

Sawamura Y, Kishida K and Kimura M (2015) Centrifuge model test and FEM analysis of dynamic interactive behavior between embankments and installed culverts in multiarch culvert embankments, International Journal of Geomechanics 15(3, June).

Schnabel P B (1973) Effects of Local Geology and Distance from Source on Earthquake Ground Motions.

Seed H B and Idriss IM (1970) Soil moduli and damping factors for dynamic response analysis. Report no. EERC 70-10. Berkeley, Calif: College of Engineering, University of California, 1970.

Sparkes J, El Naggar H and Valsangkar A (2019) Compressibility and shear strength properties of tire-derived aggregate mixed with lightweight aggregate. Journal of

Pipeline Systems Engineering and Practice **10(1)**, https://doi.org/10.1061/(ASCE)PS.1949-1204.0000354.

Taleb B and Moore I (1999) Metal culvert response to earth loading: performance of two-dimensional analysis, Transportation Research Record: Journal of the Transportation Research Board 1656, 25–36. doi:10.3141/1656-04.

Tweedie JJ, Humphrey DN and Sandford TC (1998) Full-scale field trials of tire shreds as lightweight retaining wall backfill under at-rest conditions. Transportation Research Record **1619**: 64–71, https://doi.org/10.3141/1619-08.

Vucetic M and Dobry R (1991) Effect of soil plasticity on cyclic response, Journal of Geotechnical Engineering 117(1), 89–107. doi:10.1061/(ASCE)0733-9410(1991)117:1(89).

Wang J (1993) Seismic design of tunnels: a simple state-of-the-art design approach. 1991 William Barclay Parsons Fellowship, Parsons Brinckerhoff, Monograph 7. New York: Jaw-Nan Wang and Parsons Brinckerhoff Inc.

Webb M C, Selig E T, Sussman JA and McCarthy, TJ (1999) Field tests of a large-span metal culvert. Transportation Research Record 1653, Paper No. 99-1425. Washington, DC: Transportation Research Board.

White HL and Layer JP (1960) The corrugated metal conduit as a compression ring, Paper presented at the Highway Research Board Proceedings, Washington, DC.

Wolfe SL, Humphrey DN and Wetzel EA (2004) Development of tire shred underlayment to reduce groundborne vibration from LRT track. In GeoTrans 2004, Los Angeles, CA. ASCE, Reston, VA, USA, pp. 750–759.

Wood JH and Jenkins DA (2000) Seismic analysis of buried arch structures, Paper presented at the Proc. of the 12th World Conference of Earthquake Engineering (0768), Auckland, New Zealand.

Wood JH and Lower HT (2007) Earthquake design of rectangular underground structures, Bulletin of the New Zealand Society for Earthquake Engineering 40(1), 1–6.

Yoon S, Prezzi M, Siddiki NZ and Kim B (2006) Construction of a test embankment using a sand-tire shred mixture as fill material. Waste Management **26(9)**: 1033–1044, https://doi.org/10.1016/j.wasman.2005.10.009.

Youd TL and Beckman CJ (1997) Performance of corrugated metal pipe (CMP) culverts during past earthquakes, Proceedings of the Workshop on Earthquake Engineering Frontiers in Transportation Facilities NCEER-97-005 (eds G. C. Lee and I. M. Friedland), Buffalo, NY, USA, National Center for Earthquake Engineering, Pp 137–151.

Youd TL and Beckman CJ (1996) Highway culvert performance during past earthquakes (Rep. NCEER-96-0015). Buffalo, NY: National Center for Earthquake Engineering Research.

Youd TL and Beckman CJ (2003) Performance of corrugated metal pipe (CMP) culverts during past earthquakes Advancing mitigation technologies and disaster response for lifeline systems (pp. 294–307). Seattle, Washington, USA: ASCE.

Xiao M, Bowen J, Graham M and Larralde J (2012) Comparison of seismic responses of geosynthetically reinforced walls with tire-derived aggregates and granular backfills. Journal of Materials in Civil Engineering **24(11)**: 1368–1377, https://doi.org/10.1061/(ASCE)MT.1943- 5533.0000514.

CHAPTER 8 CONCLUSION

Many new and pre-existing pipeline networks will share space with other infrastructure and be subject to traffic and construction loads in addition to the dead weight of the soil. In urban areas these pipelines are often buried in the ground beneath roads at shallow depths, which can result in substantial additional earth pressure and loads, leading to overstressing and/or unacceptable deformation of the buried pipe. This dissertation describes the results of a comprehensive experimental and numerical study aimed at enhancing the soil arching mechanism above shallow buried infrastructure by using lightweight tire-derived aggregate (TDA) backfill materials. These shredded tire products have several desirable geotechnical properties that can improve the overall performance of civil engineering infrastructure under static and seismic conditions.

8.1 SUMMARY AND CONCLUSIONS

The work presented in this thesis essentially addresses three major aspects. The first part deals with protecting pre-existing pipes located beneath shallow foundations by using a layer of TDA above the pipes (Chapters 2, 3 and 4). The second part investigates the performance of corrugated steel plate (CSP) culverts surrounded by a layer of TDA. In addition, a coupled TDA geocell stress bridging system is developed to induce a stress arching mechanism capable of controlling the surface settlement and reducing the stresses imposed on the pipe beneath (Chapters 5 and 6). Finally, the third part explores the effectiveness of TDA in the mitigation of seismic hazards for long-span metal culverts in regions with high seismicity. The following sections present a summary of the research and main findings.

8.1.1 Using TDA as an Engineered Stress-Reduction Fill above Pre-Existing Buried Pipes beneath Rigid Footings

Chapter 2 describes two full-scale field tests that were conducted to evaluate the benefits of using a layer of TDA above pre-existing metal pipes to enhance the stress arching mechanism (i.e., stress bridging). In addition, the complex pipe-soil interaction was investigated by monitoring the surface settlement, changes in pipe wall strains, and pressure distribution over the pipe. Furthermore, 3D finite element models of the tests were developed to study the interaction mechanism of the problem considered; the models developed were validated against the field test results. A parametric study was then conducted to examine the effects of the thickness of the TDA layer, the shape and configuration of the TDA cross-section, and the pipe stiffness (i.e., pipe flexibility) on the performance of the system investigated. The study concluded that using a layer of TDA above pre-existing pipe has a significant effect in reducing buried pipe stresses and transferred pressures, in comparison to the use of conventional backfill. It was found that the use of TDA reduced pipe stresses in the range of 20% to 50%, for TDA thicknesses of 0.25B to 1B, respectively (where B is the footing width).

The study was extended, as described in Chapter 3, by conducting three full-scale field tests to investigate the advantages of using TDA as a backfill material beneath footings and to compare TDA performance with that of conventional backfill materials. The field test results show that, in comparison to the use of conventional backfill, the use of a TDA layer beneath shallow foundations achieves a significant improvement in transferring the stresses and reducing the stress influence zone underneath the footing. Subsequently, 3D finite element analyses were carried out to verify the tests. A parametric study was then

conducted to examine the effects of TDA layer thickness, footing geometry, foundation depth, and soil type on the performance of the system investigated.

Chapter 4 presents design equations that are integrated into a design procedure to calculate the sustained pressure for rigid footings over backfill with a TDA layer, for different settlement values. The equations were developed by using the field tests and intensive FE analyses described in Chapter 4. In addition, FE models of three design examples with hypothetical dimensions were created in order to compare the results with those of the design equations. Very good agreement between the results demonstrates the soundness of the design equations.

8.1.2 Using TDA around CSP Culverts

Chapter 5 presents the results of four full-scale tests that were conducted to evaluate the effectiveness of using a layer of TDA material in three different configurations around corrugated steel plate (CSP) culverts with a diameter of 600 mm. The first test was designed to examine the behaviour of the CSP culvert in conventional backfill conditions and serves as a reference case. The other three tests utilized a 150 mm layer of TDA above the culvert crown; a layer of TDA around the upper half of the culvert (down to the culvert springlines); and a layer of TDA around the whole culvert down to the invert (but not underneath the culvert). Furthermore, three-dimensional finite element models of the tests were developed to study the interaction mechanism of the problem considered. After the finite element models were validated against the results of the full-scale tests, intensive parametric studies were conducted to examine the effect of the culvert burial depth, the envelope shape of the backfill area around the culvert, the granular backfill stiffness, and the performance of the proposed system under embankment loads. The study showed that

during backfilling, the existence of a TDA layer around the culvert significantly reduced the culvert deformation by around 80% of that observed with conventional backfill materials. Furthermore, the study demonstrated that due to external surface loading, before punching shear failure occurred beneath the loaded area, there was a significant decrease in culvert stresses and deformation. The study also showed that, at shallow depths, using TDA around the whole culvert down to the invert resulted in greater deformation and stresses than was the case for culverts with a layer of TDA only above the crown or down to the springlines. This was because the utilization of a TDA layer around the whole culvert resulted in less confinement, thus inducing greater deformation and stresses. The parametric study showed that using stiffer material in the top layer increased the punching shear capacity of the proposed system and consequently enhanced the arching mechanism. In addition, using a layer of TDA around the culvert under embankment load conditions enhanced the culvert behaviour significantly in comparison to using only conventional backfill. The study also found that using rigid pavement above buried culverts with a TDA layer distributed the stresses over a wider area above the culvert trench (stress bridging) and prevented the incidence of punching shear failure of the top layer above the TDA, thus notably improving the culvert performance.

Chapter 6 presents a continuation of the work described in Chapter 5. A coupled TDA geocell stress bridging system for metal pipes is proposed, to decrease the loaded surface settlement that may result from the presence of TDA at shallow depths. The use of reinforced granular backfill over a TDA layer was investigated by conducting three full-scale tests with a geocell layer in the upper part of the granular material above the TDA. In order to illustrate geocell effectiveness in reducing the surface settlement and enhancing

the arching mechanism, these tests made use of the same layout, loading conditions, and construction sequence as the set of tests described in Chapter 5 (where a TDA backfill envelope was placed around a corrugated steel culvert). 3D finite element analyses were carried out. After the models developed were validated with the test results, an extensive parametric study was conducted to examine the influence of the geocell installation depth, the granular backfill stiffness, the number of geocell layers used, and the culvert embedment depth, as well as the effect of extending the geocell width in the top layer above the buried culvert. The study demonstrated that reinforcing the top layer with geocells significantly decreased the loaded surface and prevented extended failure. The geocell layer acted as a stress mattress, with the ability to sustain tension forces and enhance the stress distribution underneath the loaded area. In addition, the use of a geocell layer in the top layer above the TDA increased the sustained loads by 45%. Moreover, the study found that in some cases, a configuration utilizing coupled geocells with a weaker material in the top layer could match the behaviour of a stronger layer (above TDA).

8.1.3 Using TDA as a Dampening Material around a Large-Span Metal Arch Culvert

Chapter 7 describes the use of full dynamic finite element modelling to investigate the seismic performance of large-span CSP culverts. First, the static behaviour of a long-span culvert was verified by using a field case study. Dynamic analyses were then performed with the aid of seismic records for different levels of seismicity. The finite element analysis results were subsequently compared with the simplified seismic provisions of the Canadian Highway Bridge Design Code (CHBDC). A parametric study was then developed to investigate the seismic behaviour of CSP culverts under different subsurface conditions, and to examine the effect of changing the culvert rigidity and configuration. This study

clearly shows that the simplified equations commonly used underestimate the internal forces. Consequently, for culverts located in zones of high seismicity, a full dynamic finite element analysis is required. The study also used TDA to develop an innovative system to mitigate seismic hazards in regions with high seismicity. Based on the results of the study conducted, a set of recommendations for the analysis and design of buried structures is proposed.

8.2 RECOMMENDATIONS FOR FUTURE WORK

Some aspects that should be considered in future research are outlined below.

1) Conducting large-scale (or even small-scale) shaking table tests to examine experimentally the seismic soil-structure interaction characteristics of metal arch culverts.
2) In addition, the seismic performance of the proposed TDA mitigation scheme should be experimentally investigated using scale-down arch culverts.
3) Exploring the effect of extreme temperatures on the performance of TDA backfills.

REFERENCES

AASHTO (2007) LRFD Bridge Design Specifications, 4th ed., American Association of State Highway and Transportation Officials, Washington, DC.

Abdel-Sayed G, Bakht B and Jaeger LG (1993) Soil-Steel Bridges: Design and Construction, McGraw–Hill Inc, New York.

Ab-Malek K and Stevenson A (1986) The effect of 42-year immersion in seawater on natural rubber. Journal of materials science, 21(1):147-54.

Abuhajar O, El Naggar, H. and Newson, T. (2015) Seismic soil–culvert interaction, Canadian Geotechnical Journal 52(11), 1649–1667. doi:10.1139/cgj-2014-0494.

Ahmed I and Lovell CW (1993) Rubber soils as lightweight geomaterials. Transportation Research Record 1422: 61–70.

Ahmed Imtiaz (1993) Laboratory Study on Properties of Rubber-Soils.

Ahmed M, Tran V, Meguid MA (2015) On the role of geogrid reinforcement in reducing earth pressures on buried pipes. Soils Found, 55(3):588–99.

Ahn I-S and Cheng L (2014) Tire derived aggregate for retaining wall backfill under earthquake loading. Construction and Building Materials 57: 105–116, https://doi.org/10.1016/ j. conbuildmat.2014.01.091.

Ahn I-S, Cheng L, Fox PJ, Wright J, Patenaude S and Fujii B (2014) Material properties of large-size tire derived aggregate for civil engineering applications. Journal of Materials in Civil Engineering 27(9).

Ali Iranikhah (2018) Experimental Investigation on the Shear Strength Parameters and Deformability Behavior of Various Soil Types Mixed with Tire-Derived Aggregate. Master's thesis. Dalhousie University.

Al-Naddaf M, Han J, Xu C, Rahmaninezhad SM (2019) Effect of geofoam on vertical stress distribution on buried structures subjected to static and cyclic footing loads. Journal of Pipeline Systems Engineering and Practice, 10(1):04018027.

Alpan I (1970) The geotechnical properties of soils, Earth-Science Reviews 6(1), 5–49. doi:10.1016/0012-8252(70)90001-2.

Al-Qadi IL, Hughes JJ (2000) Field evaluation of geocell use in flexible pavements. Transportation research record;1709(1):26-35.

Anderson AO (1913) Vol. 31 of the theory of loads on pipes in ditches: And tests of cement and clay drain tile and sewer pipe. Ames, IA: Iowa State College of Agriculture and Mechanic Arts.

Arai T, Sawamura Y, Kishida K. and Kimura M (2011) Behavior of culvert embankment in dynamic centrifuge model test. Paper presented at the 353–356.

AS/NZS 2041 (1998) Buried Corrugated Metal Structures, Standards Australia & Standards New Zealand, Sydney and Wellington.

Ashari Ghomi M (2018) Large-scale triaxial testing of sustainable TDA backfilling alternatives. Master's thesis. Dalhousie University.

Ashari M and El Naggar H (2017) Evaluation of the physical properties of TDA-sand mixtures. In GeoOttawa, the 70th Canadian Geotechnical Conference Ottawa. Canadian Geotechnical Society.

ASTM (1997) Nonrepetitive static plate load tests of soils and flexible pavement components, for use in evaluation and design of airport and highway pavements. D 1196-93. West Conshohocken, PA: ASTM International.

ASTM (2012) Standard practice for use of scrap tires in civil engineering applications. D6270-12. West Conshohocken, PA: ASTM International.

ASTM (2017) D 2487-17: Classification of soils for engineering purposes (Unified Soil Classification System). ASTM International, West Conshohocken, PA, USA.

Atkinson GM (2009) Earthquake time histories compatible with the 2005 national building code of Canada uniform hazard spectrum, Canadian Journal of Civil Engineering 36(6), 991–1000. doi:10.1139/L09-044.

Atkinson GM (2012) White Paper on Proposed Ground-Motion Prediction Equations (GMPEs) for 2015 National Seismic Hazard Maps. doi:10.1094/PDIS-11-11-0999-PDN

Atkinson GM and Boore DM (2006) Earthquake ground-motion prediction equations for eastern North America, Bulletin of the Seismological Society of America 96(6), 2181–2205. doi:10.1785/0120050245.

Azevedo F, Pacheco-Torgal F, Jesus C, De Aguiar JB, and Camões AF (2012) Properties and durability of HPC with tyre rubber wastes. Constr. Build. Mater. 34: 186–191. https://doi.org/10.1016/j .conbuildmat.2012.02.062.

Bali Reddy S, Pradeep Kumar D and Murali Krishna A (2015) Evaluation of the Optimum Mixing Ratio of a Sand-Tire Chips Mixture for Geoengineering Applications. Journal of Materials in Civil Engineering, 28(2), 6015007. https://doi.org/10.1061/(ASCE)MT.1943-5533.0001335

Benson CH, Olson MA and Bergstrom WR (1996) Temperatures of insulated landfill liner. Transportation Research Record 1534(1): 24–31, https://doi.org/10.3141/1534-05.

Benz T (2006) Small-Strain Stiffness of Soils and Its Numerical Consequences, Mitteilung Des Instituts Für Geotechnik, Der Universität Stuttgart, Stuttgart, Germany.

Biarez J and Hicher P (1994) Elementary Mechanics of Soil Behaviour: Saturated Remoulded Soils, AA Balkema, Rotterdam, Netherlands.

Black WL and Hardin BO (1969) Closure to vibration modulus of normally consolidated clays, Journal of the Soil Mechanics and Foundation Division, 95(6), 1531–1537.

Bobet A, Fernandez G, Huo H and Ramirez J (2008) A practical iterative procedure to estimate seismic-induced deformations of shallow rectangular structures, Canadian Geotechnical Journal 45(7), 923–938. doi:10.1139/T08-026.

Boore DM and Atkinson GM (2008) Ground-motion prediction equations for the average horizontal component of PGA, PGV, and 5%-damped PSA at spectral periods between 0.01 s and 10.0 s, Earthquake Spectra 24(1), 99–138. doi:10.1193/1.2830434.

Bosscher PJ, Edil TB and Eldin NN (1992) Construction and performance of shredded waste-tire test embankment. Transportation Research Record 1345: 44–52.

Bowels, J. E. (2001). Handbook of foundation analysis and design, (international edition).

Brown CB, Green DR and Powsey S (1968) Flexible culverts under high fills, Journal of the Structural Division 94(4), 905–917.

Byrne P, Anderson D and Jitno H (1996) Seismic analysis of large buried culvert structures, Transportation Research Record: Journal of the Transportation Research Board 1541, 133–139. doi:10.1177/0361198196154100117.

Canadian Standards Association (CSA) (2014). CAN/CSA-S6-14 – Canadian Highway Bridge Design Code. Mississauga, Ontario.

Cetin H, Fener M, and Gunaydin O (2006) Geotechnical properties of tire-cohesive clayey soil mixtures as a fill material. Engineering Geology, 88(1–2), 110–120. https://doi.org/10.1016/j.enggeo.2006.09.002

Chu, C-J (1998). A geotechnical investigation of the potential use of shredded scrap tires in soil stabilization. Ph.D. Dissertation, Kent State University, Kent, Ohio.

Costa YD, Zornberg JG, Bueno BS, and Costa CL (2009) Failure mechanisms in sand over a deep active trapdoor. J. Geotech. Geoenviron. Eng. 135 (11): 1741–1753. https://doi.org/10.1061/(ASCE)GT.1943-5606.0000134.

Cuelho E, Perkins S (2009) Field investigation of geosynthetics used for subgrade stabilization. Montana. Dept. of Transportation. Research Programs.

Das BM and Sivakugan N (2016) Fundamentals of Geotechnical Engineering, CENGAGE Learning, Stamford, CT.

Dash SK, Sireesh S, Sitharam TG (2003) Model studies on circular footing supported on geocell reinforced sand underlain by soft clay. Geotextiles and Geomembranes.21(4):197-219.

Davis CA and Bardet JP (2000) Responses of buried corrugated metal pipes to earthquakes, Journal of Geotechnology and Geoenvironmental Engineering ASCE 126(1), 28–39.

Debiasi E, Gajo A and Zonta D (2013) On the seismic response of shallow-buried rectangular structures, Tunnelling and Underground Space Technology 38, 99–113. doi:10.1016/j.tust.2013.04.011.

Dickson T, Dwyer D, and Humphrey D, (2001) Prototype tire-shred embankment construction. Transp. Res. Rec. 1755: 160–167. https://doi.org/10.3141/1755-17.

Duncan J M (1976) Finite element analysis of buried flexible metal culvert structures, Laurits Bjerrum Memorial Volume, 213–222.

Duncan JM, and Chang CY (1970) Nonlinear analysis of stress and strain in soils. J. Soil Mech. Found. Div. 96 (5): 1629–1653.

Eaton RA, Roberts RJ and Humphrey DN (1994) Gravel Road Test Sections Insulated with Scrap Tire Chips: Construction and First Year's Results. US Army Corps of Engineers, Cold Regions Research and Engineering Laboratory, Hanover, NH, USA. Special Report 94-21.

Edil TB, and Bosscher P J (1992) Development of engineering criteria for shredded or whole tires in highway applications. Report No. WI 14-92, Department of Civil and Environmental Engineering, University of Wisconsin, Madison, Wisconsin.

Edil TB, Fox PJ and Ahl SW (1992) Hydraulic conductivity and compressibility of waste tire chips. In 15th Madison Waste Conference, University of Wisconsin-Madison, Engineering Professional Development Department, Madison, WI, USA, pp. 49–61.

El Naggar H (2014) Seismic Design of Pipelines. Encyclopedia of Earthquake Engineering, Springer, Berlin, pp. 1–20.

El Naggar H, Soleimani P, and Fakhroo A (2016) Strength and stiffness properties of green lightweight fill mixtures. Geotech. Geol. Eng. 34 (3): 867–876. https://doi.org/10.1007/s10706-016-0010-1.

El Naggar H, Turan A. and Valsangkar A. (2015) Earth pressure reduction system using geogrid-reinforced platform bridging for buried utilities. Journal of Geotechnical and Geoenvironmental Engineering, 141, No. 6, 04015024.

Elias V, Welsh J, Warren J, Lukas R, Collin JG, and Berg RR (2006) Ground Improvement Methods, Volumes I and II, Publication No.'s FHWA NHI-06-019 and FHWA NHI-06-020, US Dept. of Transportation, Federal Highway Administration.

Elshimi TM, Brachman, RW and Moore I D (2013) Effect of truck position and multiple truck loading on response of long-span metal culverts, Canadian Geotechnical Journal 51(2), 196–207. doi:10.1139/cgj-2013-0176.

Engstrom G, and Lamb R (1994) Using shredded waste tires as a lightweight fill material for road surfaces. Rep. No. MN-RD- 94-10. Minnesota, US: Dept. of Transportation.

Esmaeili M, Zakeri JA, Ebrahimi H, Khadem Sameni M. (2016) Experimental study on dynamic properties of railway ballast mixed with tire derived aggregate by modal shaker test. Advances in Mechanical Engineering; 8(5):1687814016640245.

Fairless G J and Kirkaldie D (2008) Earthquake performance of long-span arch culverts. New Zealand Transport Agency Research Report, (366).

Feng ZY, Sutter KG. (2000) Dynamic properties of granulated rubber/sand mixtures. Geotechnical Testing Journal; 23(3):338-44.

Fortin Vallée JH (2015) Investigation of increased wall stiffness on load effect equations for soil metal structures.

GC (Geosyntec Consultants) (2008). Guidance Manual for Engineering Uses of Scrap Tires, Geosyntec Project No.: ME0012-11. Maryland Department of the Environmental Scrap Tire Programme, Columbia, MD, USA.

Gu Z, Song G, Liu W, Li P, Gao L, Li H, Hu X (2009) Preparation and properties of styrene butadiene rubber/natural rubber/organo-bentonite nanocomposites prepared from latex dispersions. Applied Clay Science, 46(3):241-4.

Hardin BO and Drnevich VP (1972) Shear modulus and damping in soils: design equations and curves, Journal of Soil Mechanics & Foundations Div 98, 667–692.

Hashash, YM, Hook JJ, Schmidt B, John I and Yao C (2001) Seismic design and analysis of underground structures, Tunnelling and Underground Space Technology 16(4), 247–293. doi:10.1016/S0886-7798(01)00051-7.

Hazarika H, Hyodo M, Yasuhara K (2010) Investigation of tire chips-sand mixtures as preventive measure against liquefaction. InGround Improvement and Geosynthetics; pp. 338-345.

Hegde A, Sitharam TG (2017) Experiment and 3D-numerical studies on soft clay bed reinforced with different types of cellular confinement systems. Transportation Geotechnics.10:73-84.

Hennebert P, Lambert S, Fouillen F and Charrasse B (2014) Assessing the environmental impact of shredded tires as embankment fill material. Canadian Geotechnical Journal, 51(5):469-78.

Hindy A and Novak M (1979) Earthquake response of underground pipelines, Earthquake Engineering & Structural Dynamics 7(5), 451–476. doi:10.1002/eqe.4290070506.

Hoppe EJ (1998) Field study of shredded-tire embankment. Transportation Research Record 1619(1): 47–54, https://doi.org/10.3141/1619-06.

Hudson M, Idriss I M and Beikae M (1994) QUAD4M—A Computer Program to Evaluate the Seismic Response of Soil Structures Using Finite Element Procedures and Incorporating a Compliant Base, Center for Geotechnical Modeling, Dept. of Civil and Environmental Engineering, Univ. of California, Davis, CA.

Humphrey D, and Blumenthal M (2010) The use of tire-derived aggregate in road construction applications. In Green Streets and Highways 2010: An Interactive Conf. on the State of the Art and How to Achieve Sustainable Outcomes, 299–313. Reston, VA: ASCE.

Humphrey DN (2005) Tire Derived Aggregate – A New Road Building Material. In Seventh International Conference on the Bearing Capacity of Roads, Railways and Airfields, Trondheim, Norway, ARRB Group Limited, Vermont South, Australia.

Humphrey DN (2008) Tire derived aggregate as lightweight fill for embankments and retaining walls. In Scrap Tire Derived Geomaterials — Opportunities and Challenges (Hazarika H and Yasuhara K (eds)). Taylor & Francis Group, London, UK, pp. 59–81.

Humphrey DN and Eaton RA (1995) Field performance of tire chips as subgrade insulation for rural roads. In Sixth International Conference on Low-Volume Roads, Minneapolis, MN, Transportation Research Board, Washington, DC, USA, pp. 77–86.

Humphrey DN and Manion WP (1992) Properties of tire chips for lightweight fill. Proceeding: Grouting, Soil Improvement, and Geosynthetics, ASCE, New York, 1344–1355.

Humphrey DN, and Swett M (2006) Literature review of the water quality effects of tire derived aggregate and rubber modified asphalt pavement. Department of Civil and Environmental Engineering, University of Maine, Orono, ME, for U.S. Environmental Protection Agency Resource Conservation Challenge, November 29, 2006.

Humphrey DN, and Thomas Sandford (1993) Tire Chips as Lightweight Subgrade Fill and Retaining Wall Backfill, Symposium on Recovery and Effective Reuse of Discarded Materials and By- Products for Construction of Highway Facilities, no. 207: 20.

Humphrey DN, Whetten N, Weaver J, and Recker K (2000) Tire shreds as lightweight fill for construction on weak marine clay. Proceeding International Symposium on Coastal Geotechnical Engineering in Practice, Balkema, Rotterdam, The Netherlands, 611–616.

Huo H, Bobet A, Fernandez G. and Ramirez J (2006) Analytical solution for deep rectangular structures subjected to far-field shear stresses, Tunnelling and Underground Space Technology 21 (6), 613–625. doi:10.1016/j.tust.2005.12.135.

Hurd JO, Hazen GA, Masada T and Sargand SM (1994) Long-term field study of a deep-corrugated metal box type culvert, Canadian Geotechnical Journal 31(2), 175–180.doi:10.1139/t94-023.

Jiang F, Gu A (2008) Breakage mitigation method for culverts under high embankments using Eps geofoam. In: Liu, H., Deng, A., Chu, J. (Eds.), Geotechnical Engineering for Disaster Mitigation and Rehabilitation. Springer, Berlin, Heidelberg.

Kargar M, Mir Mohammad Hosseini SM (2016) Influence of reinforcement stiffness and strength on load settlement response of geocell-reinforced sand bases. Eur. J. Environ. Civ. Eng. 8189, https://doi.org/10.1080/19648189.2016.1214181.

Katona MG (2010) Seismic design and analysis of buried culverts and structures, Journal of Pipeline Systems Engineering and Practice 1(3), 111–119. doi:10.1061/(ASCE)PS.1949- 1204.0000057.

Katona MG, Smith JM, Odello RS and Allgood JR (1976) CANDE-A modern approach for the structural design and analysis of buried culverts. Report No. FHWA-RD-77-5, doi:10.1084/jem.143.4.741

Kolymbas D (2005) Tunnelling and Tunnel Mechanics: A Rational Approach to Tunneling, Springer Science & Business Media, Berlin.

Kuhlemeyer RL and Lysmer J (1973) Finite element method accuracy for wave propagation problems, Journal of Soil Mechanics & Foundations Div 99, 289–304.

Latha G, Nair A, Hemalatha M (2010) Performance of geosynthetics in unpaved roads. International journal of geotechnical engineering;4(3):337-49.

Lawrence B, Humphrey D and Chen L-H (1999) Field trial of tire shreds as insulation for paved roads. In Tenth International Conference on Cold Regions Engineering: Putting Research into Practice. ASCE, Reston, VA, USA, pp. 428–439.

Leclerq B, Schaeffner M, Delmas P, Blivet JC and Matichard Y (1990) Durability of geotextiles: Pragmatic approach used in France. Geotextiles, Geomembranes and Related Products, Ed. Hoedt, D., Balkema, Rotterdam, 679-684.

Lefebvre G (1981) Fourth Canadian Geotechnical Colloquium: Strength and slope stability in Canadian soft clay deposits. Canadian Geotechnical Journal, 18(3), pp.420-442.

Liedberg NSD (1997) Load reduction on a rigid pipe: pilot study of a soft cushion installation. Transp. Res. Rec. 1594, 217e223.

Look B (2014) Handbook of geotechnical investigation and design tables. CRC Press.

Luscher U and Hoeg K (1964) The beneficial action of the surrounding soil on the load-carrying capacity of buried tubes. In Proc., Symp. On Soil-Structure Interaction. Tucson, AZ: University of Arizona.

Macias M, Atkinson GM and Motazedian D (2008) Ground-motion attenuation, source, and site effects for the 26 September 2003 M 8.1 Tokachi-Oki earthquake sequence, Bulletin of the Seismological Society of America 98(4), 1947–1963. doi:10.1785/0120070130.

Madhusudhan BR, Boominathan A, Banerjee S (2019) Properties of Sand–Rubber Tyre Shreds Mixtures for Seismic Isolation Applications. InSoil Dynamics and Earthquake Geotechnical Engineering; pp. 267-274; Springer, Singapore.

Mahgoub A and El Naggar H (2017) Assessment of the seismic provisions of the CHBDC for CSP culverts, GeoOttawa 2017, the 70th Canadian Geotechnical Conference, Ottawa, Canada.

Mahgoub A and El Naggar H (2019) Using TDA as an engineered stress-reduction fill over preexisting buried pipes. Journal of Pipeline Systems Engineering and Practice 10(1), https://doi.org/10.1061/(ASCE)PS.1949-1204.0000362.

Mahgoub A and El Naggar H (2019b) Using TDA underneath shallow foundations: field tests and numerical modelling. Geotechnique (under review)

Mahgoub A, El Naggar H (2019) Using TDA as an Engineered Stress-Reduction Fill over Preexisting Buried Pipes. Journal of Pipeline Systems Engineering and Practice;10(1):04018034.

Manion WP and Humphrey DN (1992) Use of tire chips as light weight and conventional embankment fill, Phase I-laboratory. Technical paper 91-1, Technical Services Division, Maine department of transportation, Maine.

Marston A (1930) The theory of external loads on closed conduits in the light of the latest experiments. In Vol. 9 of Proc., Highway research board. Washington, DC: Highway Research Board.

McAffee RP, Valsangkar AJ, (2008) Field performance, centrifuge testing, and numerical modelling of an induced trench installation. Can. Geotechnical J. 45 (1), 85e101.

McGrath TJ, Moore ID, Selig ET, Webb MC and Taleb, B (2002) National research council. Recommended specifications for large-span culverts. National Cooperative Highway Research Program (NCHRP) Report 473, Washington, DC: Transportation Research Board.

McGuigan BL, and Valsangkar AJ (2011) Earth pressures on twin positive projecting and induced trench box culverts under high embankments. Can. Geotech. J. 48 (2): 173–185. https://doi.org/10.1139/T10-058.

Meguid MA, Youssef TA (2018) Experimental investigation of the earth pressure distribution on buried pipes backfilled with tire-derived aggregate. Transportation Geotechnics, 14:117-25.

Mehrjardi GT, Tafreshi SM, Dawson AR (2013) Pipe response in a geocell-reinforced trench and compaction considerations. Geosynthetics International; 20(2):105-18.

Meles D, Bayat A, Shafiee MH, Nassiri S and Gul M (2013) Field study on construction of highway embankment made from two tirederived aggregate types and tire-derived aggregate mixed with soil as fill materials. In Transportation Research Board, 92 Annual meeting. Washington, DC. Washington, DC: Transportation Research Board.

Meyerhof GG and Fisher CL (1963) Composite design of underground steel structures, Engineering Journal 46(9), 36–41.

Mills, B., H. El Naggar, and A. J. Valsangkar. 2015. “North American overview and Canadian perspective on the use of tire derived aggregate in highway embankment construction.” Chap. 22 in Vol. 2 of Ground improvement case histories, edited by Indraratna and Chu. New York: Elsevier.

Mirza C and Porter WA (1981) Construction considerations and controls for soil–steel bridge structures, Canadian Journal of Civil Engineering 8(4), 519–534. doi:10.1139/l81-065.

Moo-Young, Sellasie K, Zeroka D, and Sabnis G (2003) Physical and chemical properties of recycled tire shreds for use in construction, Journal of Environmental Engineering, 129(10), 921-929.

Moussa A and El Naggar H (2019) Dynamic properties of tire derived aggregates. In GeoSt.John's, the 72th Canadian Geotechnical Conference St John’s, Canada. Canadian Geotechnical Society.

National Research Council of Canada. Associate Committee on the National Building Code. (2015) National building code of Canada associate committee on the national building code, National Research Council.

Newcomb DE and Drescher A (1994) Engineering properties of shredded tires in lightweight fill applications. Transportation Research Record 1437, National Research Council, Transportation Research Board, Washington, D.C., 1-7.

Ni P, Qin X, Yi Y (2018) Numerical study of earth pressures on rigid pipes with tire-derived aggregate inclusions. Geosynthetics International, 25(5): 494-506.

Nickels WL (1995) The effect of tire shreds as subgrade fill on paved roads. M.S. Thesis, Department of Civil Engineering, University of Maine, Orono, Maine, 215.

Obrzud R and Truty A (2012) The hardening soil model-a practical guidebook z soil. PC100701 Report.

Oshati OS, Valsangkar AJ, Schriver AB (2012) Earth pressures exerted on an induced trench cast-in-place double-cell rectangular box culvert. Canadian Geotechnical Journal, 49(11):1267–84.

Palmeira EM, Andrade HK (2010) Protection of buried pipes against accidental damage using geosynthetics. Geosynthetics International; 17(4):228-41.

Parker BA, McAffee RP, Valsangkar AJ (2008) Field performance and analysis of 3-m-diameter induced trench culvert under a 19.4-m soil cover. Transp Res Rec 2045(08):68–76.

Pierre DKS (2013) Canadian waste tire practices and their potential in sustainable construction. Dalhousie Journal of Interdisciplinary Management 9(1).

Plaxis, B. (2017) Reference Manual for PLAXIS 2D, PLAXIS bv, Delft, Netherlands.

Pokharel SK, Han J, Manandhar C, Yang X, Leshchinsky D, Halahmi I, Parsons RL (2011) Accelerated pavement testing of geocell-reinforced unpaved roads over weak subgrade. Transportation Research Record;2204(1):67-75.

Quigley RM (1980) Geology, mineralogy, and geochemistry of Canadian soft soils: a geotechnical perspective. Canadian Geotechnical Journal, 17(2), pp.261-285.

Rashwan S and Charette P (2015) Demonstration of the Viability of Using Tire Derived Aggregate (TDA) to Replace Natural Material (NM) in Residential Home Basement Construction. Summary report of the demonstration project at 263 Waverly Street, Winnipeg, Manitoba, Canada.

Regier C, Moore I D and Hoult NA (2018) Remaining strength of deteriorated corrugated steel culverts, Journal of Pipeline Systems Engineering and Practice 9, 04018002. doi:10.1061/(ASCE)PS.1949-1204.0000309.

Rezaei A, Kolahdouz EM, Dargush, GF and Weber AS (2012) Ground source heat pump pipe performance with tire derived aggregate. International Journal of Heat and Mass Transfer, 55, No. 11, 2844–2853.

Rodríguez LM, Arroyo M, Cano MM (2018) Use of tire-derived aggregate in tunnel cut-and-cover. Canadian Geotechnical Journal, 55(7):968-78.

Rowe RK and McIsaac R (2005) Clogging of tire shreds and gravel permeated with landfill leachate. Journal of Geotechnical and Geoenvironmental Engineering, 131(6):682-93.

Rubber Manufacturers Association (2017) US scrap tire management summary 2005–2009. Rubber Manufacturers Association, Washington, DC, USA.

Rui R., Van Tol AA, Xia YY, Van Eekelen SJM, and Hu G (2016) Investigation of soil-arching development in dense sand by 2D model tests. Geotech. Test. J. 39 (3): 415–430. https://doi.org/10.1520/GTJ20150130.

Salgado R, Yoon S and Siddiki NZ (2003) Construction of Tire Shreds Test Embankment. FHWA/IN/JTRP-2002/35, Joint Transportation Research Program, Indiana Department of Transportation and Purdue University, West Lafayette, IN, USA https://doi.org/10.1520/JAI103711.

Sawamura Y, Kishida K and Kimura M (2015) Centrifuge model test and FEM analysis of dynamic interactive behavior between embankments and installed culverts in multiarch culvert embankments, International Journal of Geomechanics 15(3, June).

Schanz T, Vermeer PA, and Bonnier PG (1999) The hardening soil model: Formulation and verification. In Beyond 2000 in computational geotechnics: 10 years of Plaxis, 281–296. Rotterdam, Netherlands: A.A. Balkema.

Schlick W J (1932) Loads on pipe in wide ditches, Bul. 108, Iowa Eng., Exp. Sta., 1–49. Ames, IA: Iowa State College.

Schnabel P B (1973) Effects of Local Geology and Distance from Source on Earthquake Ground Motions.

Seed H B and Idriss IM (1970) Soil moduli and damping factors for dynamic response analysis. Report no. EERC 70-10. Berkeley, Calif: College of Engineering, University of California, 1970.

Shalaby A, and Khan RA (2002) Temperature monitoring and compressibility measurement of a tire shred embankment: Winnipeg, Manitoba, Canada. In Transportation research record 1808, 67–75. Washington, DC: National Research Council, Transportation Research Board.

Sladen, J A. and Oswell, J M. (1988). The induced trench method - a critical review and case history. Canadian Geotechnical Journal, 25(3), pp.541-549.

Spangler MG, and Handy RL (1973) Soil engineering. New York: Intext Educational.

Sparkes J, El Naggar H and Valsangkar A (2019) Compressibility and shear strength properties of tire-derived aggregate mixed with lightweight aggregate. Journal of Pipeline Systems Engineering and Practice 10(1), https://doi.org/10.1061/(ASCE)PS.1949-1204.0000354.

Stark TD, Arellano D, Horvath JS and Leshchinsky D (2004) Geofoam applications in the design and construction of highway embankments. NCHRP Web Document 65 (project 24-11), National Cooperative Highway Research Program, Washington, DC.

Tafreshi SM, Mehrjardi GT, Dawson AR (2012) Buried pipes in rubber-soil backfilled trenches under cyclic loading. Journal of Geotechnical and Geoenvironmental Engineering;138(11):1346-56.

Taleb B and Moore I (1999) Metal culvert response to earth loading: performance of two-dimensional analysis, Transportation Research Record: Journal of the Transportation Research Board 1656, 25–36. doi:10.3141/1656-04.

Terzaghi, K (1936) A fundamental fallacy in earth pressure computations. J. Boston Soc. Civ. Eng. 23: 71–88.

Thakur JK, Han J, Pokharel SK, Parsons RL (2012) Performance of geocell-reinforced recycled asphalt pavement (RAP) bases over weak subgrade under cyclic plate loading. Geotextiles and Geomembranes 35:14-24.

Turan A, El Naggar MH, and Dundas D (2013) Investigation of induced trench method using a full-scale test embankment. Geotech. Geol. Eng. 31 (2): 557–568. https://doi.org/10.1007/s10706-012-9608-0.

Tweedie JJ, Humphrey DN and Sandford TC (1998) Full-scale field trials of tire shreds as lightweight retaining wall backfill under at-rest conditions. Transportation Research Record 1619: 64–71, https://doi.org/10.3141/1619-08.

Upton, R. J., and G. Machan. (1993) Use of shredded tires for lightweight fill. Transp. Res. Rec. 1422: 36–45.

Vucetic M and Dobry R (1991) Effect of soil plasticity on cyclic response, Journal of Geotechnical Engineering 117(1), 89–107. doi:10.1061/(ASCE)0733-9410(1991)117:1(89).

Wang WL and Yen BC (1974) Soil arching in slopes. J. Geotech. Eng. 100 (GT1): 61–78.

Wartman J, Natale M and Strenk P (2007) Immediate and time-dependent compression of tire derived aggregate. Journal of geotechnical and geoenvironmental engineering, 133(3), pp.245-256.

Webb M C, Selig E T, Sussman JA and McCarthy, TJ (1999) Field tests of a large-span metal culvert. Transportation Research Record 1653, Paper No. 99-1425. Washington, DC: Transportation Research Board.

White HL and Layer JP (1960) The corrugated metal conduit as a compression ring, Paper presented at the Highway Research Board Proceedings, Washington, DC.

Wolfe SL, Humphrey DN and Wetzel EA (2004) Development of tire shred underlayment to reduce groundborne vibration from LRT track. In GeoTrans 2004, Los Angeles, CA. ASCE, Reston, VA, USA, pp. 750–759.

Wood JH and Lower HT (2007) Earthquake design of rectangular underground structures, Bulletin of the New Zealand Society for Earthquake Engineering 40(1), 1–6.

Xiao M, Bowen J, Graham M and Larralde J (2012) Comparison of seismic responses of geosynthetically reinforced walls with tire-derived aggregates and granular backfills. Journal of Materials in Civil Engineering 24(11): 1368–1377, https://doi.org/10.1061/(ASCE)MT.1943- 5533.0000514.

Yoon S, Prezzi M, Siddiki NZ and Kim B (2006) Construction of a test embankment using a sand-tire shred mixture as fill material. Waste Management 26(9): 1033–1044, https://doi.org/10.1016/j.wasman.2005.10.009.

Youd TL and Beckman CJ (1997) Performance of corrugated metal pipe (CMP) culverts during past earthquakes, Proceedings of the Workshop on Earthquake Engineering Frontiers in Transportation Facilities NCEER-97-005 (eds G. C. Lee and I. M. Friedland), Buffalo, NY, USA, National Center for Earthquake Engineering, Pp 137–151.

Youd TL and Beckman CJ (2003) Performance of corrugated metal pipe (CMP) culverts during past earthquakes Advancing mitigation technologies and disaster response for lifeline systems (pp. 294–307). Seattle, Washington, USA: ASCE.

Zhang L, Ou Q, Zhao M (2018) Double-beam model to analyze the performance of a pavement structure on geocell-reinforced embankment. Journal of Engineering Mechanics ;144(8):06018002

APPENDIX A: Supplementary Data for the Fieldwork

Photos from the Site

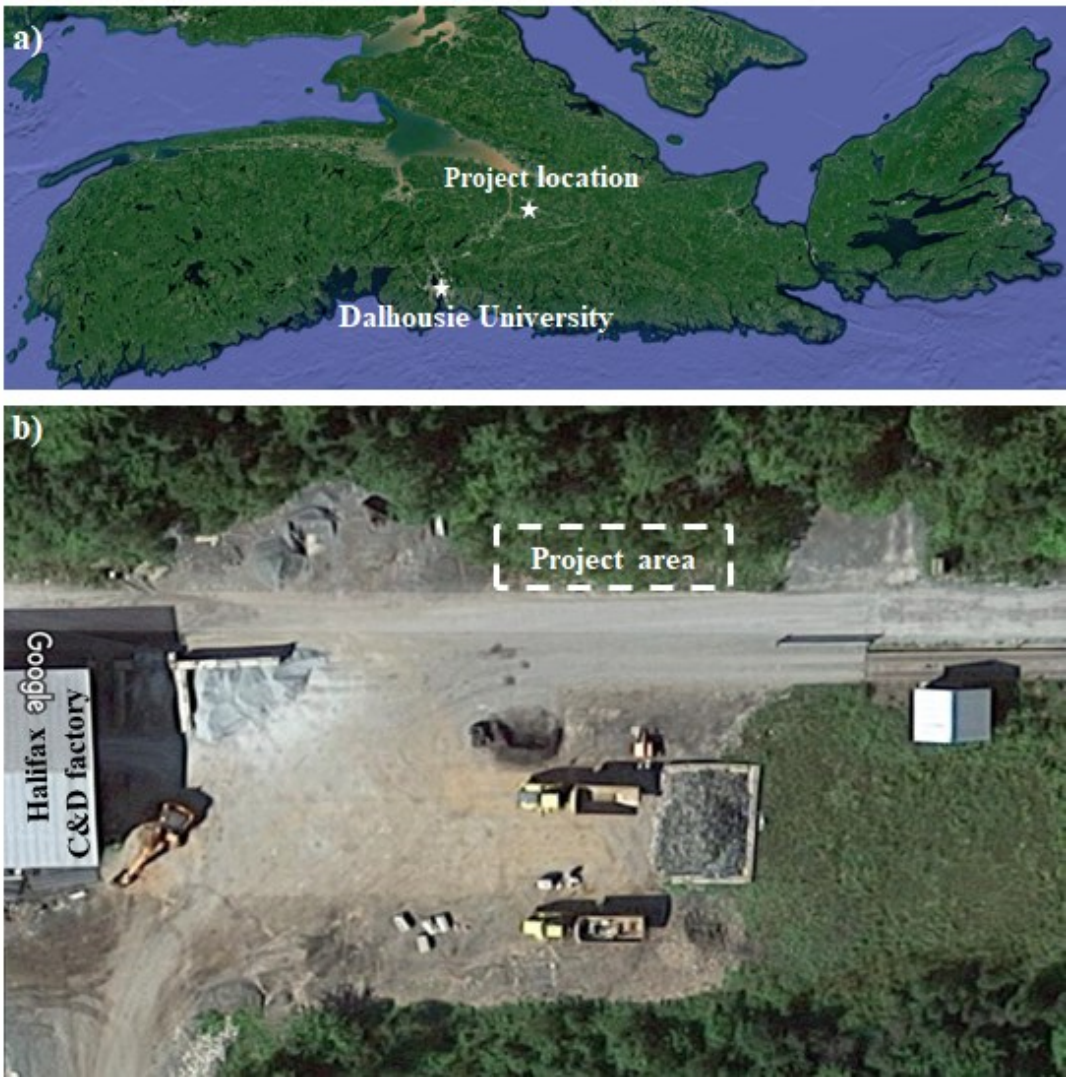

Figure A1. Satellite images of the project site

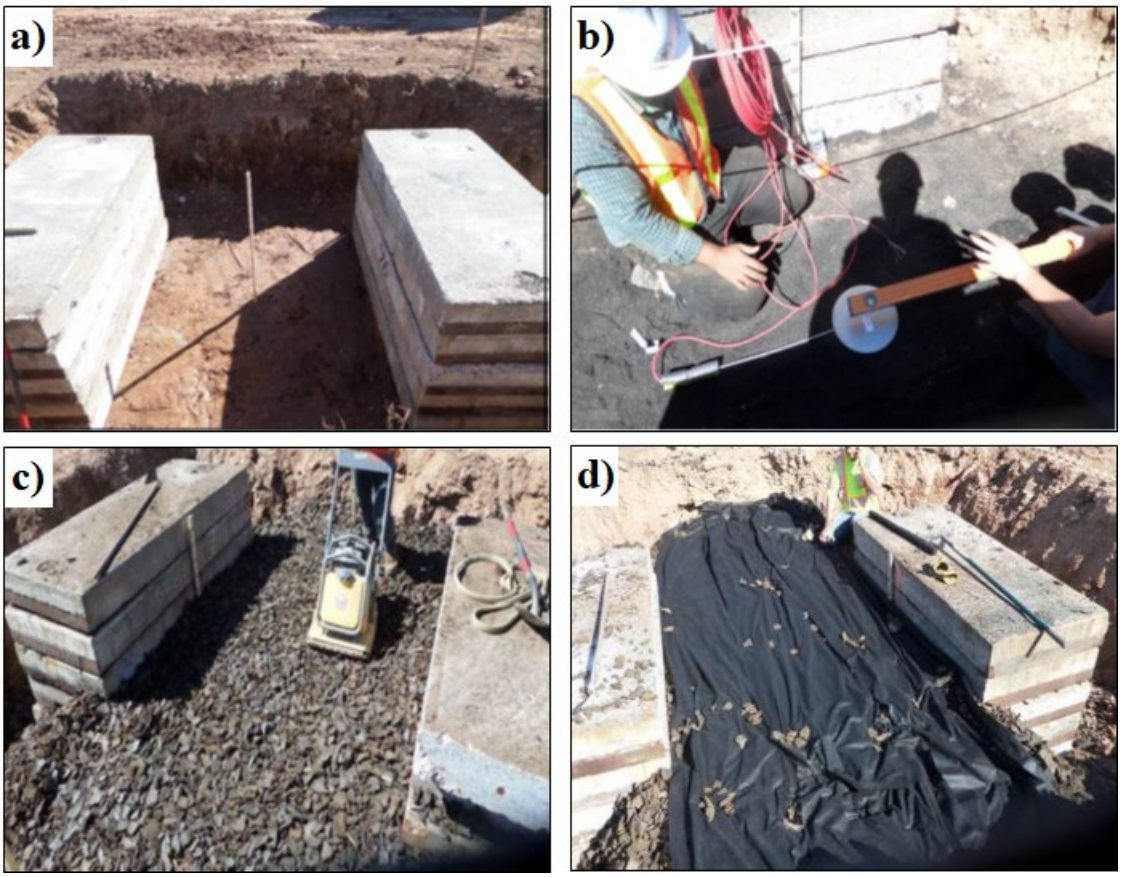

Figure A2. Test procedures a) excavation, b) pressure cell installation, c) compaction, and d) installation of the membrane sheet

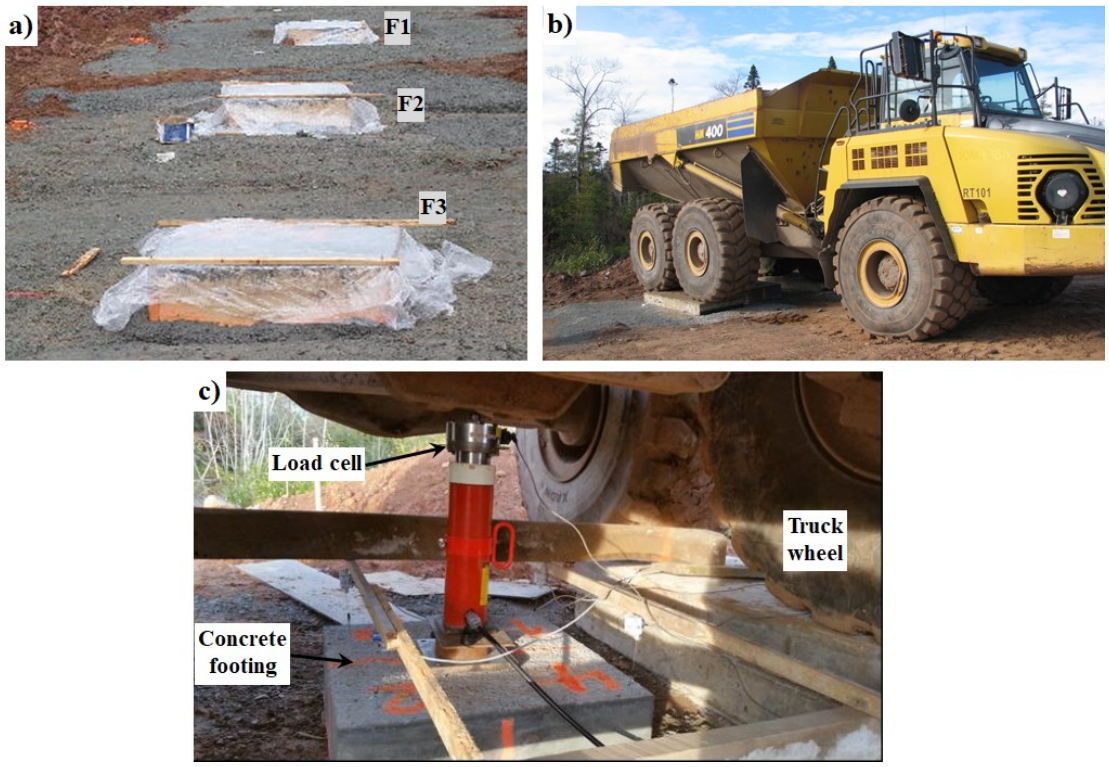

Figure A3. Test procedures a) pouring the concrete, b) aligning the loading truck, and c) applying the load

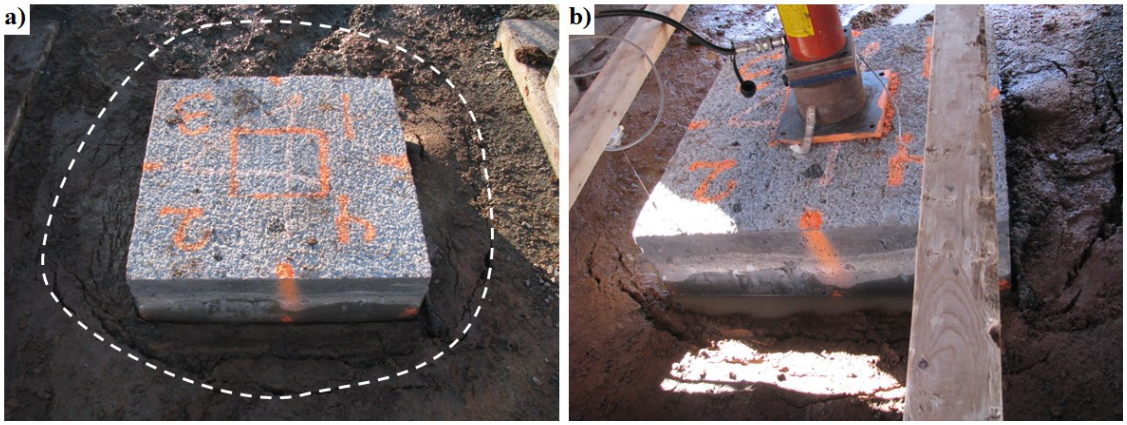

Figure A4. Punching shear failure

Calibration sheets of the pressure cells

innovation in geotechnical instrumentation

RST Instruments Ltd., 11545 Kingston St., Maple Ridge, British Columbia, Canada V2X 0Z5
Tel: 604 540 1100 • Fax: 604 540 1005 • Toll Free: 1 800 665 5599 (North America only)
e-mail: info@rstinstruments.com • Website: www.rstinstruments.com

Calibration Record

Strain Gauge Total Earth Pressure Cell

Customer:	HOSKIN SCIENTIFIC LTD.	
Model:	LPTPC09-S	
Serial Number:	TP2770	
Mfg Number:	380155	
Range:	1000	kPa
Date of Calibration:	11-Jul-16	
Temperature:	23	°C
Barometric Pressure:	1015.4	millibars
Order Number:	210516	
Cable Length:	20	m
Cable Markings:	882650 m - 882670 m	
Excitation:	9-28	Vdc
Cable Colour Code:	Red (Vdc +)	Black (Vdc -)
	Green (Signal +)	White (Signal -)
Cable Type:	EL380004	

Applied Pressure (kPa)	First Reading (V)	Second Reading (V)	Average Reading (V)	Calculated Out Put (kPa)	Calculated Error (%)
0.00	0.046	0.045	0.046	1.28	0.13
100.00	0.538	0.538	0.538	100.19	0.02
200.00	1.034	1.034	1.034	199.80	-0.02
300.00	1.530	1.531	1.531	299.51	-0.05
400.00	2.028	2.028	2.028	399.42	-0.06
500.00	2.525	2.526	2.526	499.33	-0.07
600.00	3.024	3.024	3.024	599.45	-0.06
700.00	3.523	3.523	3.523	699.66	-0.03
800.00	4.023	4.023	4.023	800.07	0.01
900.00	4.523	4.523	4.523	900.49	0.05
1000.00	5.023	5.022	5.023	1000.80	0.08

m= 200.828 kPa/V
b= -7.8578 kPa
x = Measured Output (V)

Load (kPa) = mx+b

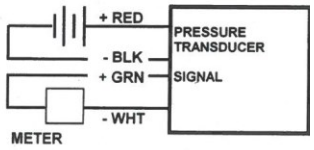

Calibrated by

Pressure Reference: Crystal 0-300 PSI S/N:2535-919715
Digital Multimeter HP34401A s/n: US36053118
Calibrated Annually to National Standards

This instrument has been calibrated using standards traceable to the NIST in compliance with ANSI Z540-1

Document version: LPL0041D

innovation in geotechnical instrumentation

RST Instruments Ltd., 11545 Kingston St., Maple Ridge, British Columbia, Canada V2X 0Z5
Tel: 604 540 1100 • Fax: 604 540 1005 • Toll Free: 1 800 665 5599 (North America only)
e-mail: info@rstinstruments.com • Website: www.rstinstruments.com

Calibration Record

Strain Gauge Total Earth Pressure Cell

Customer:	HOSKIN SCIENTIFIC LTD.
Model:	LPTPC09-S
Serial Number:	TP2771
Mfg Number:	380143
Range:	1000 kPa
Date of Calibration:	11-Jul-16
Temperature:	22.8 °C
Barometric Pressure:	1015.4 millibars
Order Number:	210516
Cable Length:	20 m
Cable Markings:	882692 m - 882711 m
Excitation:	9-28 Vdc
Cable Colour Code:	Red (Vdc +) Black (Vdc -) Green (Signal +) White (Signal -)
Cable Type:	EL380004

Applied Pressure (kPa)	First Reading (V)	Second Reading (V)	Average Reading (V)	Calculated Out Put (kPa)	Calculated Error (%)
0.00	0.039	0.040	0.040	0.78	0.08
100.00	0.533	0.533	0.533	100.20	0.02
200.00	1.027	1.028	1.028	199.81	-0.02
300.00	1.523	1.523	1.523	299.63	-0.04
400.00	2.019	2.020	2.020	399.64	-0.04
500.00	2.516	2.516	2.516	499.66	-0.03
600.00	3.012	3.013	3.013	599.68	-0.03
700.00	3.509	3.510	3.510	699.80	-0.02
800.00	4.007	4.007	4.007	800.02	0.00
900.00	4.505	4.504	4.505	900.23	0.02
1000.00	5.002	5.003	5.003	1000.55	0.06

m= 201.445 kPa/V
b= -7.1735 kPa
x = Measured Output (V)

Load (kPa) = mx+b

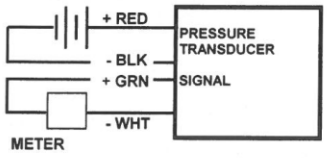

Calibrated by: C

Pressure Reference: Crystal 0-300 PSI S/N:2535-919715
Digital Multimeter HP34401A s/n: US36053118
Calibrated Annually to National Standards

This instrument has been calibrated using standards traceable to the NIST in compliance with ANSI Z540-1

Document version: LPL0041D

innovation in geotechnical instrumentation

RST Instruments Ltd., 11545 Kingston St., Maple Ridge, British Columbia, Canada V2X 0Z5
Tel: 604 540 1100 • Fax: 604 540 1005 • Toll Free: 1 800 665 5599 (North America only)
e-mail: info@rstinstruments.com • Website: www.rstinstruments.com

Calibration Record

Strain Gauge Total Earth Pressure Cell

Customer:	HOSKIN SCIENTIFIC LTD.		
Model:	LPTPC09-S		
Serial Number:	TP2772		
Mfg Number:	380150		
Range:	1000 kPa		
Date of Calibration:	11-Jul-16		
Temperature:	22.8 °C		
Barometric Pressure:	1015.4 millibars		
Order Number:	210516		
Cable Length:	20 m		
Cable Markings:	882671 m - 882690 m		
Excitation:	9-28 Vdc		
Cable Colour Code:	Red (Vdc +)	Black (Vdc -)	
	Green (Signal +)	White (Signal -)	
Cable Type:	EL380004		

Applied Pressure (kPa)	First Reading (V)	Second Reading (V)	Average Reading (V)	Calculated Out Put (kPa)	Calculated Error (%)
0.00	0.042	0.043	0.043	0.63	0.06
100.00	0.539	0.538	0.539	100.07	0.01
200.00	1.036	1.036	1.036	199.80	-0.02
300.00	1.535	1.534	1.535	299.74	-0.03
400.00	2.033	2.033	2.033	399.68	-0.03
500.00	2.532	2.532	2.532	499.72	-0.03
600.00	3.032	3.031	3.032	599.86	-0.01
700.00	3.532	3.530	3.531	699.99	0.00
800.00	4.031	4.030	4.031	800.13	0.01
900.00	4.530	4.529	4.530	900.17	0.02
1000.00	5.029	5.028	5.029	1000.21	0.02

m= 200.477 kPa/V
b= -7.8912 kPa
x = Measured Output (V)

Load (kPa) = mx+b

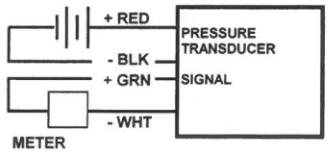

Calibrated by:

Pressure Reference: Crystal 0-300 PSI S/N:2535-919715
Digital Multimeter HP34401A s/n: US36053118
Calibrated Annually to National Standards

This instrument has been calibrated using standards traceable to the NIST in compliance with ANSI Z540-1

Document version: LPL004iD
MIG0106B

innovation in geotechnical instrumentation

RST Instruments Ltd., 11545 Kingston St., Maple Ridge, British Columbia, Canada V2X 0Z5
Tel: 604 540 1100 • Fax: 604 540 1005 • Toll Free: 1 800 665 5599 (North America only)
e-mail: info@rstinstruments.com • Website: www.rstinstruments.com

Calibration Record

Strain Gauge Total Earth Pressure Cell

Customer:	HOSKIN SCIENTIFIC LTD.	
Model:	LPTPC09-S	
Serial Number:	TP2773	
Mfg Number:	380139	
Range:	1000	kPa
Date of Calibration:	11-Jul-16	
Temperature:	22.7	°C
Barometric Pressure:	1015.4	millibars
Order Number:	210516	
Cable Length:	20	m
Cable Markings:	882629m - 882649 m	
Excitation:	9-28	Vdc
Cable Colour Code:	Red (Vdc +)	Black (Vdc -)
	Green (Signal +)	White (Signal -)
Cable Type:	EL380004	

Applied Pressure (kPa)	First Reading (V)	Second Reading (V)	Average Reading (V)	Calculated Out Put (kPa)	Calculated Error (%)
0.00	0.050	0.051	0.051	0.79	0.08
100.00	0.544	0.545	0.545	100.23	0.02
200.00	1.039	1.039	1.039	199.78	-0.02
300.00	1.534	1.535	1.535	299.53	-0.05
400.00	2.032	2.032	2.032	399.67	-0.03
500.00	2.529	2.529	2.529	499.72	-0.03
600.00	3.025	3.026	3.026	599.67	-0.03
700.00	3.523	3.523	3.523	699.82	-0.02
800.00	4.021	4.020	4.021	800.00	0.00
900.00	4.519	4.519	4.519	900.32	0.03
1000.00	5.017	5.016	5.017	1000.47	0.05

m= 201.305 kPa/V
b= -9.3769 kPa
x = Measured Output (V)

Load (kPa) = mx+b

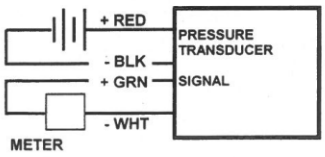

Calibrated by:

Pressure Reference: Crystal 0-300 PSI S/N:2535-919715
Digital Multimeter HP34401A s/n: US36053118
Calibrated Annually to National Standards

This instrument has been calibrated using standards traceable to the NIST in compliance with ANSI Z540-1

innovation in geotechnical instrumentation

RST Instruments Ltd., 11545 Kingston St., Maple Ridge, British Columbia, Canada V2X 0Z5
Tel: 604 540 1100 • Fax: 604 540 1005 • Toll Free: 1 800 665 5599 (North America only)
e-mail: info@rstinstruments.com • Website: www.rstinstruments.com

Calibration Record

Strain Gauge Total Earth Pressure Cell

Customer:	HOSKIN SCIENTIFIC LTD.
Model:	LPTPC09-S
Serial Number:	TP2745
Mfg Number:	418053
Range:	1.0 Mpa
Date of Calibration:	10-Jul-16
Temperature:	22.6 °C
Barometric Pressure:	1016.2 millibars
Work Order Number:	210472
Cable Length:	20 m
Cable Markings:	1412693 m - 1412712 m
Excitation:	9-28 Vdc
Cable Colour Code:	Red (Vdc +) Black (Vdc -)
Cable Type:	EL380004

Applied Pressure (kPa)	First Reading (mA)	Applied Pressure (kPa)	Second Reading (mA)	Average Pressure (kPa)	Average Reading (mA)	Calculated Pressure (kPa)	Full Scale Error (%)
0.0	4.110	0.0	4.110	0.0	4.110	0.7	0.07
100.0	5.694	100.0	5.695	100.0	5.695	100.0	0.00
200.0	7.285	200.0	7.286	200.0	7.286	199.8	-0.02
300.0	8.880	300.0	8.882	300.0	8.881	299.8	-0.02
400.0	10.475	400.0	10.475	400.0	10.475	399.7	-0.03
500.0	12.070	500.0	12.071	500.0	12.071	499.7	-0.03
600.0	13.667	600.0	13.667	600.0	13.667	599.8	-0.02
700.0	15.265	700.0	15.264	700.0	15.265	699.9	-0.01
800.0	16.862	800.0	16.861	800.0	16.862	800.1	0.01
900.0	18.459	900.0	18.459	900.0	18.459	900.2	0.02
1000.0	20.057	1000.0	20.055	1000.0	20.056	1000.3	0.03
						Max Error (%):	0.07

Scale Factor (m): 62.687 kPa/mA
Offset (b): -256.942 kPa

Pressure is calculated with the following equation:
Pressure (kPa) = mX+b

m = Scale Factor in kPa/mA
X = Current in mA
b = Offset in kPa

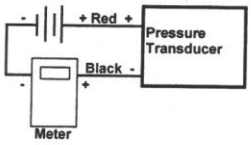

Pressure Reference: Crystal 0 -300 PSI s/n: 2535-919715
Digital Multimeter HP34401A s/n: US36053118
Calibrated Annually to National Standards

Calibrated by: Da

This instrument has been calibrated using standards traceable to the NIST in compliance with ANSI Z540-1

Document Number.: LPL0012G

Recycled

MIG0106B

APPENDIX B: Copyright Permissions

Copyright permission for Chapter 2

September 9th, 2019

ASCE's Journal of Pipeline Systems - Engineering and Practice,

I am preparing my Ph.D. thesis for submission to the Faculty of Graduate Studies at Dalhousie University, Halifax, Nova Scotia, Canada. I am seeking your permission to include a manuscript version of the following paper as a chapter in the thesis:

[Ahmed Mahgoub and Hany El Naggar, "Using TDA as an Engineered Stress Reduction Fill Over Pre-existing Buried Pipes", Journal of Pipeline Systems - Engineering and Practice]

Canadian graduate theses are reproduced by the Library and Archives of Canada (formerly National Library of Canada) through a non-exclusive, world-wide license to reproduce, loan, distributor or sell these. I am also seeking your permission for the material described above to be reproduced and distributed by the LAC (NLC). Further details about the LAC (NLC) thesis program are available on the LAC (NLC) website (www.nlc-bnc.ca) Full publication details and a copy of this permission letter will be included in the thesis.

Yours Sincerely,

Ahmed Mahgoub

Ahmed Mahgoub

From: PERMISSIONS <permissions@asce.org>
Sent: Tuesday, September 10, 2019 11:08 AM
To: Ahmed Mahgoub; ASCE Journal-Submissions5
Subject: RE: Copyright permission for Ahmed Mahgoub's PhD thesis

Dear Ahmed Mahgoub,

Thank you for your inquiry. As an original author of an ASCE journal article or proceedings paper, you are permitted to reuse your own content (including figures and tables) for another ASCE or non-ASCE publication or your thesis, provided it does not account for more than 25% of the new work.

A full credit line must be added to the material being reprinted. For reuse in non-ASCE publications, add the words "With permission from ASCE" to your source citation. For Intranet posting, add the following additional notice: "This material may be downloaded for personal use only. Any other use requires prior permission of the American Society of Civil Engineers. This material may be found at [URL/link of abstract in the ASCE Library or Civil Engineering Database]."

Each license is unique, covering only the terms and conditions specified in it. Even if you have obtained a license for certain ASCE copyrighted content, you will need to obtain another license if you plan to reuse that content outside the terms of the existing license. For example: If you already have a license to reuse a figure in a journal, you still need a new license to use the same figure in a magazine. You need a separate license for each edition.

For more information on how an author may reuse their own material, please view:
http://ascelibrary.org/page/informationforasceauthorsreusingyourownmaterial

Sincerely,

Leslie Connelly
Senior Marketing Coordinator
American Society of Civil Engineers
1801 Alexander Bell Drive
Reston, VA 20191

PERMISSIONS@asce.org

703-295-6169
Internet: www.asce.org/pubs | www.ascelibrary.org | http://ascelibrary.org/page/rightsrequests

Copyright permission for Chapter 7

Journal of Earthquake Engineering,

I am preparing my Ph.D. thesis for submission to the Faculty of Graduate Studies at Dalhousie University, Halifax, Nova Scotia, Canada. I am seeking your permission to include a manuscript version of the following paper as a chapter in the thesis:

[Ahmed Mahgoub and Hany El Naggar, "Seismic Design of Metal Arch Culverts: Design Codes Vs. Full Dynamic Analysis", Journal of Earthquake Engineering]

Canadian graduate theses are reproduced by the Library and Archives of Canada (formerly National Library of Canada) through a non-exclusive, world-wide license to reproduce, loan, distributor or sell these. I am also seeking your permission for the material described above to be reproduced and distributed by the LAC (NLC). Further details about the LAC (NLC) thesis program are available on the LAC (NLC) website (www.nlc-bnc.ca) Full publication details and a copy of this permission letter will be included in the thesis.

Yours Sincerely,

Ahmed Mahgoub